CVD de la zircone à partir du système ZrCl -H -CO -Ar : application aux matériaux composites céramique-céramique

Jacky Minet

N° d'ordre : 938

THÈSE

PRÉSENTÉE A

L'UNIVERSITÉ DE BORDEAUX I

POUR OBTENIR LE GRADE DE

DOCTEUR D'ÉTAT ÈS SCIENCES

PAR

Jacky MINET

Ingénieur E.N.S.C.P.B.

CVD DE LA ZIRCONE A PARTIR DU SYSTÈME $ZrCl_4$-H_2-CO_2-Ar. APPLICATION AUX MATÉRIAUX COMPOSITES CÉRAMIQUE-CÉRAMIQUE.

Soutenue le 14 septembre 1988, devant la Commission d'examen :

MM.	P. HAGENMULLER	*Président.*
	C. BERNARD	*Examinateurs.*
	P. BOCH	
	J. ÉTOURNEAU	
	P. LAMICQ	
	F. LANGLAIS	
	R. NASLAIN	
	J.M. QUENISSET	

— 1988 —

A Monsieur le Professeur HAGENMULLER

Hommage de ma respectueuse reconnaissance

A Monsieur le Professeur R. NASLAIN

Témoignage de ma sincère gratitude

A mes Parents,

A Marie-José, Michaël,

A tous ceux qui me sont chers

Ce travail a été réalisé au Laboratoire de Chimie du Solide du CNRS, sous la direction de Monsieur le Professeur P. HAGENMULLER. Je tiens à lui exprimer ma profonde reconnaissance pour l'accueil qu'il m'a réservé dans son laboratoire et pour avoir accepté la présidence de mon jury de thèse.

Monsieur le Professeur J. ETOURNEAU, Directeur du Laboratoire de Chimie du Solide du CNRS, m'a fait l'honneur de juger ce mémoire. Je lui adresse mes remerciements les plus sincères.

Monsieur le Professeur P. BOCH, de l'Ecole Nationale Supérieure de Céramique Industrielle de Limoges, a bien voulu nous faire l'honneur de juger ce travail, je le prie d'accepter l'expression de ma respectueuse reconnaissance.

Monsieur C. BERNARD, Directeur de Recherches au Laboratoire de Thermodynamique et Physico-Chimie Métallurgiques (LA 29) de Grenoble, m'a apporté une aide précieuse lors de l'étude des équilibres complexes de CVD. Il m'a toujours reçu avec beaucoup de sympathie dans son laboratoire et a bien voulu juger ce travail. Je lui exprime toute ma gratitude.

Monsieur P. LAMICQ, Ingénieur en Chef à la Société Européenne de Propulsion - Division Propulsion à Poudre et Composites - a aimablement accepté de participer à mon jury de thèse. Je le remercie vivement.

Monsieur le Professeur R. NASLAIN, Directeur du Laboratoire des Composites Thermo-structuraux, a dirigé le présent travail en me faisant profiter de ses précieux conseils et de sa grande connaissance des matériaux composites. Je tiens à lui exprimer ma profonde gratitude pour tout ce qu'il m'a enseigné au cours de ces années de recherche.

Monsieur le Professeur J.M. QUENISSET, Directeur du Laboratoire d'Essai des Métaux, m'a apporté une aide précieuse dans la réflexion et la compréhension des comportements thermomécaniques des matériaux élaborés lors de cette étude. Il a aimablement accepté de participer à mon jury de thèse. Qu'il trouve, ici, l'expression de ma sincère gratitude.

Je tiens à remercier, tout particulièrement, Monsieur F. LANGLAIS qui, grâce à ses compétences scientifiques mais aussi sa gentillesse et sa disponibilité, m'a permis de mener à bien ce travail. Il a également accepté de participer à mon jury de thèse. Je tiens à l'assurer de ma très profonde reconnaissance et ma sincère amitié.

Je remercie la Société Européenne de Propulsion qui m'a accordé son aide pour la réalisation de ces recherches. Mes remerciements s'adressent notamment à Messieurs CHATEIGNER, HERAUD et ROBIN-BROSSE qui ont suivi avec intérêt le déroulement de mes travaux, à Messieurs COTTERET, MACE, TAWILL et leurs collaborateurs pour leur participation à la caractérisation des matériaux.

Mes remerciements s'adressent à Messieurs LAHAYE, CRUEGE, CAZORLA, TRUT et CHAMBON qui m'ont fait profiter de leurs compétences en microanalyse X ou Raman, en diffraction X et en microscopie électronique, à Messieurs RABARDEL et VILLOT pour leur collaboration lors des études d'oxydation par thermogravimétrie.

Je ne saurais oublier Messieurs R. PAILLER, L. ALBINGRE et P. DURAND qui ont été souvent présents à mes côtés, me faisant profiter de leurs conseils scientifiques, leur assistance technique et leur gentillesse.

De même, je tiens vivement à remercier Madame M. GEORGY qui a largement contribué à la réalisation de ce mémoire.

Enfin, c'est avec un grand plaisir que j'exprime mon amitié à tous les membres du laboratoire et notamment à ceux et celles du groupe "matériaux composites", qui ont contribué, par leur sympathie et leur bonne humeur, à créer une ambiance de travail agréable.

La DRET doit être remerciée pour son aide financière, ainsi que la SEP qui a également fourni la plupart des préformes nécessaires à la réalisation de ce travail.

SOMMAIRE

INTRODUCTION

I - GENERALITES

Dans leur forme la plus commune, les matériaux composites sont définis comme des solides hétérogènes constitués de deux phases. L'une, à base d'éléments renforçants à texture généralement fibreuse, forme un squelette chargé de supporter l'effort mécanique appliqué au matériau. L'autre, appelée **matrice,** lie ces éléments, leur transmet les efforts en les répartissant et éventuellement protège le squelette fibreux contre les agressions du milieu extérieur (1).

C'est sur la base de ce concept et pour répondre à des applications spécifiques que la notion de "composite" naquit en associant à l'échelle microscopique plusieurs composants dont les propriétés sont complémentaires pour que le matériau puisse avoir à l'échelle macroscopique les caractéristiques requises.

Dans la plupart des applications, les matériaux composites sont constitués de fibres à hautes performances mécaniques (fibres de verre borosilicaté, de carbone ou de polyamides aromatiques) enrobées dans une matrice **organique** (époxyde ou polyester, par exemple). En raison de leur faible

densité (inférieure à 2), ces matériaux possèdent des caractéristiques mécaniques spécifiques supérieures, à celles des meilleurs aciers (dont les densités sont de l'ordre de 8). C'est pourquoi, ces matériaux présentent, pour des températures n'excédant pas 250°C environ, un très grand intérêt dans des applications structurales concernant de nombreux domaines (aéronautique, spatial, nautisme, automobile, etc ...)

Par la suite, les conditions d'utilisation devenant plus sévères (environnement chimique, chargement mécanique et température plus élevées), les matrices organiques ne possèdent pas une stabilité thermique suffisante. C'est pourquoi des composites à **matrice métallique** ont été imaginés pour des utilisations à moyenne température ($\theta < 500°C$), étant entendu que les fibres doivent avoir, également, une bonne stabilité thermique. Ces composites sont constitués d'alliages métalliques à faible densité (alliages de magnésium, d'aluminium ou éventuellement de titane). En raison des problèmes d'élaboration et de compatibilité fibre-matrice, les composites à matrice métallique n'ont reçu, à ce jour, qu'un développement industriel limité. Toutefois, l'arrivée de nouvelles fibres sur le marché (fibres de carbure de silicium, d'alumine par exemple) et la mise au point de nouveaux procédés tels que le forgeage liquide, ou "squeeze casting", laissent à penser que les composites à matrice métallique pourraient rapidement connaître un développement industriel, dans le secteur automobile, par exemple.

Enfin, pour des applications à températures encore plus élevées ($\theta > 500°C$), la matrice ne peut être que ***céramique*** . C'est à partir des composites

fibreux carbone-carbone, qu'a été développée la nouvelle famille de matériaux **composites céramique-céramique** dans lesquels fibres et matrice sont des matériaux réfractaires (de nature identique ou différente). Dans une autre optique, tout aussi importante, il est apparu que le concept du composite fibreux devrait permettre de réaliser des céramiques non fragiles et plus fiables.

2 - LES COMPOSITES CARBONE-CARBONE

Les matériaux composites carbone-carbone constitués de fibres de carbone enrobées dans une matrice elle-même de carbone, sont élaborés par des méthodes variées avec divers types de fibres et de matrices (2-4). Quelques généralités sur la nature des constituants des composites C-C permettront de situer les préformes carbonées enployées dans cette étude.

2.1. Les fibres de carbone

Les fibres de carbone sont obtenues par pyrolyse (1000 - 1100°C) puis éventuellement graphitation à haute trempérature de précurseurs organiques fibreux comme le polyacrylonitrile (PAN) ou les brais. Les cristallites élémentaires qui les constituent sont toutes orientées par un traitement d'étirage mécanique, de telle sorte que les feuillets de graphite à symétrie hexagonale soient parallèles à l'axe des fibres. Le traitement de graphitation réalisé à très haute température (2500 - 2800°C) est facultatif. Il permet d'augmenter considérablement la rigidité de la fibre, mais provoque, en revanche, une

diminution de la résistance à la rupture (5). Les fibres de carbone sont utilisées sous forme de feutres de fils, de mèches, de tissus ou d'architectures multidirectionnelles à n directions de renforcement (avec $2 < n < 12$). Leur mode d'arrangement au sein d'une ébauche de la pièce à réaliser, qui est appelée **préforme,** détermine la texture de celle-ci qui peut être mono, bi ou tridimentionnelle. Il détermine par conséquent le degré d'anisotropie du futur composite. Les préformes fibreuses carbonées sont ensuite densifiées par une matrice à base de carbone.

2.2. La matrice de carbone

La matrice peut être introduite dans les espaces interfibres: 1) en **phase gazeuse,** par dépôt chimique, (Chemical Vapor Infiltration ou CVI) à partir d'un hydrocarbure comme le méthane, conduisant à la formation de pyrocarbone, ou 2) en **phase liquide** par imprégnation à l'aide de résines organiques (résines phénolique ou furanique, par exemple) ou de brais suivie d'une cokéfaction (2, 3, 6-8). La structure, la texture et l'aptitude à la graphitation de ces carbones sont très différentes. Les carbones pyrolytiques présentent divers types de textures (laminaire lisse, laminaire rugueux, isotrope) suivant les conditions de dépôt (température, pression, ...) (3, 9, 10). La graphitation des cokes est beaucoup plus aisée lorsque le précurseur est un produit organique à structure réticulée fortement aromatique et de poids moléculaire élevé: un brai par exemple (substance complexe constituant le résidu de la distillation de la houille, du bois ou du pétrôle brut). La densification complète des préformes aboutissant au matériau composite carbone-carbone nécessite, suivant la

technique, plusieurs cycles d'infiltration en phase gazeuse et d'usinages superficiels (réouverture des pores) ou plusieurs cycles d'imprégnation-carbonisation. La porosité résiduelle de ces matériaux est alors très faible (2).

Compte tenu de leur grande réfractairité, de leurs performances thermomécaniques élevées et de leur excellente résistance à l'ablation à très haute température, conjuguées à leur faible densité, les composites carbone-carbone sont très largement utilisés dans le secteur aérospatial (tuyère, divergent, protections thermiques, ...). De plus, en raison de propriétés spécifiques du carbone (coefficient de friction élevé à haute température, conductivité thermique, biocompatibilité), les applications de ces composites se sont étendues à d'autres secteurs. Ainsi ils sont utilisés en tant que **dispositif de freinage** pour véhicules terrestres et aéronautiques, mais aussi en tant que **prothèses osseuses et vasculaires** du fait de l'excellente biocompatibilité du carbone par rapport aux autres matériaux prothétiques.

Toutefois, malgré les nombreux avantages des composites carbone-carbone, ces matériaux ont un champ d'application limité en raison de leur **faible résistance à l'oxydation** (le carbone s'oxyde dès 500 - 600°C à l'air). De plus, sur le plan mécanique, ces composites, notamment ceux à texture 2D présentent une faible résistance au cisaillement interstrates, en raison de la matrice pyrocarbone qui est moins performante que de nombreuses autres céramiques, les rendant fortement **anisotropes.**

3 - LES COMPOSITES A MATRICE HYBRIDE

C'est pour pallier le mauvais comportement à l'oxydation des composites carbone-carbone, qu'il a été proposé de remplacer partiellement la matrice de carbone par un matériau céramique réfractaire, plus performant, tout en utilisant le procédé d'infiltration chimique par voie gazeuse (CVI).

C'est ainsi que, partant de cette idée, F. CHRISTIN puis C. MALLET, ont pû réaliser des composites 2D-C-C / SiC pour lesquels le carbure de silicium (pur ou associé à du carbone) est élaboré à partir de mélanges de méthyltrichlorosilane (CH_3SiCl_3) et d'hydrogène (ou d'argon) (4, 11). De même, J.Y. ROSSIGNOL a mis au point des composites 2D-C-C / TiC, à partir de mélanges ternaires $TiCl_4$-CH_4-H_2 (12). Enfin, H. HANNACHE a également synthétisé des composites 2D-C-C / BN puis 2D-C-C / B_4C, partant respectivement de mélanges BF_3 (ou BCl_3)-NH_3-H_2 et BCl_3-CH_4-H_2 (13, 14). Les différents matériaux composites à matrice hybride 2D-C-C / X (X = SiC, TiC, B_4C ou BN) présentent des propriétés mécaniques améliorées (résistance et module d'Young plus élevés, anisotropie plus faible) ainsi que de meilleurs comportements vis-à-vis de l'oxydation, étendant le domaine d'utilisation dans l'air des carbone-carbone jusqu'à des températures de 900-1000°C pour les composites 2D-C-C / BN (ou B_4C), et jusqu'à 1400 - 1500°C pour les composites 2D-C-C / SiC (15, 16).

Compte tenu de ces résultats et de l'apparition ultérieure sur le marché de fibres céramiques (SiC, Al_2O_3, par exemple) il a été envisagé d'élargir

le champ d'investigation des composites en développant de nouvelles familles de matériaux.

C'est ainsi que la Société Européenne de Propulsion (SEP) a développé industriellement les composites 2D-SiC-SiC dans lesquels fibres et matrices sont en carbure de silicium, présentant une résistance à l'oxydation encore accrue par rapport aux 2D-C-C / SiC, notamment lors d'oxydations de longue durée (17, 18).

Parallèlement, étant à la recherche de matrices céramiques plus performantes (du point de vue tenue à l'oxydation), il était naturel d'étudier les composites fibreux à matrice d'oxydes réfractaires.

4 - LES COMPOSITES CERAMIQUE - CERAMIQUE A MATRICE OXYDES:

4.1. Composites à matrice d'alumine

Sur la base de travaux visant la compréhension des phénomènes physico-chimique qui contrôlent la qualité des revêtements d'alumine déposés à la surface des outils de coupe en carbure cémentés, R. COLMET a pu établir que les composites fibreux à matrice d'alumine pouvaient être obtenus par infiltration chimique en phase vapeur, à partir de mélanges $AlCl_3$-H_2-CO_2, dans la porosité ouverte de préformes à bases de fibres d'alumine ou de carbure de silicium (19, 20).

Moyennant des conditions de température, pression et débit corrects, deux types de composites alumine-alumine ont pû être élaborés. Les résultats d'essais mécaniques, réalisés en flexion et à température ambiante, montrent: (i) une augmentation de la résistance à la rupture au fur et à mesure que la fraction volumique d'alumine infiltrée croît; (ii) des ruptures à **caractère fragile** (qui se produisent en général pour des faibles déformations), (iii) une diminution de la résistance à la rupture au delà de 1200°C, traduisant une mauvaise stabilité thermique de ces matériaux, amplifiée, vraisemblablement, par des fibres d'alumine de qualité insuffisante (20).

4.2. Composites à matrice à base de zircone

4.2.1. Intérêt des composites à matrice à base de ZrO_2

De par ses propriétés (tableau I) la zircone est déjà largement utilisée dans le domaine des céramiques thermomécaniques (21).

Aussi, il est apparu intéressant de transposer l'expérience acquise sur l'alumine, au cas des composites à matrice de zircone, avec les avantages potentiels suivants:

- la zircone est beaucoup **plus réfractaire** que l'alumine ($\theta_F(ZrO_2) \approx 2700°C$ contre $\theta_F(Al_2O_3) \approx 2050°C$)

- l'existence **d'un polymorphisme dans ZrO_2** et la posibilité de stabiliser les variétés quadratique ou cubique à l'aide de certains oxydes, peuvent se traduire par **une amélioration de la ténacité** (c'est à dire, par augmentation du facteur critique d'intensité de contrainte),

- la zircone est un oxyde de très **grande stabilité chimique** et, un très **bon isolant thermique,**

- enfin, sous forme stabilisée, la zircone est un **bon conducteur ionique.**

4.2.2. Elaboration de zircones par voie gazeuse:
Approche bibliographique

Une étude bibliographique souligne que la zircone a été l'objet de multiples travaux dans le domaine des céramiques thermomécaniques, en revanche, les études portant sur l'élaboration de la zircone à partir de précurseurs gazeux, restent limitées.

Parmi les différentes réactions chimiques qui conduisent à un dépôt de zircone monoclinique, on distingue:

- **les réactions de décomposition d'organo-métalliques** qui consistent à décomposer thermiquement (CVD), ou au sein d'un plasma froid (PACVD), des composés organométalliques (généralement des alcoolates, des carboxylates ou des phénolates de zirconium) préalablement vaporisés (22 - 28). Ces réactions

peuvent être réalisées à des températures relativement faibles (entre 200 et 500°C), mais avec des cinétiques de formation de zircone très lentes.

- **les réactions d'hydrolyse d'halogénures de zirconium,** pour lesquelles la phase hydrolysante peut être:

* **de la vapeur d'eau** (28), conduisant à la réaction:

$$ZrX_{4(g)} + 2H_2O_{(g)} \text{-----> } ZrO_{2(s)} + 4HX_{(g)} \qquad \text{(avec X = Cl, Br, I)}$$

néanmoins, la zircone ainsi obtenue est partiellement hydratée, ce qui la rend chimiquement moins inerte.

* **un mélange H_2 / O_2** , réaction généralement mise en oeuvre à l'aide de réacteurs à flamme (ou chalumeaux):

$$ZrX_{4(g)} + 2H_{2(g)} + O_{2(g)} \text{-----> } ZrO_{2(s)} + 4\,HX_{(g)} \qquad \text{(avec X = Cl, Br, I)}$$

* **un mélange H_2 / CO_2** (28,29) pour lequel la cinétique de formation de la vapeur d'eau est favorisée aux températures supérieures à 900 K (30):

$$ZrX_{4(g)} + 2H_{2(g)} + CO_{2(g)} \text{----> } ZrO_{2(s)} + 2CO_{(g)} + 4HX_{(g)} \text{ (avec X = Cl, Br, I)}$$

- **les réactions d'oxydation de vapeurs d'halogénures métalliques ou de composés organométalliques** (26 - 28, 31 - 32), pour lesquelles on distingue deux

principaux agents d'oxydation: l'oxygène et le dioxyde de carbone. Toutefois, ce type de réaction devient rapidement défavorable, du point de vue thermodynamique et cinétique, par rapport aux réactions d'hydrolyse à partir de mélanges d'hydrogène et de dioxyde de carbone, lorsque la température est supérieure à 1000 K.

Par ailleurs, des tentatives de dépôt de zircone partiellement stabilisée (PSZ) ont été effectuées. C'est ainsi que K.S. MAZDIYASNI et al. (24) ont obtenu de la zircone cubique (ZrO_2 + 5% Y_2O_3). De même, WHEELER et al. (33) ont déposé un brevet pour l'obtention de PSZ (ZrO_2 + 8% SC_2O_3) par dépôt chimique en phase gazeuse. G. WAHL et al (34) ont préparé de la zircone cubique (ZrO_2 + 9% Y_2O_3) à partir des chlorures correspondants. Enfin, K. KAMATA et al. (35) et K. BRENNFLECK et al. (36) ont obtenu de la zircone cubique (ZrO_2 + 30% Y_2O_3) à partir de précurseurs gazeux organométalliques.

4.2.3. Objectifs et contenu du présent travail

La présente étude s'est donnée comme objectifs: (1) de transposer l'expérience acquise sur l'alumine au cas des composites céramique-céramique à matrice à base de zircone, en démontrant que de tels matériaux peuvent être élaborés par CVI à partir de préformes fibreuses et microporeuses de carbone ou d'alumine; (2) d'évaluer les principales propriétés des composites à matrice à base de ZrO_2 sur les plans physico-chimique et thermo-mécanique.

Le choix du système chimique permettant de former ZrO_2, à partir d'une phase gazeuse, a été guidé par des considérations théoriques (les espèces sources pour le zirconium et l'oxygène doivent avoir de faibles poids et encombrements moléculaires) et économiques (précurseurs gazeux facilement disponibles, de mise en oeuvre commode et de coût relativement faible) en vue d'une éventuelle application industrielle. Compte tenu des travaux antérieurs, le système le plus apte à donner des dépôts de zircone est un mélange $ZrCl_4$ -H_2-CO_2 (dilué éventuellement avec un gaz neutre; ici de l'argon).

Le chlorure de zirconium, choisi comme agent de transport, est obtenu par réaction directe du chlore sur de l'éponge de zirconium à 300 - 350°C. Ainsi formé, $ZrCl_4$ est transporté jusqu'au réacteur, à pression réduite, et à une température voisine de 350°C.

Tout comme l'alumine, la zircone est formée chimiquement par hydrolyse de $ZrCl_4$ à l'aide de la vapeur d'eau résultant de l'oxydation, à haute température de l'hydrogène par le dioxyde de carbone, selon le schéma réactionnel:

$$2H_{2(g)} + 2CO_{2(g)} \rightleftharpoons 2H_2O_{(g)} + 2CO_{(g)} \qquad (1)$$

$$ZrCl_{4(g)} + 2H_2O_{(g)} \rightleftharpoons ZrO_{2(s)} + 4HCl_{(g)} \qquad (2)$$

$$ZrCl_{4(g)} + 2H_{2(g)} + 2CO_{2(g)} \rightleftharpoons ZrO_{2(s)} + 2CO_{(g)} + 4HCl_{(g)} \qquad (3)$$

Dans cette méthode, l'eau nécessaire à la réaction (2) n'est formée qu'au contact immédiat du substrat à densifier porté à haute température, évitant l'hydrolyse prématurée de $ZrCl_4$ au sein du mélange gazeux initial. La cinétique de la réaction (1) étant lente, tout se passe comme si le mélange H_2 / CO_2 constituait un "réservoir d'eau" dans le réacteur.

Afin de connaître les conditions d'infiltration (i.e. les paramètres température, pression et débit), ce travail a nécessité une approche fondamentale qui se base à la fois sur des considérations théoriques (calculs thermodynamiques) et expérimentales (cinétiques de dépôt et d'infiltration).

L'approche thermodynamique permet de prévoir les conditions de dépôt, à l'équilibre, des solides purs (ZrO_2, C par exemple) ainsi que les rendements par rapport aux espèces sources, la nature des sous-produits susceptibles de se former et l'existence d'éventuelles attaques chimiques du substrat. Dans le cadre du présent travail, cette étude s'est attachée à déterminer, en fonction des divers paramètres de dépôt (P, T, composition du système gazeux initial) **la composition à l'équilibre** des phases gazeuses et condensées, ainsi que **les rendements thermodynamiques** pour différents substrats (alumine, carbone et mullite).

L'étude thermodynamique a dû être complétée par une **étude expérimentale des vitesses de dépôt sur substrats plans** puis, étendue à des **substrats poreux,** permettant de mettre si possible en évidence la transition entre

le régime de dépôt contrôlé par les réactions de surface et régime de dépôt gouverné par la diffusion des espèces gazeuses dans la couche limite.

Sur la base de cette double approche, diverses préformes à base de fibres d'alumine (ou silicoalumineuses) et de carbone ont été densifiées par ZrO_2. Les composites céramique-céramique à matrice à base de zircone ont été caractérisés sur les plans microstructural, physico-chimique puis thermo-mécanique (de la température ambiante à 1400°C). Au cours de cette caractérisation, un accent particulier a été mis sur l'influence de la texture fibreuse, de la fraction volumique de zircone, de la porosité résiduelle et de la liaison fibre-matrice sur le comportement mécanique des composites alumine-zircone.

Notre mémoire est articulé autour de cinq publications qui ont été soumises à des revues internationales et qui sont, de ce fait, rédifées en langue anglaise (certaines d'entre elles sont d'ailleurs déjà parues).

- le premier article (Chapitre I) concerne l'approche thermodynamique du dépôt chimique en phase gazeuse (CVD) de zircone, à partir du système $ZrCl_4$-H_2-CO_2-Ar;

- le deuxième (Chapitre II) présente l'étude expérimentale de la cinétique de dépôt de ZrO_2 sur substrat plan, complétée par une caractérisation physico-chimique des divers dépôts, en fonction des paramètres expérimentaux (T, P, D).

Ces deux premières publications ont, par ailleurs, fait l'objet d'une récente communication à un congrès international (37);

- le troisième (Chapitre III) relate l'approche expérimentale de l'optimisation des paramètres d'infiltration CVI (température, pression, débit total) de ZrO_2 pour diverses préformes fibreuses et microporeuses;

- le quatrième (Chapitre IV) présente les propriétés mécaniques des composites alumine-zircone et carbone-zircone;

- Enfin, le dernier article (Chapitre V) rassemble les caractéristiques thermiques ainsi que le comportement en milieu oxydant des composites alumine-zircone et carbone-zircone.

Compte tenu du mode de présentation qui a été adopté ici, un chapitre de conclusions générales, relativement développé, reprend les résultats présentés dans chaque article, tout en tentant de proposer de nouvelles ouvertures.

Propriétés	Alumine	Zircone
Densité	3,98	5,6 à 6,0
Point de fusion	2040	~ 2700
Coefficient de dilatation thermique ($°C^{-1}$)	8×10^{-6}	8×10^{-6} à 10×10^{-6}
Conductivité thermique ($w . m^{-1} . K^{-1}$)	30 - 35 (20°C) 5 - 6 (1000°C)	1,0 - 1,5 (20°C) 2 (1000°C)
Diffusivité thermique ($m^2 . s^{-1}$)	5×10^{-6} à 7×10^{-6} (20°C)	1×10^{-6} à 2×10^{-6} (20°C)
Dureté VICKERS ($kg. mm^2$)	3100	1100
Module d'Young (GPa)	380 (20°C)	≈ 200

Tableau I - Quelques propriétés physiques de l'alumine et de la zircone

REFERENCES

(1) Introduction aux matériaux composites R. Naslain, éd.) CNRS/IMC, Bordeaux, 2 (1985), Chap. 1 et 13.

(2) B. BROQUERE, B. BUTTAZZONI, et J.J. CHOURY, dans "Introduction aux matériaux composites " (R. Naslain, éd.), CNRS/IMC, Bordeaux, 2 (1985) chap. 17.

(3) P. DELHAES, A. MARCHAND, A. PACAULT, M. TRINQUECOSTE et B; CHATTERJEE, Rev. Chimie Minérale, 18 (1981) 476-485.

(4) F. CHRISTIN, Thèse de doctorat d'état, n° 641, Univ. Bordeaux 1, 1979.

(5) P. OLRY, L'Industrie Textile, n° 1150 (décembre 1984) 1107-1110.

(6) W.V. KOTLENSKY and D.H. LEEDS, Proc. 3rd Ind. Conf CVD (F.A. Glaski ed.), The Electrochem. Soc. , Princeton (1972) 574 - 589.

(7) W.V. KOTLENSKY, Proc. 16th Nat. SAMPE, Soc. Aerosp. Mater. Process. Eng., Azusa (1971) 257 - 265.

(8) J.D. THEIS, Proc. 3rd Int. Conf. CVD (F.A. Glaski, éd.), The Electrochem. Soc. Princeton (1972) 561 - 573.

(9) H.O. PIERSON et M.L. LIEBERMAN, Carbon, 13 (1975) 159 - 166.

(10) M.L. LIEBERMAN, Proc. 3rd Conf. CVD (F.A. Glaski, éd.), The Electrochem. Soc., Princeton (1972) 95 - 119.

(11) C. MALLET, Thèse de doctorat de 3° cycle, n° 1811, Univ. Bordeaux I, 1982.

(12) J.Y. ROSSIGNOL, R. NASLAIN, P. HAGENMULLER, L. HERAUD et J.J. CHOURY, Proc. Euro-CVD-III, Neuchâtel, (H.E. Hintermann, ed.), LSRH, Neuchâtel, (1980) 162 - 168.

(13) H. HANNACHE, R. NASLAIN and C. BERNARD, Journal of the Less-Common Metals, 95 (1983) 221 - 246.

(14) H. HANNACHE, J.Y. ROSSIGNOL, F. LANGLAIS, R. NASLAIN and P. HAGENMULLER, soumis à "Journal of the Less-Common Metals".

(15) E. FITZER et D. HEGEN, Angew. Chem. Int. Ed. Engl., 18, 295 (1979) 295.

(16) E. FITZER, D. HEGEN et H. STROHMEIER, Rev. Int. Hautes Temper. Refract. 77 (1980) 23.

(17) L.H. HERAUD, F. CHRISTIN, R. NASLAIN et P. HAGENMULLER, Proc. CVD-VIII (J.M. Blocher et al., éds), The Electrochem. Soc., Pennington, (1981) 782.

(18) M. DAUCHIER, P. LAMICQ, et J. MACE, Mem. Etudes Sc. Rev. Metallurgie, Sept (1982) 453.

(19) R. COLMET, R. NASLAIN, P. HAGENMULLER and C. BERNARD, J. of the Electrochem. Soc., 129, 6 (1982) 1367 - 1372.

(20) R. COLMET, I. LHERMITTE-SEBIRE and R. NASLAIN, J. of American Society (to be published).

(21) P. BOCH, G. FANTOZZI, G. ORANGE, Rev. Int. Hautes Tempér. Refract., 19 (1982) 119 - 157.

(22) MAZDIYASNI K.S., USAF Rept. ASD. T.R. 62 - 90.

(23) MAZDIYASNI K.S. et C.T. LYNCH, USAF Rept. ASD - TDR - 63 - 322 (May, 1963).

(24) MAZDIYASNI K.S. and LYNCH C.T., Special Ceramics 1964, (P. Popper, éd.), p 115 - 138.

(25) L. RALPH et HOUGH, Proc. Int. Conf. Chem. Vap. Deposition, 3rd, (1972) pp. 232 - 241.

(26) M. BALOG, M. SHIEBER, M. MICHMAN et S. PATAI, Thin Solid Films, 47 (1977) 109 - 120.

(27) L. BEN DOR, A. ELSHTEIN et J. SHAPPIR, Euro CVD-IV, Proc. of the 4 th. European Conf. on Chem. Vap. Deposition, (May 31, June 2) 1983 - Eindhoven - The Netherlands.

(28) CF. POWEL, J.H. OXLEY et J.M. BLOCHER, Vapor Deposition, (WILEY, éd.), New-York, 1966.

(29) K. BREENFLECK, E. FITZER et G. MACK, Proceedings of the 8th International Conference on Chem. Vapor. Deposition (Paris) 1981 pp. 672-683.

(30) G.L. TINGEY, J. Phys. Chem. 70 (1966) 1406 - 1412.

(31) R.W. VEST, ASTIA. DOC. AD. 255079 (May 3, 1961).

(32) G. WAHL, S. SCHLOSSER et F. SCHMADERER, Int. Conf. CVD VII, Los Angeles, (1979) 536 - 543.

(33) WHEELER V.J., MARKIN T.L. and BONES R.J., Brit, (240572) P, 2pp. Pat. n° 1275044.

(34) G. WAHL, S. SCHLOSSER and F. SCHMADERER, Proc. CVD VII (T.O. Sedwich et al., éds.), (1979) 536 - 548.

(35) K. KAMATA, S. MATSUMOTO and Y. SHIBATA, Yogyo, Kyokai-Shi 90 (1) 1982 - pp. 54 - 55.

(36) K. BRENNFLECK, E. FITZER and G. SCHOCH, Proc. Euro CVD V (J.O. Carlsson et al., éds.), (1985) 63 - 70.

(37) J. MINET, F. LANGLAIS, R. NASLAIN and C. BERNARD, Proc. Euro CVD VI (R. Porat, éd.), (1987) 68 - 75.

Chapitre I

APPROCHE THERMODYNAMIQUE

Journal of the Less-Common Metals, 119 (1986) 219 - 235

ON THE CHEMICAL VAPOUR DEPOSITION OF ZIRCONIA FROM $ZrCl_4$-H_2-CO_2-Ar GAS MIXTURES: I. - A THERMODYNAMIC APPROACH

J. MINET, F. LANGLAIS and R. NASLAIN,
Laboratoire de Chimie du Solide du CNRS, Université de Bordeaux I
351, Cours de la Libération - 33405 Talence cédex, France

C. BERNARD
Laboratoire de Thermodynamique et Physico-Chimie Métallurgiques, ENSEEG, 38401 - Saint-Martin-d'Hères (France)

ABSTRACT

Chemical vapour deposition of zirconia from the $ZrCl_4$-CO_2-H_2-Ar system is investigated, from a thermodynamic point of view, as a function of initial gas composition, total pressure and temperature, including the influence of the nature of the substrate. On an inert substrate, pure zirconia is deposited with a 100% yield when water is in excess at equilibrium and carbon-zirconia codeposition can be obtained for hydrogen-rich initial compositions. Under conditions for ZrO_2 yields close to 100%, a carbon substrate is found to be oxidized while a mullite one is thermodynamically stable.

1 - INTRODUCTION

Zirconia is a refractory material which exhibits outstanding thermal, mechanical, electrical and optical properties in connection with its crystal structure and phase transitions (1). ZrO_2 is one of the most refractory oxides with a melting point close to 2600°C. The high **ionic conductivity of CaO or Y_2O_3-stabilized zirconia** is used in various devices, such as oxygen sensors, high temperature electrochemical cells, resistance heating elements ... . Moreover, recent developments in fracture mechanics evidence a **toughening** effect in ZrO_2 - based ceramics related to the use of **partially stabilized zirconia P.S.Z.** (essentially a mixture of cubic and tetragonal phases). It has been shown that the martensitic transformation of the metastable tetragonal particles to the stable monoclinic phase is the mechanism which absorbs energy and inhibits crack propagation, thereby strengthening and toughening the material (2-5).

The marked electronic insulating character of pure zirconium dioxide and its extreme chemical inertia led TAUBER et al.,to consider ZrO_2 thin films as alternatives to SiO_2, Si_3N_4 and Al_2O_3 for **microelectronic devices** (6). Considering another application field, it would be interesting to use zirconia as a matrix (or part of a matrix) in **ceramic-ceramic composite materials** reinforced

with various carbon or alumina-based refractory fibers, in the same way than for alumina matrix composite materials (7). One of the best method for preparing both kinds of materials is chemical vapour deposition, since it needs relatively low temperatures compared with the high melting point of these materials.

Several chemical reactions involving a gaseous precursor can result in zirconia deposition. Organometallics (e.g. zirconium alcoholates, carboxylates and phenolates) have been used as source species, their decomposition occurring at low temperatures (473-773 K) (8-12). ZrO_2 has also been deposited by hydrolysis of zirconium halides (usually chlorides) directly with H_2O vapour or with H_2-O_2 or H_2-CO_2 (13) gaseous mixtures. Another ZrO_2 deposition process is to oxidize a zirconium halide with O_2 or CO_2 (14).In most cases, deposition reactions are so irreversible that homogeneous nucleation in the gas phase occurs in considerable amount leading to unwanted soot formation and obstruction of the tubings. **The $ZrCl_4$-CO_2-H_2 system** seems to be the most convenient one is as much as the overall process kinetics is controlled by the water formation (13).

A detailed thermodynamic study of such system has not been carried out to date. The aim of the present contribution is to study the influence of the main CVD parameters (initial gaseous mixture, temperature, pressure) on the gas phase and solid deposit composition, assuming that the heterogeneous equilibrium is achieved. Two cases have been considered: (i) the deposition on a chemically inert substrate and (ii) the deposition on a reactive substrate. In the second case, carbon and mullite ($3Al_2O_3$, $2SiO_2$) substrates have been chosen in

order to try to understand the initial steps of the deposition process on the corresponding fibers (that could be used in zirconia matrix composite materials).

The thermodynamic computations have been performed, as usual, based on the minimization of the overall Gibbs free energy of the system. Ar is introduced in the calculations only as diluent gas.

2 - ZIRCONIA CVD FROM $ZrCl_4$-H_2-CO_2-Ar SYSTEM ON A CHEMICALLY INERT SUBSTRATE

Zirconia deposition is performed according to the generally accepted following reactions (13):

$$2H_{2(g)} + 2CO_{2(g)} \rightleftharpoons 2H_2O_{(g)} + 2CO_{(g)} \quad [1]$$

$$ZrCl_{4(g)} + 2H_2O_{(g)} \rightleftharpoons ZrO_{2(s)} + 4HCl_{(g)} \quad [2]$$

$$ZrCl_{4(g)} + 2H_{2(g)} + 2CO_{2(g)} \rightleftharpoons ZrO_{2(s)} + 4HCl_{(g)} + 2CO_{(g)} \quad [3]$$

The water formation from H_2-CO_2 gaseous mixture is favoured by increasing temperature (T > 900 K), thereby permitting a good control of zirconium chloride hydrolysis by monitoring the substrate temperature (15).

For the thermodynamic computations, a set of 21 chemical species are taken into account (table 1). The corresponding data, i.e. enthalpies of formation and entropies, are taken from the Scientific Group Thermodata Europe data bank. The experimental parameters introduced in the calculations are, on the one hand, composition parameters: $\alpha = [H_2]_{in} / [CO_2]_{in}$ ratio between the hydrogen and carbon dioxide mole fractions ($10^{-2} \leq \alpha \leq 10^3$) and the mole fraction of $ZrCl_4$ ($10^{-3} \leq [ZrCl_4]_{in} \leq 1$), in the initial gas mixture; on the other hand, total pressure ($0,01 \leq P \leq 0,5$ atm.) and temperature ($1000 < T < 1400$ K) are considered.

The computation results show that only the following species are present in significant concentrations at equilibrium: $ZrCl_4$, HCl, H_2, CO_2, H_2O, CO for the gas phase and ZrO_2 and carbon for the deposit. The thermodynamic yields of these various species are calculated as defined in table 2.

2.1. Influence of the ratio α on equilibrium composition

On figure 1, the various thermodynamic yields are drawn as a function of α for T = 1200 K, P = 0.05 atm. and $[ZrCl_4]_{in} = 5.10^{-3}$. Three α ranges can be seen, limited by two critical values α_i and α_s.

- **For initial gaseous mixtures with a lack of H_2** ($\alpha < \alpha_i$) the concentration of H_2O resulting from reaction [1] is limited by H_2 concentration. Hydrolysis reaction (2), which is highly irreversible ($\Delta G°_{1200\ K} = -50.5$ kcal. mole^{-1}), consumes all the H_2O, the resulting gas phase contains unreacted $ZrCl_4$, so ZrO_2

[Ar]	<ZrC>	<ZrO_2>
[H_2O]	[CH_4]	[$ZrCl_2$]
[Cl]	[Cl_2]	[ZrCl]
[$ZrCl_3$]	[$ZrCl_4$]	[O_2]
[H]	[H_2]	[HCl]
<C>	[CO]	[CO_2]
[C_2H_2]	[C_2H_4]	[C_2H_6]

Table I - Chemical species introduced in the thermodynamic computations (chemically inert substrate)

$\eta_{ZrCl_4}(\%) = 100 \cdot \frac{[ZrCl_4]_{eq.}}{[ZrCl_4]_{in.}}$	$\eta_{HCl}(\%) = 100 \cdot \frac{[HCl]_{eq.}}{4[ZrCl_4]_{in.}}$
$\eta_{H_2}(\%) = 100 \cdot \frac{[H_2]_{eq.}}{[H_2]_{in.}}$	$\eta_{CO_2}(\%) = 100 \cdot \frac{[CO_2]_{eq.}}{[CO_2]_{in.}}$
$\eta_{H_2O}(\%) = 100 \cdot \frac{[H_2O]_{eq.}}{[H_2]_{in.}}$	$\eta_{CO}(\%) = 100 \cdot \frac{[CO]_{eq.}}{[CO_2]_{eq.}}$
$\eta_{<ZrO_2>}(\%) = 100 \cdot \frac{<ZrO_2>_{eq.}}{[ZrCl_4]_{in.}}$	$\eta_{<C>}(\%) = 100 \cdot \frac{<C>_{eq.}}{[CO_2]_{in.}}$

Table 2 - Thermodynamic yields η of the main chemical species (chemically inert substrate)

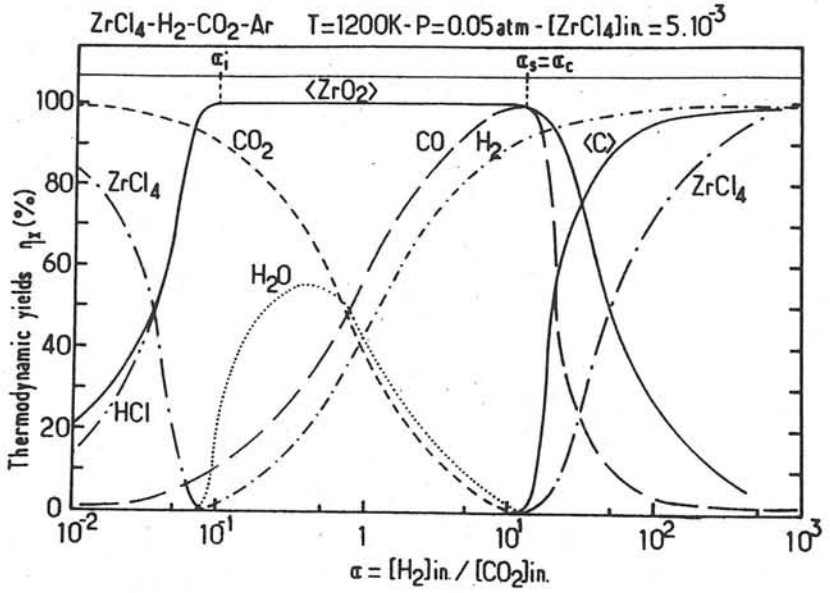

Fig. 1 - Influence of the ratio α on the various thermodynamic yields in the CVD of zirconia on a chemically inert substrate (T = 1200 K, P = 0.05 atm, $[ZrCl_4]_{in.} = 5 \times 10^{-3}$)

yield is less than 100%. When the ratio α is increased, H_2O concentration increases, consumption of $ZrCl_4$ becomes more and more complete and zirconia yield rises (up to 100% for $\alpha = \alpha_i$).

- **For initial gaseous mixture with** $\alpha_i < \alpha < \alpha_s$, i.e. a composition not too far from stoechiometry, water is formed in sufficient amount to react with the wole of the zirconium chloride, leading to a ZrO_2 yield of 100%, an excess of H_2O and a $ZrCl_4$ yield of 0%.

- **For initial gaseous mixtures with an excess of** H_2 ($\alpha > \alpha_s$), water formation reaction is limited by CO_2 concentration resulting in a progressive decrease of ZrO_2 yield as α ratio is increased. Here, besides the hydrolysis reaction which gives zirconia deposit, carbon monoxide formed from reaction [1] reacts with part of the excess of hydrogen leading to H_2O and solid carbon according to the reaction:

$$CO_{(g)} + H_{2(g)} \rightleftharpoons C_{(s)} + H_2O_{(g)} \qquad [4]$$

Combining reactions [1], [2] and [4] results in the following overall reaction, which gives a mixture of zirconia and free carbon (ZrO_2/C codeposit)

$$ZrCl_{4\,(g)} + 2H_{2\,(g)} + CO_{2\,(g)} \rightleftharpoons ZrO_{2\,(s)} + C_{(s)} + 4HCl_{(g)} \qquad [5]$$

Reaction [4], which is endothermic ($\Delta G°_{1200\ K} = 17{,}5$ kcal. mole^{-1}) is shifted to the right water formation only if ZrO_2 yield is less than 100% with a lack of water ($\eta\,(H_2O) = 0\%$).

2.2. Influence of $ZrCl_4$ concentration on equilibrium composition

Figure 2 shows the variation of the thermodynamic yields previously defined as a function of $ZrCl_4$ initial mole fraction for various α ratio values, at a temperature of 1200 K and a pressure of 0.05 atm.

The hydrolysis reaction of $ZrCl_4$ is complete (η (ZrO_2) = 100%) only if $[ZrCl_4]_{in}$ is lower than a critical value, i.e. when water is in excess, owing to high concentrations of CO_2 (α = 0.166), H_2 (α = 13) or both CO_2 and H_2 (α = 1). This critical value of $\eta\ [ZrCl_4]_{in}$ seems to rise to a maximum for $\alpha \approx 1$. Above this critical value, η (ZrO_2) decreases down to 0% as $[ZrCl_4]_{in}$ increases. For α =13, this η (ZrO_2) decrease occurs simultaneously with the rise of free carbon yield, which permits an initial composition range favourable to a ZrO_2/C codeposit.

2.3. Zirconia and carbon isoyield curves

In order to define the experimental conditions which favour, from a thermodynamic point of view, a pure ZrO_2 deposition or a ZrO_2/C codeposition, it is convenient to draw zirconia and carbon isoyield curves, as shown in figures 3 and 4 for T = 1200 K and P = 0.05 atm.. The first plot (Fig. 3), in ($[ZrCl_4]_{in}$, α) coordinates, evidences clearly the $[ZrCl_4]_{in}$ upper limit for obtaining a ZrO_2 yield of 100% (ZrO_2 isoyields are in dashed lines) the maximum of that limit occuring for α = 1. ZrO_2/C codeposit conditions, represented by the hatched area of the drawing, are defined by high values of both $[ZrCl_4]_{in}$ and α ratio.

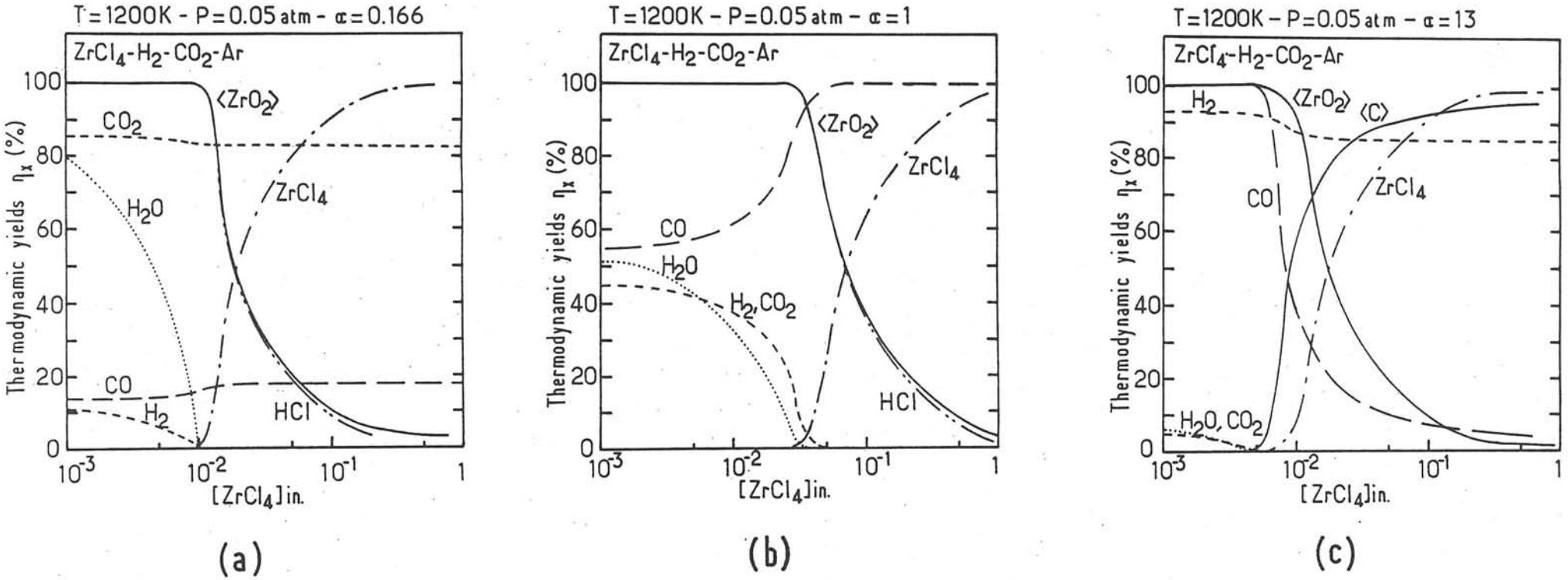

Fig. 2 - Influence of $ZrCl_4$ initial mole fraction on the thermodynamic yields in the CVD of zirconia on a chemically inert substrate: (a) $\alpha = 0.166$; (b) $\alpha = 1$; (c) $\alpha = 13$ ($T = 1200$ K, $P = 0.05$ atm.)

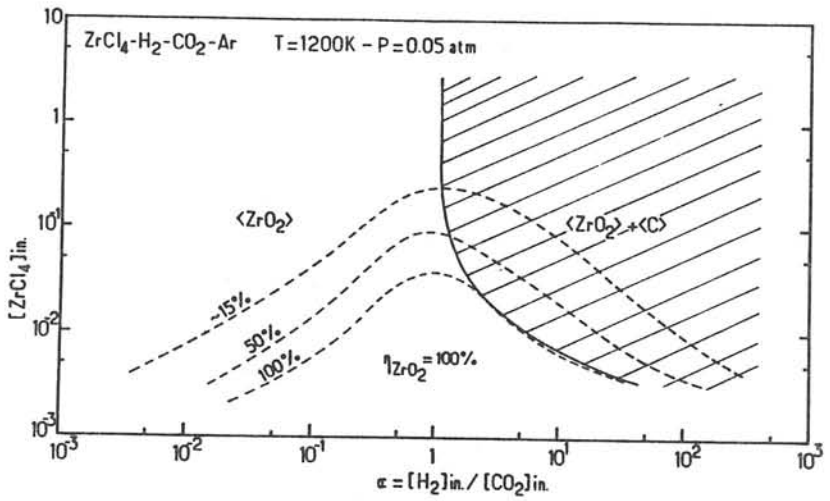

Fig. 3 - Zirconia and carbon isoyield curves in $([ZrCl_4]_{in.}, \alpha)$ coordinates (chemically inert substrate; T = 1200 K; P = 0.05 atm.)

The plots in figure 4, in ($[H_2]_{in}$, $[CO_2]_{in}$) coordinates, give more details about the deposition diagram. In order to get a total hydrolysis of $ZrCl_4$, i.e. a ZrO_2 yield of 100%, the initial gaseous mixture must contain at least twice as much H_2 and CO_2 as $ZrCl_4$, which is in good agreement with the stoechiometry of reaction [3]. A pure ZrO_2 deposition domain with $\eta(ZrO_2) < 100\%$ can also be deduced and defined approximately by $\alpha < 1$ and $[H_2]_{in} < 2\,[ZrCl_4]_{in}$: $\eta\,(ZrO_2)$ decreases with decreasing $[\,H_2\,]_{in}$; water formation is limited by hydrogen molar fraction, which limits hydrolysis of $ZrCl_4$. Concerning the initial composition range which leads to a ZrO_2 / C codeposit, it is nearly defined (hatched area) by $\alpha > 1$ and $[CO_2]_{in} < 2\,[ZrCl_4]_{in}$: if the initial amount of zirconium chloride increases, the codeposition limit becomes closer to $\alpha = 1$.

2.4. Influence of temperature and pressure on the deposition diagram

The shift of ZrO_2 / C codeposition limit as a function of temperature and total pressure is investigated in figures 5 and 6 respectively.

For a $ZrCl_4$ initial molar fraction of 2.10^{-2} and a total pressure of 0.05 atm., the codeposition area is shifted towards the high values of α (i.e. gaseous mixtures with an excess of hydrogen) as temperature increases from 1000 K to 1400 K (Fig. 5a). For a given initial composition, a temperature rise is unfavourable to deposition process and particularly to occurrence of free carbon. This feature is also seen in the plots in figure 5b (for an initial gaseous mixture defined as point 1 in figure 5a), except in the low temperature range ($T < 1150K$) where a slight increase of η_c is observed.

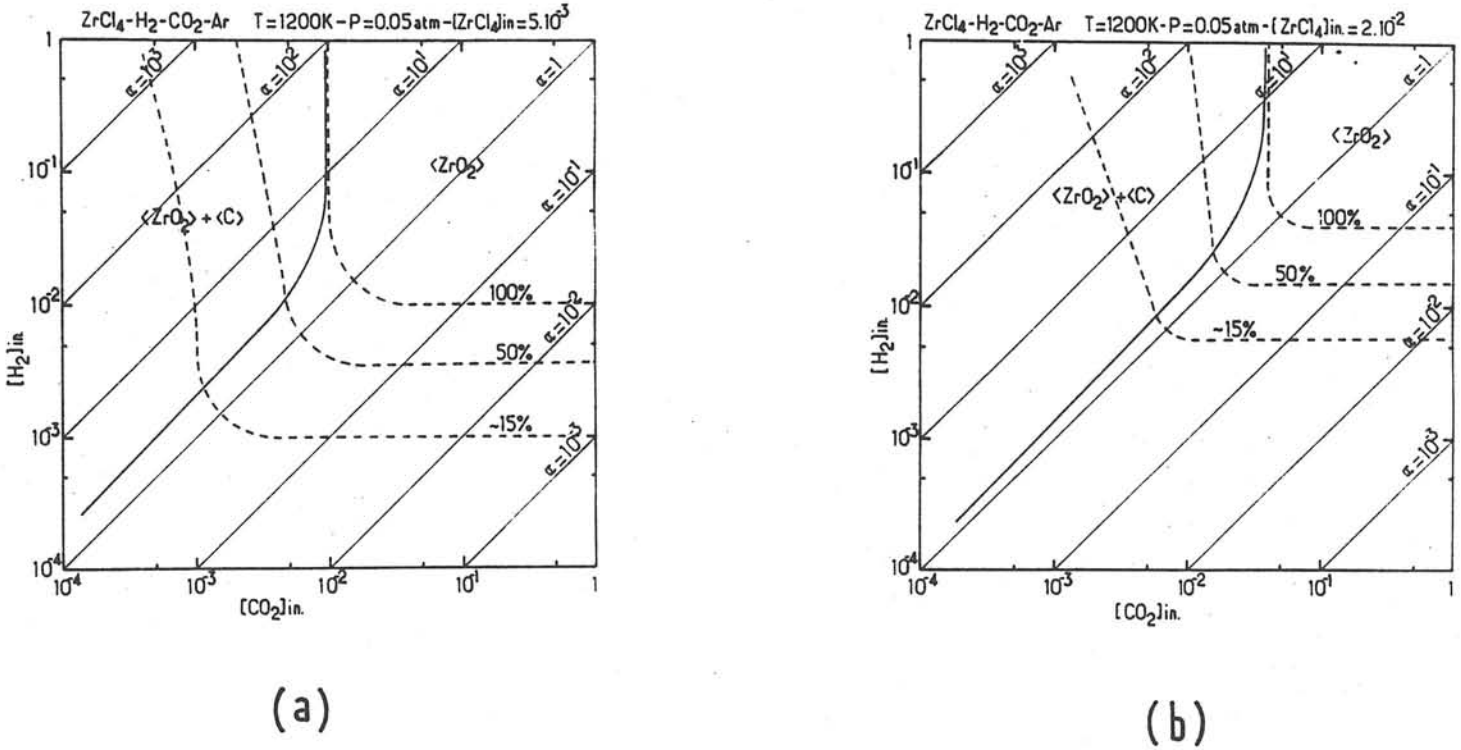

Fig. 4 - Zirconia and carbon isoyield curves in ($[H_2]_{in.}$, $[CO_2]_{in.}$) coordinates and (a) $[ZrCl_4]_{in.} = 5 \times 10^{-3}$ and (b) $[ZrCl_4]_{in.} = 2 \times 10^{-2}$ (chemically inert substrate; T = 1200 K; P = 0.05 atm).

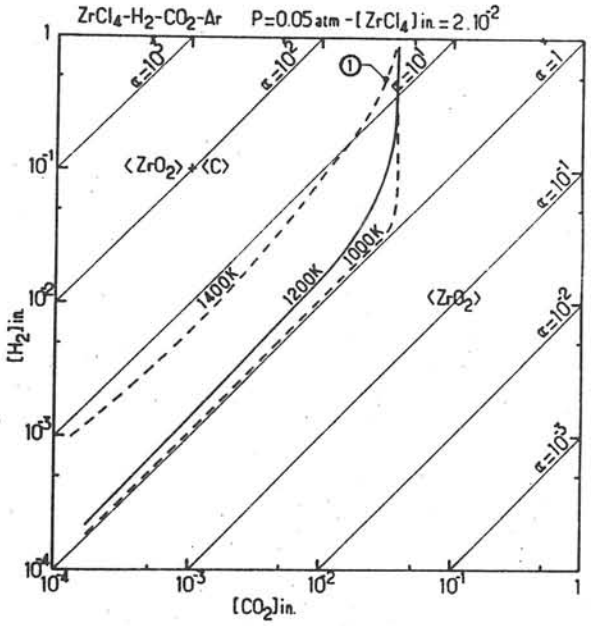

(a)

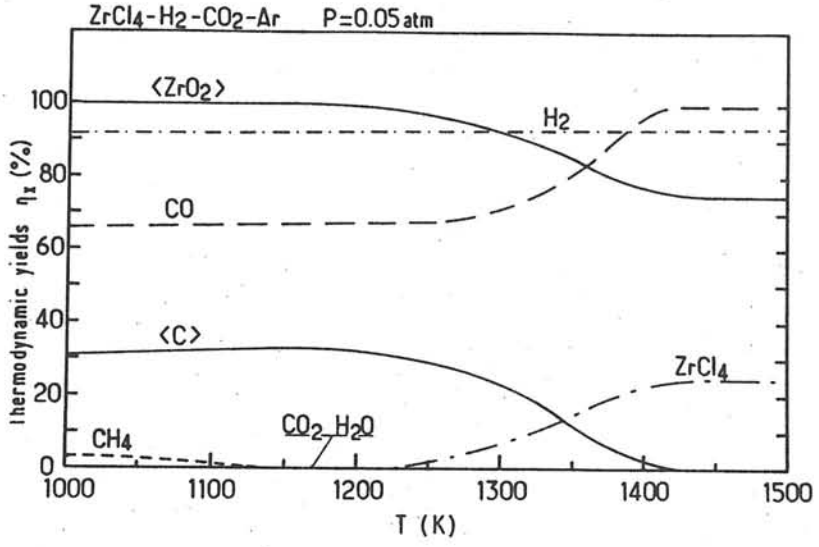

(b)

Fig. 5 - Influence of temperature on ZrO_2-C codeposition (chemically inert substrate): (a) carbon isoyields in ($[H_2]_{in.}$,$[CO_2]_{in.}$) coordinates; (b) zirconia and carbon thermodynamic yields for initial gas phase composition defined by point 1: $[ZrCl_4]_{in.} = 2 \times 10^{-2}$; $[Ar]_{in.} = 0.45$; $[H_2]_{in.} = 0.5$; $[CO_2]_{in.} = 3 \times 10^{-2}$ (P = 0.05 atm.)

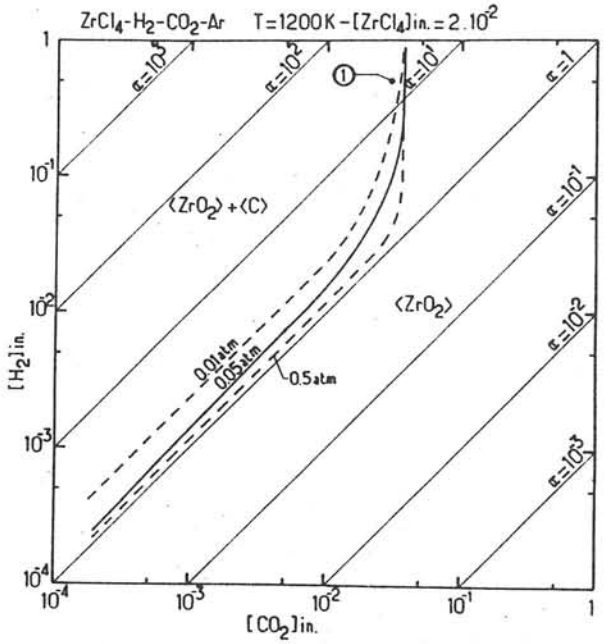

(a)

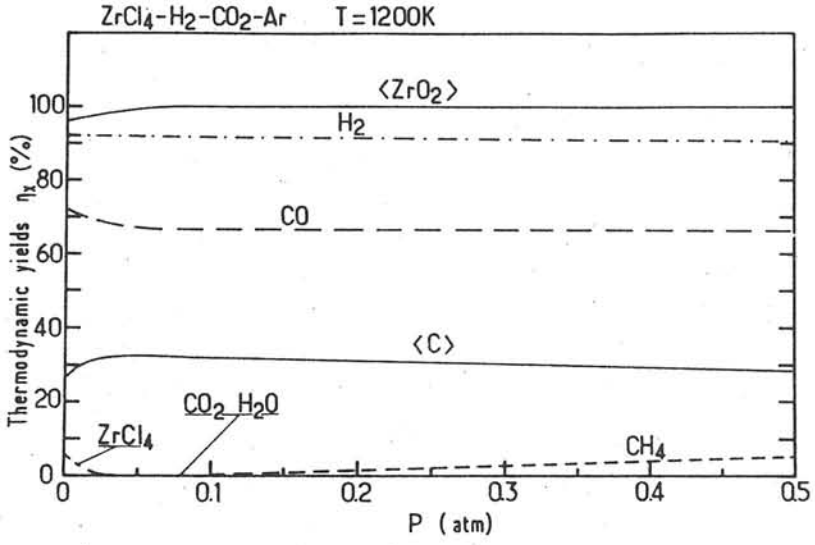

(b)

Fig. 6 - Influence of pressure on ZrO_2-C codeposition (chemically inert substrate): (a) carbon isoyields in $([H_2]_{in.}, [CO_2]_{in.})$ coordinates; (b) zirconia and carbon thermodynamic yields for initial gas phase composition defined by point 1: $[CO_2]_{in.} = 3 \times 10^{-2}$ (T = 1200 K)

As total pressure increases from 0.01 to 0.5 atm. for T = 1200 K and $[ZrCl_4]_{in} = 2.10^{-2}$, the ZrO_2 / C codeposition limit drawn in ($[H_2]_{in}$, $[CO_2]_{in}$) coordinates (Fig. 6a), is shifted towards the $\alpha = 1$ composition line, but that parameter has not an actual great influence. This behaviour can be related to the slight increase of carbon yield with total pressure between 0 and 0.05 atm. (Fig. 6b) for an initial composition given by point 1 in figure 6a.

It turns out from this thermodynamic approach that conditions for ZrO_2 / C codeposition can be found in the $ZrCl_4$-CO_2-H_2-Ar system, which are similar to those already reported by I. Lhermitte-Sebire et al. in the case of alumina CVD: i.e. an excess of hydrogen ($\alpha > 1$), an excess of zirconium chloride ($[ZrCl_4]_i > 1/2\ [CO_2]_{in}$) and a low enough temperature (18). The various chemical reactions taken into account in the CVD process have been derived on the basis of initial and equilibrium chemical compositions of the system. If the high reactivity of the gaseous mixture is considered, it seems interesting to include in thermodynamic calculations a reactive substrate such as carbon or mullite which are commonly used as fibers in ceramic matrix composite materials.

3 - ZIRCONIA CVD FROM ZrCl4 - H2 - CO2 - Ar SYSTEM ON REACTIVE SUBSTRATES

The role played by a given substrate can be taken into account in the thermodynamic approach by introducing an excess of the substrate material in the initial composition, as previously carried out for other CVD systems (16 - 18).

3.1. Reactive carbon substrate

The chemical species considered here are the same than for a chemically inert substrate. The thermdoynamic yields are defined by the same expressions, except for the carbon-based species, such as CO_2, CO and C (table 3). The computations are performed for a temperature of 1200 K, a total pressure of 0.05 atm., and various initial compositions. Figure 7 shows the variations of the thermodynamic yields as a function of α for an initial $ZrCl_4$ molar fraction of 5.10^{-3}. Zirconia and $ZrCl_4$ yields are very similar to those obtained with a chemically inert substrate. On the contrary, H_2O or CO_2 are not present at equilibrium, whatever the initial composition. H_2 yield curve is above the corresponding one in the case of an inert substrate. With regard to the carbon-based species, the yield variations are not significant over the wole α range, owing to the large excess of carbon introduced in the calculation. So it seems to be convenient to express the concentrations of CO and CO_2 species and variations of free carbon between equilibrium and initial state, with respect to $[CO_2]_{in} + \langle C_{eq} \rangle - \langle C \rangle_{in}$ according to the definition given in table 4. These rates τ are

$\eta_{CO_2}(\%) = 100 \cdot \dfrac{[CO_2]_{eq.}}{[CO_2]_{in.} + \langle C \rangle_{in}}$
$\eta_{CO}(\%) = 100 \cdot \dfrac{[CO]_{eq.}}{[CO_2]_{in.} + \langle C \rangle_{in.}}$
$\eta_{\langle C \rangle}(\%) = 100 \cdot \dfrac{\langle C \rangle_{eq.}}{[CO_2]_{in.} + \langle C \rangle_{in.}}$

Table 3 - Thermodynamic yields η of the carbon-based species (reactive carbon substrate)

$\tau_{CO_2}(\%) = 100 \cdot \dfrac{[CO_2]_{eq.}}{[CO_2]_{in.} + \lvert \langle C \rangle_{in.} - \langle C \rangle_{eq.} \rvert}$
$\tau_{CO}(\%) = 100 \cdot \dfrac{[CO]_{eq.}}{[CO_2]_{in.} + \lvert \langle C \rangle_{in.} - \langle C \rangle_{eq.} \rvert}$
$\tau_{\langle C \rangle_{eq.} - \langle C \rangle_{in.}}(\%) = 100 \cdot \dfrac{\langle C \rangle_{eq.} - \langle C \rangle_{in.}}{[CO_2]_{in.} + \lvert \langle C \rangle_{in.} - \langle C \rangle_{eq.} \rvert}$

Table 4 - Thermodynamic rates τ of the carbon-based species (reactive carbon substrate)

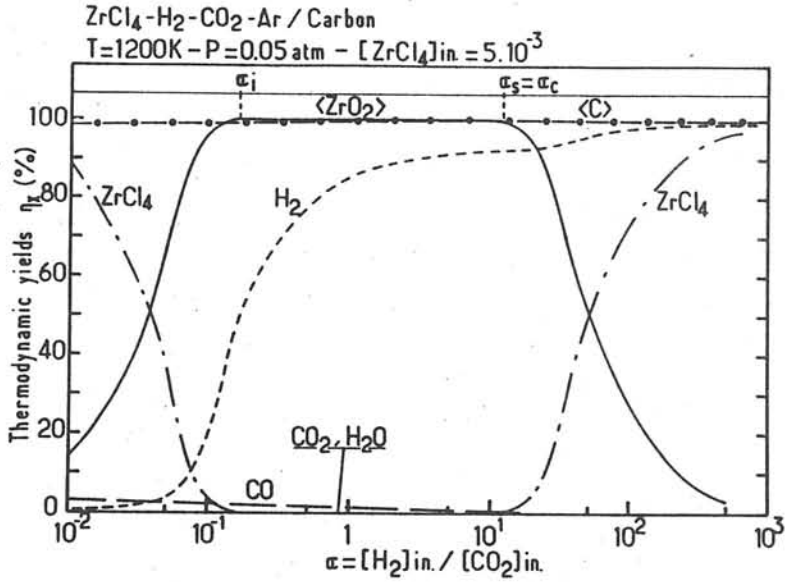

Fig. 7 - CVD of zirconia on a reactive carbon substrate: influence of ratio α on the thermodynamic yields (T = 1200 K, P = 0.05 atm.)

plotted in figure 8 as a function of $\alpha = [H_2]_{in} / [CO_2]_{in}$ ratio. The free carbon curve evidences for $\alpha \sim 10$ a transition from a substrate consumption process to a carbon deposition one. ZrO_2 deposition is evidently obtained after reaction [3], but other reactions simultaneously occur.

- **For** $\alpha < \alpha_i$ (ZrO_2 yield less than 100%) CO_2 which is still in excess is totally reacted; it oxydises the carbon substrate, giving CO species according to the reaction:

$$CO_{2(g)} + C_{(s)} \rightleftharpoons 2CO_{(g)} \qquad [6]$$

Another reaction which consumes carbon must be considered here:

$$H_2O_{(g)} + C_{(s)} \rightleftharpoons CO_{(g)} + H_{2(g)} \qquad [7]$$

This oxidization is a concurrent reaction of the $ZrCl_4$ hydrolysis, which slightly decreases zirconia deposition yield and increases H_2 yield with respect to the case of an inert substrate.

- **For** $\alpha_i < \alpha < \alpha_s$ (ZrO_2 yield of 100%), the increase of H_2 and decrease of CO_2 initial concentrations with rising α, involve a lower and lower etching of carbon substrate, the more so as the reverse of reaction [7] is more and more favoured. For T = 1200 K, P = 0.05 atm., $[ZrCl_4]_{in.} = 5.10^{-3}$ and $\alpha = 1$, the etched carbon mass is very close to deposited ZrO_2 mass. This result must not be neglected, particularly if zirconia deposition is carried out on small diameter

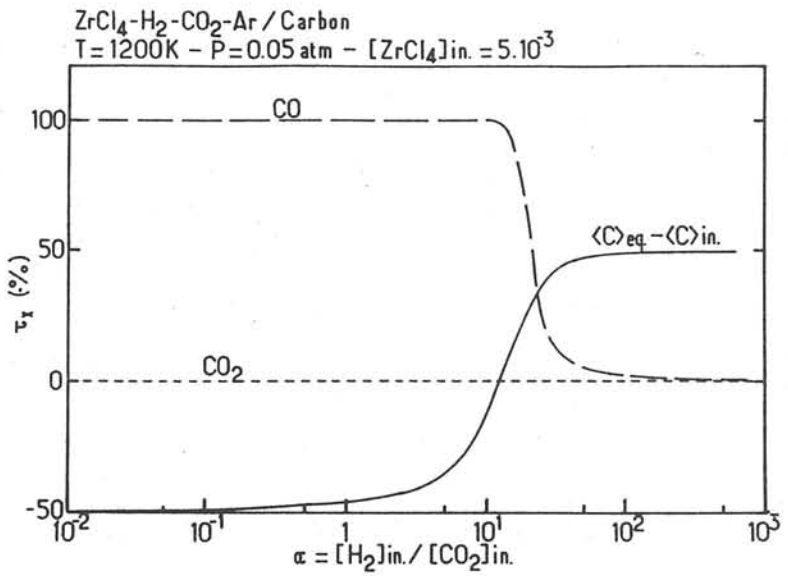

Fig. 8 - CVD of zirconia on a reactive carbon substrate: infuence of ratio α on the τ rates of the carbon-based species (T = 1200 K, P = 0.05 atm., $[ZrCl_4]_{in.} = 5 \times 10^{-3}$)

carbon fibers which could be attacked with a possible strength alteration as long as their surface is not totally covered by ZrO_2.

- **For** $\alpha > \alpha_s$ (excess of initial H_2), reaction [6] does not occur and a deposition of free carbon is possible according to reaction [4] which is the reverse of reaction [7]:

$$CO_{(g)} + H_{2(g)} \rightleftharpoons C_{(s)} + H_2O_{(g)} \qquad [4]$$

Under the previously defined conditions, the amount of carbon deposited for $\alpha = 30$ is ten times lower than the etched carbon mass for $\alpha = 2$.

Figures 9, 10 and 11 shows for various α values the influence of $ZrCl_4$ initial concentration on the various thermodynamic yields and the τ rates defined in table 4. A $[ZrCl_4]_{in}$ increase favours hydrolysis reaction [2] against oxidation reaction [7], which involves a less significant etching of carbon substrate. For $\alpha = 13$, the transition from substrate consumption to carbon deposition process is clearly visible at $[ZrCl_4]_{in} = 5.10^{-3}$ (for T = 1200 K and P = 0.05 atm.).

The main difference between an inert and a reactive carbon substrate is that under conditions of zirconia deposition with a good yield ($\alpha \sim 1$; low $ZrCl_4$ initial concentration), the latter is thermodynamically etched by the oxidising vapour phase. In both cases, for high α values and high $ZrCl_4$ initial concentrations, a C/ZrO_2 codeposit can be performed.

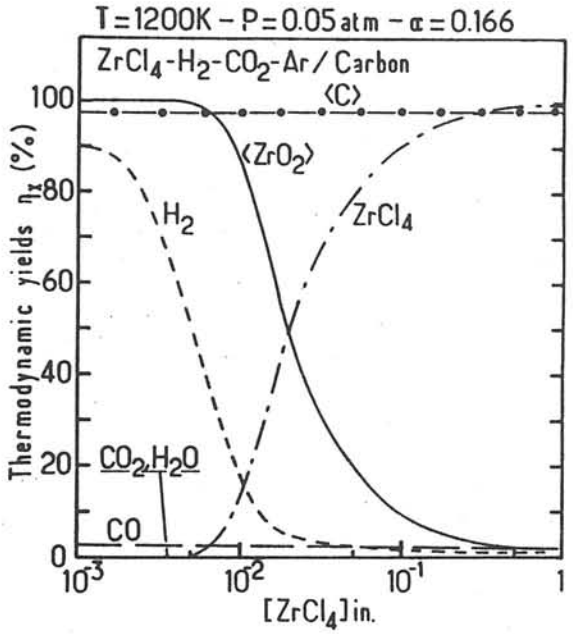

(a)

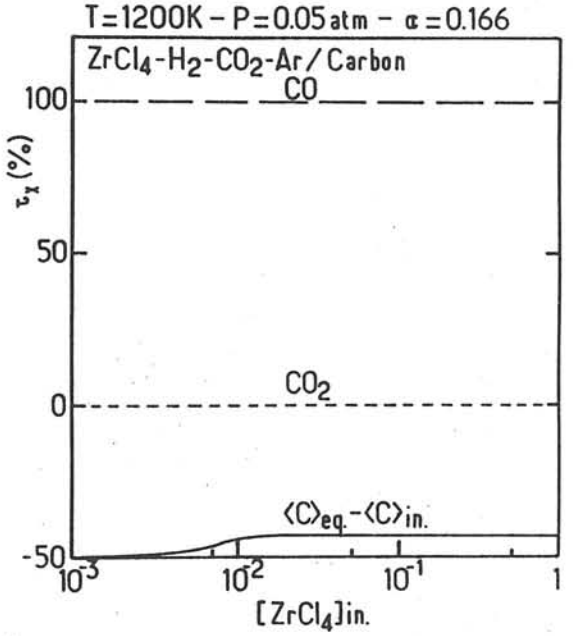

(b)

Fig. 9 - CVD of zirconia on a reactive carbon substrate: influence of initial $ZrCl_4$ mole fraction (a) the thermodynamic yields η and (b) rates τ, for $\alpha = 0.166$ (T = 1200 K, P = 0.005 atm.)

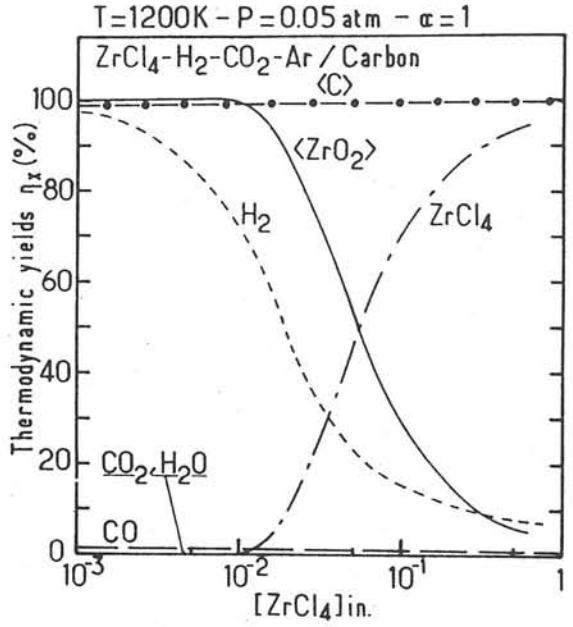

(a)

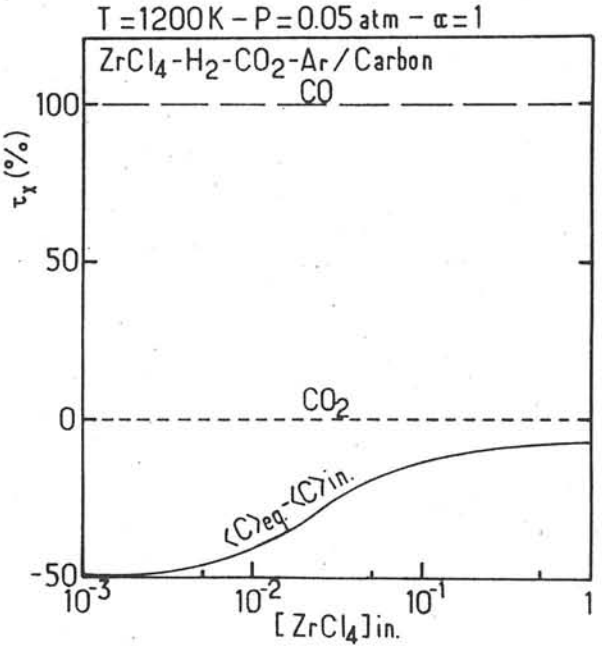

(b)

Fig. 10 - CVD of zirconia on a reactive carbon substrate: influence of initial $ZrCl_4$ mole fraction on (a) the thermodynamic yields η and (b) rates τ, for $\alpha = 1$ (T = 1200 K, P = 0.05 atm.)

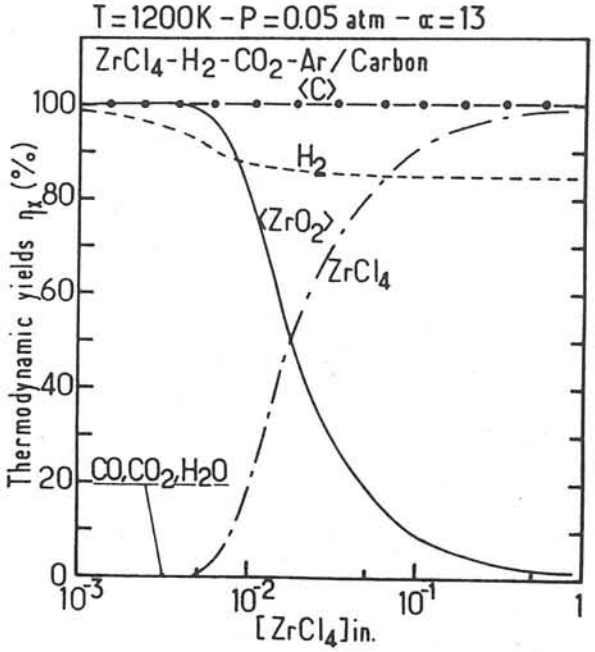

(a)

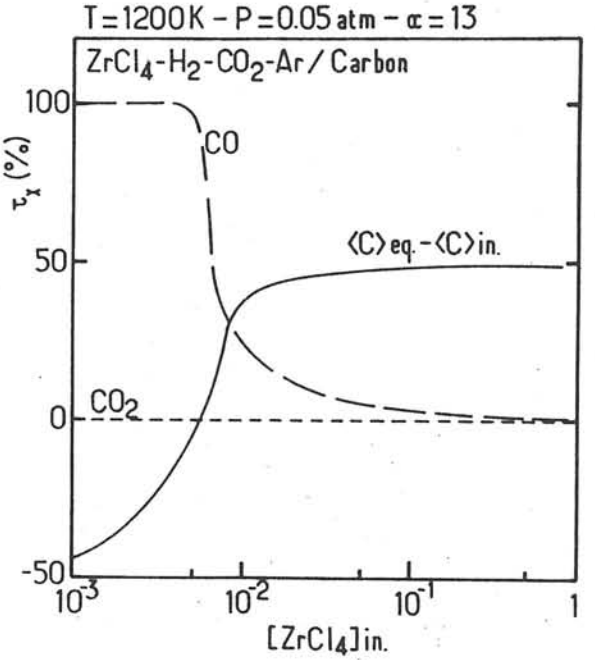

(b)

Fig. 11 - CVD of zirconia on a reactive carbon substrate: influence of initial $ZrCl_4$ mole fraction on (a) the thermodynamic yields η and (b) rates τ, for $\alpha = 13$ (T = 1200 K, P = 0.05 atm.)

3.2. Reactive mullite substrate (Zr-Cl-O-H-C-Al-Si-Ar system)

As mentioned above, it could be interesting to deposit zirconia on alumina-based substrates, such as mullite whose formula is $3Al_2O_3$, $2SiO_2$ (or $Al_6O_{13}Si_2$). Here, 18 new species, including for instance silicon carbide, zirconium silicate, aluminium and silicon chlorides, are introduced in the calculations (table 5), leading to a total of 39 gaseous or solid species effectively retained (aluminum and zirconium oxicarbides are not taken into account, owing to the low probability of their occurence). Thermodynamic yields are defined as usual and definition of the main new species yields are given in table 6.

Figures 12 and 13 show the variations of the thermodynamic yields as a function of ratio α for $[ZrCl_4]_{in} = 5.10^{-3}$ and of $[ZrCl_4]_{in}$ for α ratio values of 0.166, 1 and 13 respectively (with T = 1200 K, P = 0.05 atm. in all cases). The reactive mullite substrate seems to have a negligible influence on the equilibrium composition if $\alpha_i < \alpha < \alpha_s$, zirconia yield remaining very close to 100% with no etching of the mullite substrate. On the contrary, for $\alpha < \alpha_i$, substrate etching is indicated by the occurrence of new species at equilibrium, such as $AlCl_3$ and $ZrSiO_4$. Under these conditions, three reactions should be taken into account, which are given in table 7 with their standard free enthalpics and equilibrium constants. Reaction [8] is not favourable because of the high positive free enthalpy; reaction [9] is thermodynamically favourable, but it is a solid state reaction kinetically slow. The following reaction:

$$9ZrCl_{4\,(g)} + 2Al_6O_{13}Si2_{\,(s)} \rightleftharpoons 5ZrO_{2\,(s)} + 4ZrSiO_{4\,(s)} + 12AlCl_{3\,(g)} \qquad [10]$$

$<Al_2O_3(\alpha)>$	$[AlCl]$	$[AlCl_2]$	$[AlCl_3]$	$[Al_2Cl_6]$	$[AlClO]$	$<ZrC>$
$<Al_4C_3>$	$[SiO]$	$<SiO_2>$	$<ZrSiO_4>$	$[SiCl]$	$[SiCl_3]$	
$[SiCl_4]$	$<SiC(\alpha)>$	$<Al_6O_{13}Si_2>$	$<ZrSi_2>$	$[SiH_2Cl_2]$	$[SiH_3Cl]$	

Table 5 - New chemical species introduced in the thermodynamic computations in the case of a reactive mullite substrate

$\eta_{AlCl_3}(\%) = 100 \cdot \frac{3\,[AlCl_3]_{eq.}}{4\,[ZrCl_4]_{in.}}$	$\eta_{SiCl_4}(\%) = 100 \cdot \frac{[SiCl_4]_{eq.}}{[ZrCl_4]_{in.}}$
$\eta_{<SiC>}(\%) = 100 \cdot \frac{<SiC>_{eq.}}{\lvert CO_2 \rvert_{in.}}$	$\eta_{<ZrSiO_4>}(\%) = 100 \cdot \frac{<ZrSiO_4>_{eq.}}{[ZrCl_4]_{in.}}$

Table 6 - Thermodynamic yields of the main new species in the case of reactive mullite substrate

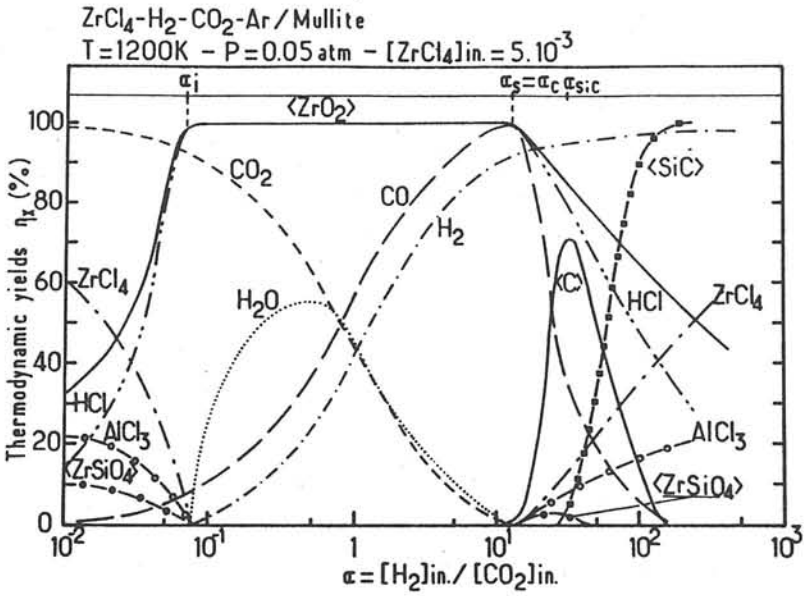

Fig. 12 - CVD of zirconia on a reactive mullite substrate: influence of ratio α on the thermodynamic yields (T = 1200 K, P = 0.05 atm., $[ZrCl_4]_{in.} = 5 \times 10^{-3}$)

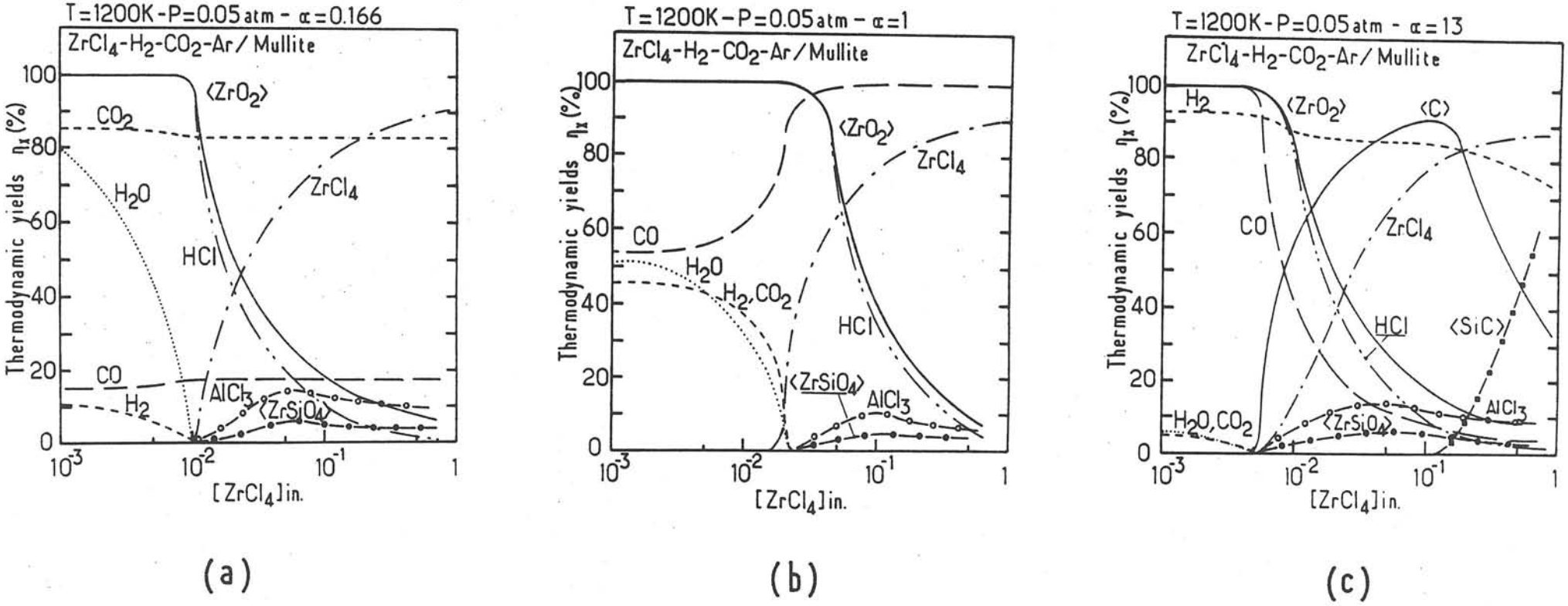

Fig. 13 - CVD of zirconia on a reactive mulite substrate: influence of initial $ZrCl_4$ mole fraction on the thermodynamic yields for (a) $\alpha = 0.66$, (b) $\alpha = 1$ and (c) $\alpha = 13$ ($T = 1200$ K, $P = 0.05$ atm.)

$26\ HCl + Al_6O_{13}Si_2 \rightleftharpoons 6\ AlCl_3 + 2\ SiCl_4 + 13\ H_2O$	$\Delta G°_{1200\ K} = 354\ Kcal\ mole^{-1}$	[8]
$2\ ZrO_2 + Al_6O_{13}Si_2 \rightleftharpoons 2\ ZrSiO_4 + 3\ Al_2O_3$	$\Delta G°_{1200\ K} = 1 kcal\ mole^{-1}$	[9]
$9 ZrCl_4 + 2Al_6O_{13}Si_2 \rightleftharpoons 5\ ZrO_2 + 4\ ZrSiO_4 + 12\ AlCl_3$	$\Delta G°_{1200\ K} = 82 kcal\ mole^{-1}$	[10]

Table 7 - Possible mullite etching reactions

seems to be the most convenient one to represent the mullite etching process. It explains the enhancement of ZrO_2 yield and consumption of part of $ZrCl_4$ excess with respect to the case of inert substrate.

For a values higher than α_s, two composition ranges must be considered, with a boundary at $\alpha = \alpha_{SiC}$ associated with the occurrence of solid SiC at equilibrium. If $\alpha_s < \alpha < \alpha_{SiC}$, $ZrCl_4$ excess involves the same mullite etching reaction [10] and H_2 excess reacts with CO obtained from water formation reaction:

$$H_2 + CO \rightleftharpoons C + H_2O \qquad [4]$$

which shows C/ZrO_2 codeposition as previously reported for an inert substrate. If $\alpha > \alpha_{SiC}$, the occurrence of SiC, Al_2O_3 and $AlCl_3$ species suggests that the following solid state reaction:

$$6C_{(s)} + Al_6O_{13}Si_{2\,(s)} \rightleftharpoons 2SiC_{(s)} + 4CO_{(g)} + 3Al_2O_{3\,(s)}$$

and

$$3C_{(s)} + ZrSiO_{4\,(s)} \rightleftharpoons SiC_{(s)} + ZrO_{2\,(s)} + 2CO_{(g)}$$

must be taken into account.

In order to give more details about the mullite etching, the species originating in this substrate material are represented in figure 14 as a function of α using other rate definitions. These rates refer to the total etched mullite amount as reported in table 8.

This investigation shows that a mullite substrate can be etched, but under conditions which do not give a high zirconia yield, which is in contrast with the case for a carbon substrate.

CONCLUSIONS

This contribution, based on a thermodynamic approach, gives a detailed analysis of the conditions of formation of zirconia from the $ZrCl_4$-CO_2-H_2-Ar system including the influence of the substrate nature.

If deposition is performed on an inert substrate, a pure ZrO_2 deposit is obtained with a 100% yield as long as water is present at equilibrium (i.e.for $\alpha = [H_2]_{in} / [CO_2]_{in}$ ratio close to 1) and zirconium chloride initial amount is low enough (i.e. $[ZrCl_4]_{in} < 1/2\ [CO_2]_{in}$). Under other conditions, the ZrO_2 yield is lower and when $\alpha >> 1$, a ZrO_2 / C codeposition can be obtained. These results are very similar to those obtained previously by Colmet et al. as well as by I. Lhermitte-Sebire et al. in the case of alumina CVD (7,18).

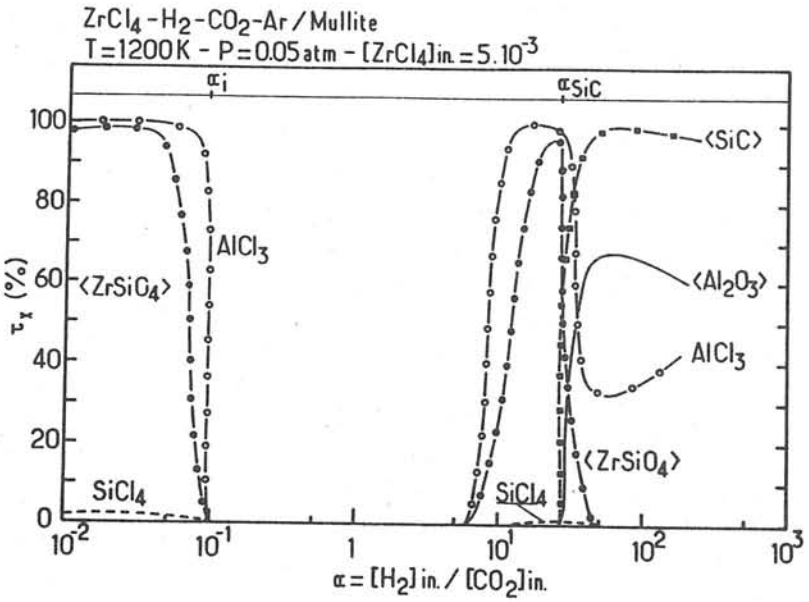

Fig. 14 - CVD of zirconia on a reactive mullite substrate: influence of ratio α on some thermodynamic rates defined in table 8 (T = 1200 K, P = 0.05 atm., $[ZrCl_4]_{in.} = 5 \times 10^{-3}$)

$\tau_{AlCl_3}(\%) = 100 \cdot \frac{[AlCl_3]_{eq.}}{6(<Al_6O_{13}Si_2>_{in.} - <Al_6O_{13}Si_2>_{eq.})}$
$\tau_{SiCl_4}(\%) = 100 \cdot \frac{[SiCl_4]_{eq}}{2(<Al_6O_{13}Si_2>_{in} - <Al_6O_{13}Si_2>_{eq.})}$
$\tau_{<SiC>}(\%) = 100 \cdot \frac{<SiC>_{eq.}}{2(<Al_6O_{13}Si_2>_{in.} - <Al_6O_{13}Si_2>_{eq.})}$
$\tau_{<ZrSiO_4>}(\%) = 100 \cdot \frac{<ZrSiO_4>_{eq.}}{2(<Al_6O_{13}Si_2>_{in.} - <Al_6O_{13}Si_2>_{eq.})}$
$\tau_{<Al_2O_3>}(\%) = 100 \cdot \frac{<Al_2O_3>_{eq}}{3(<Al_6O_{13}Si_2>_{in.} - <Al_6O_{13}Si_2>_{eq.})}$

Table 8 - Thermodynamic rates τ of some species originating in reactive mullite substrate

If deposition is carried out on a reactive substrate, this substrate can be etched by reactive mixture, depending on its nature and the experimental conditions. If the initial gas phase composition is monitored so that ZrO_2 yield is very close to 100% ($[H_2]_{in} / [CO_2]_{in}$ ratio close to 1 and $[ZrCl_4]_{in}$ low enough), a carbon substrate can be oxidised into carbon monoxide, while a mullite one is thermodynamically stable. These conclusions should be noted and will be correlated to kinetic results concerning the first steps of the ZrO_2 deposition process: a transient stage could be observed in zirconia CVD on carbon based substrates (19).

ACKNOWLEDGEMENTS

The authors wish to thank the French Ministry of Defense (DRET) and Société Européenne de Propulsion for their financial support.

REFERENCES

1 - E.C. SUBBARAD, in "Science and Technology of Zirconia", A.H. Hener and L.W. Hobbs, eds. (The American Ceramic Society, Columbus, 1981) p.1.

2 - R.C. GARVIE, R.H. HANNINK and R.T. PASCOE, Nature, 258 (1975) 703.

3 - D.L. PORTER and A.H. HEVER, J. Am. Ceram. Soc., 62 (1979) 298.

4 - D.L. PORTER and A.H. HEVER, J. Am. Ceram. Soc., 60 (1977) 183.

5 - D.L. PORTER, A.G. EVANS and A.H. HEVER, Acta Metall., 27 (1979) 1649.

6 - R.N. TAUBER, A.C. DUMRI and R.E. CAFFREY, J. Electrochem. Soc., 118 (1971) 747.

7 - R. COLMET, I. LHERMITTE-SEBIRE and R. NASLAIN, J. Am. Ceram. Soc., to be published.

8 - K.S. MAZDIYASNI and C.T. LYNCH, USAF Rept. ASD-TDR-63-322.

9 - K.S. MAZDIYASNI and C.T. LYNCH, in Special Ceramics 1965 (P. POPPER, ed.) p.115.

10- L.R. HOUGH, Proc. CVD-III, The Electrochemical Society, Princeton (1972) 232.

11- M. BALOG, M. SCHIEBER, M. MICHMMAN and S. PATAI, J. Cryst. Growth, 47, (1977) 109.

12- L. BEN DOR, A. ELSHTEIN and J. SHAPPIR, Proc. Euro CVD-IV (J. Bloem et al., eds.) Eindhoven, (1983) 444.

13- K. BRENNFLECK, E. FITZER and G. MACK, Proc. CVD-VIII (J.M. Blocher et al., eds) The Electrochemical Society, Pennington (1981) 672.

14- G. WAHL, S. SCHLOSSER and F. SCHMADERER, Proc. CVD-VII (T.O. Sedwick et al., eds.) The Electrochemical Society, Princeton (1979) p.536.

15- G.L. TINGEY, J. Phys. Chem. 70 (1966) 1406.

16- J. THEBAULT, R. NASLAIN and C. BERNARD, J. Less-Common Metals, 57 (1978) 1.

17- H. HANNACHE, R. NASLAIN and C. BERNARD, J. Less-Common Metals, 95 (1983) 221.

18- I. LHERMITTE-SEBIRE, R; COLMET, R. NASLAIN and C. BERNARD, J. Less-Common Metals, to be published.

19- J. MINET, F. LANGLAIS and R. NASLAIN, to be published.

Chapitre II

DEPOT DE ZIRCONE SUR SUBSTRAT PLAN:

ETUDE CINETIQUE ET CARACTERISATION PHYSICO - CHIMIQUE

Journal of the Less-Common Metals, 132 (1987) 273 - 287

ON THE CHEMICAL VAPOUR DEPOSITION OF ZIRCONIA FROM ZrO_2-H_2-CO_2-Ar GAS MIXTURE II: AN EXPERIMENTAL APPROACH

J. MINET, F. LANGLAIS and R. NASLAIN
Laboratoire de Chimie du Solide du CNRS, Université de Bordeaux I
351, Cours de la Libération - 33405 Talence cédex, France

ABSTRACT

Zirconia chemical vapor deposition, from $ZrCl_4$-H_2-CO_2-Ar gas mixture, is experimentally studied.

On the basis of a kinetic approach, the deposition process is shown to be governed by chemical reactions (probably water formation) with an apparent activation energy of about 100 kcal.mole^{-1}. With increasing the total gas flow rate and the total pressure, the occurence of an important homogeneous nucleation in the gas phase ("soot" formation) cannot be prevented.

The zirconia deposited films are found polycrystalline. A structural analysis by X-ray diffraction shows the possibility of depositing both monoclinic and tetragonal modifications of zirconia; such a mixture remaining stable down to room temperature. By Raman spectroscopic analysis, a small amount of weakly graphitized free carbon can be detected in the deposited films, depending on the deposition parameters. The stabilization of the tetragonal phase, at room temperature, can be explained on the basis of the effect of grain size, which has been thermodynamically studied by Lange et al.

I - INTRODUCTION

Compared to the CVD of alumina from $AlCl_3$-H_2-CO_2 system [1-4] the deposition process of zirconia from $ZrCl_4$-H_2-CO_2 gas mixture, whose advantages were previously discussed [5], has not been described, as yet, in much detail. Whereas a lot of articles have been devoted to the properties of sintered zirconia (particularly stabilized or partially stabilized zirconia) [6], very few studies concerned the physical and chemical characteristics of CVD zirconia thin films prepared by hydrolysis of zirconium chloride [7]. The only contribution in this field is , to our knowledge, that of Brennfleck et al. [8] who asserts, through a kinetic study of the deposition process as a function of temperature and total pressure, that the formation of water ($CO_2 + H_2$ -----> $CO + H_2O$) is the rate controlling step of the overall reaction process. Their characterization of the so-prepared ZrO_2 thin films is limited to a morphological analysis carried out by scanning electronic microscopy.

The present experimental study gives, on the basis of a specific deposition apparatus, an extended investigation of the influence of the deposition parameters on the growth rate and the physicochemical properties of ZrO_2

deposited on alumina flat substrates (*). Composition, structure and morphology of the deposits have been more particularly studied, in order to establish some correlations with the deposition parameters.

2 - EXPERIMENTAL ARRANGEMENT

Zirconia deposition experiments were performed using a CVD apparatus with a hot-wall reactor working under reduced pressure (fig. 1).

The initial gaseous mixture contains: (i) CO_2 and H_2 used to form H_2O, (ii) Cl_2 used to prepare $ZrCl_4$ by passing accross a small specific chamber containing zirconium sponge and heated to about 300°C, as well as eventually (iii) argon. The various gas flow rates and consequently the composition of the gas phase were controlled by means of mass flow-meters. The deposition chamber, made of alloys with high mechanical and chemical resistance, was heated resistively (up to about 1000°C) by electrical resistances embedded in a thermal insulator. The size of the isothermal hot-zone was 60 mm in diameter and 50 mm in height. The gaseous mixture produced by the CVD reactions was classically condensed in liquid nitrogen traps. A vacuum pump maintains in the reactor a reduced pressure (down to about 1 KPa) whose value can be regulated electronically.

(*) Degussa-France: Degussit AL 23

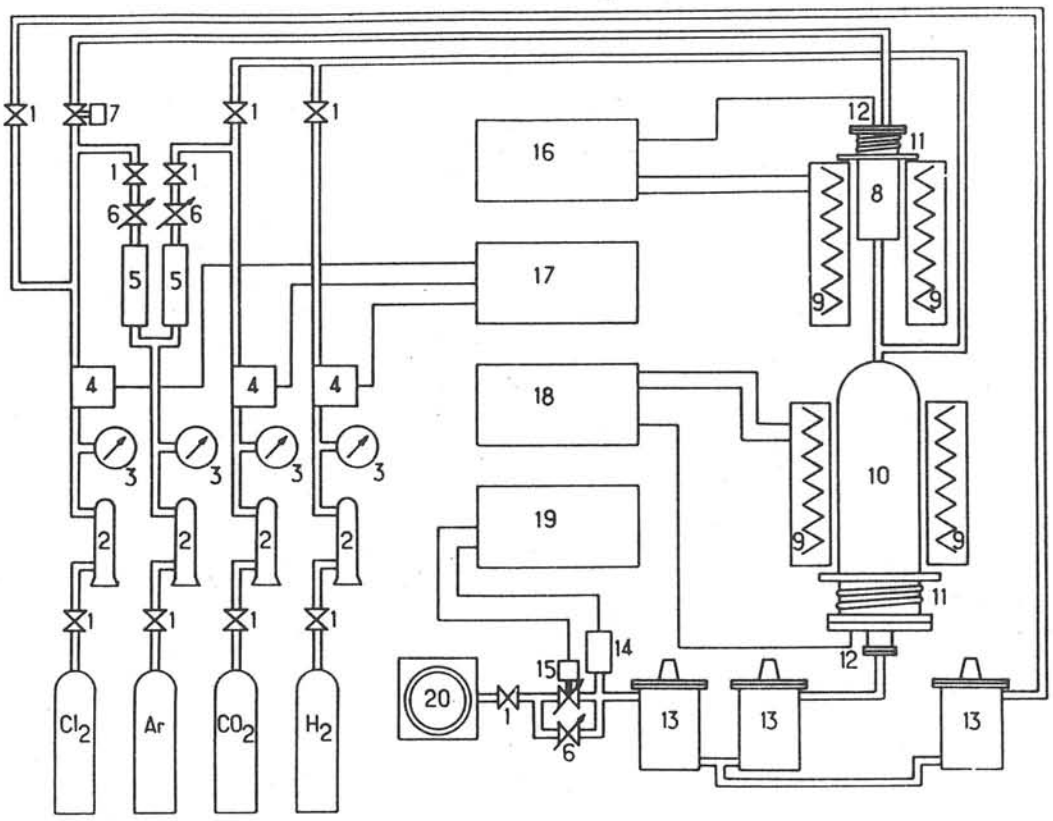

Fig. 1 - Schematic diagram of the experimental apparatus used for ZrO_2 chemical deposition:

1, shut -off valve;
2, P_2O_5 purification;
3, manometer;
4, mass flowmeter;
5, flowmeter;
6, adjusting valve;
7, security valve;
8, Chlorinator;
9, heating furnace;
10, CVD reactor;
11, water cooling;
12, thermocouple;
13, liquid nitrogen trap;
14, pressure sensor;
15, adjusting valve;
16, Chlorinator temperature controller;
17, (Cl_2, CO_2, H_2) flow controller;
18, CVD reactor temperature controller;
19, pressure controller;
20, vacuum pump.

3 - EXPERIMENTAL DEPOSITION RATE OF ZIRCONIA

Before examining the characteristics of the deposited thin films, a short kinetic study was performed as a function of total flow rate, temperature and total pression, for a ratio α (H_2/CO_2) = 1.

3.1- Influence of the total gas flow rate

The deposition rate of ZrO_2 is plotted in fig. 2 as a function of the total gas flow rate for a total pressure of 4 kPa and a temperature of 965°C. A rapid increase is observed between 250 and 400 $cm^3.mn^{-1}$ and then the deposition rate does not seem to increase any further. Moreover, for higher gas flow rates (D > 500 $cm^3.mn^{-1}$), an important homogeneous nucleation occurs in the gas phase (soot formation), which resuls in very poorly adherent deposits and consequently decreases the growth rate of the deposit on the substrate.

3.2 - Influence of the temperature

The variations of zirconia deposition rate versus reciprocal temperature (semi-logarithmic scale) are reported in figure 3 for a total gas flow rate of 300 $cm^3.mn^{-1}$ and a total pressure of 2 kPa. The temperature range is limited to 800-1000°C. At temperatures lower than 900°C, the deposition rate is very low and the measurement not very accurate. Between 900 and 1000°C, the

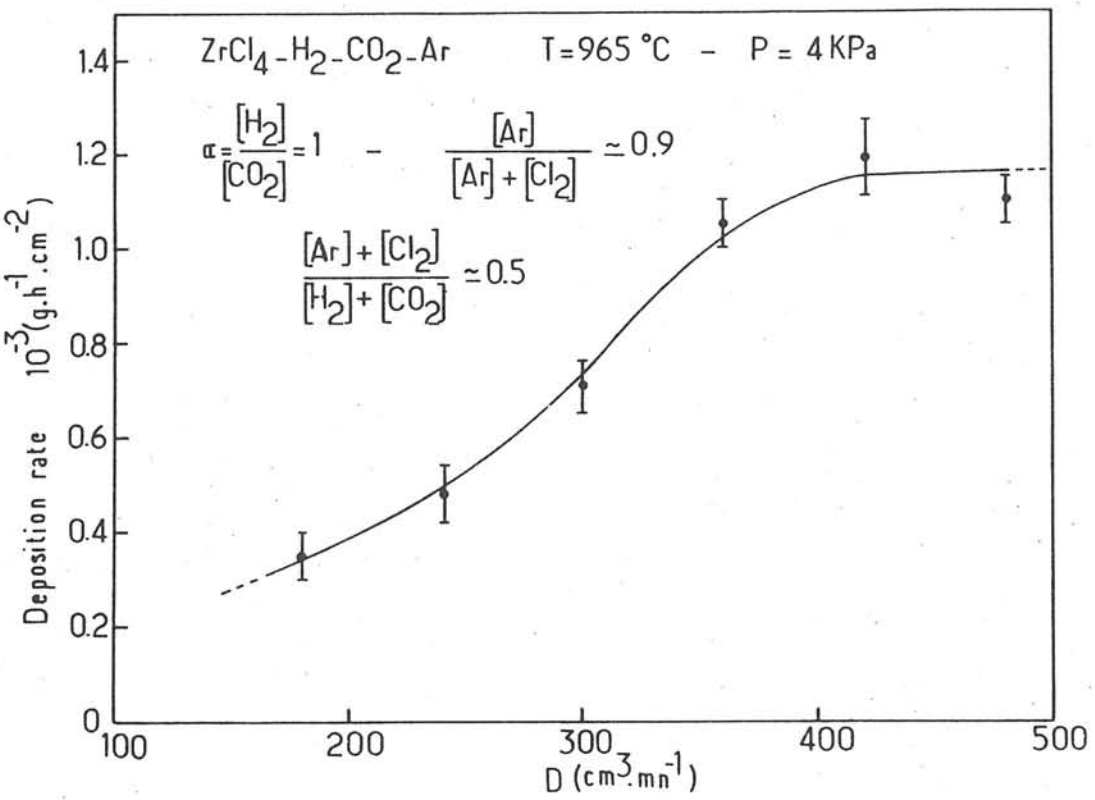

Fig. 2 - Influence of the total gas flow rate on the zirconia deposition rate

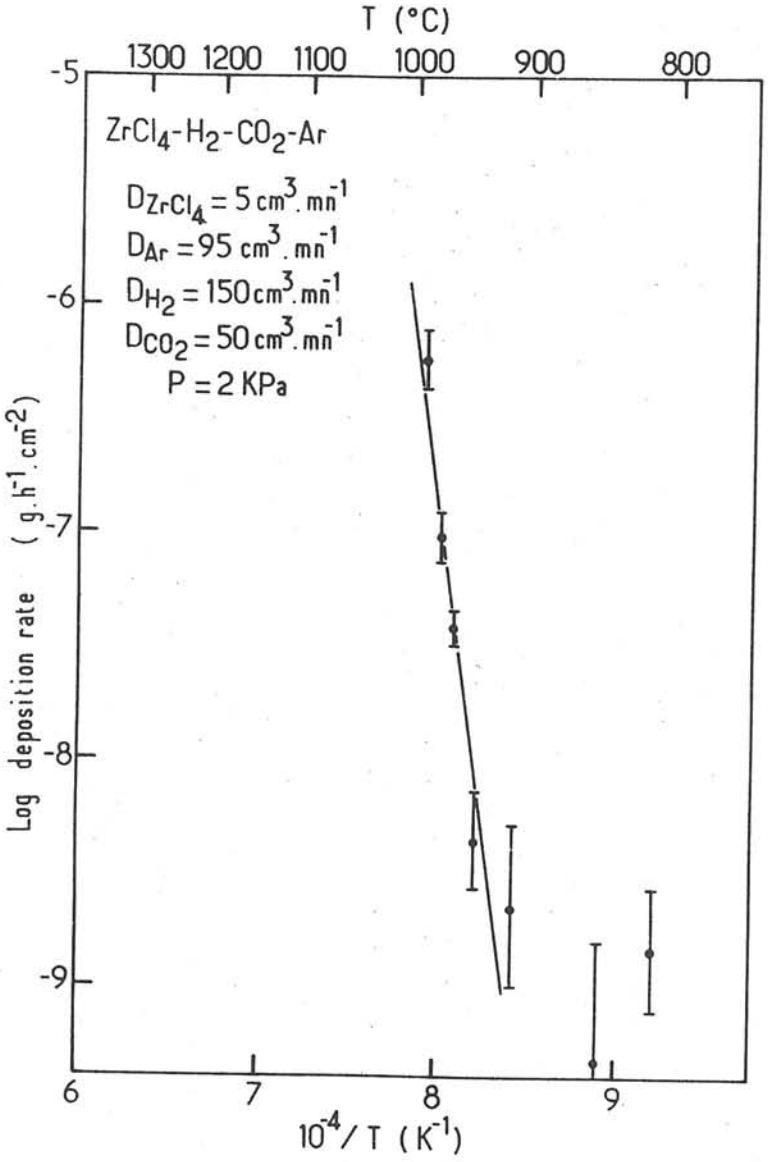

Fig. 3 - Variation in the logarithm of the zirconia deposition rate with reciprocal temperature

variation seems to follow an exponential Arrhenius law, with a very high apparent activation energy of about 100 kcal.mole^{-1}.

3.3 - Influence of the total pressure

The deposition rate of zirconia is plotted in figure 4 as a function of the total pressure (in the range 2 - 10 kPa) for a temperature of 965°C and two values of the total gas flow rate: 300 and 420 cm^3.mn^{-1}. A marked maximum is observed in both cases, for 3 kPa at 300 cm^3.mn^{-1} and for 4 kPa at 420 cm^3.mn^{-1}. At pressures higher than 6 kPa, the growth rate seems to become almost constant (about 0.5 mg.h^{-1}.cm^{-2}). In this relatively high pressure range, an important homogeneous nucleation phenomenon occurs, which makes an accurate measurement of the deposition rate difficult.

3.4 - Discussion

The very high activation energy is probably a consequence of a deposition process kinetically controlled by chemical reactions. This value is not far from the one estimated by Brennfleck et al. [8] (i.e. 86 kcal.mole^{-1}) between 860 and 900°C. On the basis of the high activation energy (78 kcal.mole^{-1}) reported by Tingey for the homogeneous reaction of CO_2 with H_2 to form CO and H_2O at temperatures higher than 800°C [9], that reaction of water formation can be supposed to be the kinetic controlling step of the overall deposition process. A further kinetic investigation, e.g. as a function of the H_2 and CO_2 concentrations, giving reaction orders with respect to these species, should be very useful to confirm the

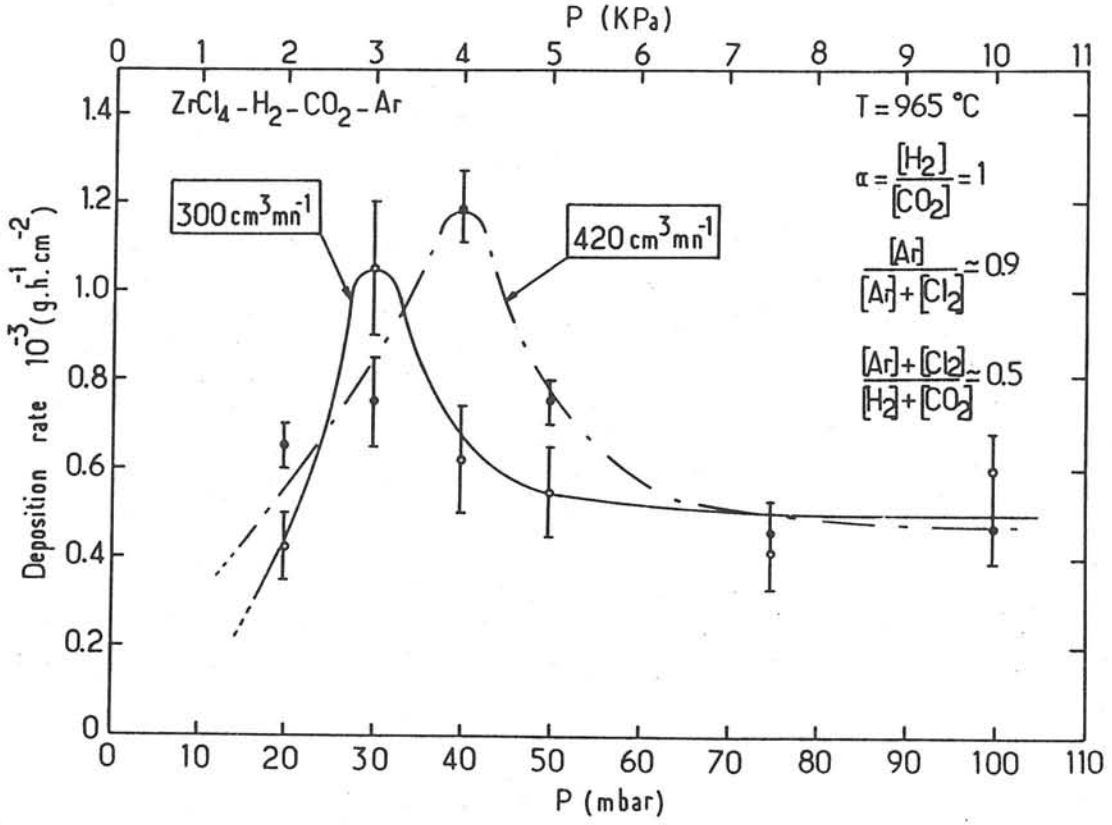

Fig. 4 - Influence of the total pressure on the zirconia deposition rate

hypothesis and to approach more accurately the reactional mechanism. Moreover, the present experimental result does not reveal, up to 1000°C, the transition usually observed in CVD towards a deposition process kinetically limited by diffusion of gaseous species through the boundary layer.

As a consequence , at a temperature of 965°C and a total gas flow rate of about 300 $cm^3.mn^{-1}$, i.e. with a deposition mechanism governed by chemical reaction kinetics, the increase of the growth rate with increasing total flow rate can be explained by a supersaturation increase at the gas-substrate interface. For a total gas flow rate lower than 400 $cm^3.mn^{-1}$, the depletion of the gas phase (owing to, for instance, unwanted deposits on the hot walls of the reactor) is probably less and less important while the total gas flow rate increases, as previously found by Hannache et al. for boron carbide CVD [10]. At a sufficiently high gas flow rate (i.e. D > 400 $cm^3.mn^{-1}$), the amount of gaseous reactants consumed by ZrO_2 deposition on the reactor walls becomes negligible with respect to that flowing at the gas inlet; the supersaturation at the gas-substrate interface does not vary significantly any longer and the deposition rate becomes almost constant.

4 - PHYSICO-CHEMICAL PROPERTIES OF CVD ZIRCONIA THIN FILMS

The investigation of Brennfleck et al. in this field was limited to some morphological observations by S.E.M. [8]. These authors have not characterized their CVD zirconia thin films from a chemical and structural point of view. The present paper gives the influence of the experimental parameters particularly on the occurrence of carbon in the deposited films and the transition between the various phases (particularly the monoclinic-tetragonal phases).

4.1- Morphological analysis of zirconia deposits

The S.E.M. micrographs presented in figure 5 illustrate the influence of deposition temperature (in the range 800 - 1000°C) on the morphology of zirconia deposited under a total pressure of 2 kPa and for a ratio $\alpha = 3$. The so-prepared deposits are polycrystalline, with a small grain size (of about 0.1 μm) which increases slightly with temperature. In the same way, they are the more homogeneous and dense as the temperature is increased.

Figure 6 shows micrographs of zirconia deposits obtained at a temperature of 965°C, for a ratio $\alpha = 1$ and various total pressures between 2 and 10 kPa. This parameter seems to have a marked influence on the grain size which increases with deposition pressure from about 0.1 μm under 2 kPa up to more than 1 μm under 10 kPa.

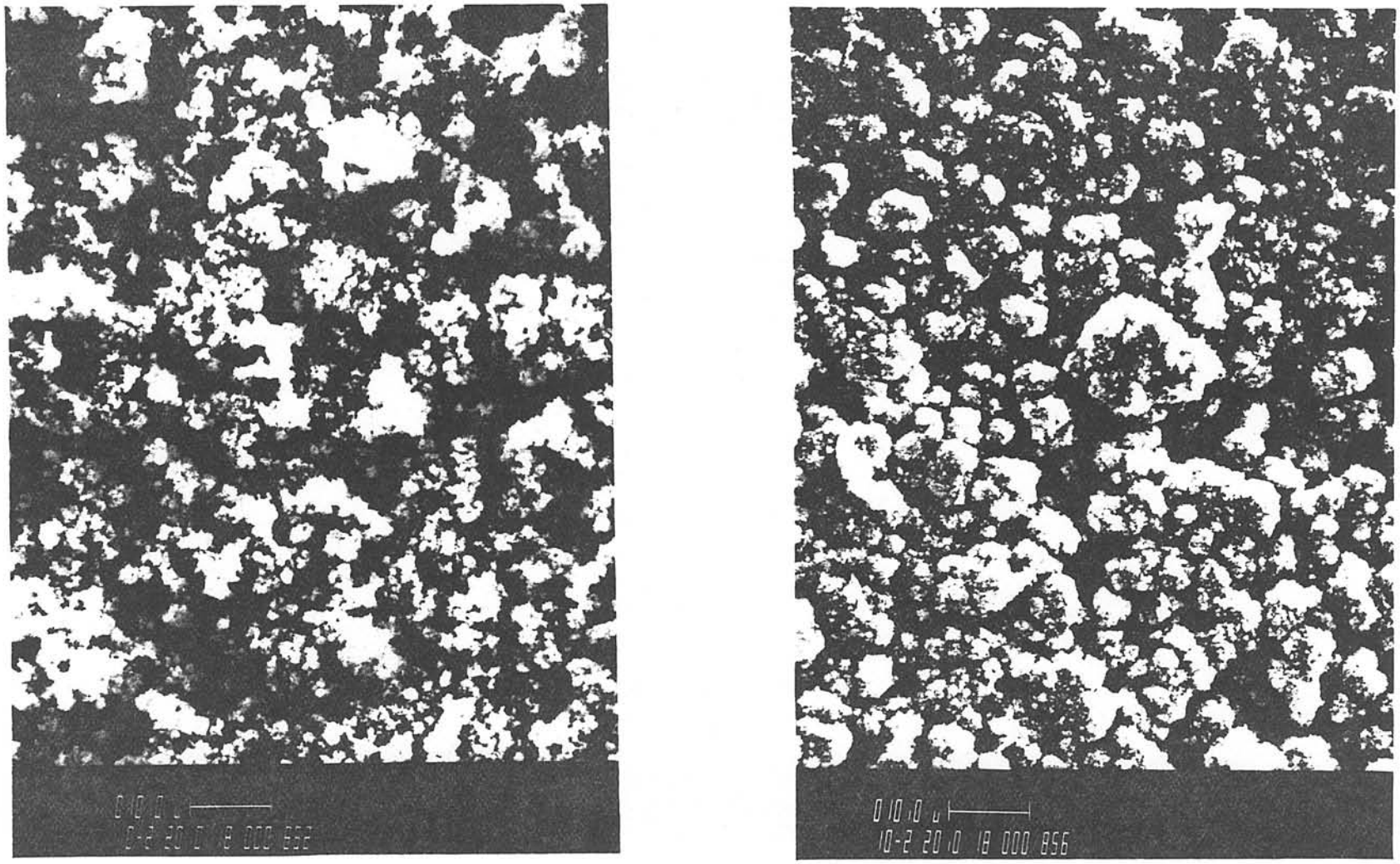

Fig. 5 Influence of the deposition temperature on the morphology of zirconia deposited under a total pressure of 2 kPa, a total flow rate of 300 cm^3 min^{-1} and a ratio $\alpha = 3$: (a) T = 815°C, (b) T = 975°C

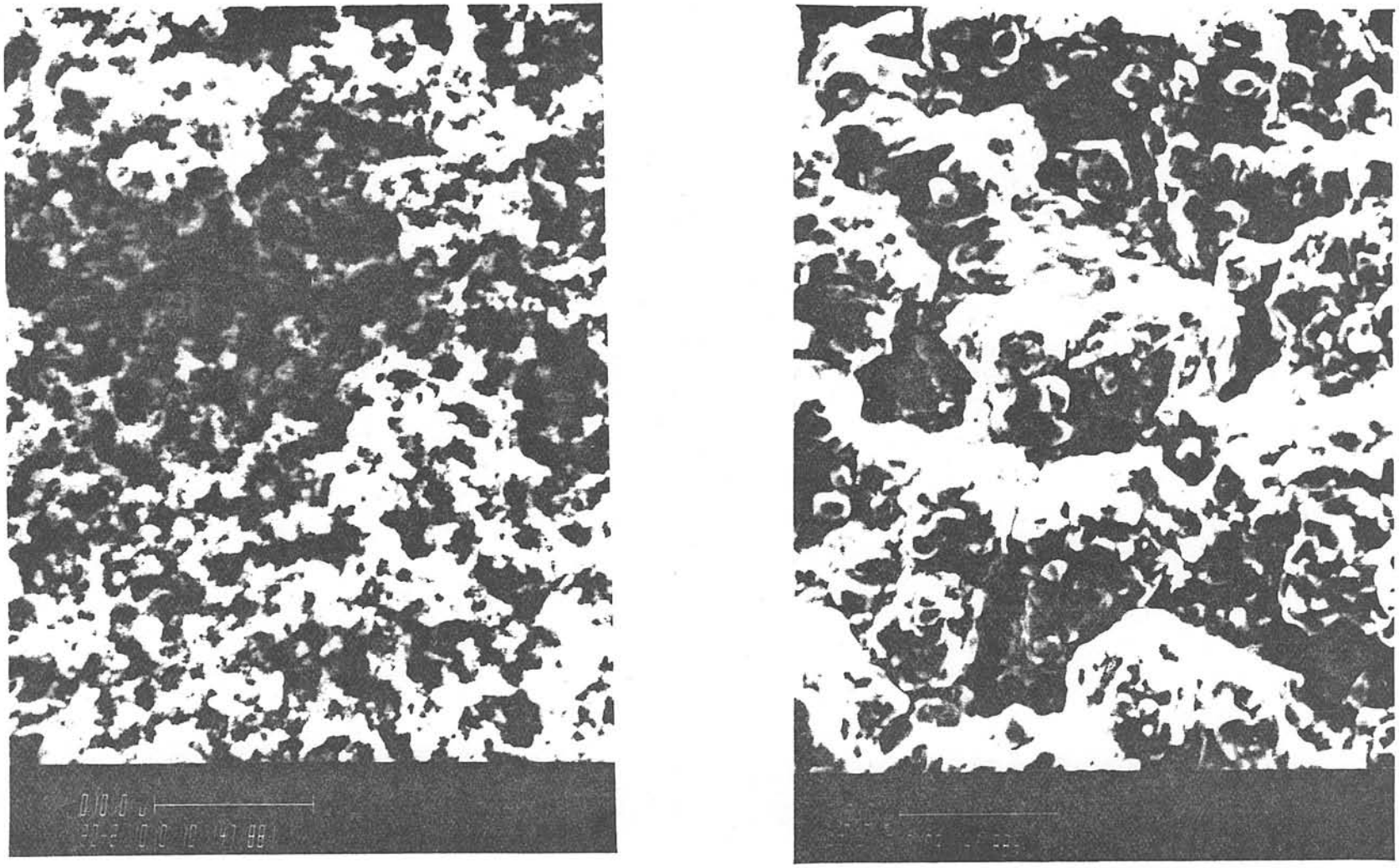

(a) (b)

Fig. 6 - Influence of the deposition total pressure on the morphology of zirconia deposited under a deposition temperature of 965°C, a total flow rate of $300 cm^3 . min^{-1}$ and a ratio $\alpha = 1$: (a) P = 2 kPa; (b) P = 10 kPa

4.2 - Structural analysis of zirconia deposits

X-ray diffraction patterns gives evidence of the occurrence,after cooling at room temperature, of both monoclinic and tetragonal modifications of zirconia in the thin films deposited on alumina substrates, the ratio of each phase depending on the experimental conditions (Figs.7-8).

The fraction of tetragonal phase, given by:

$$x_t = \frac{I_t(111)}{I_t(111) + I_m(111) + I_m(11\bar{1})}$$

where $I_t(111)$ is the intensity of (111) peak of tetragonal ZrO_2, $I_m(111)$ that of (111) peak of monoclinic ZrO_2 and $I_m(11\bar{1})$ that of $(11\bar{1})$ peak of monoclinic ZrO_2 [11,12] is reported in figure 9, for the same total pressure and α ratio, as defined in 4.1. as a function of deposition temperature. This plot seems to reveal a marked maximum for a temperature of 975°C, with a tetragonal phase ratio of 75%. The observation of all the X-ray diffraction patterns, particularly the relative intensities of the various peaks, permits to exclude the influence of some preferred orientations in the deposited films, which could result in false interpretation of the diffraction data.

Figure 10 gives the influence of deposition total pressure on the tetragonal ZrO_2 ratio in the deposit. For both values of total gas flow rates studied here (300 and 420 $cm^3.mn^{-1}$), a pressure increase decreases drastically the

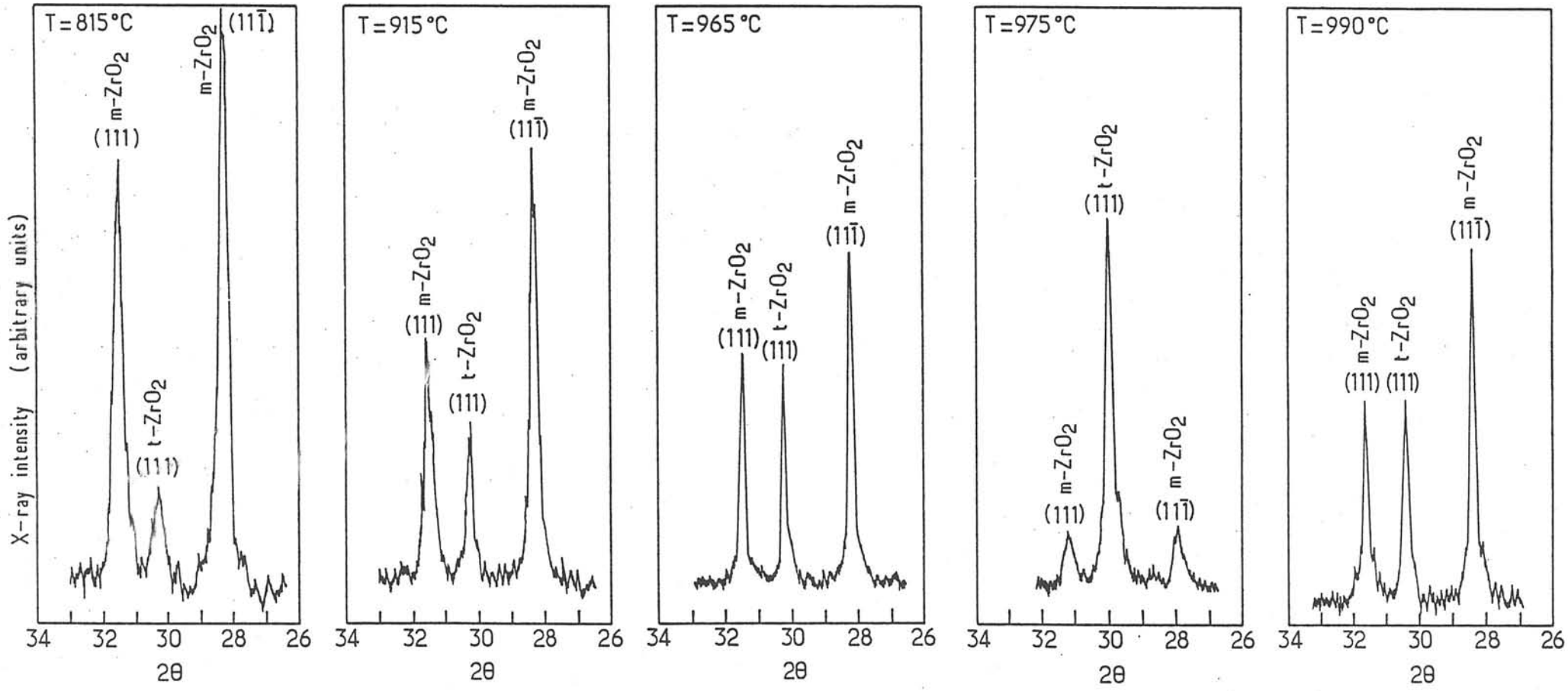

Fig. 7 - Room temperature X-ray diffraction patterns of the zirconia deposits for various deposition temperatures (P = 2 KPa; D = 300 $cm^3 . min^{-1}$, $\alpha = 3$)

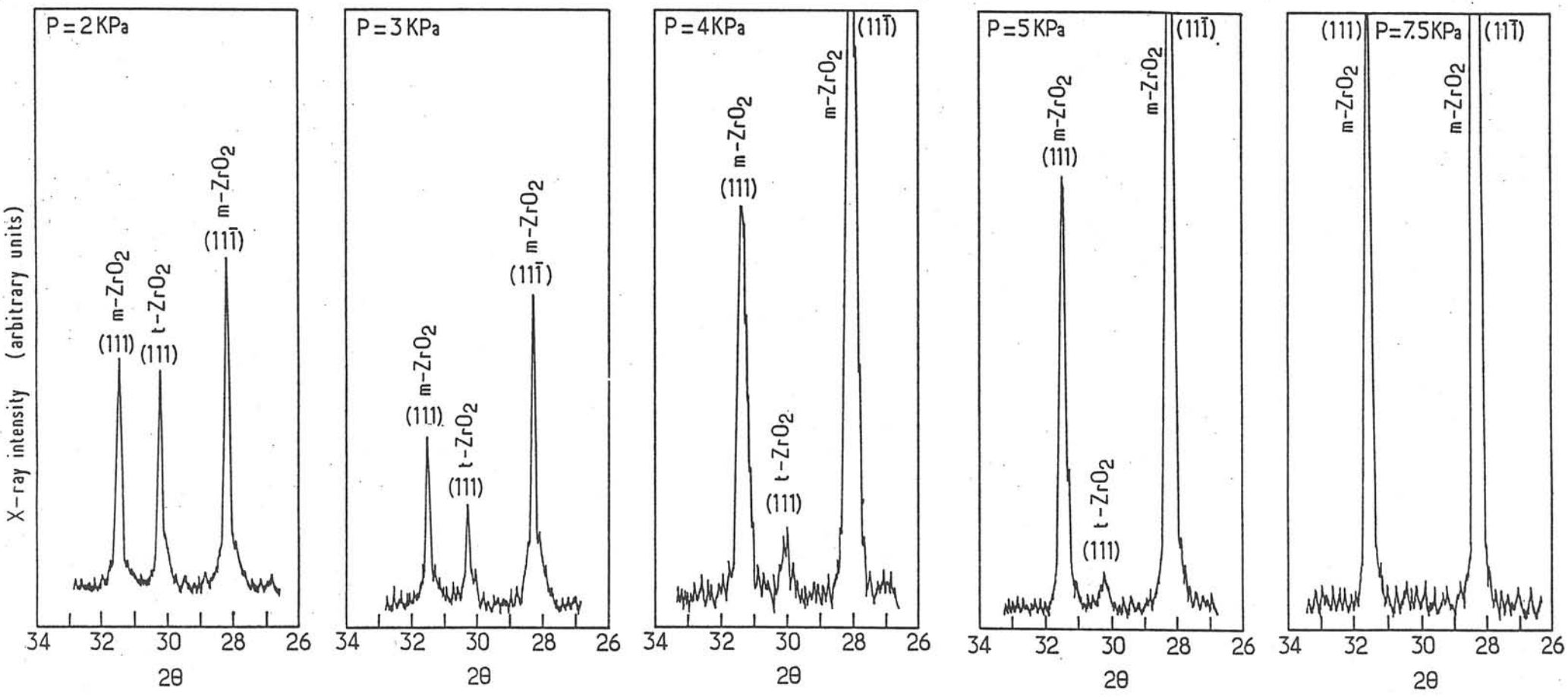

Fig. 8 - Room temperature X-ray diffraction patterns of the zirconia deposits for various deposition total pressures (T = 965°C, D = 300 $cm^3 . min^{-1}$, $\alpha = 1$)

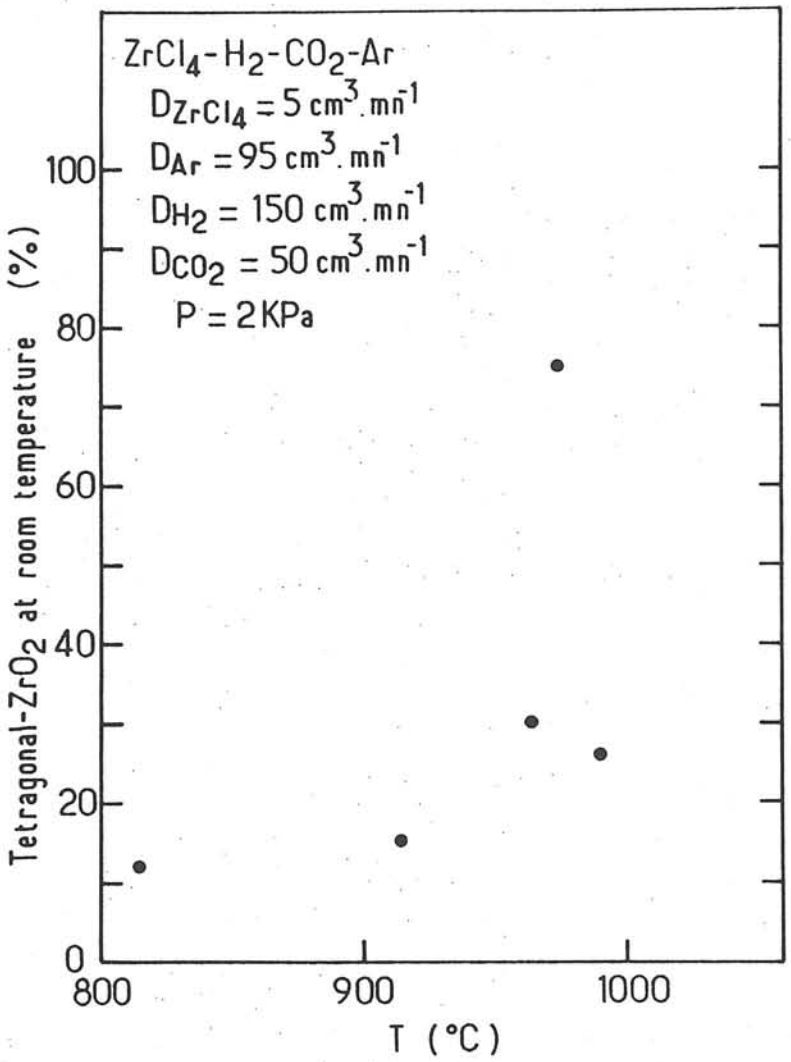

Fig. 9 - Influence of the deposition temperature on the tetragonal ZrO_2 ratio in the deposits at room temperature

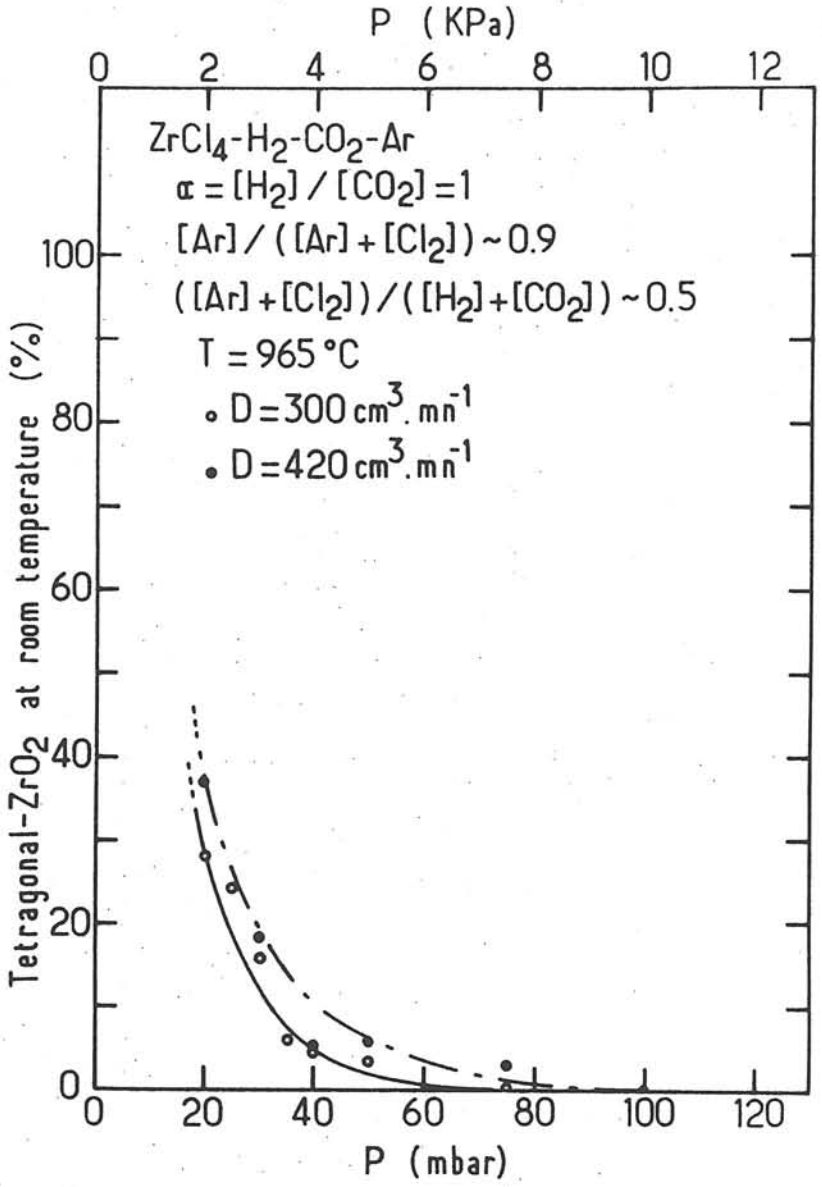

Fig. 10 - Influence of the deposition total pressure on the tetragonal ZrO_2 ratio in the deposits at room temperature

tetragonal phase percentage down to a negligible value at about 8 kPa. On the contrary, the influence of total flow rate is very weak.

The tetragonal modification of zirconia, which is not usually stable under ambient conditions, seems to be stabilized by the CVD process, the stabilization extent being dependent on the values of the experimental deposition parameters, essentially temperature and total pressure.

4.3 - Chemical analysis of zirconia deposits

The observed stabilization of tetragonal zirconia could be explained by the occurence in the deposit of some contaminants, such as elements originating in the alloy of the reaction chamber wall. This hypothesis has been eliminated, on the basis of a microanalysis performed with an electron microprobe analyser which did not give evidence in the deposited films any constitutive element of the CVD chamber. The only element detected besides zirconium and oxygen was carbon. However the small amount of carbon actually found in the deposits formed on flat alumina substrates made very difficult the study of the influence of the various experimental parameters on the carbon content and eventually the stabilization of ZrO_2-tetragonal phase.

Raman spectroscopy is a very sensitive method which has been used by Couzi and Cruege to characterize the state of crystallization of carbon (which can be detected down to 0.2%) in C-C composites [13]. C-BN composites have been

recently investigated by Hannache et al. [14] as well as SiC-C deposits by P. Martineau et al. [15] using in the same manner a Raman microanalyser (laser excitation, 5145 Å). This method is used in the present work to give a further description of the characteristics of ZrO_2 films as a fonction of deposition parameters.

The raman spectra of ZrO_2-deposits are reported in figure 11 for various deposition temperatures ranging from 815 up to 975°C, the other CVD parameters being defined in the figure. As previously found by X-ray diffraction, the Raman spectrum of films deposited at 815°C permits to identify the monoclinic zirconia which seems to be the only phase. Table 1 gives the main lines observed in that spectrum, which is very consistent with those given by various authors for bulk zirconia ceramics [16-20]. As deposition temperature increases, the intensity of the lines of monoclinic phase decreases and two characteristic lines of carbon occur simultaneously (wave numbers=1350 and 1600 cm^{-1}). When the deposition temperature reaches 975°C, the carbon lines are very strong, the monoclinic ZrO_2 lines very weak and one line of the tetragonal phase can be observed at 265 cm^{-1} (Table 2), however it is very weak.

The influence of the deposition pressure on the Raman spectra under conditions defined in 4.1, is shown in figure 12. The spectrum of the deposit performed at 3 kPa reveals a mixture of monoclinic and tetragonal (line at 265 cm^{-1}) zirconia phases combined with pyrocarbon. As CVD pressure increases, the monoclinic ZrO_2 lines become stronger and

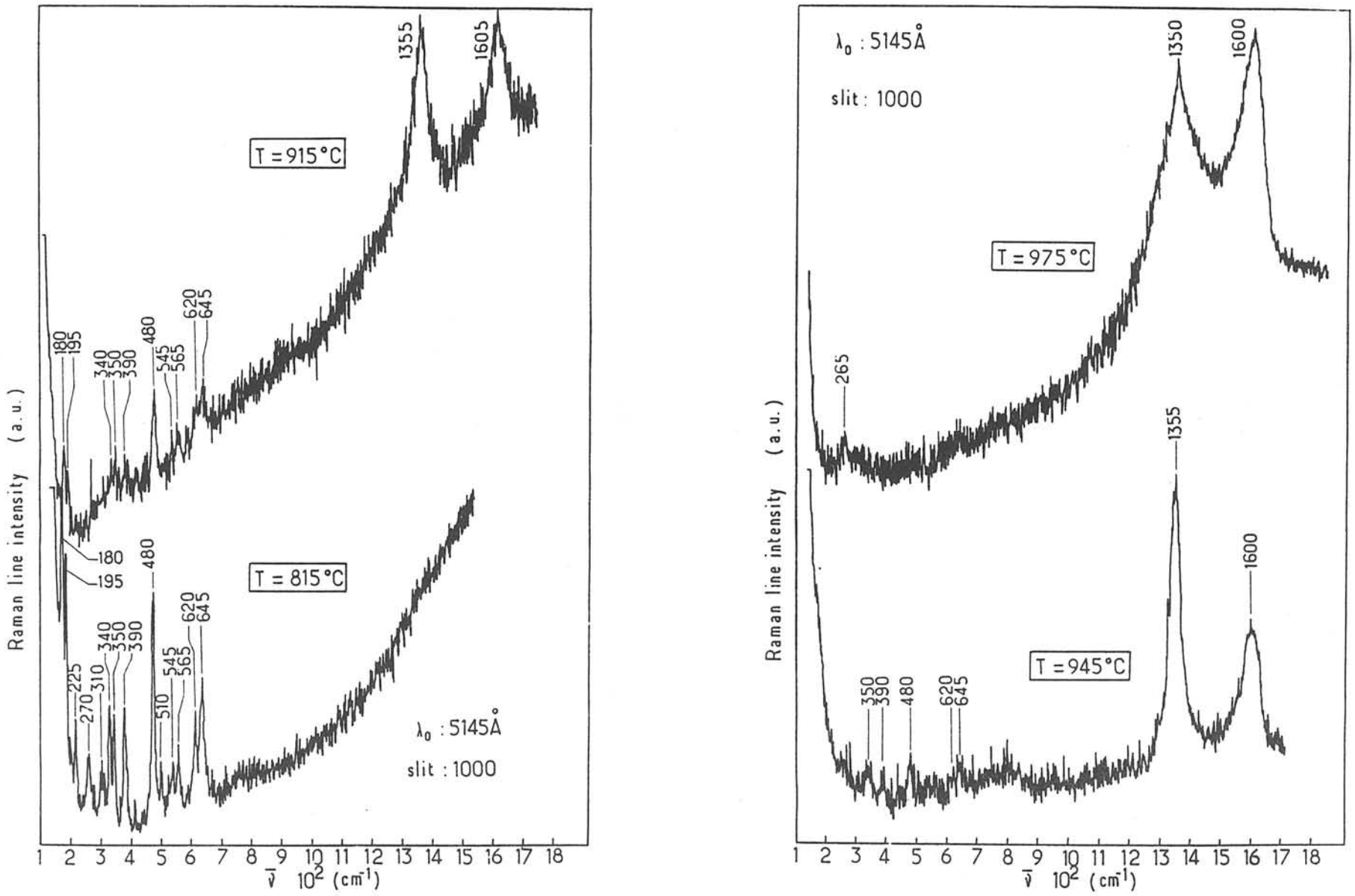

Fig. 11 - Raman spectra of zirconia deposits for various deposition temperatures ($P = 2$ kPa, $D = 300$ cm^3 . min^{-1}, $\alpha = 3$)

E. ANASTASSAKIS B. PAPANICOLAOU M. ASHER (15)		D.R. CLARKE F. ADAR (16)		M. ISHIGAME T. SAKURAI (17)		Y.G. KERAMIDAS W.B. WHITE (18)		C.M. PHILLIPPI K.S. MAZDIYASNI (19)		Present work	
$\bar{\nu}$ (cm^{-1})	Intensity	$\bar{\nu}$ (cm^{-1})	Intensity	$\bar{\nu}$ (cm^{-1})	Intensity	$\bar{\nu}$ (cm^{-1})	Intensity	$\bar{\nu}$ (cm^{-1})	Intensity	$\bar{\nu}$ (cm^{-1})	Intensity
92	m										
101	m	105	m	102	m	103	m	104	m		
177	s	181	s	179	s	180	s	180	s	180	s
189	s	192	s	190	s	192	s	192	s	190	s
222	w	224	w	222	w	224	w	223	w	225	w
315	m	309	w	305	w	308	w	307	w	310	w
335	m	335	m	334	m	335	m	337	m	340	m
347	m	349	m	348	m	349	m	348	m	350	m
382	m	385	m	381	m	383	m	382	m	390	m
476	s	480	s	476	s	476	s	476	s	480	s
502	w	524	w	500	w	503	w	502	w	510	w
537	w	543	w	534	w	539	w	538	w	545	w
559	w	563	w	556	w	561	w	559	w	565	w
616	m	619	m	615	m	617	m	617	m	620	m
637	m	636	m	637	m	638	m	638	m	645	m
						755	w				

Table 1 - Frequency-level (from various authors) of the Raman spectrum main peaks for monoclinic-ZrO_2. w, m, and s, respectively designate weak, medium and strong scattering intensity

E. ANASTASSAKIS B. PAPANICOLAOU M. ASHER (15)		D.R. CLARKE F. ADAR (16)		C.M. PHILIPPI K.S. MAZDIYASNI (19)		Present work	
$\bar{\nu}$ (cm^{-1})	Intensity	$\bar{\nu}$ (cm^{-1})	Intensity	$\bar{\nu}$ (cm^{-1})	Intensity	$\bar{\nu}$ (cm^{-1})	Intensity
145	s	148	s	148	s		
178	s			179	s		
188	s			189	s		
222	w			223	w		
262	s	264	s	263	s	265	s
332	m	319	w	332	m		
380	m	404	w	380	m		
473	s	461	w	473	s		
536	w			536	w		
562	w			561	w		
615	w	606	w	615	w		
640	s	643	m	640	s		

Table 2 - Frequency-level (from various authors) of the Raman spectrum main peaks for tetragonal-ZrO_2. w, m and s, respectively designate weak, medium and strong scattering intensity

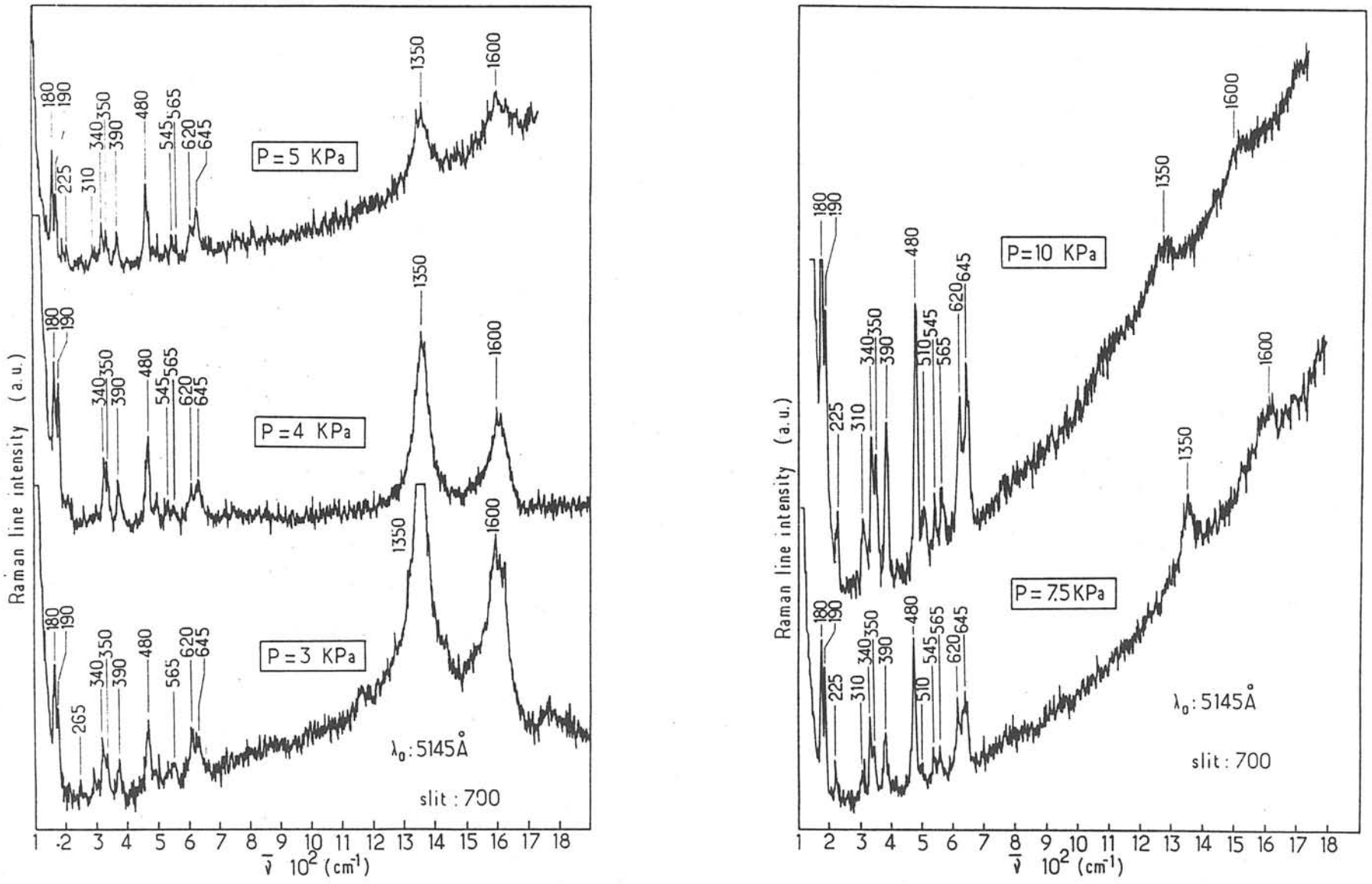

Fig. 12 - Raman spectra of zirconia deposits for various deposition total pressures (T = 965°C, D = 300 $cm^3 . min^{-1}$, $\alpha = 1$).

stronger, tetragonalone disappears and those of carbon decrease and become rather weak for 10 kPa.

4.4 - Discussion

These results confirm the occurence of weakly graphitized free carbon in zirconia deposits. Its content increases with rising deposition temperature and decreases when CVD pressure increases. This C-ZrO_2 codeposition is not exactly in accordance with the thermodynamic approach which predicts a deposition of pure zirconia [5]. This disagreement emphasizes the importance of the kinetic factors in a CVD process. Here the water formation reaction, which is probably the limiting step of the reaction process, controls the water concentration whose value at the gas / substrate interface is lower than that at equilibrium . As a consequence, the actual situation can be described by the thermodynamic diagrams, but with different values of the initial composition of the gas phase, probably lower concentrations of CO_2 and H_2 species and higher values of the α ratio [5], giving rise to the reaction:

$$CO + H_2 \text{ -----> } C + H_2O$$

Nevertheless, the influence of CVD temperature and pressure on the carbon yield assessed in the thermodynamic approach, is in good agreement with the experimental results previously given concerning the carbon content of the deposit.

Moreover, Raman microanalysis confirms the stabilization of zirconia tetragonal phase which has been suggested by X-ray diffraction particularly for a deposition temperature of 975°C and a CVD pressure of 3 kPa. However, the amount of the tetragonal phase in the deposited films seems to be low. On the other hand, the amount of free carbon in the deposits varies with deposition temperature and pressure in the same manner as that observed for tetragonal zirconia, and this could be a determining factor in the stabilization of that tetragonal phase. Nevertheless, the decrease of tetragonal zirconia ratio for temperatures higher than 975°C cannot be explained on the basis of this argument.

Another important parameter must be taken into account in the understanding of such a stabilization phenomenon: the effect of grain size. In order to study the toughness enhancement in partially stabilized zirconia, Lange et al. have recently reported a thermodynamic approach of tetragonal-monoclinic zirconia transition, in connexion with grain size [21,22]. This approach takes into account not only the chemical free energy variation associated to that transition (ΔG_c), but also the deformation and surface energy variation (ΔU_{se}). On this basis, Lange et al. define a critical grain diameter D_c as a function of these various energy terms including surface energy and interfaces areas. Only zirconia grains whose diameter is higher than that critical value D_c, can be transformed from tetragonal to monoclinic structure as temperature is decreased. These authors have been able to plot a phase diagram, reported here in figure 13, which gives the ratio of grain diameters (D/D_c) versus an energy ratio $\Delta U_{se}/\Delta G_c$ proportional e.g. to temperature. According to this

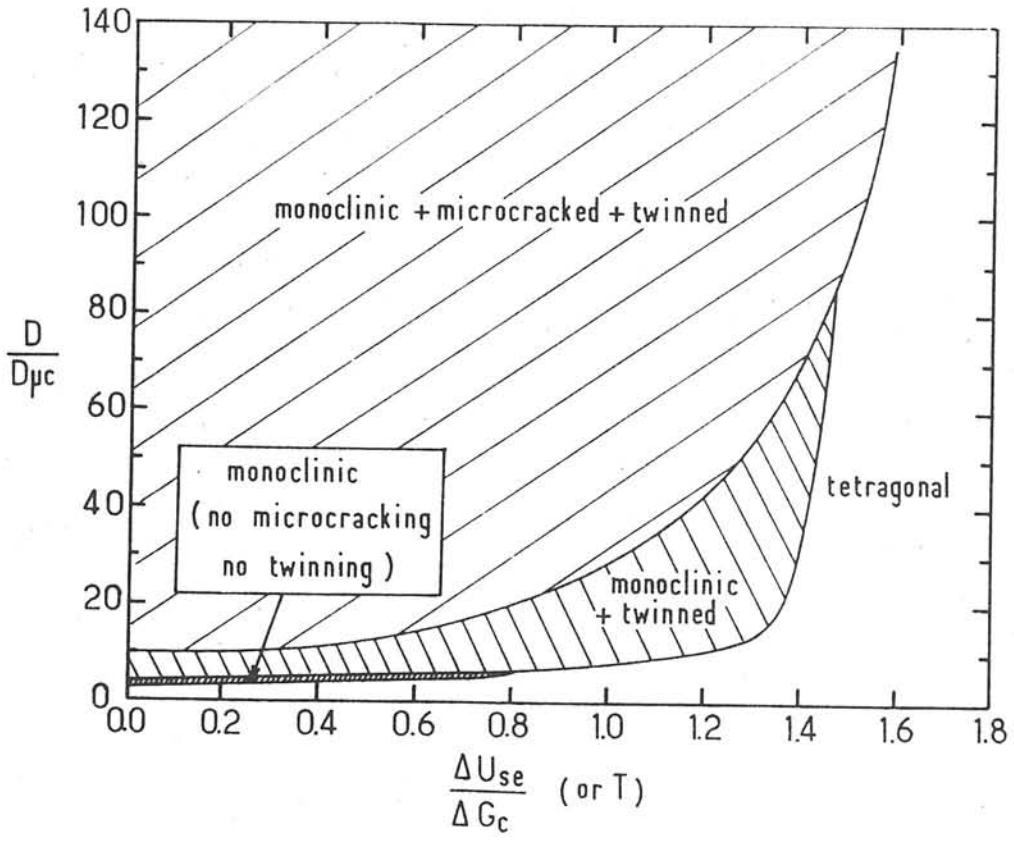

Fig. 13 - Phase diagram of Lange et al. [20]

diagram, for grains of large size, the transition tetragonal ----> monoclinic occurs at relatively high temperature (close to equilibrium temperature of 1170°C) with microcracking and twinning; for grains of lower size ($5 < D / D_c < 10$), the transition occurs at low temperature with only twinning and for grains of much lower size ($3 < D / D_c < 5$), the transition occurs at temperature without microcracking and twinning. Finally, for very small grains ($D / D_c < 3$), the tetragonal phase could be stabilized down to room temperature. Such results have also been found by Anderson and Gupta who have shown that the stabilization of the tetragonal modification of zirconia is achieved when the grain size was lower than 0.3 μm [23].

If such an approach, which concerns the bulk material of partially stabilized zirconia, can be extended to the case of CVD thin films, it is possible to explain the observed stabilization phenomenon on the basis of an accurate morphological study of the deposits. The first analysis in this field, previously given in the present paper, permits the following preliminary remarks: (i) the rapid decrease of tetragonal zirconia content for deposition temperatures higher than 975°C could be due to the effect of grain size increasing in the CVD films; and (ii) in the same manner, when deposition pressure rises, the resulting increase in mean grain size (from about 0.1 to 1μm) could disfavour the stabilization of the tetragonal phase, which is observed experimentally.

5 - CONCLUSION

This experimental approach of zirconia CVD process has led to a rather accurate study of the main deposition parameters and of their influence upon both the process itself (from a kinetic point of view) and some physicochemical properties of the so-prepared zirconia thin films.

On the basis of the high activation energy exhibited by the deposition rate over the whole temperature range studied , a kinetic process controlled by chemical reactions has been assumed, the limiting step being probably the water formation reaction. The kinetic approach has shown a determining interest for e.g. the understanding of the occurrence of ZrO_2/C codeposition under experimental conditions, when the only thermodynamic study predicted a pure zirconia deposit. In spite of homogeneous nucleation unwanted phenomenon, the influence of total pressure and total gas flow rate has been established. A more advanced investigation of the reactional mechanisms would need more results particularly on the reaction order with respect to the main gaseous species.

The microanalysis of the deposited thin films based on various techniques (such as X-ray diffraction and Raman spectroscopy) has shown the possibility of stabilizing the tetragonal modification of zirconia by choosing adequate deposition conditions, e.g. a temperature of 975°C and a total pressure of about 2kPa. A preliminary explanation of this result, supported by the thermodynamic approach of tetragonal-monoclinic transition by Lange et al.,

has been proposed on the basis of the effect of grain size. This interesting correlation must now be corroborated by other investigations (e.g. an accurate method should be used in order to measure precisely the mean grain size in the deposit).

ACKNOWLEDGEMENTS

The authors, wish to thank the French Ministry of Defense (DRET) and the Société Européenne de Propulsion for their financial support. They are also indebted to Dr. COUZI and CRUEGE for their assistance in Raman microanalysis and the Electronic Microscopy Department of Université de Bordeaux I for the S.E.M. studies. They wish to acknoledge Cabot Alloy France company for providing the high performance "hastelloy" alloys of the CVD reactor.

REFERENCES

1 - C.S. PARK, J.G. KIM and J.S. CHUN, J. Vac. Technol. A, 1, 4 (1983)1820.

2 - J.G. KIM, C.S. PARK and J.S. CHUN, Thin Solid Films, 97 (1982) 97.

3 - R. COLMET, R. NASLAIN, P. HAGENMULLER and C. BERNARD, J. Electrochem. Soc., 129 , 6 (1982) 1367.

4 - K. IIDA and T. TSUJIDE, Jpn. J. Appl. Phys., 11 (1972) 840.

5 - J. MINET, F. LANGLAIS, R. NASLAIN and C. BERNARD, J. Less-Common Met., 119 (1986) 219 - 235.

6 - E.C. SUBBARAD, in "Science and Technology of Zirconia", A.H. Hener and L.W. Hobbs, eds. (The American Ceramic Society, Columbus, (1981) p.1.

7 - R.N. TAUBER, A.C. DUMBRI and R.E. CAFFREY, J. Electrochem. Soc.,118 (1971) 747.

8 - K. BRENNFLECK, E. FITZER and G. MACK, Proc. CVD-VIII (J.M. BLOCHER and al., eds.). The Electrochemical Society, Pennington (1981) 672.

9 - G.L. TINGEY, J. Phys. Chem. 70 (1966) 1406.

10 - H. HANNACHE, J.Y. ROSSIGNOL, F. LANGLAIS, R. NASLAIN and P.HAGENMULLER, J. Less-CommonMetals, to be published.

11 - R.C. GARVIE and P.S. NICHOLSON, J. Am. Ceram. Soc., 55, 6 (1972) 303.

12 - E.D. WHITNEY, Trans. Faraday Soc., 61 (1965) 1991.

13 - M. COUZI and F. CRUEGE, Actual. Chim., 4 (1980) 62.

14 - H. HANNACHE, R. NASLAIN and C. BERNARD, J. Less-Common Metals, 95 (1983) 221.

15 - P. MARTINEAU, M. LAHAYE, R. PAILLER, R. NASLAIN, M. COUZI and F. CRUEGE, J. Mater. Sc., 19 (1984) 2731.

16 - E. ANASTASSAKIS, B. PAPANICOLAOU and I.M. ASHER, J. Phys. Chem. Solids, 36 (1975) 667.

17 - D.R. CLARKE and F. ADAR, J. Am. Ceram. Soc., 65, 6 (1982) 284.

18 - N. ISHIGAME and T. SAKURAI, J. Am. Ceram. Soc., 60, 7-8 (1977) 367.

19 - V.G. KERAMIDAS and W.B. WHITE, J. Am. Ceram. Soc., 57, 1 (1974) 22.

20 - C.M. PHILIPPI and K.S. MAZDIYASNI, J. Am. Ceram. Soc., 54, 5 (1971) 254.

21 - F.F. LANGE and D.J. GREEN, Advances in Ceramics - Vol.3 - The American Ceramic Society, Inc, Columbus, Ohio (1981) pp. 217-225.

22 - F.F. LANGE, J. Mat. Sci., 17 (1982) 225.

23 - C.A. ANDERSON and T.K. GUPTA. Advances in Ceramics - Vol. 3 - The American Ceramic Society, Inc., Columbus, Ohio (1981) pp.184-201.

Chapitre III

INFILTRATION DE PREFORMES FIBREUSES ET MICROPOREUSES PAR DE LA ZIRCONE : OPTIMIZATION EXPERIMENTALE

Soumis à " Composite Science and Technology "

CHEMICAL VAPOR INFILTRATION OF ZIRCONIA WITHIN THE PORE NETWORK OF FIBROUS CERAMIC MATERIALS FROM $ZrCl_4$-H_2-CO_2 GAS MIXTURES

J. MINET(*) , F. LANGLAIS and R. NASLAIN,
Laboratoire de Chimie du Solide du CNRS, Université de Bordeaux I
351, Cours de la Libération - 33405 Talence cédex, France

ABSTRACT

On the basis of an experimental approach, new ceramic-ceramic composites have been prepared by the CVI of ZrO_2 within the pore network of various fibrous preforms.

The optimization of the CVI parameters has been carried out on the basis of: (i) a kinetic study (overall mass of deposited zirconia), (ii) mercury porosimetry (actual infiltration ratio τ_i) and (iii) microprobe analysis (ZrO_2 distribution profiles) utilizing mainly transition alumina fiber based substrates.

SEM observations of failure surfaces evidence a strong adhesion between alumina and zirconia in alumina fibers composites, and a weak adhesion with delaminations between pyrocarbon and zirconia in 2D-C-C/ZrO_2 composites.

From a kinetic point of view, the variations of the residual porosity as a function of the densification time follow an exponential law. The different behaviours of preforms towards the same CVI conditions has been shown to be strongly dependent on the features of the pore network. A low porosity and a low mean pore size are unfavourable to a good densification.

(*) Present adress: Société Européenne de Propulsion, Division Propulsion à Poudres et Composites - B.P. 37 - 33165 Saint Médard en Jalles, France.

I - INTRODUCTION

Recently chemical vapor infiltration (CVI) has been succesfully used to prepare new families of ceramic-ceramic composite materials. Most of them were derived from carbon-carbon composites by replacing totally or partially the carbon matrix by more suitable ceramics, so giving improved mechanical and oxydation resistance. Thus, C-C/SiC, SiC-SiC, C-C/TiC, C-C/B_4C or C-C/BN fibrous composite materials have been synthesized and characterized (1-5).

R. COLMET et al. have shown that CVI could also be used to densify with alumina (deposited from $AlCl_3$-H_2-CO_2 mixtures) porous preforms made of alumina-based fibers. An analysis of the main thermomechanical properties of alumina-alumina composite materials revealed a relatively high bending strength to failure up to 1000°C but a rather poor toughness probably due to strong fiber-matrix interfaces (6).

On the basis of the outstanding thermomechanical properties of zirconia, it seemed to us particularly attractive to try to prepare zirconia matrix composite materials: (i) zirconia is much more refractory than alumina, (ii) it

has various cristallographic forms and can be stabilized under given conditions in the tetragonal or cubic modifications, an improvement in toughness being related to the phase transformation, (iii) zirconia exhibits a high chemical stability, and finally it is a very good thermal insulator (7).

On the basis of a thermodynamical approach, J. MINET et al. have given a detailed analysis of zirconia deposition conditions in the Zr-C-H-O-Cl system as well as a study of the influence of the nature of the substrate. As in the case of alumina, pure zirconia can be deposited as long as water is present at equilibrium to hydrolyse zirconium chloride. On the contrary, a ZrO_2/C mixture can be obtained particularly when H_2 is in excess with respect to CO_2 (8).

Experimental studies of the CVD of ZrO2 from $ZrCl_4$-H_2-CO_2 gaseous mixtures have been recently reported (9,10). The high activation energy of the growth rate has been related to a kinetic process controlled by chemical reactions, such as water formation. On the other hand, a microanalysis of the deposited thin films has shown the possibility of stabilizing the tetragonal modification of zirconia by choosing adequate CVD conditions which induce a very low grain size (less than 0.3 μm) (9).

The aim of this contribution is to give an experimental optimization of ZrO_2 CVI conditions for various fibrous preforms in order to demonstrate the possibility of preparing by this technique ceramic-ceramic composite materials. The morphology of the materials is then characterized. At last, the CVI processes of various refractory preforms are kinetically compared.

II - EXPERIMENTAL

II.1. Apparatus

The laboratory-scale equipment used in the present study has been described previously (9): it is a hot-wall CVD reactor operated under reduced pressure. Zirconium chloride is formed in line by direct chlorination of zirconium sponge. It is mixed with H_2/CO_2 at the entrance of the infiltration chamber which results in hydrolysis and oxide formation according to the overall following reactions:

$$2H_2(g) + 2CO_2(g) \rightleftharpoons 2H_2O(g) + 2CO(g)$$

$$ZrCl_4(g) + 2H_2O(g) \rightleftharpoons ZrO_2(s) + 4HCl(g)$$

During a CVI run, the experimental parameters (gas flow rate, temperature and total pressure) should be maintained at constant values for several hundred hours, thus requiring automatic regulations.

II.2. Fibrous preforms

The starting materials have been chosen within two main types of fibrous substrates which could lead to thermomechanical applications: oxide preforms for use at medium temperatures under oxidizing atmosphere on one

hand, and carbon-based preforms for applications at very high temperatures on the other hand.

II.2.1. Alumina-based fibrous preforms

Two starting preforms made of alumina-based fibers were chosen on the basis of their microstructure and their ability to be densified from the gaseous phase. Some of these characteristics are given in table 1.

The first type - named "alumina preform 1" in the following - is made with transition alumina fibers ("Saffil" from ICI), impregnated by an alumina slurry and pyrolyzed. These preforms, whose overall silica content is small (about 3 %), exhibit an initial porosity of about 60% with two main pore size ranges (i.e. 0.05-0.3μm and 1-20μm). The microstructural characteristics, particularly the occurrence of very small pores, render the infiltration of these porous substrates difficult.

On the contrary, the second type of alumina-based preforms, made of alumina fibers with a silico-aluminous binder (from "Zircar" Company), - named "alumina preform 2" in this paper - shows a very high initial porosity (close to 90%) with rather wide pores ranging from 3 to 50 μm in size. They were exposed to result in easier densification and higher zirconia volume fractions.

Kind of preforms / Characteristics	Alumina preform [1] Transition alumina fibers + Alumina powder	Alumina preform [2] Alumina fibers + silico-aluminous binder	Carbon preform 2D-C-C (40 PAN)
Fiber type	SAFFIL alumina fibers (ICI) mat	Alumina fibers (ZIRCAR)	2D carbon (ex-PAN) woven fabrics
Fiber volume fraction	∿ 0.20	∿ 0.05	∿ 0.30
Initial porosity	∿ 0.60	∿ 0.90	0.30 - 0.60
Pore size	2 ranges: { 0.05 - 0.3 µm { 1 - 20 µm	3 - 50 µm	10 - 300 µm
Apparent density	1.5 - 1.6	0.5 - 0.6	0.9 - 1.4
Skeleton density	3.7	3.1 - 3.2	1.8 - 1.9
Chemical composition (weight %)	Al_2O_3: ∿ 99 SiO_2 : ∿ 1	Al_2O_3: 70 SiO_2 : 30	Carbon fiber: 40 - 75 Pyrocarbon : 25 - 60

Table I: Some characteristics of the starting fibrous preforms

The first substrate, which is the most unfavorable case, has been used to demonstrate the feasibility of zirconia CVI and to optimize the process. Whereas, the densification kinetics have been studied on both preforms .

II.2.2. Carbon-based fibrous preforms

In this preform family, - named here "carbon preform" - 2D-C-C substrates made of a stack of carbon woven fabric layers consolidated with pyrocarbon, have been chosen as a reference material (many studies have been devoted to ceramic-ceramic composites deriving from 2D-C-C substrates). Thus the synthesis conditions and properties of 2D-C-C/ZrO_2 composite materials could be compared with those of related 2D-C-C/ceramic composites (10).

III - OPTIMIZATION OF ZIRCONIA CVI-CONDITIONS

III.1. Outline of the optimization method

The optimization of ZrO_2 CVI main parameters (total flow rate, temperature and total pressure) has been carried out on the basis of three experimental approaches previously used for other ceramic matrices. A kinetic study gives as a function of time, the overall mass of zirconia deposited (i.e. including zirconia deposited both within the pore network and the substrate external surface). A mercury porosimetry study is used to calculate the volume fraction of actually infiltrated zirconia by measuring the residual porosity at an

arbitrary stage of densification. At last, the conclusions drawn from these approaches were confirmed by ZrO_2 distribution profiles recorded, with an electron microprobe X-ray spectrometer analyzer, ($Zr_{K\alpha}$ X-ray line) along a polished cross-section.

By measuring the total zirconia volume fraction $V(ZrO_2)$ and the residual porosity Vp of the sample at an arbitrary stage of the densification (i.e. after 100 hour experiments), it is possible to determine the volume fraction of both surface $V(ZrO_2)_s$ and in-depth $V(ZrO_2)_p$ zirconia deposits.

If W_0 is the apparent initial volume of the sample and Vp_0 the initial open porosity, the initial volume of the pores p_0 is given by:

$$p_0 = W_0 Vp_0 \qquad (1)$$

and the residual volume of the pores at a given stage of densification, by:

$$p = p_0 - Wp = W_0 Vp_0 - Wp \ , \qquad (2)$$

where Wp is the volume of zirconia infiltrated within the pore network. The residual open porosity can be deduced:

$$Vp = \frac{p}{W_0+W_s} = \frac{W_0.Vp_0 - Wp}{W_0+W_s} \ , \qquad (3)$$

W_s being the volume of zirconia deposited on the external surface of the sample.Thus:

$$Vp = \frac{Vp_o - V(ZrO_2)_p}{1 + V(ZrO_2)_s} \qquad (4)$$

$V(ZrO_2)_p$ and $V(ZrO_2)_s$ can be obtained by solving the following system of equations:

$$\begin{cases} V(ZrO_2)_p + Vp.V(ZrO_2)_s = Vp_o - Vp & (5) \\ V(ZrO_2)_p + V(ZrO_2)_s = V(ZrO_2) & (6) \end{cases}$$

Finally,

$$\begin{cases} V(ZrO_2)_p = \dfrac{Vp_o - (1+V(ZrO_2)).Vp}{1 - Vp} & (7) \\ V(ZrO_2)_s = \dfrac{V(ZrO_2) - (Vp_o - Vp)}{1 - Vp} & (8) \end{cases}$$

In order to assess the efficiency of the densification process as it is going on, an infiltration ratio has been defined as:

$$\tau_i = \frac{V(ZrO_2)_p}{V(ZrO_2)} \qquad (9)$$

$\tau_i = 1$ when deposition occurs only within the pore network.

III.2. Influence of the total gas flow rate

III.2.1. Alumina based preforms

The infiltration kinetic curves in the case of alumina preform 1, drawn in figure 1-a for three values of the total gas flow rate, T = 940°C and P = 2 kPa, reveal a marked decrease of the overall deposition rate after about a 30 hours run. This decrease is the more important as the total gas flow rate is high. For 300 $cm^3\ mn^{-1}$, zirconia formation decreases drastically as early as after 50 hours . Zirconia volume fraction obtained for a total flow rate of 123 $cm^3\ mn^{-1}$ is lower than for 180 $cm^3\ mn^{-1}$ but the overall deposition rate Ra keeps higher after 100 hours (Table II), which is probably more favorable to achieve a good densification.

The corresponding cumulative pore spectra are presented in figure 1-b. The contribution of the large pores (more than 1μm in size) seems to be reduced more rapidly than those of small pores. The volume fraction of actually infiltrated zirconia $V(ZrO_2)_p$, deduced from porosimetry data, is higher for a total flow rate of 180 $cm^3\ mn^{-1}$ (Table II). Simultaneously, the infiltration ratio τ_i

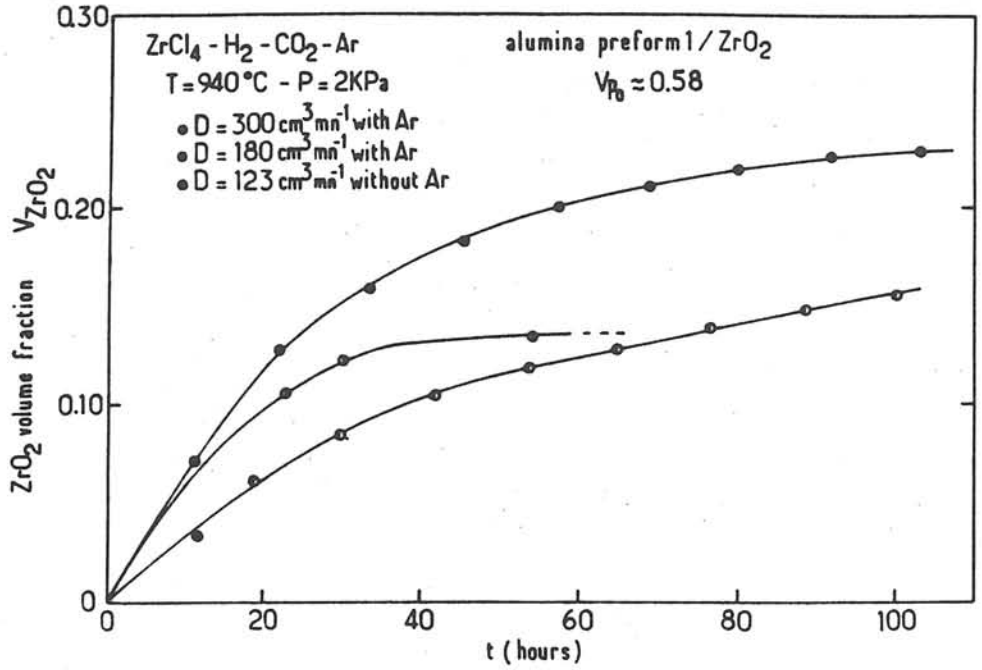

(a)

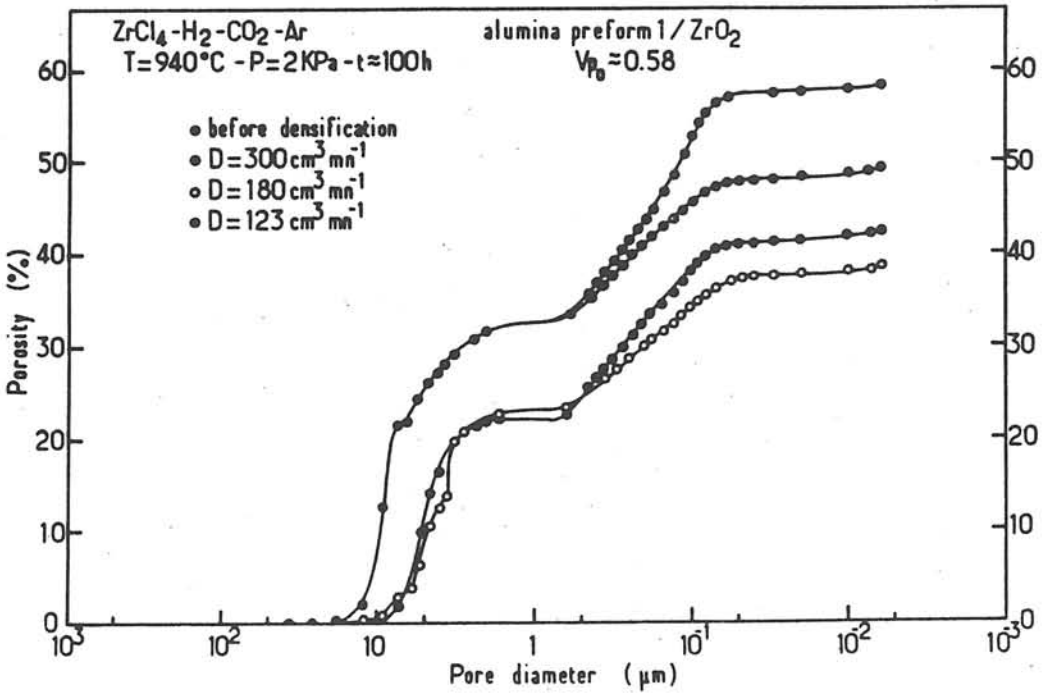

(b)

Fig. 1 - Influence of the total gas flow rate on (a) the infiltration kinetics, (b) the mercury porosimetry spectra, up to an arbitrary stage of densification of 100 hours for transition alumina fibers + alumina powder preforms

Experimental parameters			Sample n°	t (h)	Ra (h^{-1})	V_{ZrO_2}	V_p	$V_{(ZrO_2)_p}$	$V_{(ZrO_2)_s}$	τ_I
T (°C)	P (KPa)	D (cm^3/mn)								
940	2	300	1	54.2*	4.6×10^{-4}*	0.133	0.488	0.053	0.080	~0.39*
			2	54.2	4.6×10^{-4}	0.135	-	-	-	-
940	2	180	1	103.3	2.6×10^{-4}	0.232	0.383	0.175	0.057	0.75
			2	103.3	1.7×10^{-4}	0.224	-	-	-	-
940	2	123	1	100.4	6.7×10^{-4}	0.164	0.421	0.156	0.008	0.95
			2	100.4	5.0×10^{-4}	0.144	-	-	-	-
910	2	180	1	95.6	2.5×10^{-4}	0.223	0.349	0.223	0	1
			2	95.6	2.5×10^{-4}	0.184	-	-	-	-
940	2	180	1	102.5	4.8×10^{-4}	0.194	0.403	0.165	0.029	0.85
			2	102.5	9.5×10^{-4}	0.147	-	-	-	-
960	2	180	1	103.1	2.2×10^{-3}	0.122	0.518	0	0.122	0
			2	103.1	1.4×10^{-3}	0.101	-	-	-	-
910	2	180	1	95.6	2.5×10^{-4}	0.223	0.349	0.223	0	1
			2	95.6	2.5×10^{-4}	0.184	-	-	-	-
910	5	180	1	101.3	7.7×10^{-4}	0.216	0.446	0.068	0.148	0.31
			2	101.3	5.8×10^{-4}	0.205	-	-	-	-

* the values are obtained before the arbitrary stage of the densification

Table II: Influence of the experimental parameters on the infiltration ratio for alumina preform 1

is found, after 100 hours, higher for the lowest gas flow rate (0.95), which is consistent with the kinetic result.

The favorable effect of lowering the total gas flow rate has been confirmed by zirconia distribution profiles (Fig.2). The experiment performed at 123 cm^3 mn^{-1} reveals an in-depth deposition but a zirconia concentration gradient is observed from the external surface to the core of the sample.

III.2.2. Carbon based preforms

The overall zirconia volume fraction seems to increase quasi-linearly versus time over the 100 hours investigated for total flow rates lower than 180 cm^3 mn^{-1} (Fig.3-a). Only a small deviation to linearity is observed at the beginning of the infiltration process and essentially above 123 cm^3 mn^{-1}.It could be due to some transient oxidation etching of the carbon-based preforms as suggested by the thermodynamic approach of ZrO_2 CVD on reactive substrates (8).

On the basis of the mercury porosimetry spectra (Fig.3-b), the volume fractions of actually infiltrated zirconia $V(ZrO_2)_p$ are found to be lower than for the oxide substrates (table III). This result can be explained by both the slight etching of the carbon substrates (which has not been taken into account in the calculation) and the difference between initial porosities of alumina and carbon-based substrates.

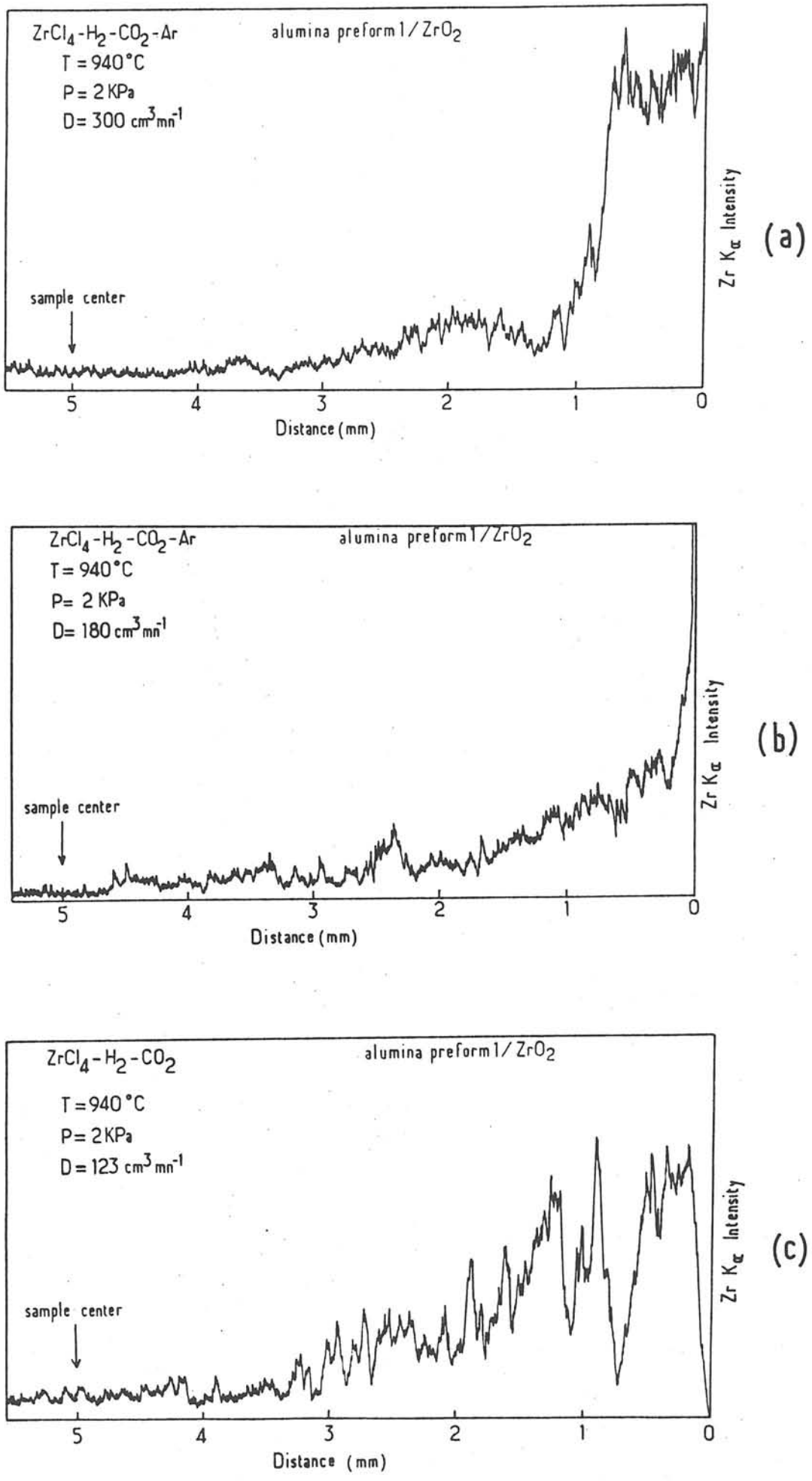

Fig. 2 - Influence of the total gas flow rate on the zirconia distribution profile within transition alumina fibers + alumina powder preforms (a) D = 300 $cm^3 . mn^{-1}$; (b) D = 180 $cm^3 . mn^{-1}$; (c) D = 123 $cm^3 . mn^{-1}$

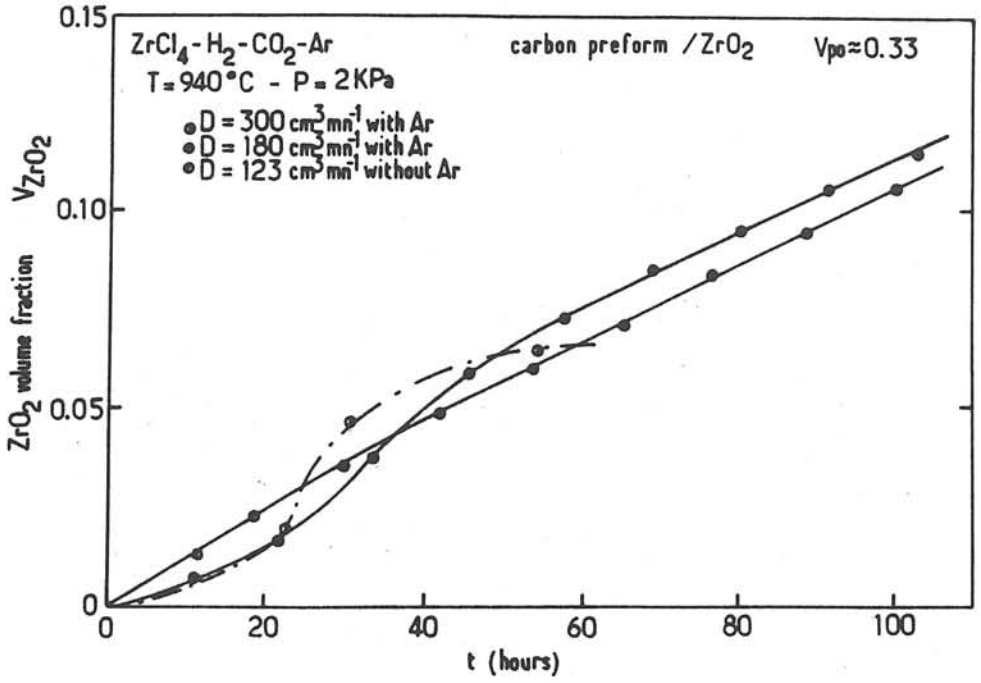

(a)

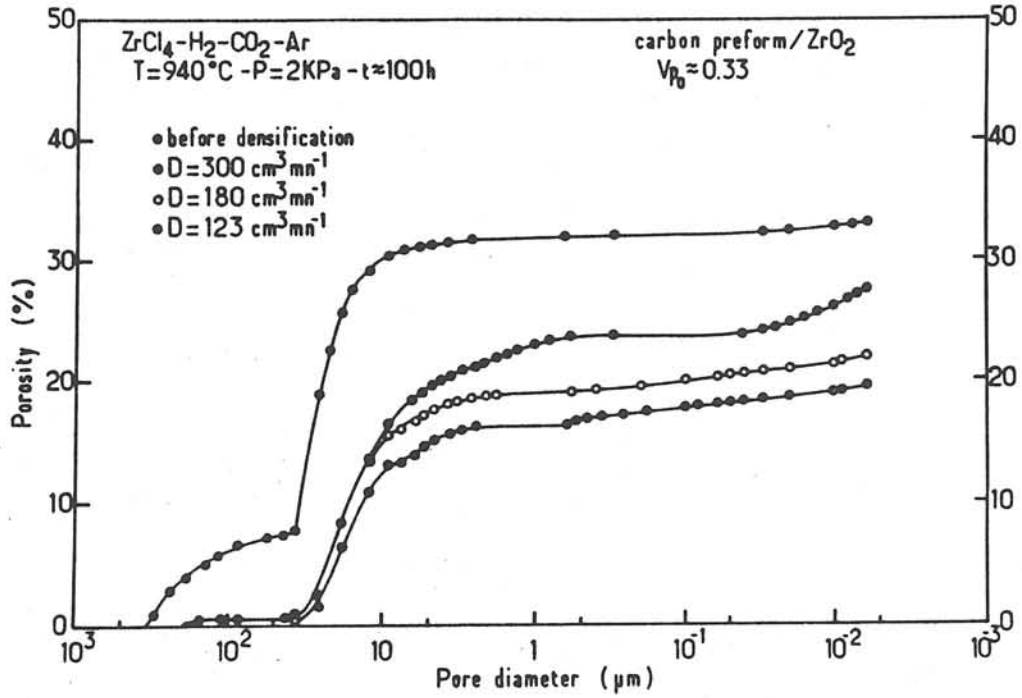

(b)

Fig. 3 - Influence of the total flow rate on: (a) the infiltration kinetics, (b) the mercury porosimetry spectra, up to an arbitrary stage of densification of 100 hours for 2D-C-C preforms

Experimental parameters			Sample n°	t (h)	Ra (h^{-1})	V_{ZrO_2}	V_p	$V_{(ZrO_2)_p}$	$V_{(ZrO_2)_s}$	τ_I
T (°C)	P (KPa)	D (cm^3/mn)								
940	2	300	1	54.2*	3.3×10^{-4}*	0.057	0.273	0.057	0	1*
			2	54.2	1.1×10^{-3}	0.071	-	-	-	-
940	2	180	1	103.3	8.8×10^{-4}	0.129	0.218	0.107	0.022	0.83
			2	103.3	7.0×10^{-4}	0.100	-	-	-	-
940	2	123	1	100.4	9.1×10^{-4}	0.114	0.195	0.114	0	1
			2	100.4	8.3×10^{-4}	0.096	-	-	-	-
910	2	180	1	95.6	3.2×10^{-4}	0.131	0.219	0.106	0.025	0.81
			2	95.6	3.8×10^{-4}	0.108	-	-	-	-
940	2	180	1	103.3	8.8×10^{-4}	0.129	0.218	0.107	0.022	0.83
			2	103.3	7.0×10^{-4}	0.100	-	-	-	-
960	2	180	1	103.1	1.4×10^{-3}	0.136	0.231	0.099	0.037	0.73
			2	103.1	1.0×10^{-3}	0.130	-	-	-	-
910	2	180	1	95.6	3.2×10^{-4}	0.131	0.219	0.106	0.025	0.81
			2	95.6	3.8×10^{-4}	0.108	-	-	-	-
910	5	180	1	101.3	2.4×10^{-3}	0.210	0.434	0	0.210	0
			2	101.3	2.4×10^{-3}	0.214	-	-	-	-

* The values are obtained before the arbitrary stage of densification

Table III: Influence of the experimental parameters on the infiltration ratio for carbon preform

The highest infiltration ratio τ_i (about 1 after 100 hours) is found here again for the lowest total gas flow rate. This result has been confirmed by the X-ray microprobe profiles, which show a quasi-homogeneous zirconia distribution profile inside the preform for $123 cm^3 mn^{-1}$ (Fig.4).

In spite of a lower overall porosity, the 2D-C-C preforms seem to be easier to densify at least at the beginning of the process. The infiltration rate is almost constant (up to 100 hours) and for the lowest value of the total gas flow rate, no zirconia concentration gradient is observed within the pore network of the preform. This behaviour can be attributed to the presence of large pores (more than 10μm) in the carbon preforms, whereas in the alumina-based substrates the contribution of small pores (hard to fill up) is more important.

III.3. Influence of temperature

A previous kinetic study of ZrO_2 CVD has shown that the deposition process is kinetically controlled by chemical reactions (probably water formation) at least up to a substrate temperature of 1000°C (9). One of the conditions for in-depth deposition is to have a kinetic process controlled by chemical reactions (4). So temperatures lower than 1000°C have been chosen to optimize this experimental parameter, the total pressure and the total flow rate being maintained respectively at 2kPa and $180 cm^3 mn^{-1}$.

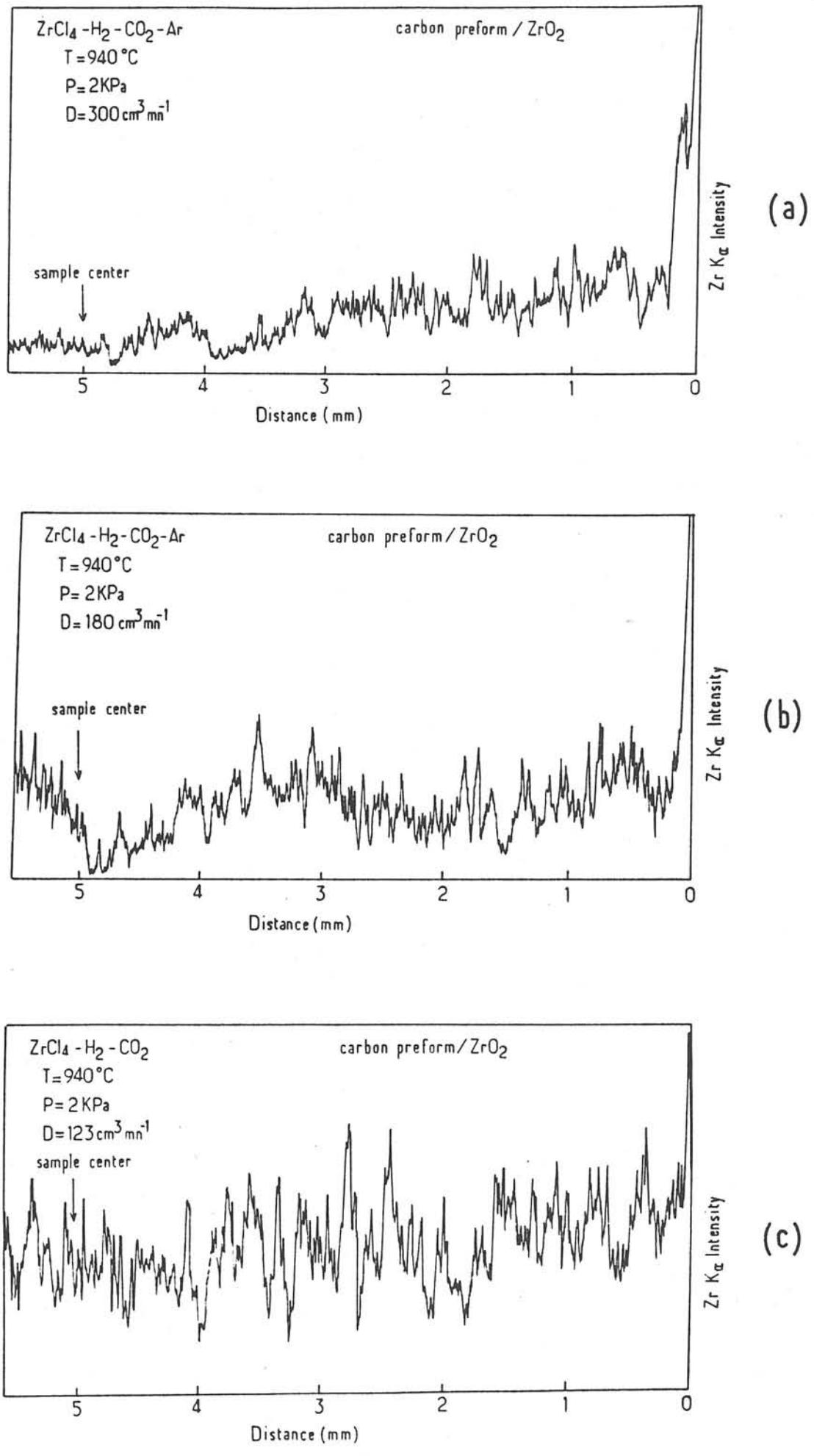

Fig. 4 - Influence of the total gas flow rate on the zirconia distribution profile within 2D-C-C preforms:
(a) D = 300 $cm^3 . mn^{-1}$; (b) D = 180 $cm^3 . mn^{-1}$; (c) D = 123 $cm^3 . mn^{-1}$

III.3.1. Alumina-based preforms

The experimental data reveal a drastic influence of the substrate temperature on the densification process (Figs. 5, 6). For a deposition temperature of 960°C, the infiltration ratio τ_i, after 100 hours, is close to 0 (table II) and the deposition is mainly localized at the external surface of the preform giving rise to a film about 0.3 mm in thickness. On the contrary, for T = 910°C, the infiltration ratio τ_i is very close to 1, the surface deposition hardly occurs and the oxide deposit reaches the center of the preform. However a significant gradient of zirconia-concentration is observed along the cross section of the sample.

III.3.2. Carbon-based preforms

The beginning of the densification of 2D-C-C preforms is not so influenced by temperature variations than that of the oxide preforms previously studied . The various experimental approaches give rather similar results for all temperatures ranging from 910 to 960°C (Fig. 7, 8). As an example, the infiltration ratio τ_i exhibits in the three cases rather high values (close to 0.8) (table III). Only a gradient of zirconia concentration and an external surface coating are observed for a deposition temperature of 960°C, which indicates here also the low temperature range as favourable to a good densification.

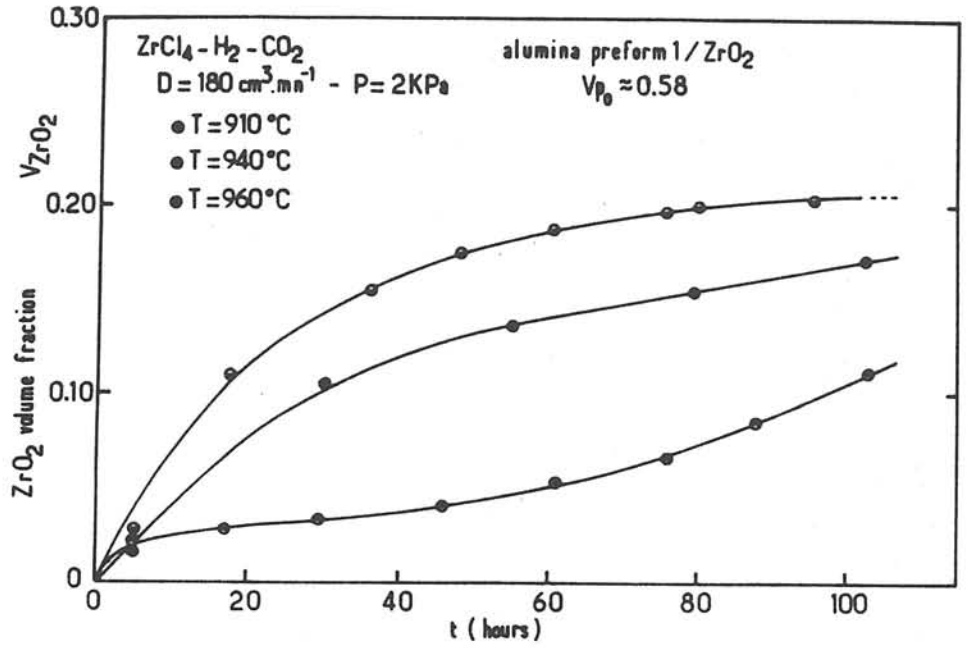

(a)

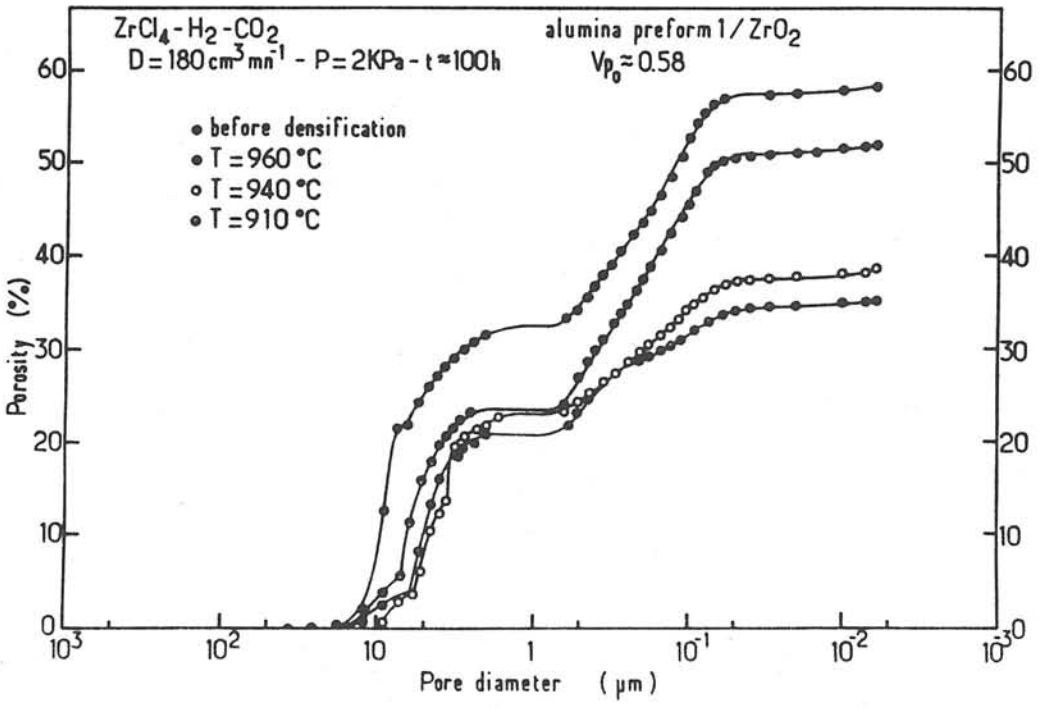

(b)

Fig. 5 - Influence of temperature on: (a) the infiltration kinetics, (b) the mercury porosimetry spectra, up to an arbitrary stage of densification of 100 hours for the transition alumina fibers + alumina powder preforms

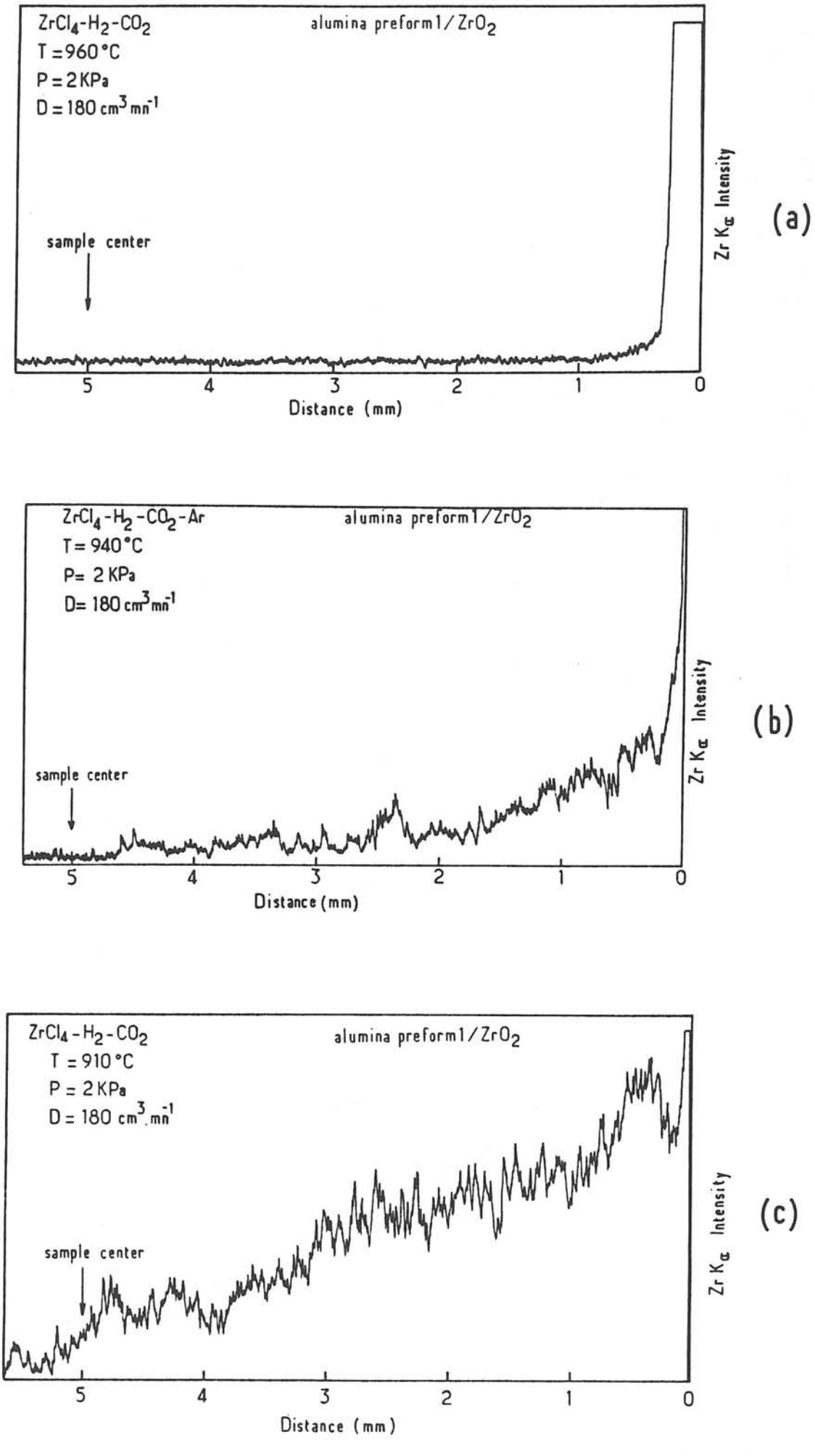

Fig. 6 - Influence of temperature of the zirconia distribution profile within the transition alumina fibers + alumina powder preforms (a) T = 960°C; (b) T = 940°C; (c) T = 910°C

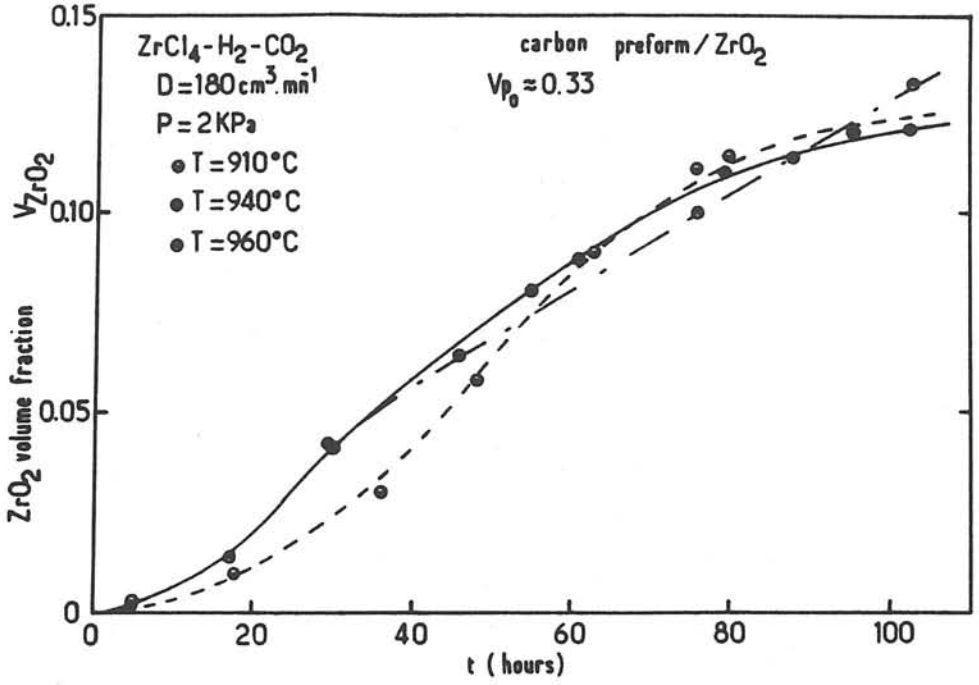

(a)

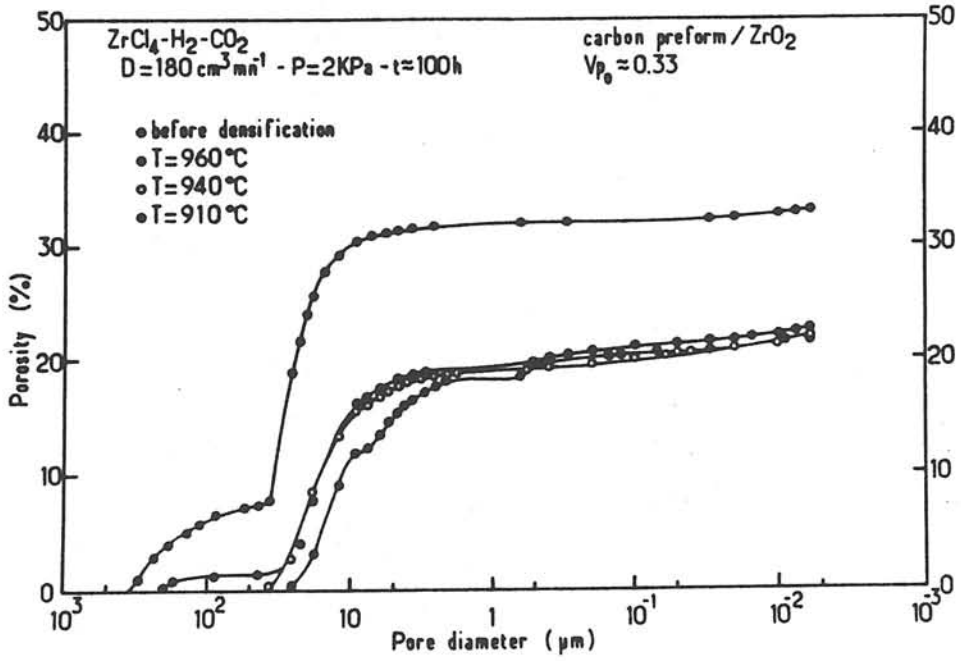

(b)

Fig. 7 - Influence of temperature on (a) the infiltration kinetics, (b) the mercury porosimetry spectra, up to an arbitrary stage of densification of 100 hours for the 2D-C-C preforms

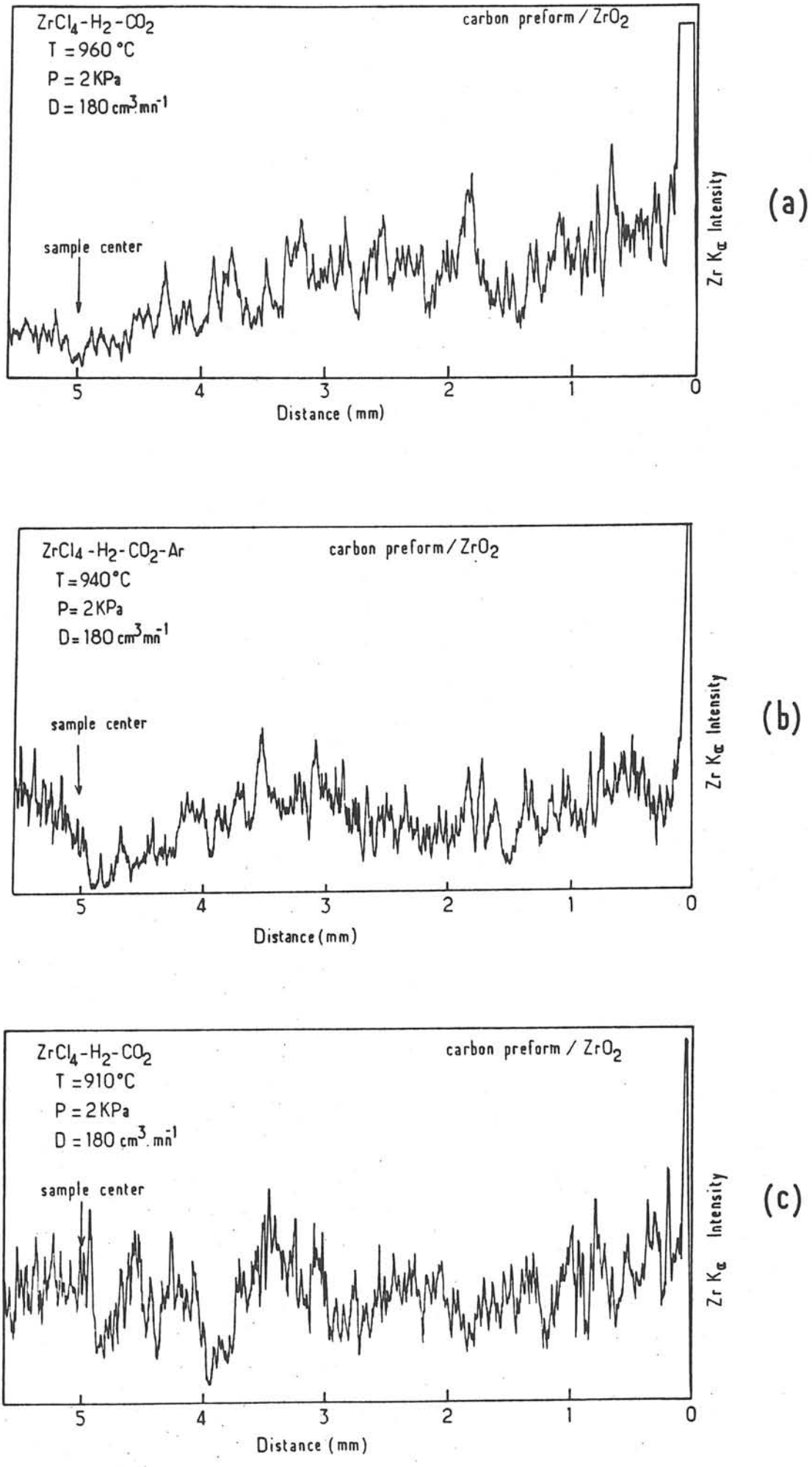

Fig. 8 - Influence of temperature on the zirconia distribution profile within the 2D-C-C preforms (a) T = 960°C; (b) T = 940°C; (c) T = 910°C

III.4. Influence of total pressure

This parameter has been investigated for a total gas flow rate of 180 cm^3 mn^{-1} and a temperature of 910°C. Two values of the total pressure have been chosen, which take into account the problem of homogeneous nucleation usually occurring for pressures higher than 5 kPa (9).

III.4.1. Alumina-based preforms

The kinetics curves do not reveal any great difference between both densification pressures (Fig.9-a). But the mercury porosimetry approach shows two different cumulative pore spectra corresponding to infiltration ratios τ_i of 1 for 2kPa and only 0.31 for 5kPa (Fig. 9-b, table II). These unfavorable conditions for 5 kPa have been confirmed by the experimental zirconia distribution profiles which evidence a ZrO_2 film of about 0.4mm in thickness at the external surface of the preform and no in-depth deposition. A much less steep zirconia gradient is observed for a densification pressure of 2kPa (Fig.10).

III.4.2. Carbon-based preforms

The optimization of the infiltration process for carbon porous substrates is again difficult as a function of total pressure. The experimental results given in figures 11 and 12, and table III, are rather similar for both pressure values. The infiltration ratio τ_i remains high and zirconia distribution is homogeneous within the whole porous sample.

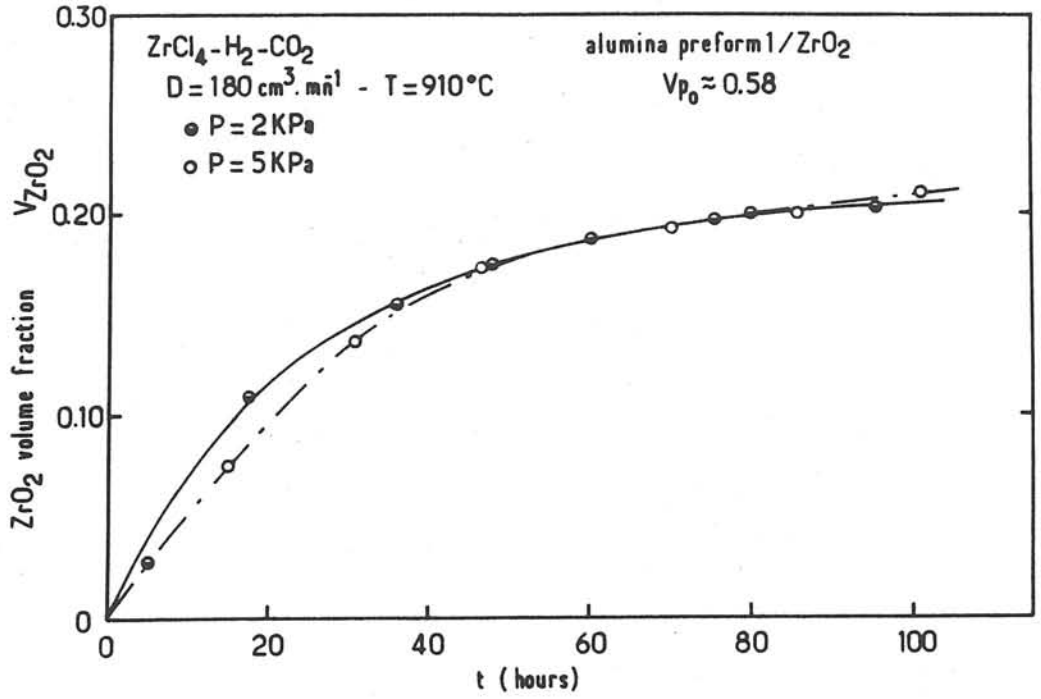

(a)

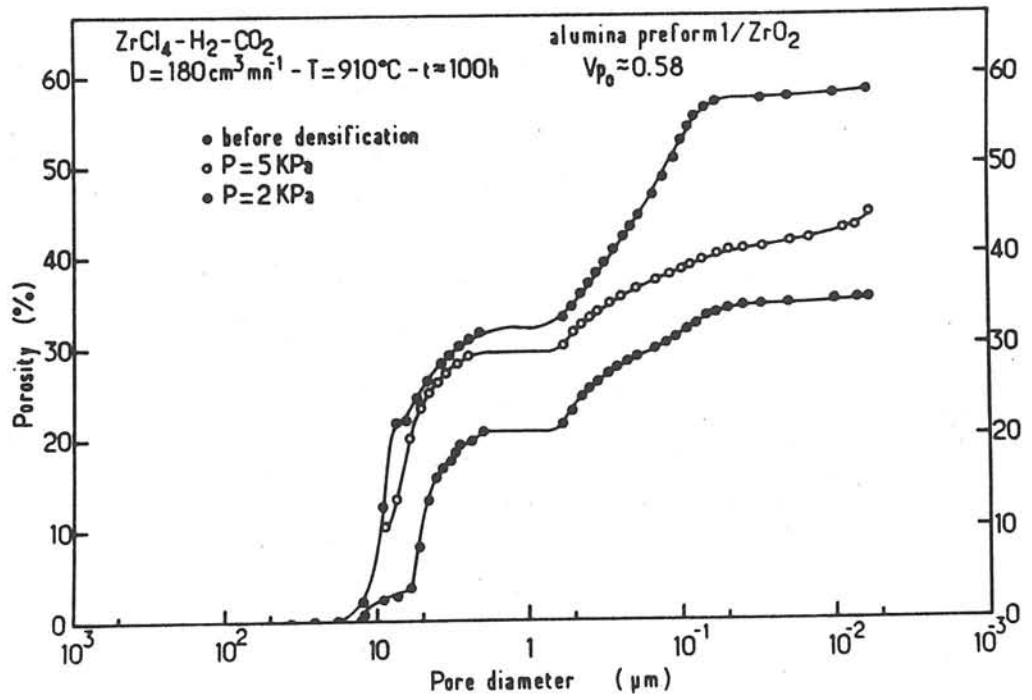

(b)

Fig. 9 - Influence of total pressure on (a) the infiltration kinetics, (b) the mercury porosimetry spectra, up to an arbitrary stage of densification of 100 hours for the transition alumina fibers + aluminapowder preforms.

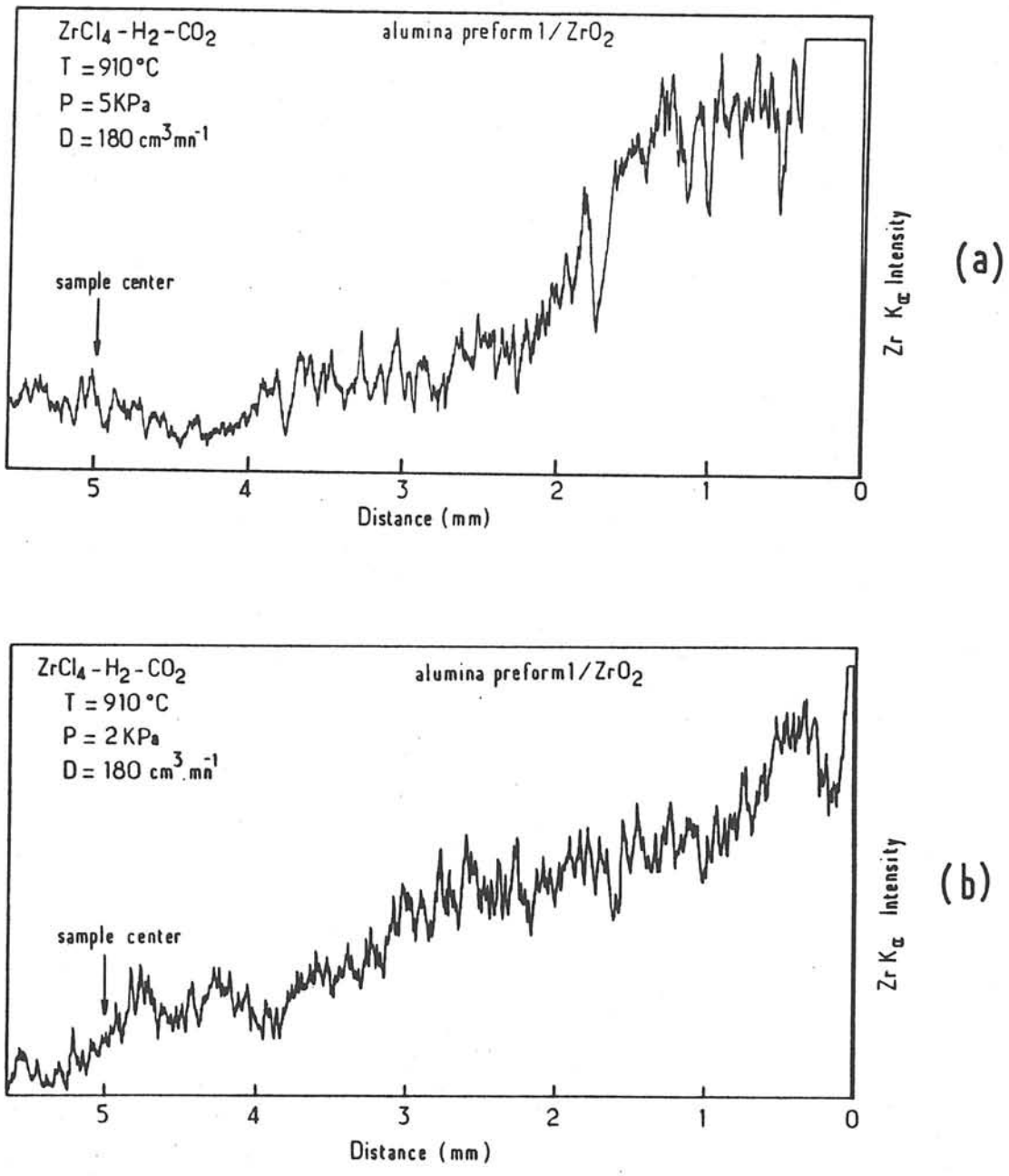

Fig. 10 - Influence of total pressure on the zirconia distribution profile within the transition alumina fibers + alumina powder preforms (a) P = 5 kPa; (b) P = 2 kPa

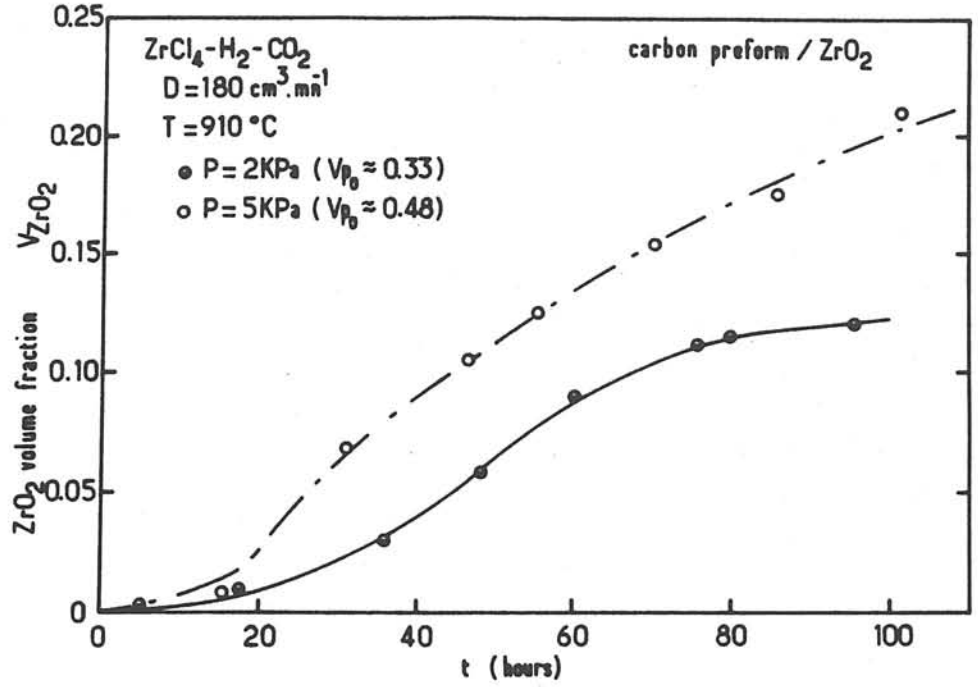

(a)

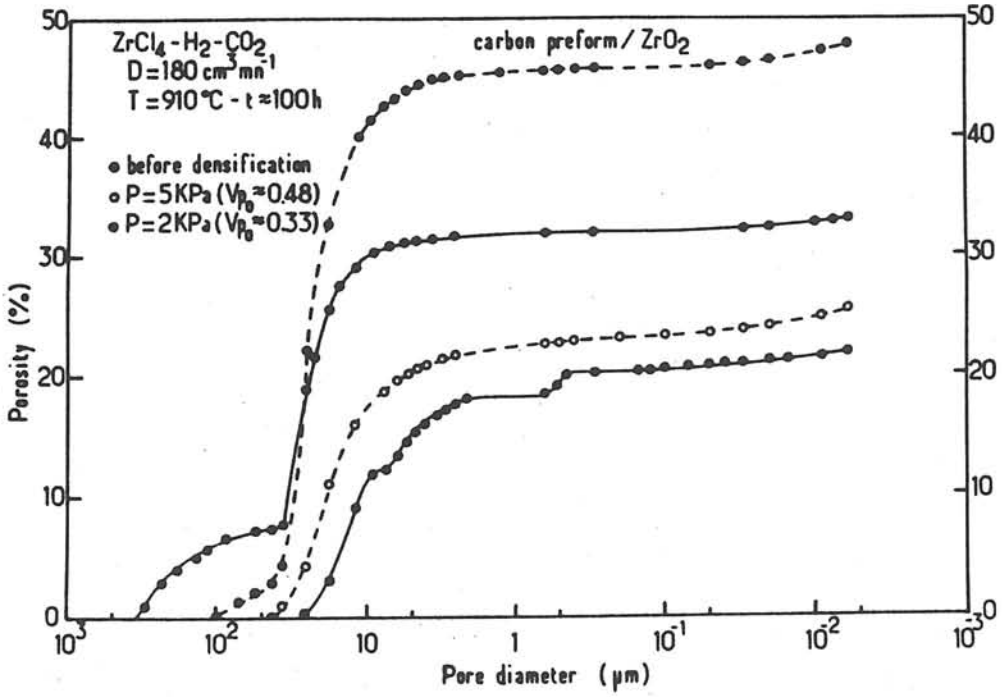

(b)

Fig. 11- Influence of the total pressure on (a) the infiltration kinetics, (b) the mercury porosimetry spectra, up to an arbitrary stage of densification of 100 hours for 2D-C-C preforms

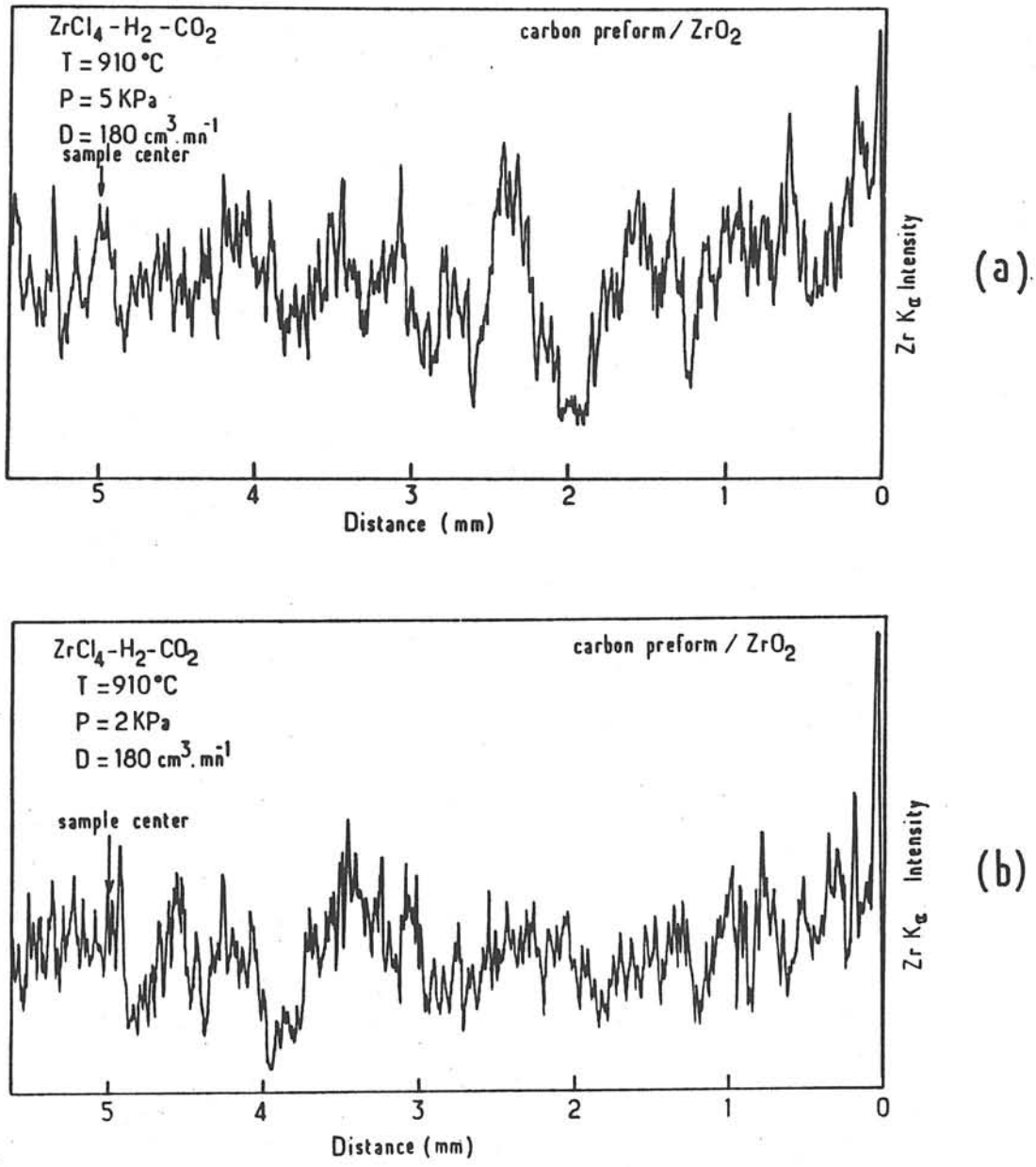

Fig. 12 - Influence of the total pressure on the zirconia distribution profil within the 2D-C-C preforms (a) P = 5 kPa; (b) 2 kPa

III.5. Discussion

Over the beginning period of densification of about 100 hours, both preforms exhibit a different behavior with respect to the infiltration process itself and to the optimization of the experimental parameters. The 2D-C-C preforms seem to be easier to densify than the alumina-based preforms, essentially because the former include only large pores of more than 10 μm in size and the latter contain small pores of about 0.1 μm whose contribution to porosity is not negligible.

The three main experimental parameters have been optimized on the basis of the conjunction of several investigation methods. It appears that zirconia CVI may be performed with various types of porous fibrous substrates under the following conditions: a total gas flow rate of $100cm^3\ mn^{-1}$, a temperature of 910°C and a total pressure of 2kPa for the kind of laboratory equipment described previously (9). As it is known in this field, the CVI parameters given here will have to be readjusted for a deposition chamber of different size.

IV - MICROSTRUCTURE OF ZIRCONIA MATRIX CERAMIC-CERAMIC COMPOSITE MATERIALS DURING THE DENSIFICATION PROCESS

X-ray diffraction patterns of zirconia matrix composite materials have shown that zirconia has, in all kinds of preforms, the monoclinic modification at room temperature.

IV.I. Alumina-based preforms

A scanning electron microscopy micrograph with backscattered electrons is shown in figure 13-a for a polished surface of an alumina-zirconia composite material. The heavy elements coming out more clearly than the light ones, this technique which permits here to distinguish zirconia/alumina matrix areas and the alumina-based fibers. Thus an in-depth infiltration of zirconia within the alumina porous structure is evidenced.

Figure 13-b represents the failure surface of the same type of preform partially densified. One can notice the polycrystalline structure of zirconia coating the fibers with a good adhesion. No delamination is observed at the fiber/matrix interface and the fracture is brittle as in the case of alumina-alumina composite materials (6).

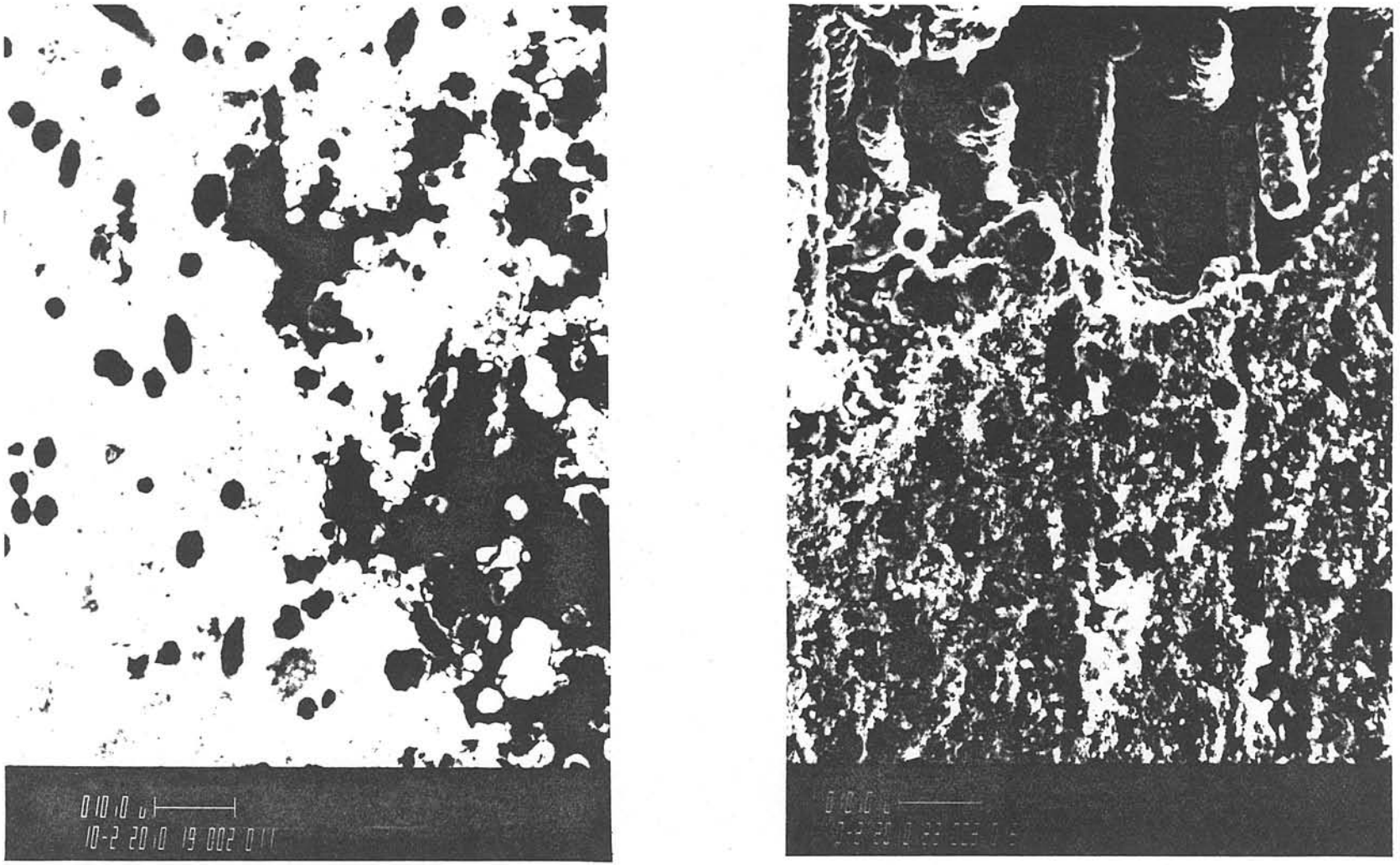

(a) (b)

Fig. 13 - SEM micrograph of zirconia-alumina composite materials: (a) polished cross section observed with backscattered electrons; (b) fracture surface

IV.2. Carbon-based preforms

The SEM micrograph in figure 14-a shows clearly zirconia infiltration within the pore network of a carbon fibrous structure predensified by pyrocarbon.

The failure surface (Fig. 14-b) exhibits some delamination at both carbon fiber/pyrocarbon and pyrocarbon/zirconia interfaces, which suggests a weaker adhesion between zirconia and pyrocarbon than between zirconia and alumina.

IV.3. Discussion

The microscopic observations seem to show that carbon/zirconia composite materials may exhibit a better toughness than alumina/zirconia ones (10). The relatively weak adhesion between zirconia and pyrocarbon can result partly from the different crystallochemical nature of each material and partly from some gas phase oxydation etching of the pyrocarbon during the first stage of the densification. This etching of the preform involves evolution of carbon monoxide which is unfavorable to the adhesion of zirconia deposit. This transient oxydation step, which is in accordance with the thermodynamic study of ZrO_2 CVD (8), has been evidenced over about 30 hours in the kinetic approach of the previous optimization study (cf. III.2.2.).

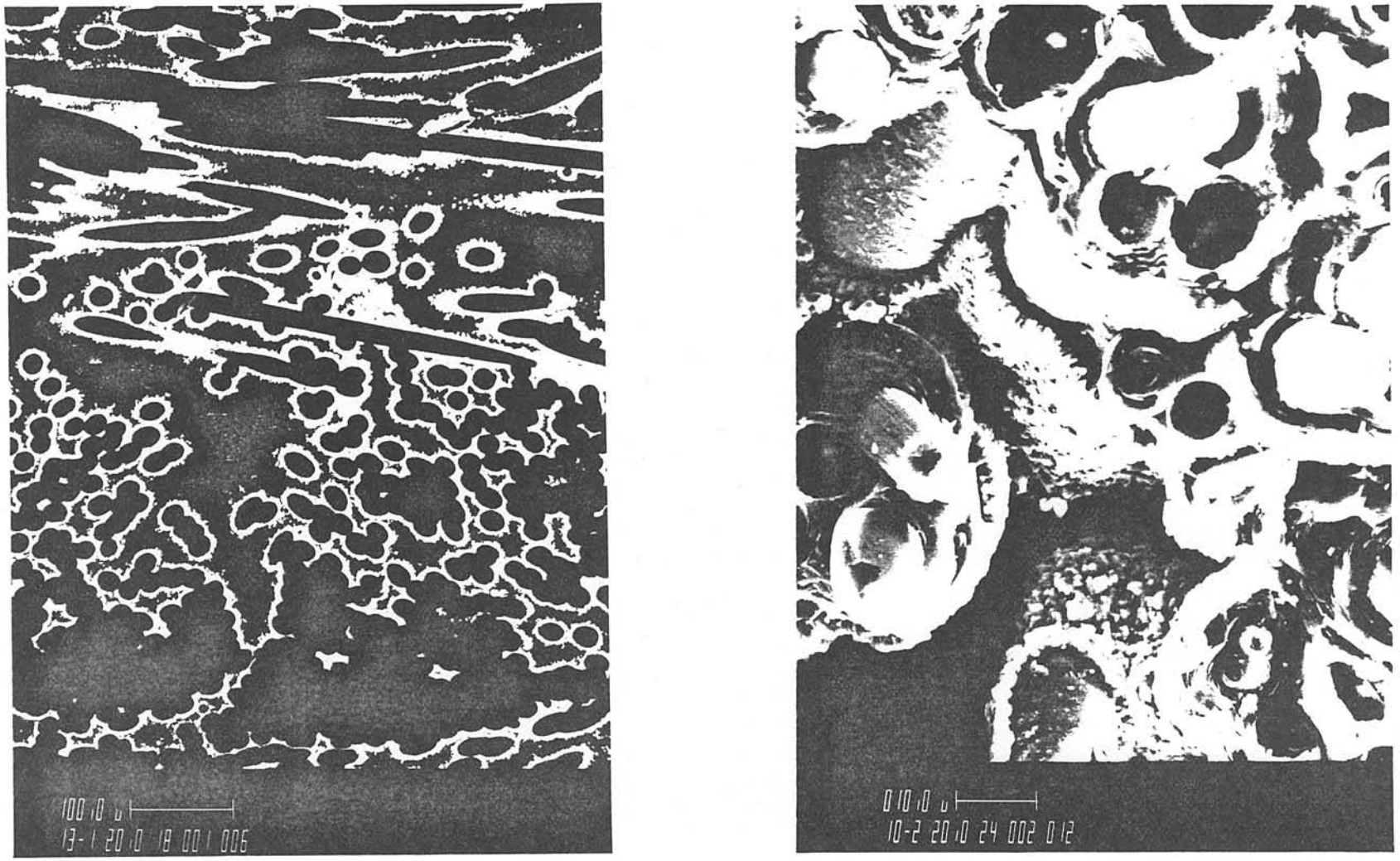

(a) (b)

Fig. 14 - SEM micrograph of zirconia-carbon composite material (a) polished cross section observed with backscattered electrons; (b) fracture surface

V - KINETIC STUDY OF THE DENSIFICATION OF CERAMIC FIBROUS PREFORMS BY ZIRCONIA

In order to prepare ceramic-ceramic composite materials with a zirconia-based matrix, it is necessary to achieve the densification process as completely as possible. Previous kinetic approaches for various CVI systems (3, 4) have shown that the overall infiltration rate usually decreases as the process is going on and depends on the features of the pore network. A kinetic study has been carried out on the basis of the variation of the total zirconia volume fraction, on the one hand, and the residual porosity, on the other hand. Moreover the volume fraction of both surface $V(ZrO_2)_s$ and in-depth $V(ZrO_2)_p$ zirconia deposits and the resulting infiltration ratio τ_i have been calculated at any stage of the densification (tables IV, V, VI).

The residual porosity p/p_0, as defined by Rossignol et al. with respect to the initial porous volume p_0 (3), can be expressed by:

$$\frac{p}{p_0} = \frac{p_0 - Wp}{p_0} = 1 - \frac{Wp}{p_0} = 1 - \frac{V(ZrO_2)_p}{Vp_0} \qquad (10)$$

It has been plotted versus time on a semi-logarithmic scale in figure 15, in the case of the infiltration conditions previously optimized.

Infiltration time ti (h)	V_{ZrO_2} (from the kinetic study)	V_p (from the mercury porosimetry)	$V_{(ZrO_2)_p}$	$V_{(ZrO_2)_s}$	τ_I	Log $\frac{p}{p_0}$
0	0	0.625	0	0	0	0
42.3	0.099	0.468	0.099	0	1	- 0.172
81.4	0.244	0.370	0.244	0	1	- 0.495
123.6	0.315	0.306	0.315	0	1	- 0.701
162.5	0.387	0.258	0.360	0.027	0.93	- 0.858
213.1	0.412	0.24	0.376	0.036	0.91	- 0.920

Table IV: Kinetics of densification of alumina preform 1
($\bar{V}_{p_0}$ = 0.625, D = 100 $cm^3 . mn^{-1}$, T = 910°C, P = 2 KPa)

Infiltration time ti (h)	V_{ZrO_2} (from the kinetic study)	V_p (from the mercury porosimetry)	$V_{(ZrO_2)_p}$	$V_{(ZrO_2)_s}$	τ_I	Log $\frac{p}{p_0}$
0	0	0.875	0	0	0	0
39.3	0.129	0.717	0.129	0	1	- 0.159
150.4	0.301	0.555	0.301	0	1	- 0.419
242.3	0.427	0.403	0.427	0	1	- 0.664
316.7	0.520	0.326	0.520	0	1	- 0.894
438.3	0.618	0.226	0.618	0	1	- 1.21
618.9	0.708	0.152	0.708	0	1	- 1.63
727.5	0.734	0.136	0.734	0	1	- 1.80

Table V: Kinetic of the densification of alumina preform 2
($\overline{V}_{p_0} \sim 0.88$, $D = 100\ cm^3.\ mn^{-1}$, $T = 910°C$, $P = 2$ KPa)

Infiltration time ti (h)	V_{ZrO_2} (from the kinetic study)	V_p (from the mercury porosimetry)	$V_{(ZrO_2)_p}$	$V_{(ZrO_2)_s}$	τ_I	Log $\frac{p}{p_0}$
0	0	0.50	0	0	0	0
116.7	0.095	0.408	0.090	0.005	0.95	- 0.198
209.4	0.193	0.327	1.163	0.03	0.85	- 0.395
513.7	0.295	0.159	0.295	0	1	- 0.892
650.7	0.342	0.129	0.375	0	1	- 1.39

Table VI: Kinetic of the densification of carbon preform
($\overline{V}_{p_0} \sim 0.50$, D = 100 $cm^3 . mn^{-1}$, T = 910°C, P = 2 KPa)

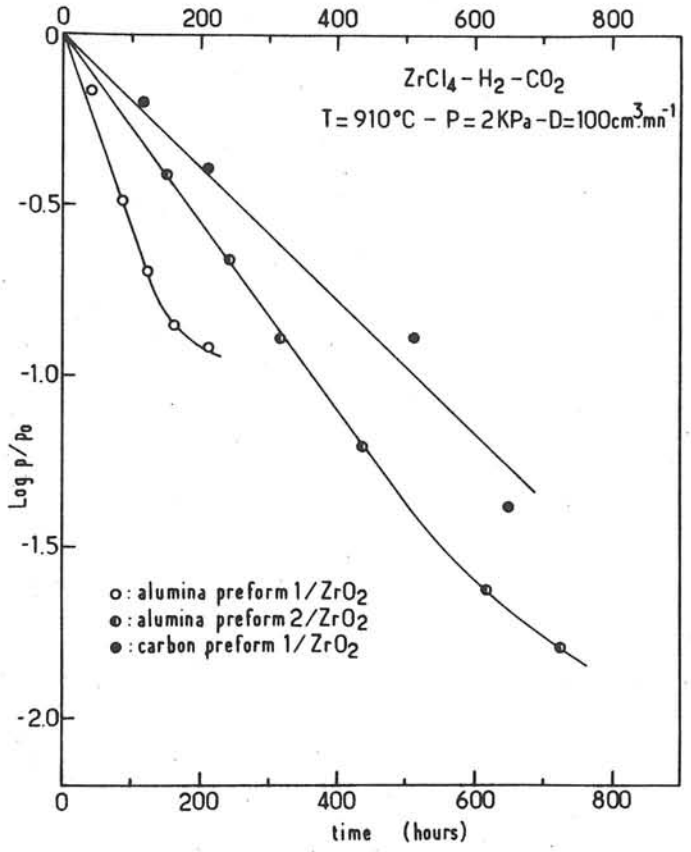

Fig. 15 - Zirconia infiltration kinetics of fibrous porous preforms ($D = 100\ cm^3 . mn^{-1}$; T = 910°C; P = 2 Kpa)

V.1. "Transition alumina fibers + alumina powder" preforms

The rapid decrease of the residual porosity as a function of densification time reveals the high efficiency of the infiltration process. The variation of Log p/p_0 is linear up to 150 hours. At the same time, the infiltration ratio τ_i is maintained close to one. This empirical linear law has been found previously for TiC and B_4C infiltration processes. Beyond 150 hours, a deviation to linearity is observed and τ_i decreases down about 0.9, which means the occurrence of some external deposition and slower infiltration process (with probably an obstruction of some pores of the preform). A residual porosity of 24% is obtained at the end of the process.

These results show that the experimental conditions are not yet totally optimized for this kind of porous substrates which are difficult to densify.

V.2. "Alumina fibers + silico-aluminous binder" preforms

The residual porosity decreases also linearly but more slowly than for the previous type of preforms. This difference is essentially due to the higher value of the initial porosity (90% instead of 60%). The infiltration ratio τ_i is very close to one over all the studied densification time (i.e. more than 700 hours). Only a small deviation to linearity seems to occur beyond 600 hours, which could be attributed to a beginning of pore obstruction. The extent of densification is much higher for this second kind of preforms probably because of the larger mean size

of the pores. Consequently a relatively low residual porosity (about 14%) is obtained at the end of the process.

The optimization previously reported is suitable for this second preform which is not so difficult to densify.

V.3. "2D-C-C" preforms

For the carbon-based preforms, whose initial porosity is the lowest (about 50%), the densification kinetics is the slowest. The decrease of the residual porosity is again linear up to a 700 hours and the corresponding slope is the lowest among the three studied substrates. The large pores between the carbon fabric layers are probably responsible for these good densification conditions without external deposition and pore obstruction. After a 650 hours, the residual porosity is lower than 13% and the infiltration ratio τ_i remains close to one.

In this last case, the experimental parameters are well optimized and the process could be further carried on in order to still improve the degree of densification.

ACKNOWLEDGEMENTS

The authors wish to thank S.E.P. for the supply of the preforms and for its financial support as well as the French Ministry of Defense (DRET).

REFERENCES

1 - R. NASLAIN, P. HAGENMULLER, F. CHRISTIN, L. HERAUD and J.J.CHOURY, Proc. of ICCM-3 "Advances in Composite Materials" (A.R. Bunsell et al., eds.) Paris, 1980, Pergamon Press, 2 (1980) 1084-1097.

2 - L. HERAUD, F. CHRISTIN, R. NASLAIN and P. HAGENMULLER, Proc. of Int. CVD-8 (J.M. Blocher et al., eds.) Paris 1981,The Electrochem. Soc., Pennington N.J. (1981) 782-789.

3 - J.Y. ROSSIGNOL, F. LANGLAIS and R. NASLAIN, Proc. of Int. CVD - 9 (Mc. D. Robinson et al., eds.) Cincinnati 1984, The Electrochem. Soc., Pennington N.J. (1984) 596-614.

4 - H. HANNACHE, F. LANGLAIS and R. NASLAIN, Proc. of Euro CVD-5 (J.O. Carlson and J. Lindström, eds.) Uppsala 1985, 219-233.

5 - H. HANNACHE, R. NASLAIN and C. BERNARD, J. Less-Common Metals, 95 (1983) 221-246.

6 - R. COLMET, I. LHERMITTE-SEBIRE and R. NASLAIN, Advanced Ceramic Materials,1, 2 (1986) 185-191.

7 - E.C. SUBBARAO, in "Science and Technology of Zirconia", A.H. Hener and L.W.Hobbs, eds. (The American Ceramic Society, Columbus (1981) 1.

8 - J. MINET, F. LANGLAIS, R. NASLAIN and C. BERNARD, J. Less-Common Metals, 119 (1986) 219-235.

9 - J. MINET, F. LANGLAIS and R. NASLAIN, J. Less-Common Metals,132 (1987) 273-287.

10 - K. BRENNFLECK, E. FITZER and G. MACK, in J.M. Blocher, G.E. Vuillard and G. Wahl (eds.), Proc. CVD-VIII, The Electrochemical Society, Pennington, N.J. 1981, 672.

11 - J. MINET et al., to be published.

List of symbols

Volumes

W_0 = apparent initial volume of the preform

Wp = $W(ZrO_2)_p$ = volume of ZrO_2 actually infiltrated within the network

W_s = $W(ZrO_2)_s$ = volume of ZrO_2 deposited at the external surface of preform

p_0 = initial pore volume

p = residual pore volume at any stage of the densification = p_0-Wp

Volume fractions

$V(ZrO_2)$ = total ZrO_2 volume fraction = $(Wp+W_s)/W_o$

$V(ZrO_2)_p$ = volume fraction of ZrO_2 actually infiltrated = Wp/W_o

$V(ZrO_2)_s$ = volume fraction of ZrO_2 deposited at the surface = W_s/W_o

Vp_o = initial open porosity = p_o/W_o

Vp = residual open porosity = $p/(W_o+W_s)$.

Chapitre IV

COMPOSITES A MATRICE A BASE DE ZIRCONE :

PROPRIETES MECANIQUES

Soumis à "Journal of Materials Science"

THERMO - MECHANICAL PROPERTIES AND RESISTANCE TO OXIDATION OF ZIRCONIA CVI - MATRIX COMPOSITES: 1 - MECHANICAL BAHAVIOR

J. MINET (*), F. LANGLAIS, J.M. QUENISSET and R. NASLAIN
Laboratoire deChimie du Solide du CNRS, Université de Bordeaux I
351, Cours de la Libération, 33405 - Talence, France

ABSTRACT

The mechanical behavior of various zirconia-based fibrous composites has been studied at ambient and high temperatures. The composites were prepared by ZrO_2-CVI densification, from preforms made of alumina or carbon fibers consolidated with a small amount of alumina, pyrocarbon or hex-BN. When loaded under compression at room temperature, 2D-C-C / ZrO_2 composites exhibit a mechanical behavior similar to that already reported for the related 2D-C-C / SiC, 2D-C-C / B_4C, 2D-C-C / TiC or 2D-C-C / BN materials with: (i) a linear elastic domain, (ii) a damaging domain prior to failure and (iii) an anisotropy which decreases as $V(ZrO_2)$ is raised. Under 3 points bending, the alumina-zirconia composites behave, at room-temperature, in a non-brittle manner when the preform has been consolidated by BN, with crack deviation and pull-out phenomena. The variations of the stiffness and strength vs $V(ZrO_2)$ obey exponential laws, at room temperature. Finally, the alumina-zirconia composites keep their strength and rigidity up to about 1000°C under an atmosphere of argon / hydrogen.

KEYWORDS: CERAMIC MATRIX COMPOSITES, ZIRCONIA MATRIX COMPOSITES, MECHANICAL BEHAVIOR, STIFFNESS, FAILURE STRENGTH, DAMAGING PHENOMENA

(*) Present adress: Société Européenne de Propulsion, B.P. 37
33165 Saint-Médard-en-Jalles-Cédex, France

INTRODUCTION

It is now well established that the fiber composite concept provides an efficient way to improve the toughness and reliability of engineering ceramics. Very recently, the key role played by the fiber-matrix interfaces (or interphases) in the mechanisms which control the crack propagation (and thus the failure and fracture work) of the ceramic matrix composites (CMC) has been identified for different fiber-matrix ceramic couples. It appears that tough composites are obtained when the fibers are not too strongly bound to the matrix allowing thus different energy-absorbing phenomena to take place (e.g. compliant load transfer at the fiber matrix interface, fiber friction against the matrix and, finally, fibers pull-out) under loading. It has been shown that a way to control crack propagation in CMC is to add a thin layer of a compliant material (e.g.) pyrocarbon or hex-BN), at the fiber-matrix interfaces, either through an in-situ reaction occuring at high temperatures during the elaboration of the composites or as a coating applied to the fibers prior to their insertion in the matrix [1- 4]. However, these interphases are sensitive to oxidation and experimental data showing the dependence of the strength of such composites on test atmosphere have been already given [5]. Therefore, the behavior of CMC with respect to long exposures at high temperatures in oxygen-containing atmospheres is an important subject for the future of CMC.

The aim of the present work was to explore the potential of zirconia as a ceramic matrix in CMC for aerospace applications at high temperatures. On the basis of the above general considerations, zirconia has several advantages

with respect to carbon and SiC : (i) it is a very refractory compound ($T_m \approx 2700°C$) and stable oxide, (ii) it is a good insulating material whereas both graphite and SiC exhibit a high thermal conductivity and (iii) it undergoes a polymorphic transition, $ZrO_{2(m)} \rightleftharpoons ZrO_{2(t)}$, with a martensitic character which has been used to increase the toughness of many ceramics. Furthermore, it has been established recently that ZrO_2 - based composites can be preparated, at moderate temperatures (i.e. about 900°C), according to the so-called chemical vapor infiltration (CVI) process already used by R. Colmet et al. to prepare Al_2O_3 - based composites [6 - 9].

Surprisingly, ZrO_2 - matrix composites reinforced with continuous fibers have not been yet the subject of much research whereas many articles have been published on the fiber reinforcement of SiO_2 - based glass - ceramics, mullite and alumina [5, 9, 10]. As a matter of fact, when the present study was started, no paper had been devoted to the subject, at least to our knowledge. In the meantime, V.K. Pujari and I. Jawed reported the results of their study on chopped alumina fiber - TZP matrix composites prepared according to a conventional powder metallurgy route. They found that the alumina fibers did result in a twofold increase in toughness with respect to the monolithic TZP but mentioned that the failure mode remained brittle [11]. Almost simultaneously, B. Bender et al. succeded in preparing ZrO_2 - SiO_2 and ZrO_2 - TiO_2 matrix composites reinforced with uncoated - or BN coated - SiC fibers, according to a liquid route (organometallic precursors). They showed that the composites exhibited a brittle failure when reinforced with uncoated SiC fibers due to a strong fiber-matrix bonding whereas they did behave in a non-brittle manner with BN-coated

SiC-fibers, the BN layer allowing the fiber pull out to occur and preventing the fibers to react with the matrix [2]. Finally, a few articles were also published on the related whisker reinforced ZrO_2 composites [12 - 14].

Our contribution, presented as two companion papers, is a continuation of three articles which have been already published on the synthesis of ZrO_2 - matrix composites by CVI [7 - 9]. The first part of our present contribution gives the results of our work on the mechanical behavior, at ambient and high temperatures of some ZrO_2 - matrix composites reinforced with either alumina or carbon continuous fibers whereas the second part is devoted to their thermal properties and resistance to oxidation.

2 - EXPERIMENTAL

The samples used in the present study were prepared, according to a CVI-technique, from five different types of fiber preforms with a marked two dimensional (or pseudo three dimensional) character (tables 1 and 2). Regarding the nature of the potential applications of ZrO_2 - matrix composites and that of the ceramic fibers available when the study was started, two kinds of reinforcements were selected: (i) alumina based fibers, for their insulating character with a view to applications at medium temperatures in oxygen-rich gas environments and (ii) carbon fibers, for their refractoriness, low coefficient of thermal expansion (CTE) with a view to applications at high temperatures in oxygen-poor gas media. It was understood that this choice might result in fiber-matrix compatibility

Préforms / Characteristics	SAFFIL alumina fibers (ICI) [16]	ZIRCAR fibers (1)	SUMITOMO fibers [17]	Carbon fibers (ex PAN) (2)	Carbon fibers (ex PAN) (2)
Chemical composition	Al_2O_3 : 96-97 wt. % SiO_2 : 3-4 wt.%	Al_2O_3 : 80 wt. % SiO_2 : 20 wt. %	Al_2O_3 : 85 wt. % SiO_2 : 15 wt. %	treated at 1600°C	treated at 1600°C
Fiber diameter (μm)	3	3 - 5	17	8-10	8.5. - 9.1
Tensile strength (MPa)	2000		1800	2300	2300
Tensile failure strain (%)	(0.67)		(0.86)		(0.96)
Young modulus (GPa)	300		210		240
Fibre length (cm)	1 - 5	≤ 5	continuous	≤15	≤15
Density ($g . cm^{-3}$)	3.3	3.1	3.2	1.7 - 1.8	1.7 - 1.8

(1) - Alumina fibers + silico - aluminous binder for insulating applications (SALI® from ZIRCAR)
(2) - carbon fibers for thermal applications (from GEPEM)

Table 1 : Mean characteristics of the alumina and carbon fibers used to prepare the preforms

Composite / Characteristics	type 1 Al_2O_3 (SiO_2) / ZrO_2	type 2 (Al_2O_3 - SiO_2) / ZrO_2	type 3 2D-(Al_2O_3 - SiO) / ZrO_2	type 4 2D-C-C/ZrO_2	type 5 p-3D-C-C / ZrO_2
Fibers	(1) Al_2O_3 : 97 wt. % SiO_2 : 3 wt. %	(2) Al_2O_3 : 80 wt. % SiO_2 : 20 wt. %	(3) Al_2O_3 : 85 wt. % SiO_2 : 15 wt. %	carbon ex - PAN	carbon ex - PAN
Fiber binder	alumina slurry (1 µm)	Al_2O_3 - SiO_2 slurry	pyro - BN (CVI)	pyrocarbon (CVI)	pyrocarbon (CVI)
Texture of the reinforcement	mat	short fibers in bulk	2D fabrics stacking	2D fabrics stacking	pseudo - 3D (NOVOLTEX) (4)
Fiber volume fraction (V_f)	0.17	0.10	0.37	0.30	0.20 - 0.25
Preform porosity (V_{p_o})	0.60	0.85	0.53	0.50	0.70
Preform true density (g. cm^{-3}) (5)	3.7	3.5	3.25	1.8 - 1.9	1.8 - 1.9
Preform apparent density (g. cm^{-3}) (6)	1.5 - 1.6	0.5	1.40 - 1.45	0.90 - 1.40	0.40
Zirconia volume fraction (V(ZrO_2))	0.44	0.75	0.31	0.38	0.62
Composite apparent density (g.cm^{-3})	3.8	4.7	3.2	3.2	4.0

(1) - SAFFIL from ICI, (2) - alumina fibers + silico - aluminous binder preform from ZIRCAR , (3) - SUMITOMO fibers, (4) - proprietary preform material from SEP, (5) - after grinding, (6) - mass / apparent volume ratio

Table 2 : Main characteristics of the preforms and ZrO_2 - matrix composites

problems at high temperatures. However, fibers made of pure or stabilized zirconia which would have been more appropriate than alumina fibers were not available at that time nor are they on the market presently [15].

Different techniques were used to prepare the preforms depending on the nature of the ceramic fibers. Preform of type 1 was obtained by impregnation of a SAFFIL mat (transition alumina fibers) with an alumina slurry (mean grain size: 1 μm), drying and firing at about 1400°C [16]. Preform of type 2 was supplied by ZIRCAR (it was made according to a paper industry technique, i.e. from Al_2O_3 - SiO_2 fibers in suspension within a liquid medium which was aspirated through a porous substrate, then the fiber cake was dried and fired). Preform of type 3 was made from a stack of alumina-silica fabrics (from SUMITOMO) which was then consolidated with a small amount of hex-BN infiltrated according to a process described in details elsewhere [17, 18]. Preform of type 4 was a conventional 2D-C-C porous material, i.e. it was obtained after consolidation of a stack of carbon fabrics (ex-PAN fibers) with a small amount of pyrocarbon deposited by CVI from a natural gas precursor [19]. Finally, preform of type 5 was a carbon fiber (ex-PAN) architecture specifically developed by SEP (trade mark NOVOLTEX) and consolidated by pyrocarbon. All the preforms had a marked two dimensional character (i.e. they are transverse isotropic) except preform of type 5 which was pseudo three dimensional (i.e. in the NOVOLTEX architecture, some carbon fibers are running in a direction perpendicular to the main 2D fiber construction). As shown in table 2, the open porosity of the preforms after consolication, V_{p_o} , range from 50 to 85% and the residual porosity after ZrO_2 - CVI densification, V_p, from 8 to 20%.

The densification of the porous preforms with zirconia was performed according to the CVI-technique which has been first worked out by F. Christin et al. for SiC-based cmposites and then extended to various CMC (namely B_4C, TiC, BN and, more recently, Al_2O_3 matrices) [20, 21]. It has been, for the particular case of zirconia, described in details elsewhere [6 - 8]. For the purpose of the discussion, it will be sufficient to recall here that the precursor of the matrix is a $ZrCl_4$-H_2-CO_2 mixture, the densification of the preforms being conducted in a CVI - laboratory apparatus under the following conditions: $T \approx 900°C$, $p = 2$ kPa and $D = 100\ m^3 . min^{-1}$ [8]. The kinetics of densification of the preforms are given in figure 1 as the variations vs time of Log p/p_0, where p and p_0 are respectively the pore volumes at $t = 0$ and at a given infiltration time t. It clearly appears that the infiltration rates remain constant over a large fraction of the overall process duration. However, near the end, i.e. when the residual pore mean diameter becomes too small, a deviation from the lienar relationship is usually observed indicating that the pores entrances begin to be obturated, a feature already reported by J.Y. Rossignol et al. for TiC and by H. Hannache et al. for B_4C infiltrations [22, 23]. Finally, the infiltration rate depends on the nature of the preform (each preform being characterized by a specific pore spectrum depending on its nature). As shown in table 2, the residual porosity of the composites after the ZrO_2 - CVI step, V_p, ranged from 0.08 to 0.20. No effort was done to better approach full densification regarding the time which will have been necessary to reach a residual porosity less than say 0.05. As a result, the volume fraction of zirconia deposited within the pore networks, $V(ZrO_2)$, ranged from 0.30 to 0.75 depending on the nature of the preforms.

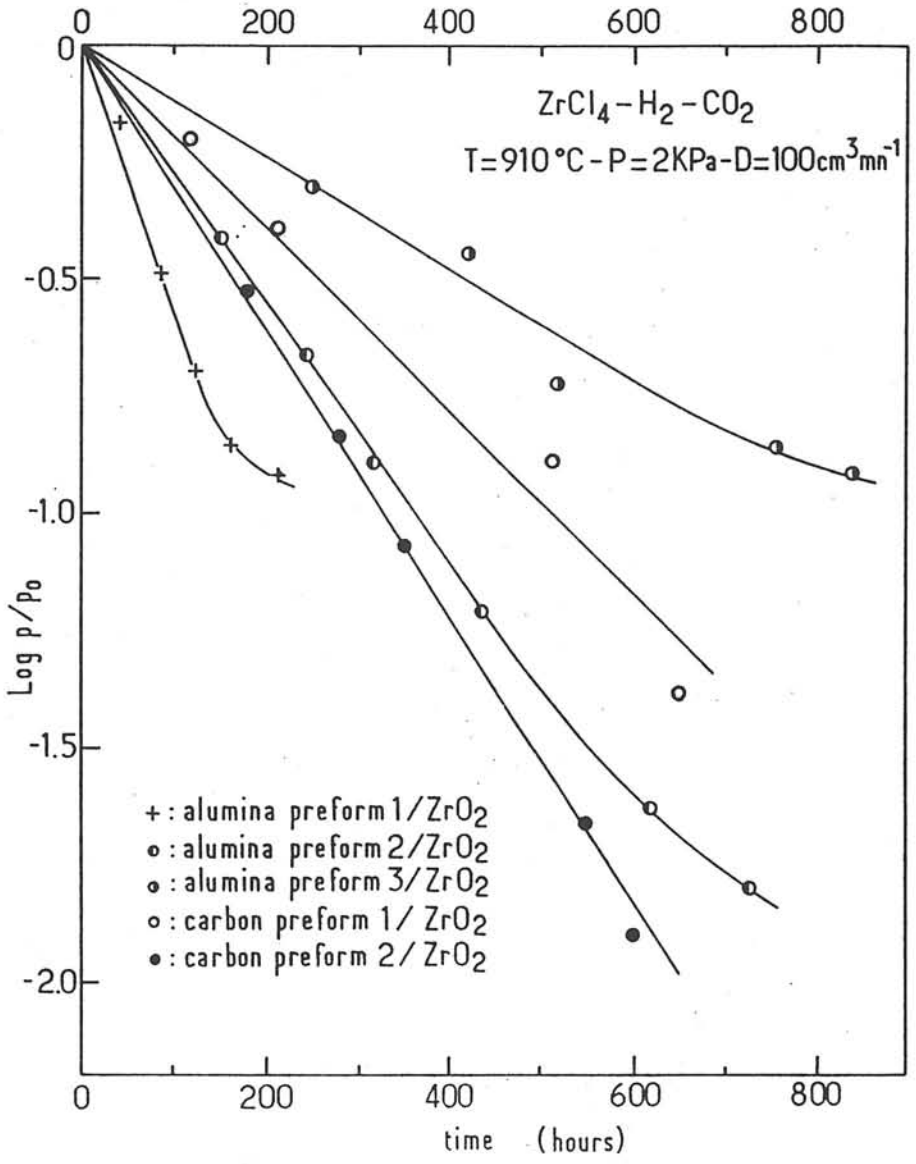

Fig. 1 - Zirconia infiltration kinetics of the fibrous porous preform

The samples used for the mechanical and thermal tests as well as those used to assess the resistance of the composites to oxidation were cut and machined from the consolidated preforms, in different directions with respect to the fiber layers, as shown in figure 2, and then densified with zirconia (up to increasing $V(ZrO_2)$ values). No machining or surfacing treatments were performed after the CVI-densification step.

The compression tests were performed on cylindrical specimens (d = 8 mm; h = 16 mm), the load being applied either along the directions 1 or 3. The tests were performed with two different displacement speeds, i.e. 0.1 mm . min^{-1} for direction 1 and 1 mm . min^{-1} for direction 3, since in 2D-composites the corresponding rupture strains are not within the same range of values, as discussed below. Due to the small size of the specimens, the approximation of the specimen deformation through the machine displacement leads to consider the Young moduli measured under compression as comparative rather than true values.

The bending tests were performed on specimens with a rectangular cross section (12 x 2 mm^2) and a length of 50 mm. The specimen length and width correspond to the composites directions 1 or 2, the load being applied in direction 3 according to a 3 points bending test configuration (span: 40 mm). The tests were performed with displacement speeds of 0.1 mm . min^{-1} at room temperature and 1 mm . min^{-1} at high temperatures (under a protective gas atmosphere of argon containing 5 vol. % of hydrogen at a total pressure of 400 mbar).

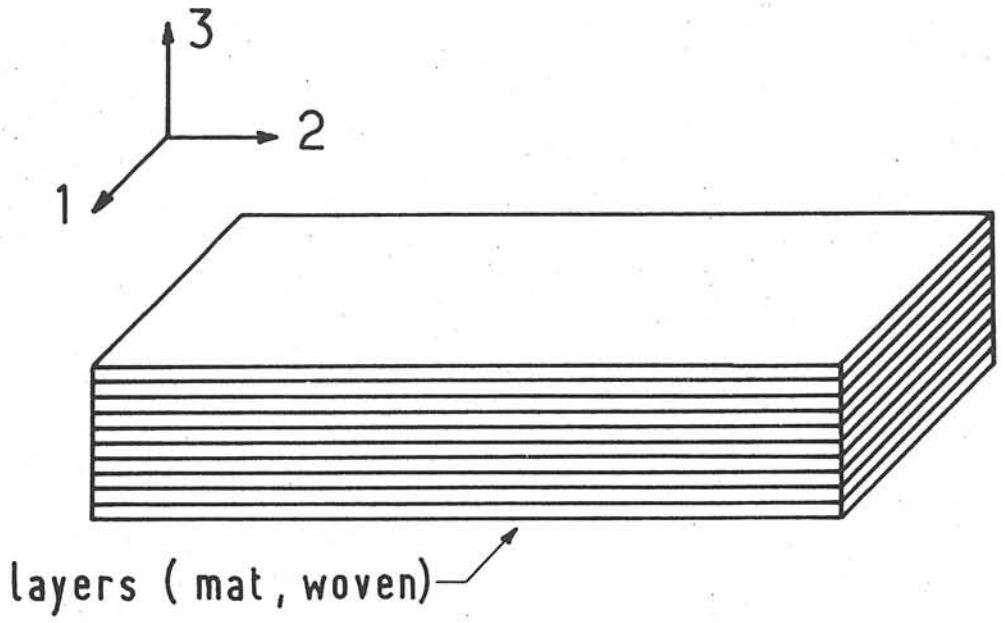

Fig. 2 - Definition of the materials natural directions

For some of the specimens, the Young modulus E_1 was measured, between room temperature and 1200°C with a Grindo Sonic Apparatus, by determining the frequency of propagation of acoustic waves along direction 1 of samples 50 mm in length with a square cross section (5 x 5 mm^2). The Young modulus is given by:

$$E_1 = \rho . C^2_1 \qquad (1)$$

where C_1 is the velocity of the tensile wave applied in the direction 1 of the composite and ρ the density.

3 - RESULTS AND DISCUSSION

3.1. Comparative behavior under compression loading

The mechanical behavior of the **2D-C-C / ZrO_2** (composites of type 4) were studied under compression loading, in both directions 1 and 3, by testing at room temperature 25 specimens whose zirconia volume fractions were ranging from 0 to 0.35 (the initial porosity of hte 2D-C-C preform being of the order of 0.45). As shown in figure 3, the stress-strain curves exhibit general features which are typical of 2D-ceramic composites [24, 25]. Their analysis can be done on the basis of three strain domains:

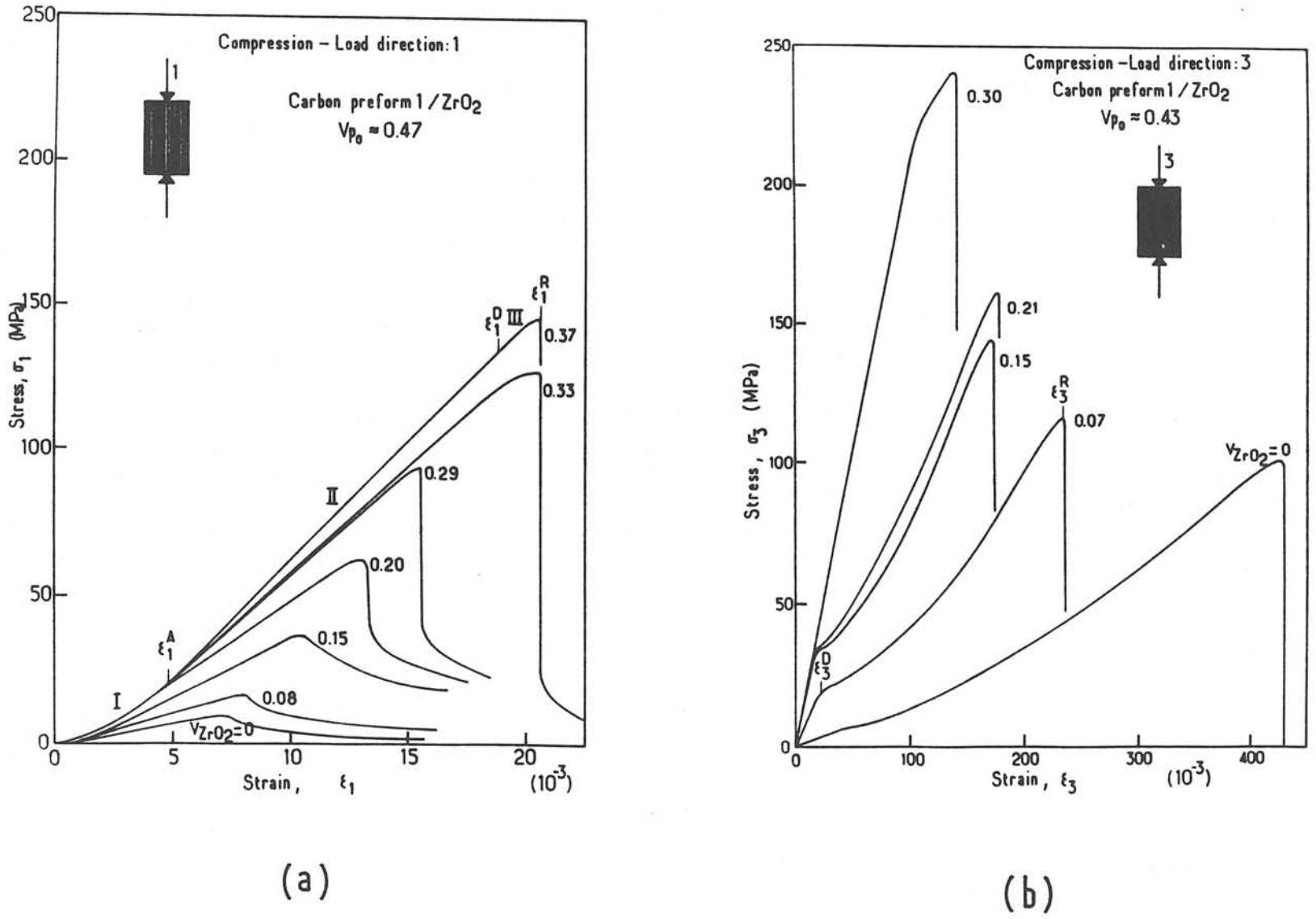

Fig. 3 - Compression behavior of 2D-C-C / ZrO_2 composites (composites of type 4): (a) load applied in direction 1, (b) load applied in direction 3.

(i) for $0 < \varepsilon < \varepsilon^A$, a first domain (I), which is particularly limited in direction 3 and for materials with high volume fractions of zirconia, is related partly to the non linearity of the loading system and, to some extend, to small rearrangements within the fibrous structure. As already discussed elsewhere, the distinction between these two effects is rather difficult when the specimens are small and it is not required for a first approach of the mechanical behavior [26].

(ii) for $\varepsilon^A < \varepsilon < \varepsilon^D$, a second domain (II) corresponds to a linear elastic behavior up to a yielding or damaging stress which strongly depends on V (ZrO_2). The elastic characteristics of the materials which are discussed below were derived from this domain.

(iii) for $\varepsilon^D < \varepsilon < \varepsilon^R$, a third domain (III) of non linear behavior leads to the rupture of the materials and is related to the occurence of damaging mechanisms within the brittle matrix. The width of this domain is quite different depending on the loading direction. In direction 3 and for incompletely densified materials this domain is so broad that it seems to correspond to a "strain hardening" effect. In fact, the damaging mechanisms related to the non-linear parts of the stress-strain curves correspond to a decrease in the material rigidity due to matrix microcracking. The apparent increase in stiffness, observed in fig. 3b, as strain increases, is the result of the compaction of the fabric layer stacking after an extensive degradation of the ceramic matrix.

Thus, the general features of the mechanical behavior of 2D-C-C / ZrO_2 composites are very similar to those already reported for other 2D-C-C / ceramic composites (where the CVI-matrix can be: carbon, SiC, SiC + C, TiC, BN or B_4C) [24, 25]. This result show how predominant is the contribution of the reinforcement architecture (which is the same for all these materials) in the mechanical behavior of the composites compared to the influence of the matrix nature.

The evolution of the Young moduli E_1 and E_3 over the range of zirconia volume fractions achieved, shows a strong increase in rigidity as $V(ZrO_2)$ is raised (Fig. 4). It can be fitted with an exponential function as proposed by R. Spriggs as well as by a parabolic law as suggested by J.Y. Rossignol et al [25, 36]. It is noteworthy that the gap between E_1 and E_3 is progressively reduced as the composites are getting more isotropic for increasing zirconia volume fractions. Although the maximum values which have been reached, for a residual porosity of 10% (i.e. for $V(ZrO_2) = 0.35$), are only of the order of 35 GPa for E_1 and 10 GPa for E_3 (and probably more due to the roughness of the measurements), much higher rigidities could be expected from an improvement in the densification level.

Regarding the yielding and rupture stresses, the two different orthotropic directions should be considered separately since, on one hand, the yielding stresses are very close to the maximum stresses in direction 1 whereas, on the other hand, the gap between these too stress levels is quite high in direction 3. However, the evolution of all these parameters vs porosity, which is

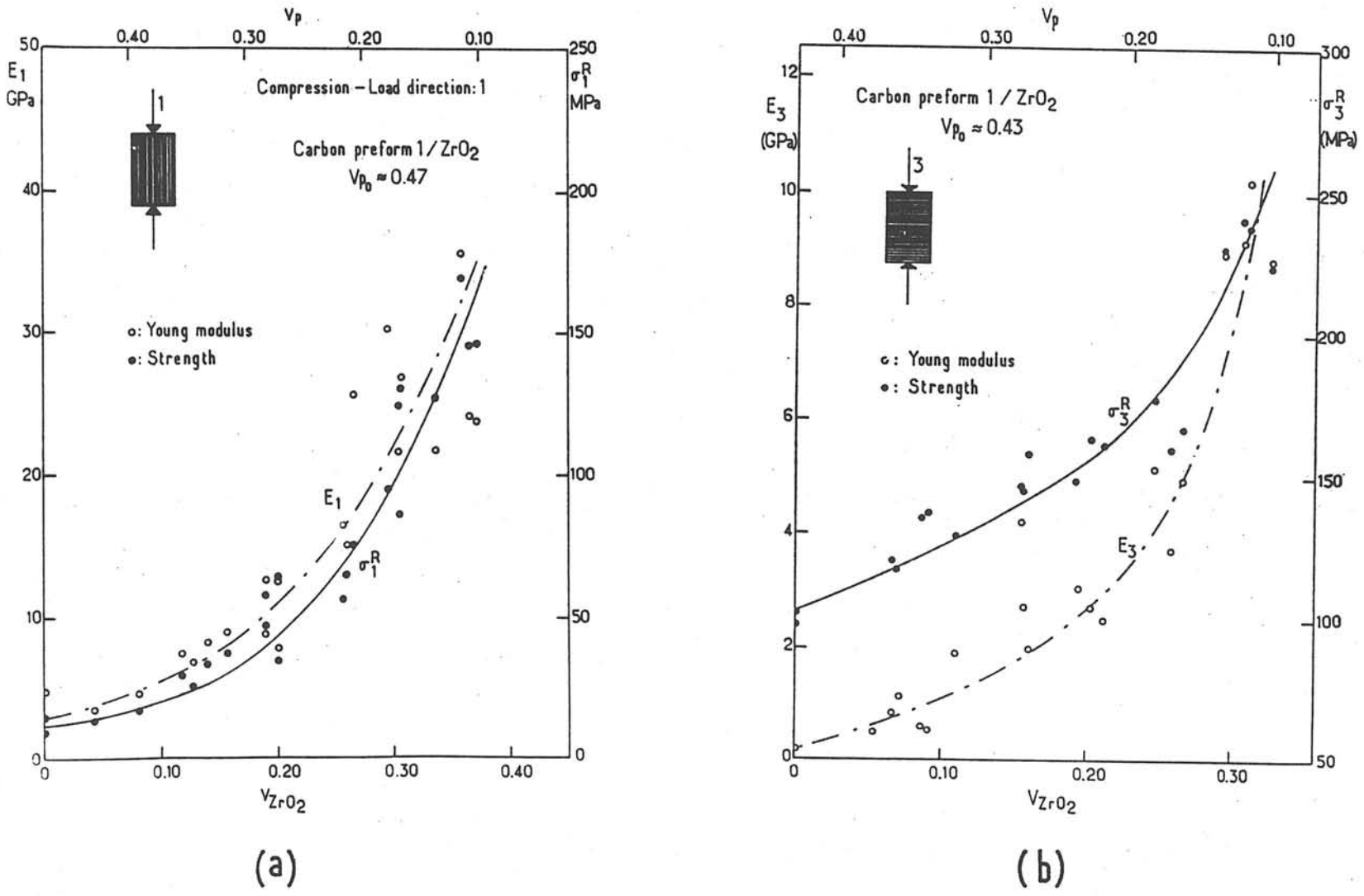

Fig. 4 - Variations of the Young modulus (E) and the stress to failure (σ^R) of 2D-C-C / ZrO_2 composites (composites of type 4) as a function of zirconia volume fraction $V(ZrO_2)$: (a) load applied in direction 1, (b) load applied in direction 3.

illustrated in figure 4, can be represented by the following general function, as proposed independently by W.H. Duckworth and by J.Y. Rossignol et al [25, 27 - 29]:

$$\sigma = \sigma(o) \exp - K_\sigma V_p \qquad (2)$$

where σ is either the yielding stress σ^D_3 or the rupture stress (σ^R_1 or σ^R_3), $\sigma(o)$ is the value of the yielding or rupture stress extrapolated to complete densification (i.e., $\sigma^D_3(o)$ = 330 MPa; $\sigma^R_3(o)$ = 280 MPa; $\sigma^R_1(o)$ = 367 MPa) and K_α is a fitting constant (K^D_3 = 9.70; K^R_3 = 2.27; K^R_1 = 7.65). Otherwise, the maximum compression stresses achieved for V_p = 0.10 (i.e. $V(ZrO_2)$ = 0.35) are σ^R_1 = 160 MPa in a direction parallel to the fiber layers and σ^R_3 = 235 MPa in a perpendicular direction. In this latter direction, the stress level above which damaging occurs is low except at the highest densifications which give the 2D-C-C / ZrO_2 composites similar behaviors in both directions 1 and 3.

The main difference in the material behavior under compression loading, between its two orthotropic directions, concerns the damaging (or yielding) strains ε^D_1 and ε^D_3 as well as the rupture strains ε^R_1 and ε^R_3. When the compression load is applied **in direction 1,** the instability of the fibrous layers of the material leads to buckling phenomena, initiates microcraks within the brittle zirconia matrix and finally results in interlayer delamination. Thus, increasing $V(ZrO)_2$ improves the buckling resistance of the fibrous layers so that failure, which occurs only by interlayer delamination, is delayed towards higher rupture strains ε^R_1. As illustrated in figure 5a, this effect also results in an increase in ε^D_1 as $V(ZrO_2)$ is raised since each fibrous layer is able to support

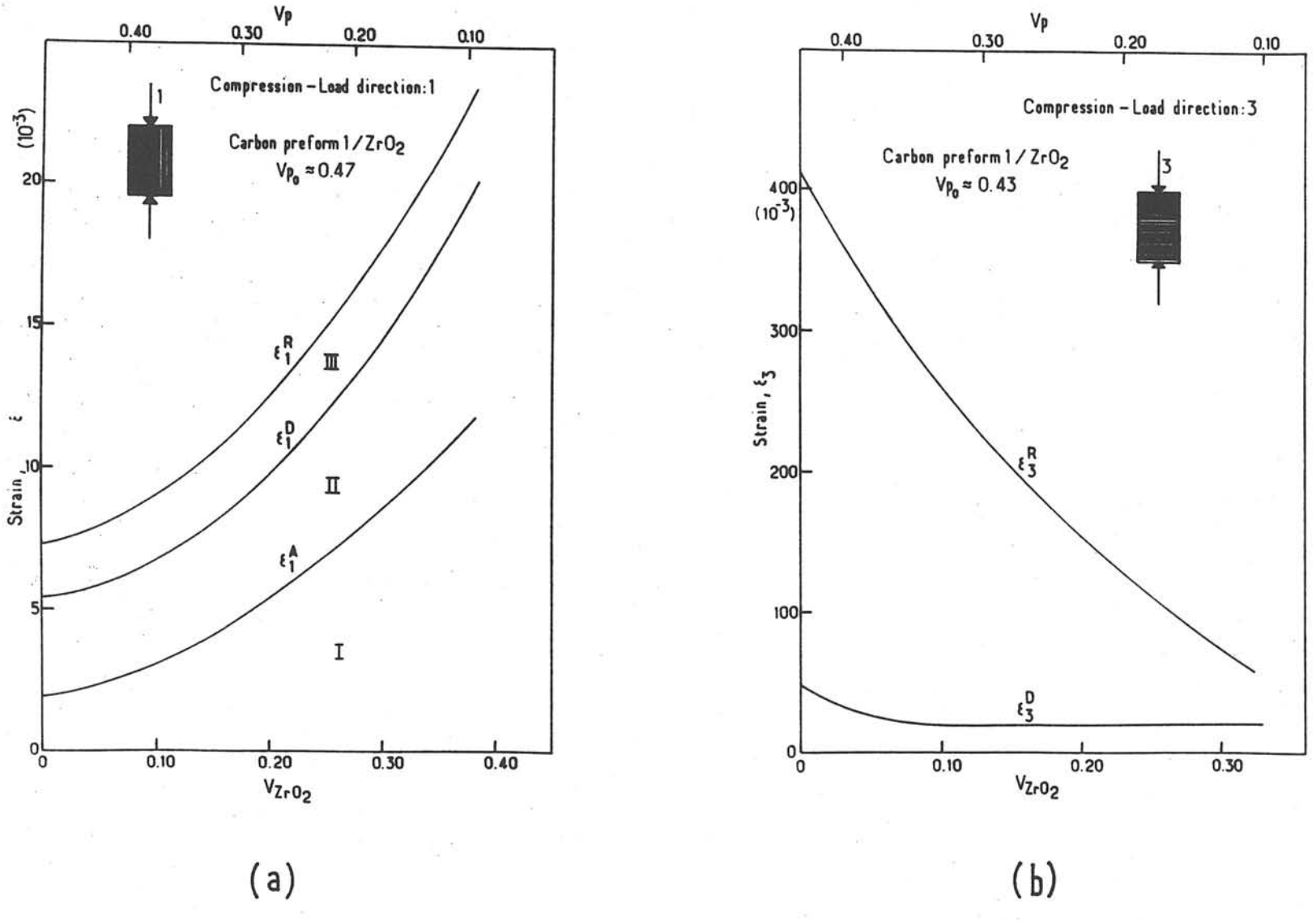

Fig. 5 - Variations of the strain (ε^D and ε^R) vs. zirconia volume fraction ($V(ZrO_2)$)for 2D-C-C / ZrO_2 composites (composites of type 4): (a) load applied in direction 1, (b) load applied in direction 3.

higher compressive strains before buckling. This effect is still more noticeable as the volume fraction of the pyrocarbon used to consolidate the preform prior to ZrO_2 densification is higher. It has been found to be more pronounced for the 2D-C-C / ZrO_2 composites than for the other 2D-C-C / ceramic composites previously studied (e.g. $\varepsilon^R_1 \approx 22.10^{-3}$ for 2D-C-C / ZrO_2 whereas $\varepsilon^R_1 \approx 6 - 8 . 10^{-3}$ for 2D-C-C / ceramic where the ceramic matrix is made of BN, B_4C, SiC or TiC) [25]. This feature could also explain the absence of transition in the rupture mode (i.e. interlayer failure ----> intralayer failure) over the range of zirconia volume fractions which have been achieved: the insufficient zirconia bridging of the fibrous layers prevents any intralayer failure. When the compression load is applied **in direction 3**, the stability of the structure allows the brittle matrix to be completely crushed into a powder before rupture. The higher the porosity in which the matrix debris can be distributed (i.e. the lower $V(ZrO_2)$) the higher the rupture strain ε^R_3, as illustrated in figure 5b. The damaging initiation corresponds to the fracture strain of the matrix which remains quasi-constant as $V(ZrO_2)$ is raised. On the other hand, it appears that the elastic energy which is required for the matrix microcracking increases as $V(ZrO_2)$ is raised whereas the rupture strain ε^R_3 simultaneous decreases. Thus, the compression behavior of 2D-C-C / ZrO_2 composites in direction 3 suggests two contradictory ways for improving the rupture work: (i) an increase in the stress level at failure initiation and (ii) an extension of the failure strain. Finally, it is noteworthy that the compression behaviors of 2D-C-C / ZrO_2 composites in their orthotropic directions (1 and 3) become more and more similar and brittle as $V(ZrO_2)$ increases. On the other hand, the embrittlement seems to be attenuated, at least to some extent, by

the presence of the pyrocarbon matrix used to consolidate the carbon fiber preform.

In order to work out, in a similar manner, the role played by the **less anisotropic mat preform,** the mechanical behavior under compression loading, of the alumina-zirconia composites (type 1) was briefly investigated. The tests were performed on two cylindrical specimens whose axes were respectively orientated along the directions 1 and 3, as shown in figure 2. The zirconia volume fractions were 0.35 and 0.43 for the specimens loaded in directions 1 and 3 respectively. As shown in figure 6, the stress-strain curves have many common features and their analysis can be done on the basis of three strain domains as already discussed for the 2D-C-C / ZrO_2 composites (Figs. 3a,b). After a wide stress-strain domain (II) in which the composite is considered to behave as linear elastic, a rather narrow damaging domain (III) is observed prior to failure. This non linearity indicates the occurence of microcracking within the brittle matrix which gives rise to a decrease in the rigidity of the material. However, the failure which follows these damaging phenomena remains rather brittle despite the fact that the failure strains are rather high ($\varepsilon^R_1 \approx \varepsilon^R_3 \approx 15 \cdot 10^{-3}$). Although the amount of data is still limited, some general aspects of the Al_2O_3-ZrO_2 composites derived from a mat preform can be expected as follows:

(1) the composite rigidity is strongly dependent on the densification level as observed for most ceramic matrix composites obtained by CVI,

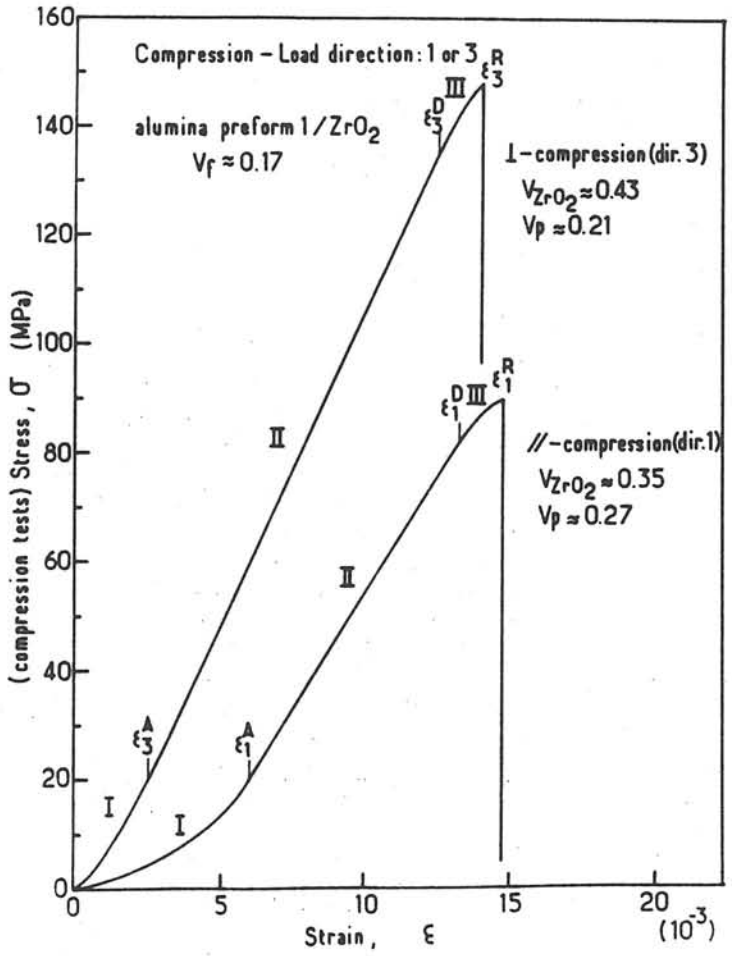

Fig. 6 - Compression behavior of composites of type 1 (SAFFIL fibers + alumina powder (1 μm) preform / ZrO_2 loaded parallely (direction 1) and perpendicularly (direction 3) to fibers layers.

(2) the alumina binder and the residual porosity is presumed to impede, at least partly, the notch effects due to the zirconia matrix microcracking thus slightly delaying the composite fracture. However, the deviations between the yielding and fracture strains recorded for rather low densification level ($V_p \approx 0.25$) are small enough to think that this type of composite should be quite brittle after complete densification,

(3) the deviation between the failure stress obtained in direction 1 and 3 ($\sigma^R_1 \approx 90$ MPa; $\sigma^R_3 \approx 150$ MPa) is thought to be more likely related to the difference in densification level rather than the material anisotropy. It is a matter of fact that the predominance of the matrix volume fraction should significantly reduce the contribution of the already moderate anisotropy of the initial preform, giving the composite a quasi isotropic behavior.

In summary, comparison between 2D-C-C / ZrO_2 composites (type 4) and the alumina-zirconia composites (type 1) leads to the following remarks:

(1) in both cases the performances of these composites are strongly dependent on the densification level,

(2) when on one hand the features of the mechanical behavior related to 2D-C-C / ZrO_2 are quite different depending on the loading direction (1 or 3), the alumina-zirconia composites (type 1) seem to be much less sensitive to the loading direction. Indeed, the toughening effect of the fibrous reinforcement is only

effective when the fiber strength and volume fraction are not small compared to those of the matrix,

(3) in direction 3, for moderate densification level of a 2D-C-C preform, the pores within the carbon network allows an extensive degradation of the zirconia matrix before failure giving rise to significant rupture strain. For high densification level, the carbon network is rigid and resistant enough to delay the matrix microcracking by building up a multiaxial stress field in the matrix. It leads to high yielding and failure strength,

(4) in direction 1, the failure mechanism deals with buckling of carbon fabric layers so that a small content of zirconia or an excessive amount of carbon matrix result in weak interlayer bounding and failure by delamination,

(5) on the contrary and although the alumina preforms derived from mats are not isotropic, the part of randomly oriented fibers is sufficient to allow macrocracking in any direction. However, the relatively low mechanical performance of the used alumina fibers compared to carbon fibers, the random orientation in mat layers, as well as the presence of alumina powder and porosities at the fiber-matrix interface are thought to facilitate the formation and coalescence of large microcracks occuring in thick zirconia coating and result in smaller failure strain.

3.2. Effect of the nature of alumina preforms on bending properties

The mechanical behavior, in bending, of the alumina-zirconia composites (types 1. 2 and 3) was studied, at room temperature, as a function of $V(ZrO_2)$. The orientation of the 3 points bending specimens with respect to the materials dierections, given in figure 2, was the same for all the composites, the load being applied in direction 3. The load - deflection curves are given in figures 7 a-c.

It clearly appears from figures 7 a,b that both composites of types 1 and 2 exhibit a brittle character which indicates that the energy dissipation related to damaging mechanisms is not significant enough (as already established under compression loading for composites 1) to prevent the catastrophic propagation of any crack initiated at the specimen surface. These two types of composites can be regarded as linear elastic. On the contrary and as shown in figure 7c, composites of type 3 (i.e. made of a stack of alumina fabrics consolidated with a small amount of hex-BN and more less densified with zirconia) exhibit, after a linear elastic domain II, extensive damaging phenomena within the zirconia matrix which result in a broad non-linear domain III prior to fracture. Thus, the continuous 2D fibrous network can fail progressively, i.e. layer after layer, since the relatively soft BN interphase impedes the microcracks propagation. As a result, the composites of type 3 exhibit an overall non-brittle behavior which contrasts strongly with the brittle behavior of composites of types 1 and 2.

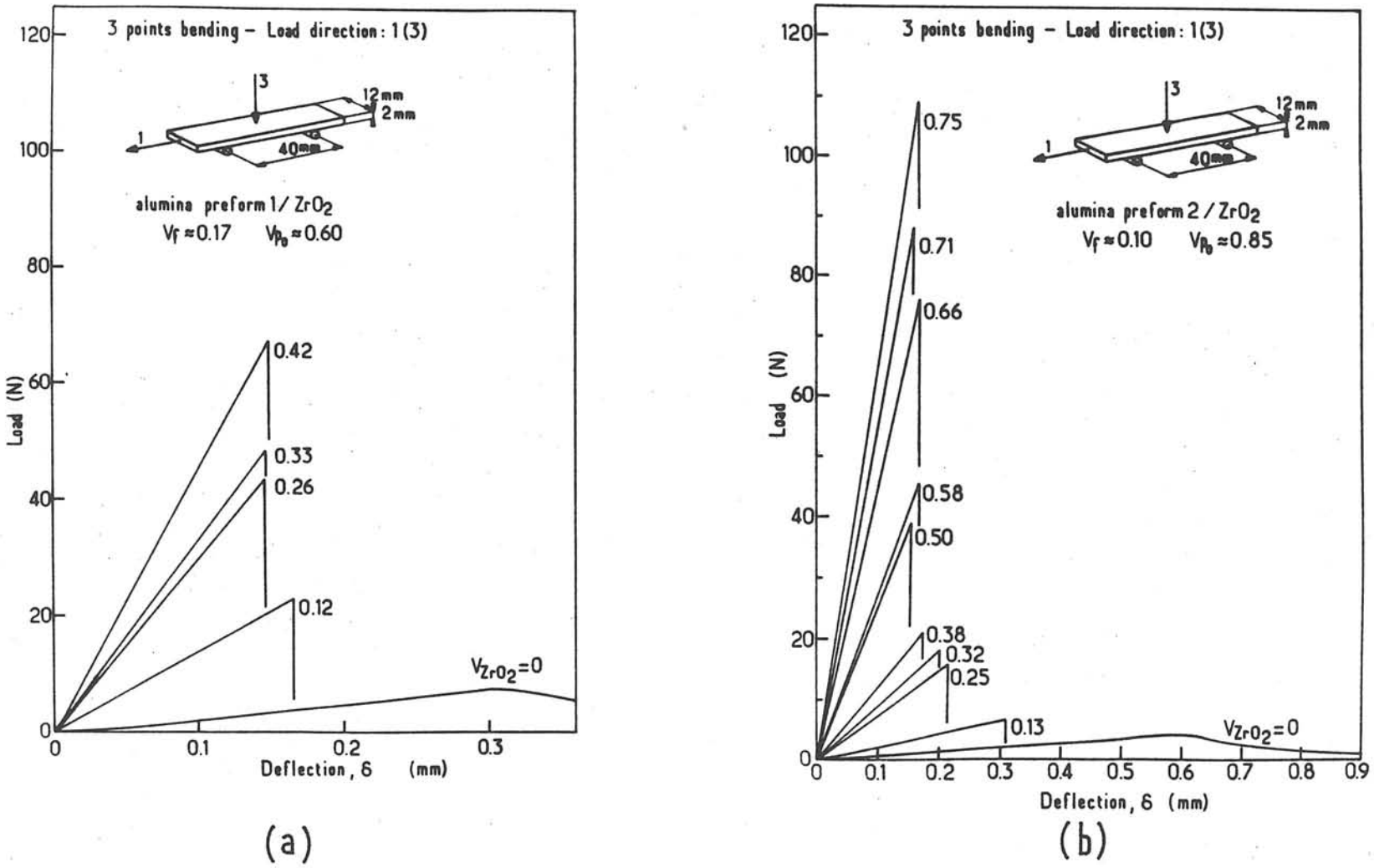

Fig. 7 - Three points bending behavior of: (a) composites of type 1 (SAFFIL fibers + alumina powder (1 μm) preform / ZrO_2); (b) composites of type 2 (Al_2O_3 fibers + silico-aluminous bounding preform / ZrO_2); (c) composites of type 3 (2D-Al_2O_3 (SUMITOMO) - BN preform / ZrO_2).

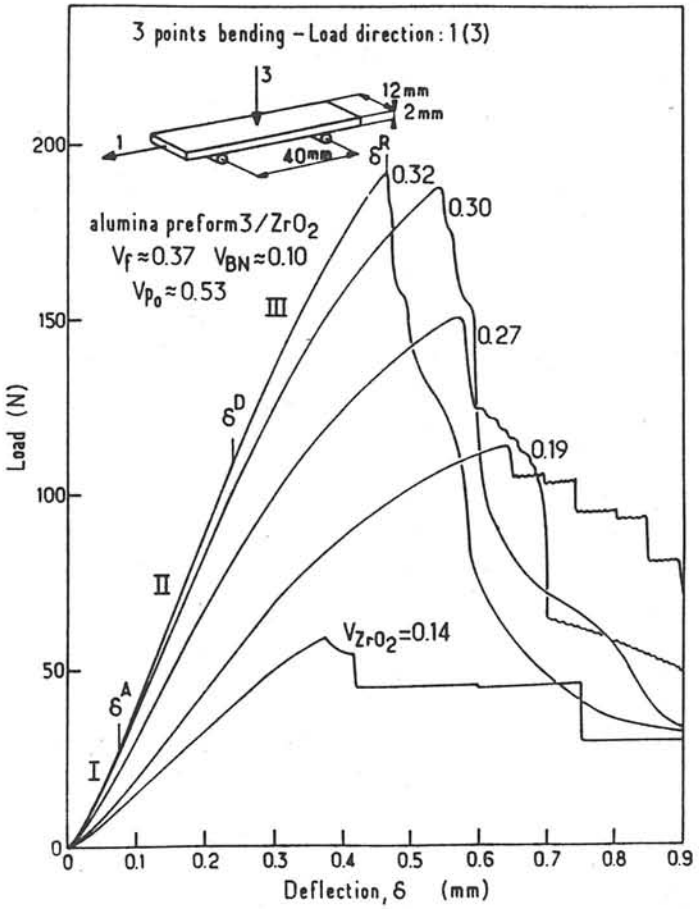
3 points bending – Load direction: 1 (3)
3
12mm
2mm
1
40mm
δ^R
0.32
0.30
0.27
0.19
alumina preform3/ZrO_2
$V_f \approx 0.37$ $V_{BN} \approx 0.10$
$V_{p_0} \approx 0.53$
III
δ^D
II
$V_{ZrO_2}=0.14$
δ^A
I
Load (N)
0
50
100
150
200
0
0.1
0.2
0.3
0.4
0.5
0.6
0.7
0.8
0.9
Deflection, δ (mm)

(c)

As shown in figures 8 a,b, the rupture deflections δ^R of the composites of types 1 and 2 decrease with increasing $V(ZrO_2)$ up to a limit of about 0.17 mm (corresponding presumably to the zirconia fracture strain). On the contrary, those observed for the composites of type 3 are much higher, as shown in figure 8c. In addition, the load-deflection curves related to the composites of type 3 allow a clear distinction between the yielding deflection δ^D which remains almost constant within the $V(ZrO_2)$ range studied and the rupture deflection δ^R whose variations vs $V(ZrO_2)$ is much significant and non monotonous. This non monotonous feature could be related to a transition between two rupture mechanisms: (1) up to about $V(ZrO_2) = 0.20$, raising $V(ZrO_2)$ increases the rigidity and strength of the fibrous layers and improves their cohesion so that rupture by delamination is delayed while the zirconia coating is not yet thick enough to induce notch effects such that matrix microcracks propagate, (2) for $V(ZrO_2) > 0.20$, the notch effects due to matrix microcracking are effective enough to embrittle the whole composite despite the presence of the soft BN interphase. This feature thus results in a decrease in δ^R.

Thus, the major differences in the mechanical behaviors of the three types of alumina fiber-zirconia matrix composites seem to be related, in a first approach, to both the fiber architecture and, as discussed below, the nature of the fiber-matrix bonding.

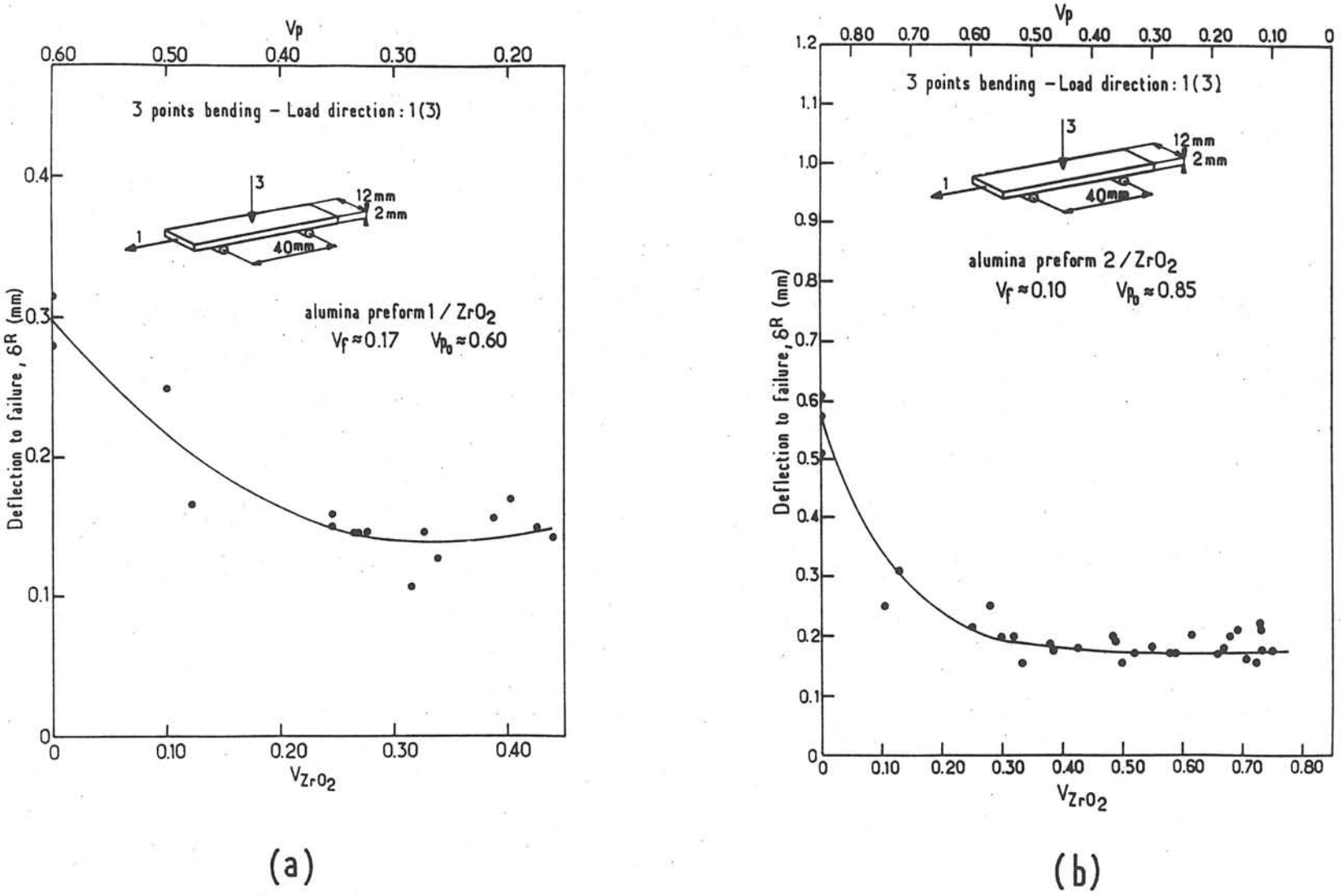

Fig. 8 - Variations of the deflexion at failure (∂^R) as a function of $V(ZrO_2)$ 3 points bending test) for: (a) composites of type 1, (b) composites of type 2, (c) composites of type 3.

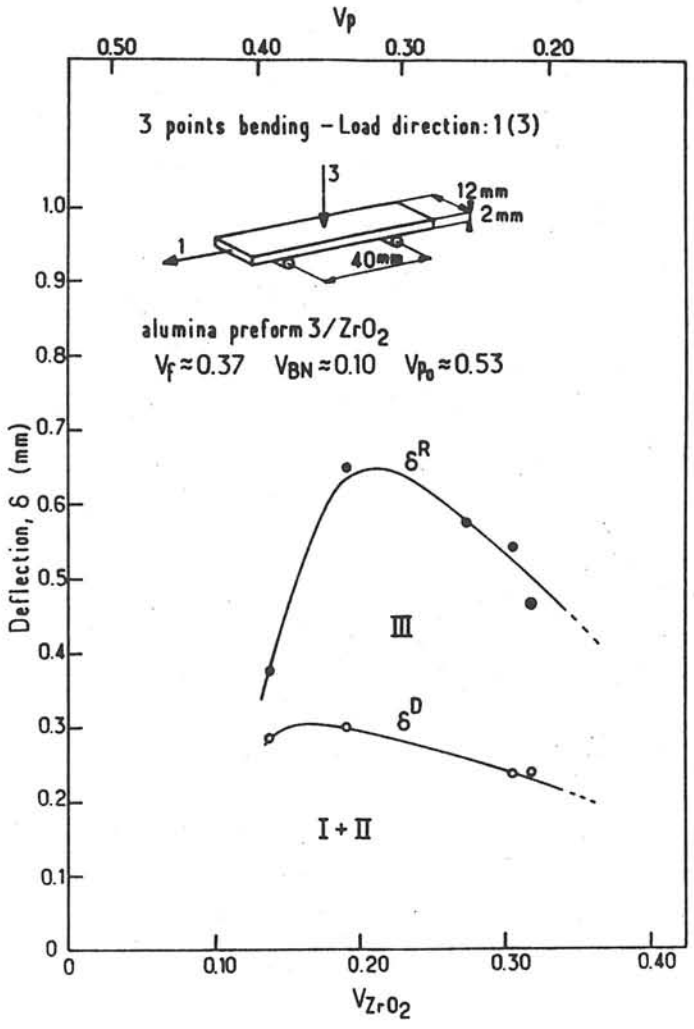
Vp
0.50
0.40
0.30
0.20
3 points bending – Load direction: 1 (3)
3
12mm
2mm
1
40mm
alumina preform 3/ZrO2
Vf ≈ 0.37 VBN ≈ 0.10 Vp0 ≈ 0.53
δR
III
δD
I + II
Deflection, δ (mm)
1.0
0.9
0.8
0.7
0.6
0.5
0.4
0.3
0.2
0.1
0
0
0.10
0.20
0.30
0.40
VZrO2

(c)

. Variations of the stiffness and rupture strength vs $V(ZrO_2)$

Both the rigidity and rupture strength of composites of types 1 to 3 increase as $V(ZrO_2)$ is raised, as shown in figure 9. These evolutions can be depicted on the basis of exponential laws similar to that given above for the compression strength (i.e. equation (2)) with the values of the constants K and the extrapolated stiffness E_1 (o) and strength σ_1(o) listed in table 3. A similar evolution of E_1 vs $V(ZrO_2)$ (with slightly lower E_1 values) has been also observed from the stiffness measurements derived from acoustic wave propagation data (recorded with the Grindo Sonic Apparatus) (Fig. 9b). All these results show again the important role played by the related residual porosity-zirconia volume fraction parameters (for composites processed by CVI from a given preform: $V_p + V(ZrO_2) = V p_o$ = constant).

Obviously, the maximum values of the rigidity and bending strength cannot be used alone to work out the influence of the components (fibers, binder, matrix) and fiber architecture on the mechanical behavior of the composites since each composite differs from the others by several parameters. However, it is noteworthy that the rigidities of the three composites are very close from one another for the same residual porosity (e. g. for $V_p \approx 0.20$, $E_1 \approx 90 - 110$ GPa), the only slight differences between them being related to the zirconia contents. On the contrary, at equal residual porosity (e.g. $V_p \approx 0.20$), the rupture strength of composite of type 3 (with a continuous reinforcement) is much higher than those corresponding to composites of types 1 and 2 (with a non woven reinforcement) whatever $V(ZrO_2)$.

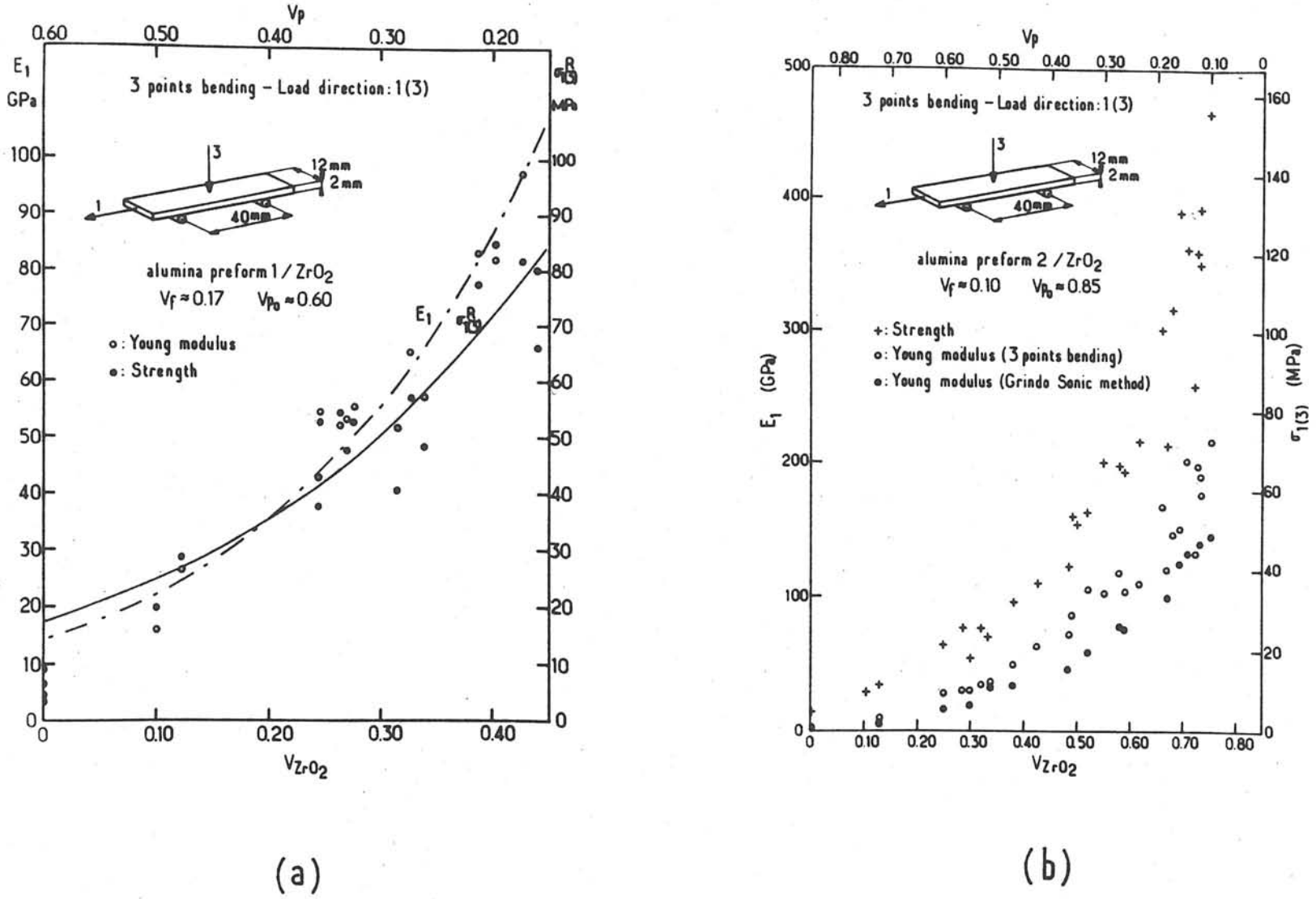

Fig. 9 - Variations of bending stiffness and strength versus $V(ZrO_2)$ for:
(a) composites of type 1, (b) composites of type 2, (c) composites of type 3.

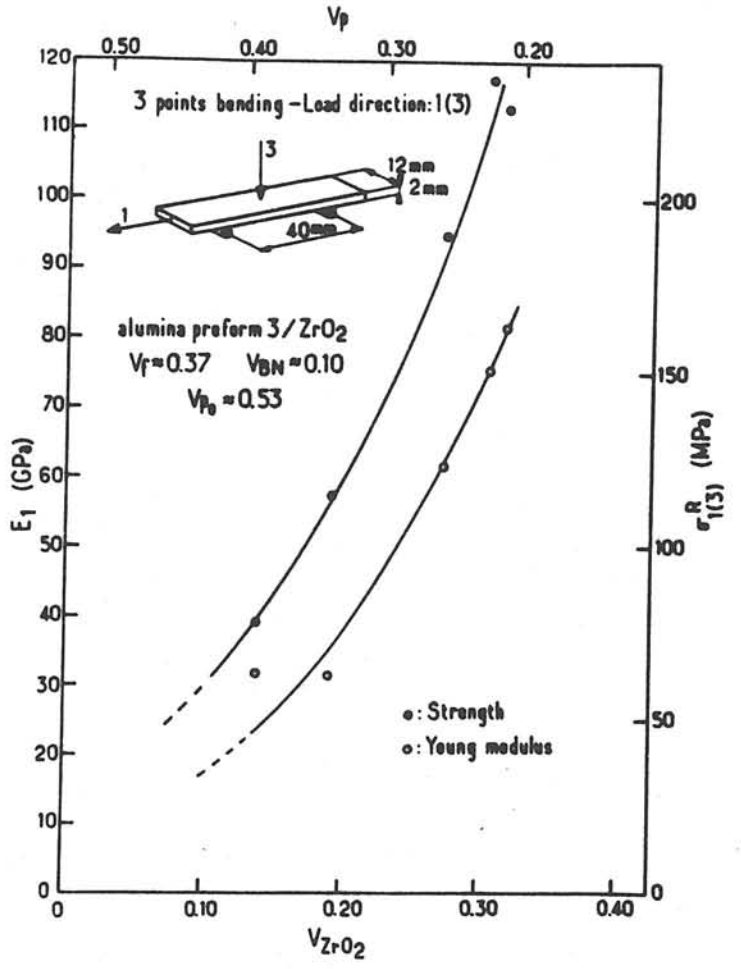
Vp
0.50
0.40
0.30
0.20
3 points bending – Load direction: 1(3)
3
12mm
2mm
1
40mm
alumina preform 3 / ZrO2
Vf ≈ 0.37 VBN ≈ 0.10
Vp0 ≈ 0.53
E1 (GPa)
σ R 1(3) (MPa)
●: Strength
○: Young modulus
VZrO2
0.10
0.20
0.30
0.40

(C)

Composite	K_{E_1}	$E_1^{(o)}$ (GPa)	K_1^R	$\sigma_1^{R\,(o)}$ (MPa)
type 1	4.46	212	3.56	147
type 2	5.42	448	4.19	209
type 3	5.84	273	6.16	893
type 4	5.07	40.4	6.54	367
type 5	4.88	47.7	4.28	242

Table 3 : Coefficients of the exponential evolution of rigidities and rupture strength vs. the porosity volume fraction V_p for alumina and carbon renforced zirconia matrix composites

. Stiffness and strength at high temperatures

The effect of temperature on the rigidity of a composite of type 1 (with $V(ZrO_2) \approx 0.20$) was studied within the temperature range 0 - 1200°C. Young modulus E_1 values were derived from the measurements of the frequency of acoustic waves propagating at hith temperatures along the direction 1 of the composites. As shown in figure 10, during the first heating, E_1 decreases from 55 to 45 GPa and the material keeps this rigidity after cooling to room temperature and agter any additional heating. Therefore, the composite seems to have been stabilized during the first treatment at high temperatures by some damaging phenomena that could be related to the thermomechanical fiber-matrix coupling or / and the allotropic transformation of the zirconia matrix (found to occur, in this composite, between 1100 - 1200°C on heating, as shown in part 2).

The high temperature bending strength was measured from room temperature to 1400°C, on composites of types 1 and 3 with zirconia volume fractions within the range 0.25 - 0.35. The variations of the bending strength as a function of the test temperature as shown in figure 11. It appears that the decrease in strength which occurs as temperature is raised occurs earlier for the composites of type 3 (i.e. the most resistant at ambient and medium temperatures). Thus, a decrease in strength of 70% is observed between 1300 and 1400°C for the composites of type 3 whereas it is only of 30% within the same temperature range for the composites of type 1. This difference may be justified by the fact that the SUMITOMO alumina-based fibers have a much higher silica content than the SAFFIL fibers (i.e. 15 and 3 wt. % respectively) [16, 17]. Although

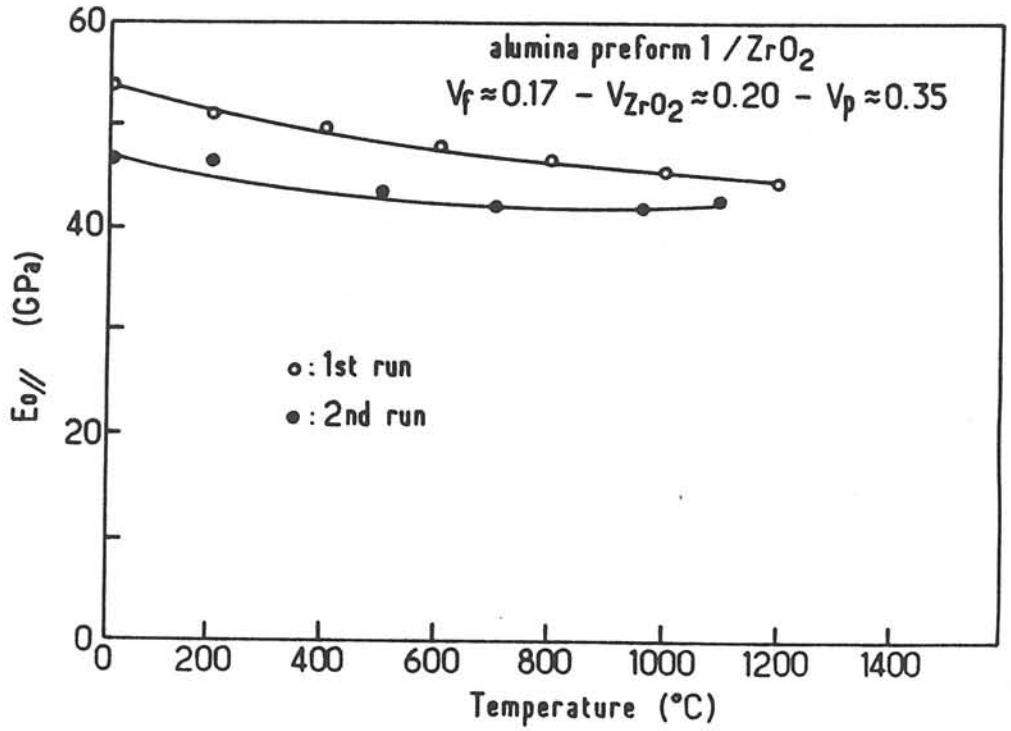

Fig. 10 - High temperature young modulus of composites of type 1.

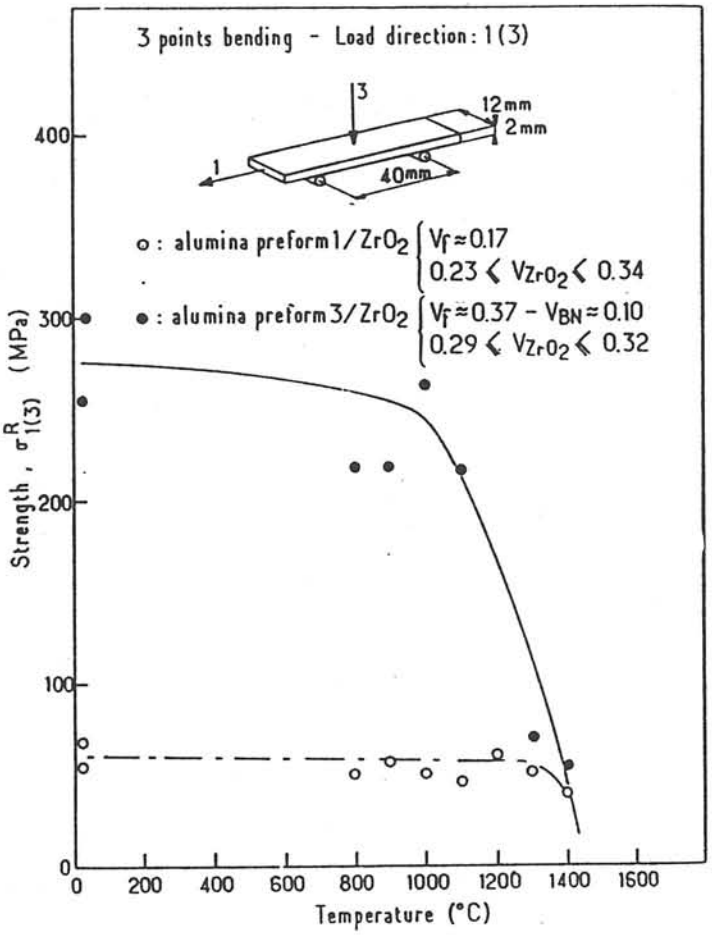

Fig. 11 - High temperature bending strength of alumina-zirconia composites (types 1 and 3).

the bending strength of the two types of composites are nearly the same at 1400°C (i.e. ≈ 40 MPa), that of the composites of type 3 (reinforced by alumina fabric layers) remains at 1000°C about four times higher than the bending strength of the composites of type 1 (derived from the mat preform).

. Discussion

From the above experimental results, it appears difficult to point out the influence of each materials parameter, on the mechanical behavior of the composites, due to the fact that several parameters are usually simultaneously modified when moving from a given material to another (e.g. fiber and preform natures, fiber-matrix bonding, $V(ZrO_2)$, V_p). This is the result of: (i) a very limited fiber or fibrous semi-product choice (e.g. the SAFFIL fiber is not available as a continuous material) and (ii) processing considerations (as said above, in CVI, increasing $V(ZrO_2)$ results in a decrease in V_p and vice versa, for a given initial preform).

Nevertheless, the above results clearly show that among the three composites studied, only one, namely the composite of type 3, appears to exhibit simultaneously the following positive features: (i) a **non brittle behavior** due to the presence of a BN-interphase (which is relatively compliant with respect to both the alumina fibers and zirconia matrix, thus enhancing the heterogeneity of the material) which reduces the stress-concentration in the vicinity of the fiber surface due to matrix microcracking and enables microcracks deviations and fiber pull out as shown in figure 12, (ii) a **sufficient volume fraction of fibers** (i.e.

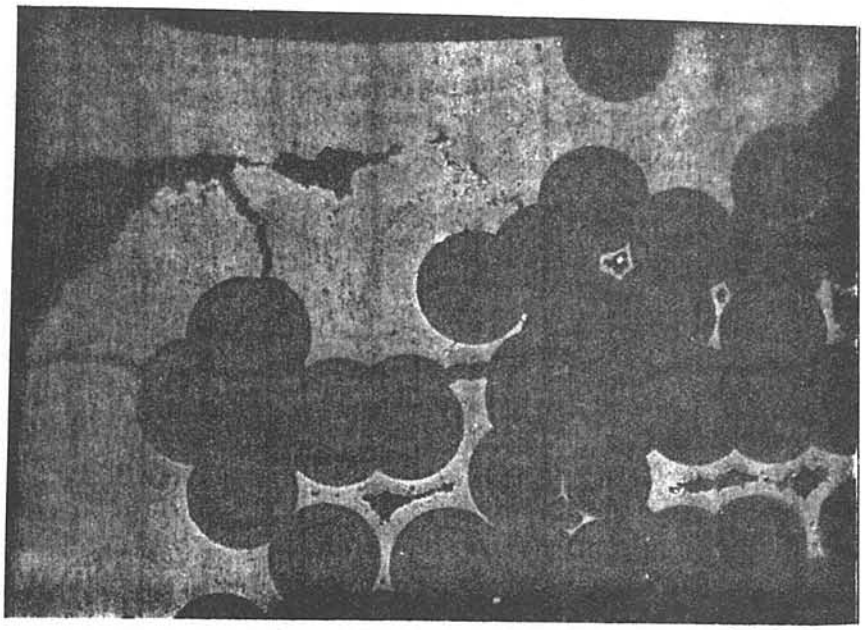

(a)

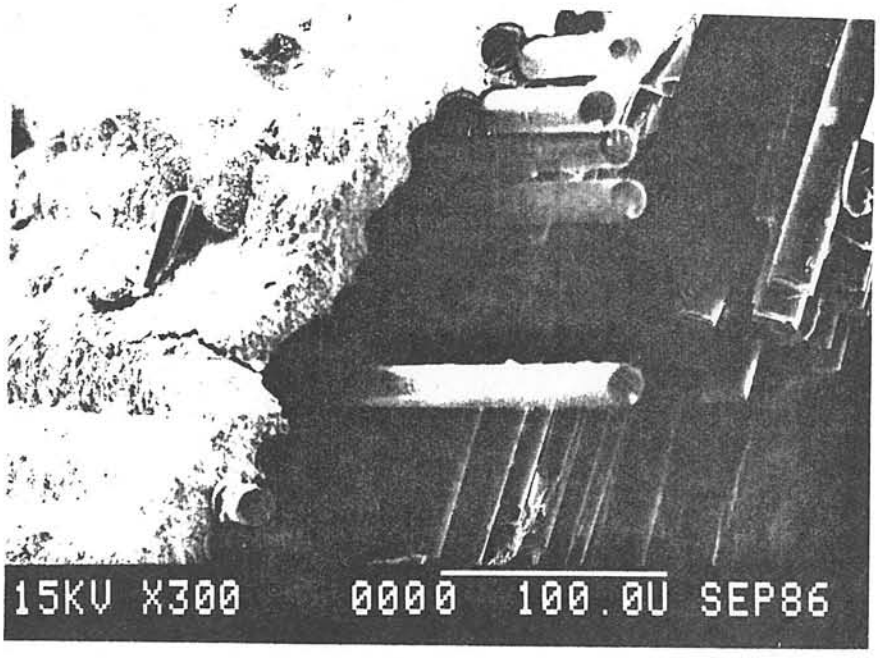

(b)

Fig. 12 - Damage and rupture of a composite of type 3 (2D-Al_2O_3 (SUMITOMO) -BN / ZrO_2) : (a) optical micrograph, (b) SEM fractograph.

Vf ≈ 0.40) allowing the fibers to support the load relaxation when the matrix undergoes microcracking and (iii) the **orientation of a significant part of the reinforcement** in the load direction (i.e. nearly half the fiber volume fraction).

On the contrary, the alumina-based binders which have been used to consolidate the preforms of the composites of types 1 and 2 do not play obviously a similar role of compliant interphase. The strong fiber-matrix bonding prevents any fiber pull out phenomena and results in catastrophic crack propagations as illustrated in figure 13.

Although the mechanical behavior of the composites of type 3 is good at ambient and medium temperatures, as illustrated in figure 11, it will have to be improved at T > 1000°C by e.g. considering more suitable ceramic fibers. This matter remains an open subject since there is presently a well known lack of thermally stable ceramic fibers (others than carbon fibers).

3.3. Effect of the architecture and carbon coating of carbon fibrous preforms on bending properties

The mechanical behavior of the carbon - zirconia composites (types 4 and 5) was also evaluated under bending with the same testing conditions used for the other zirconia matrix composites; the load being applied in direction 3. The load-deflection curves obtained for various densification level are given in figure 14.

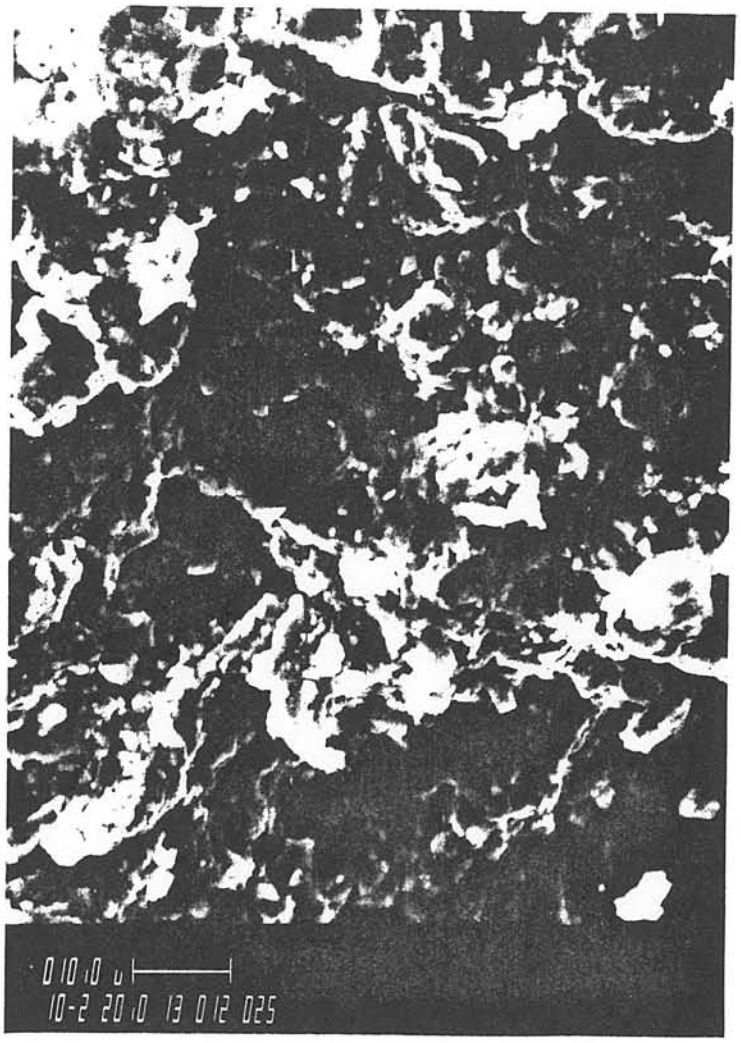

Fig. 13 - SEM fractograph of a composite of type 1.

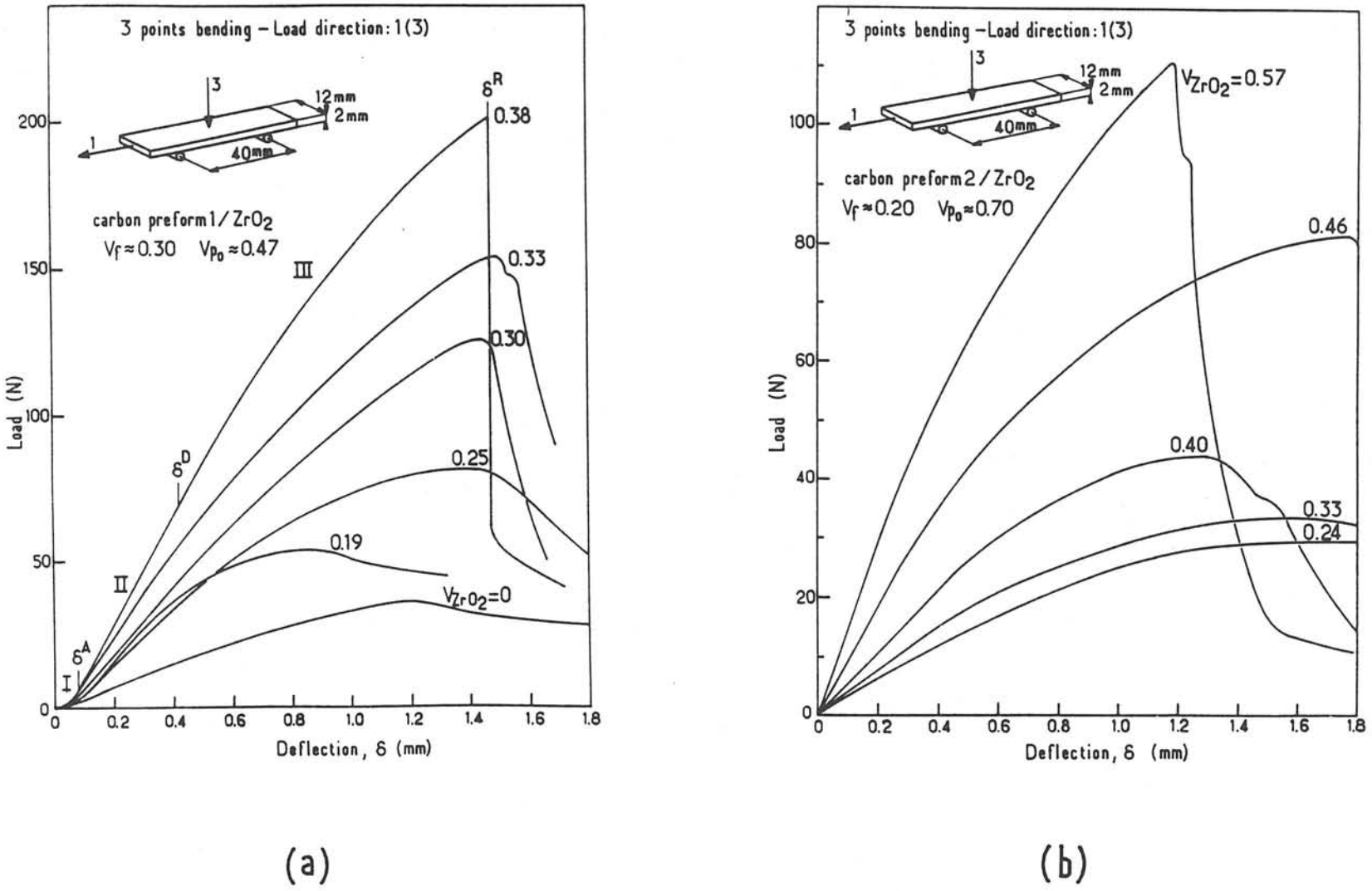

Fig. 14 - Three points bending behavior of : (a) composites of type 4 (2D-C-C/ ZrO_2), (b) composites of type 5 (p-3D-C-C/ZrO_2).

For both types of composites (4 and 5), the load-deflection curves show similar features although the levels of load are quite different. Up to deflection of about 0.4 mm the composites C-C / ZrO_2 exhibit a quasi linear elastic behavior followed by a widely spread damaging domain preceding the failure.

Furthermore the increases in stiffness and bending strength versus $V(ZrO_2)$, as illustrated in figure 15, are quite similar to those observed for alumina reinforced composites (types 1, 2 and 3). Again, the evolutions can be represented by exponential functions whose coefficients are reported in table 3.

In fact, composites 4 and 5 can be distinguished by their mode of failure which results in some differences in the evolution of the deflection at failure δ^R versus $V(ZrO_2)$ as illustrated in figure 16. As long as $V(ZrO)_2$ remains low (< 20%) the composites 4 fail by delamination so that an increase in $V(ZrO_2)$ gives the fabric layer a higher notch sensitivity during buckling of the specimen layers under compression. It results an embrittlement effect of the densification. As soon as $V(ZrO_2)$ is high enough (> 20%) the failure occurs by intralayer crack propagation. The amount of ZrO_2 is sufficient to build up bridging through the fabric layers, impeding any delamination. The rupture is initiated by the fiber fractures in the first fabric layer of the specimen surface under tension. As a matter of fact, the thickness of the carbon matrix is significant enough to inhibit the notch effects due to zirconia microcracking. Also, the specimen deflection at failure remain quasi constant versus $V(ZrO_2)$, since it is related to the tensile fracture strain of the first fiber layer. Thus, the transition in the failure mode of

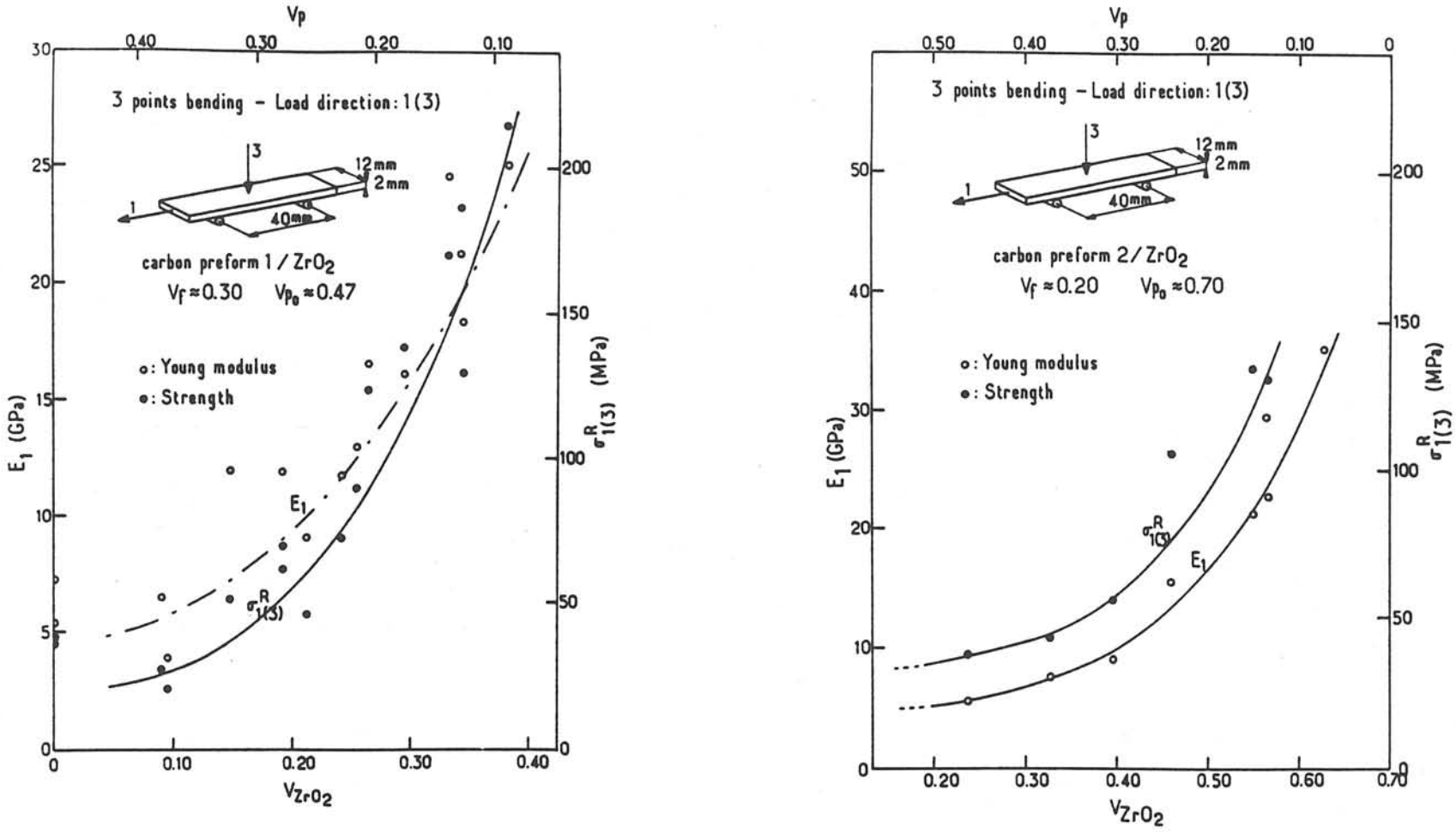

Fig. 15 - Variations of the Young modulus and bending strength versus $V(ZrO_2)$ for : (a) composites of type 4 (2D-C-C / ZrO_2), (b) composites of type 5 (p-3D-C-C/ZrO_2).

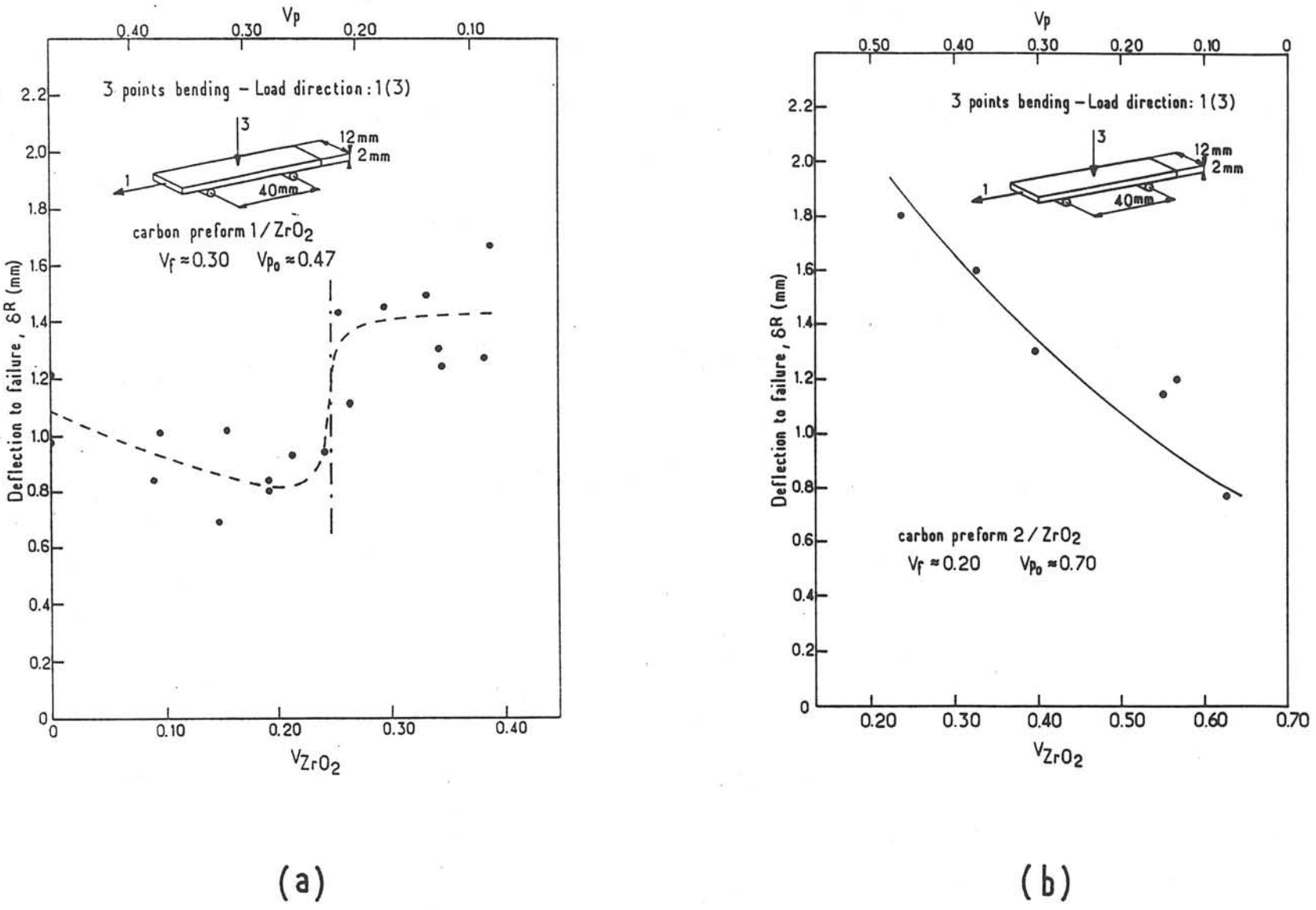

Fig. 16 - Variations of the deflexion at failure versus. $V(ZrO_2)$ for: (a) composites of type 4 (2D-C-C / ZrO_2), (b) composites of type 5 (p-3D-C-C/ZrO_2).

Fig. 17 - SEM fractograph of a composite of type 4.

composites 4 explains the non monotonous evolution of the rupture deflection versus $V(ZrO_2)$.

On the contrary, the smaller fiber volume fraction and thimer carbon coating in composites 5 (V_f = 0.20; V_{pyc} = 0.1) compared to composites 4 (V_f = 0.3; V_{pyc} = 0.2) enhance the material sensitivity to notch effect. The stress concentrations due to microcracking in particularly thick ZrO_2 coatings, control the composite failure. This mode of failure results in a decrease in the rupture deflection as $V(ZrO_2)$ is raised.

Otherwise, the evolution of the bending strength versus temperature shown in figure 18 points out for both types of composites (4 and 5) a sligth increase in their performance up to about 1000°C.

In summary, the results which have been obtained on the C / ZrO_2 composites are consistent with those already published on other ceramic matrix composites deriving from the same carbon preforms (e.g. 2D-C-C/SiC, 2D-C-C/TiC, 2D-C-C/B_4C or 2D-C-C / BN) whose comparative properties have been discussed in details elsewhere [24, 25]. Furthermore and as it will be discussed in part 2, the interest of carbon fiber reinforced zirconia is limited to specific applications due to the fact that: (i) carbon reacts with oxygen containing atmospheres above 500°C, (ii) carbon-zirconia reactions may take place in the solid state at high temperatures and (iii) carbon and zirconia are characterized by very different CTE. On the other hand, carbon fibers are presently the best

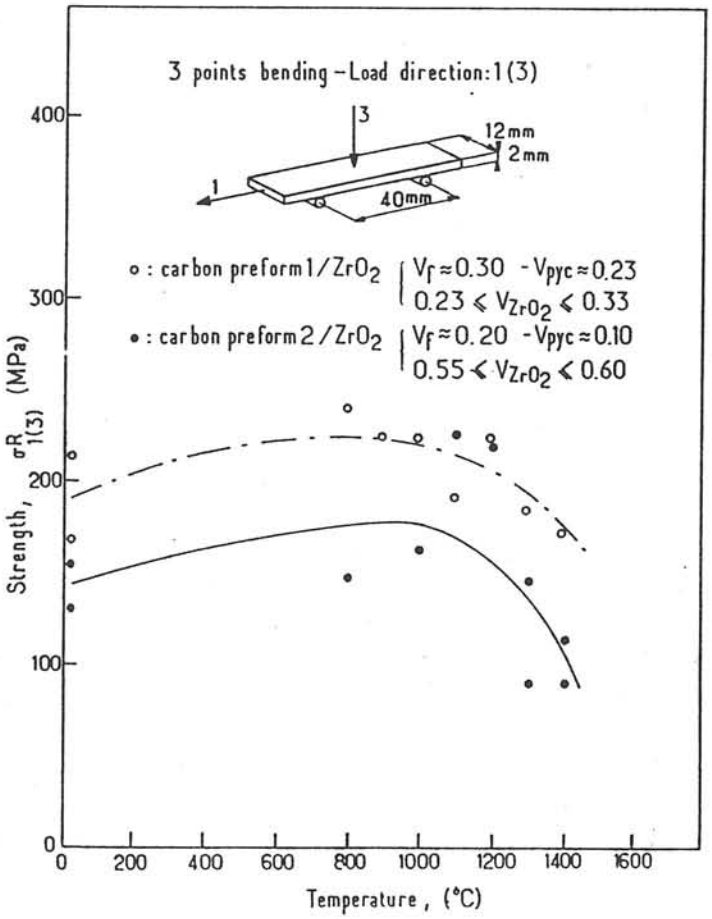

Fig. 18 - Evolution of the bending strength versus temperature for composites of types 4 and 5.

reinforcement for high temperature applications due to their refractoriness and high temperature strength.

ACKNOWLEDGEMENTS

The authors wish to acknowledge the Société Européenne de Propulsion for the supply of the preforms used in the present study and part of the mechanical tests and S.E.M. studies were performed in its laboratories.

REFERENCES

1 - J.J. BRENNAN, "Interfacial characterization of glass and glass-ceramic matrix / Nicalon SiC fiber Composites", in "Tailoring Multiphase and Composite Ceramics (R.E. Tressler et al., eds.), Mat. Sci. Res. 20 (1986) 549-570.

2- B. BENDER, D. SHADWELL, C. BULIK, L. INCORVATI and D. LEWIS III, "Effect of fiber coatings and composite processing on properties of zirconia-based matrix SiC fiber composites", Ceram. Bull., 65/2 (1986) 363-369.

3 - R.W. RICE, "BN coating of ceramic fibers for ceramic fiber composites" U.S.
Pat. 4, 642, 271, Feb. 10, 1987.

4 - R.N. SINGH and M.K. BRUN, "Effect of Boron nitride coatings on fiber-matrix interactions", Ceram. Eng. Sci. Proc., 8 (7-8) (1987) 636-643.

5 - K.M. PREWO, J.J. BRENNAN and G.K. LAYDEN, "Fiber reinforced glasses and glass-caramics for high performance applications", Ceram. Bull., 65 [2] (1986) 305 - 313.

6 - J. MINET, F. LANGLAIS, R. NASLAIN and C. BERNARD, "On the CVD of zirconia from $ZrCl_4$-H_2-CO_2-Ar gas-mixture: 1 - a thermodynamic approach", J. Less-Common Met., 119 (1986) 219 - 235.

7 - J. MINET, F. LANGLAIS and R. NASLAIN, "On the CVD of zirconia from $ZrCl_4$-H_2-CO_2-Ar gas mixture: 2 - an experimental approach", J. Less-Common Met., 132 (1987) 273 - 287.

8 - J. MINET, F. LANGLAIS and R. NASLAIN, "Chemical Vapor Infiltration of zirconia within the pore network of fibrous ceramic materials, from $ZrCl_4$-H_2-CO_2 "(to be published).

9 - R. COLMET, J. LHERMITTE-SEBIRE and R. NASLAIN, "Fibrous alumina-alumina composite materials obtained according to a CVI-technique", Adv. Ceram. Mater., 1[2] (1986) 185-191.

10 - E. FITZER and R. GADOW, "Fibre reinforced composites via the sol/gel route" in "Tailoring Multiphase and Composite Ceramics" (R.E. Tressler et al., eds.), Mat. Sci. Res., 20 (1986) 571-607.

11 - V.K. PUJARI and I. JAWED, "The alumina fibre/tetragonal zirconia polycrystal composite system", Composites, 17 [2] (1986) 137-140.

12 - N. CLAUSSEN and G. PETZOW, "Whisker reinforced zirconia-toughened ceramics", in "Tailoring Multiphase and Composite Ceramics" (R.E. Tressler et al. eds.), Mater. Sci. Res., 20 (1986) 649-662.

13 - N. CLAUSSEN and G. PETZOW, "Whisker-reinforced oxide ceramics", J. de Physique, Colloque C1, Suppl # 2, 47 (1986) C1-693 to C1-702.

14 - H. GREWE, K. DREYER and J. KOLASKA, "Whisker reinforced Ceramics",cfi/Ber, 8/9 (1987) 303-317.

15 - D.B. MARSHALL, F.F. LANGE and P.D. MORGAN, "High Strength zirconia fibers", J. Amer. Ceram. Soc., 70 [9] (1987) C 187- C 188.

16 - J.D. BIRCHALL, "The preparation and properties of polycristalline aluminum oxide fibers", Trans. J. Br. Ceram. Soc., 82 (1983) 143-145.

17 - Y. ABE, S. HORIKIRI, K. FUJIMURA and E. ICHIKI, "High performance alumina fiber and alumina/aluminum composites", in "Progress in Science and Engineering of Composites" (T. HAYASHI et al., eds.), Ed. ICCM-IV, Tokyo, 1982 (1427 - 1433).

18 - H. HANNACHE, R. NASLAIN and C. BERNARD, "Boron nitride chemical vapour infiltration of fibrous materials from BCl_3-NH_3-H_2 or BF_3-NH_3-H_2 mixtures: a thermodynamical and experimental approach", J. Less-Common Met., 95 (1983) 221-246.

19 - B. BROQUERE, B. BUTTAZZONI and J.J. CHOURY, "Les composites carbone-carbone, leurs applications industrielles", in "Introduction aux matériaux composites: 2 - Matrices Métalliques et Céramiques" (R. Naslain, ed.), CNRS-IMC Editions, Bordeaux, Chap. 17, (1985) 405-438.

20 - CHRISTIN, R. NASLAIN and C. BERNARD, "A Thermodynamic and experimental approach of silicon carbide CVD. Application to the CVI-infiltration of porous carbon-composites", Proc. Int. Conf. CVD (T.O. Sedwick and H. Lydtin, eds.), The Electrochem. Soc., Princeton, 1979, pp. 499-514.

21 - R. NASLAIN and F. LANGLAIS, "CVD-processing of ceramic-ceramic composite materials", in "Tailoring Multiphase and Composite Ceramics" (R.E. Tressler et al., eds.), Mater. Sci. Res., 20 (1986) 145-164.

22 - J.Y. ROSSIGNOL, F. LANGLAIS and R. NASLAIN, "A tentative modelization of titanium carbide CVI within the pore network of two-dimensional carbon-carbon preforms", Proc. Int. Conf. CVD (CVD-IX, Cincinnati) (Mc. D. Robinson et al., eds.), The Electrochem. Soc., Pennington, (1984), pp. 596-614.

23 - H. HANNACHE, J.Y. ROSSIGNOL, F. LANGLAIS, R. NASLAIN and P. HAGENMULLER, "Boron carbide LPCVD from BCl_3-CH_4-H_2 gas mixtures. Application to the synthesis of 2D-C-C / B_4C composite materials by CVI ", J. Less-Common Met.,

24 - R. NASLAIN, J.M. QUENISSET, J.Y. ROSSIGNOL, H. HANNACHE, P. LAMICQ, J.J. CHOURY, L. HERAUD and F. CHRISTIN, "An analysis of the properties of some ceramic-ceramic composite materials obtained by CVI-densification of 2D-C-C preforms", Proc. 5th. Int. Conf. Composite Mater. (ICCM-V, San Diego) (W.C. Harrigan et al., eds.), TMS-AIME, Warrendale, 1985, pp. 499.

25- J.Y. ROSSIGNOL, J.M. QUENISSET, H. HANNACHE, C. MALLET, R. NASLAIN and F. CHRISTIN, "Mechanical behavior in compression loading of 2D-composite materials made of carbon fabrics and a ceramic matrix", J. Mater. Sc., 22 (1987) 3240 - 3252.

26- R. SPRIGGS, J. Am. Ceram. Soc., 44 (12961) 628.

27 - J.Y. ROSSIGNOL, J.M. QUENISSET and R. NASLAIN, "Mechanical behavior of 2D-C-C / TiC composites made of a 2D-C-C preform densified with TiC by CVI", Composites, 18 [2] (1987) 135-144.

28- E. RYSHKEWITCH. "Compression strength of porous sintered alumina and zirconia", J. Am. Ceram. Soc., 36 [2] (1953) 65-68.

29 -W. DUCKWORTH, "Discussion of Ryshkewitch paper by Winston Duckworth" J. Ame. Ceram. Soc., 36 [2] (1953) 68.

Chapitre V

COMPOSITES A MATRICE A BASE DE ZIRCONE : PROPRIETES THERMIQUES ET RESISTANCE A L'OXYDATION

Soumis à "Journal of Materials Science"

THERMO - MECHANICAL PROPERTIES AND OXIDATION RESISTANCE OF ZIRCONIA CVI MATRIX COMPOSITES: 2 - THERMAL PROPERTIES AND OXIDATION RESISTANCE

J. MINET(*), F. LANGLAIS and R. NASLAIN
Laboratoire de Chimie du Solide du CNRS, Université de Bordeaux
351, Cours de la Libération, 33405 - TALENCE, France

ABSTRACT

Zirconia matrix composites, prepared by CVI from preforms (alumina or carbon fibers) having a two (or pseudo three) dimensional character, were studied from a thermal behavior and resistance to oxidation stand point. The zirconia volume fraction and residual porosity were within the 0.30 - 0.75 and 0.10 - 0.25 ranges. The experiments were carried out up to 1500°C. Thermal expansion is low and almost reversible for the C - ZrO_2 composites whereas it is more significant and partly irreversible for the Al_2O_3 - ZrO_2 composites. The ZrO_2 (m) $\rightleftharpoons$ ZrO_2 (t) transition is shifted towards the high temperatures due to the constraining effect of the carbon fibers. The Al_2O_3 - ZrO_2 composites exhibit above 1000°C an insulating character comparable to that of sintered ZrO_2. Whereas the C - ZrO_2 composites have a thermal conductivity equal to that of sintered alumina at T > 1000°C. Finally, the resistance to oxidation by air is acceptable at moderate temperatures and for short exposures. On the contrary, under more severe conditions, damaging phenomena occur (i.e. grain growth, oxidation of the carbon preform or BN interphase) which are detrimental to the mechanical behavior.

KEYWORDS

CERAMIC MATRIX COMPOSITES, ZIRCONIA MATRIX COMPOSITES
THERMAL EXPANSION, THERMAL DIFFUSIVITY, THERMALSHOCK

(*) Present adress: Société Européenne de Propulsion, B.P. 37
33165 - Saint-Médard-en-Jalles, France

1 - INTRODUCTION

Ceramic matrix composites (CMC) based on refractory oxide fibers and matrices (e.g. alumina and zirconia) have not been studied as extensively as were their carbide or nitride counterparts. However, their use at high temperatures and under oxygen-rich atmospheres should be obviously more appropriate regarding the outstanding thermal and chemical stability of refractory oxides (alumina and zirconia undergo congruent melting at about 2050°C and 2700°C respectively). Among the reasons that could explain the rather limited effort of research devoted to Al_2O_3 and ZrO_2 - based CMC are: (i) the higher densities of corundum (3.98 g . cm^{-3}) and zirconia (5.83 g . cm^{-3} for m - ZrO_2) with respect to graphite (2.27 g . cm^{-3}) and SiC (3.25 g . cm^{-3}) whereas most potential applications of CMC are presently in the field of the aerospace industry, (ii) the lack of high performance fibers suitable for reinforcing oxide matrices at high temperatures and (iii) the well known brittleness of refractory oxides which implies the use of soft fiber-matrice interphases (acting as crack arresters) in the design of oxide-based CMC (with here the specific requirement that the interphase material has to be stable towards oxidation). On the other hand, the goal of obtaining, through the use of the composite concept, tough materials stable at high temperatures and under oxygen-rich atmospheres, is a very stimulating challenge cast to researchers. This appears particularly true for ZrO_2 - based

composites where different toughening mechanisms could be combined (i.e. toughning due to phase transformation, microcracking and fiber pull-out). In that sense, zirconia is probably unique.

As a matter of fact, the number of articles on ZrO_2-CMC reinforced with long fibers is very limited whereas more attention has been paid to the reinforcement of zirconia by whiskers [1 - 6]. **V.K. Pujari and I. Jawed** reported the synthesis, according to a powder metallurgy approach, of composites made of tetragonal zirconia polycrystals (TZP) stabilized with 3.5 mole % Y_2O_3 and reinforced with 10 wt . % of chopped alumina fibers. They mentioned a twofold increase in fracture toughness over the monolithic TZP [1]. **A. Bender et al.** have prepared, through a liquid impregnation route (from organometallic precursors) ZrO_2 - SiO_2 and ZrO_2 - TiO_2 matrix composites reinforced with BN-coated SiC fibers (50 vol. %). They established the key role played by the fiber coating in the fracture mechanism (toughning by fiber pull-out) as well as in preventing the matrix-fiber reaction (diffusion barrier). Finally, they reported tensile strengths of 600 - 700 MPa and toughness of 10 - 20 MPa $m^{1/2}$ at room temperature [2]. As far as we know, no data have been published on the thermal properties of ZrO_2 - based fibrous composites.

The aim of the present work was to try to point out the effects of (i) different reinforcements (namely alumina and carbon fiber architectures characterized by very different thermal expansion coefficients, thermal diffusivities and oxidation resistances) and (ii) the monoclinic-tetragonal transition of zirconia, on the thermal behavior and oxidation resistance of ZrO_2 -

bazed CMC. The processing technique and mechanical behavior have been reported in details elsewhere but were parts of the same programme started a few years ago at University of Bordeaux within the frame of a long range effort of research on CMC [7 - 13].

2 - EXPERIMENTAL

The samples used in the present study, were obtained, starting from different fiber preforms, according to a chemical vapor infiltration (CVI) technique which has been first worked out by **F. Christin et al.** for the SiC - based composites and then extended to various CMC (namely, B_4C, TiC, BN and, more recently, Al_2O_3 matrices) [7 - 13]. It has been, in the particular case of zirconia, described in details elsewhere [7 - 13]. It has been, in the particular case of zirconia, described in details elsewhere [7 - 9]. It will be sufficient to recall here, for the purpose of the discussion, that the precursor of the matrix was a $ZrCl_4$-H_2-CO_2 mixture and that the densification of the preform was conducted in a CVI-laboratory apparatus under the following conditions: $T \approx 910°C$; $p \approx 2$ kPa and $D \approx 100\ cm^3 . min^{-1}$ [9]. Although the main purpose of this part of the study was not the optimization of toughness, a BN-coating was applied in a few cases to the fiber preforms according to a similar CVI-procedure, prior to their densification with zirconia [14].

Two kinds of reinforcements were selected: (i) alumina - based fibers characterized by an insulating character and a high positive coefficient of

thermal expansion (CTE) and (ii) carbon fibers (ex PAN) characterized by conducting properties and low CTE. Details on the nature of the fiber preforms and derived ZrO_2 - matrix composites have been given in part 1 (see tables 1 and 2) [10]. The open porosity of the preforms ranged, after consolidation, from 50 to 85 % and the residual porosity of the composites after ZrO_2 - CVI densification, from 8 to 20%. As a result, the volume fraction of zirconia deposited within the pore network was 31-75% depending on the nature of the preforms. Composites refered to as composites of types 1 to 3 derived from alumina fiber preforms (type 1: SAFFIL fiber preform / alumina binder; type 2 : ZIRCAR fiber preform / alumino - silica binder; type 3 : 2D - Sumitomo fiber preform consolidated with hex - BN by CVI) wheras composites of types 4 and 5 derived from carbon fiber preforms (type 4 : 2D - carbon fiber preform; type 5 : pseudo 3D carbon fiber preform developed by SEP under the trade mark NOVOLTEX, both consolidated with pyrocarbon by CVI). Fibers made of pure (or stabilized) zirconia would have been more appropriate than alumina fibers but were not available at that time nor are they presently on the market [15].

The thermal and oxidation resistance tests were run according to conventional procedures. The **thermal expansion** experiments were performed up to 1500°C under an argon atmosphere on samples (50 x 5 x 5 mm) cut in the preforms, parallely to the fiber reinforcement (direction 1), prior to the ZrO_2 - CVI densification; as explained in part 1 [10].

The **thermal diffusivity** of a solid can be defined in terms of the transient heat conduction equation:

$$\lambda \, \partial^2 T / \partial x^2 = Cp. \rho \, \partial T / \partial x \qquad (1)$$

where λ is the thermal conductivity, Cp the specific heat and ρ the density. The thermal diffusivity **a** is related to λ, Cp and ρ by:

$$a = \lambda / Cp. \rho \qquad (2)$$

The thermal diffusivity is a more fundamental parameter than the thermal conductivity, from a designer view point, since it is the diffusion constant which is necessary to calculate the spatial propagation of heat in a non-uniform temperature field [16]. The thermal diffusivity measurements were performed on cylindrical samples (d = 10 mm; h = 3 mm) cut in the preforms either parallely or perpendicularly to the fiber reinforcements (directions 1 and 3), prior to the ZrO_2 - CVI densification. The experiments were run, at different temperatures ranging from room temperature to 1500°C, under an argon atmosphere, according to the so-called flash method [17]. According to this technique and as illustrated in figure 1, one face of the specimen is briefly illuminated with a laser flash (duration of the flash less than one microsecond) and the temperature of the rear face is recorded vs time while the heat flux propagates through the solid. If h is the specimen thickness and $t_{1/2}$ the time which is necessary to raise the temperature of the rear face to $T_M / 2$ (where T_M is the maximum temperature reached at the rear face due to the heat flux), then the thermal diffusivity is given by [17]:

$$a = 1.38 (h^2) / (\pi^2 t_{1/2}) \qquad (3)$$

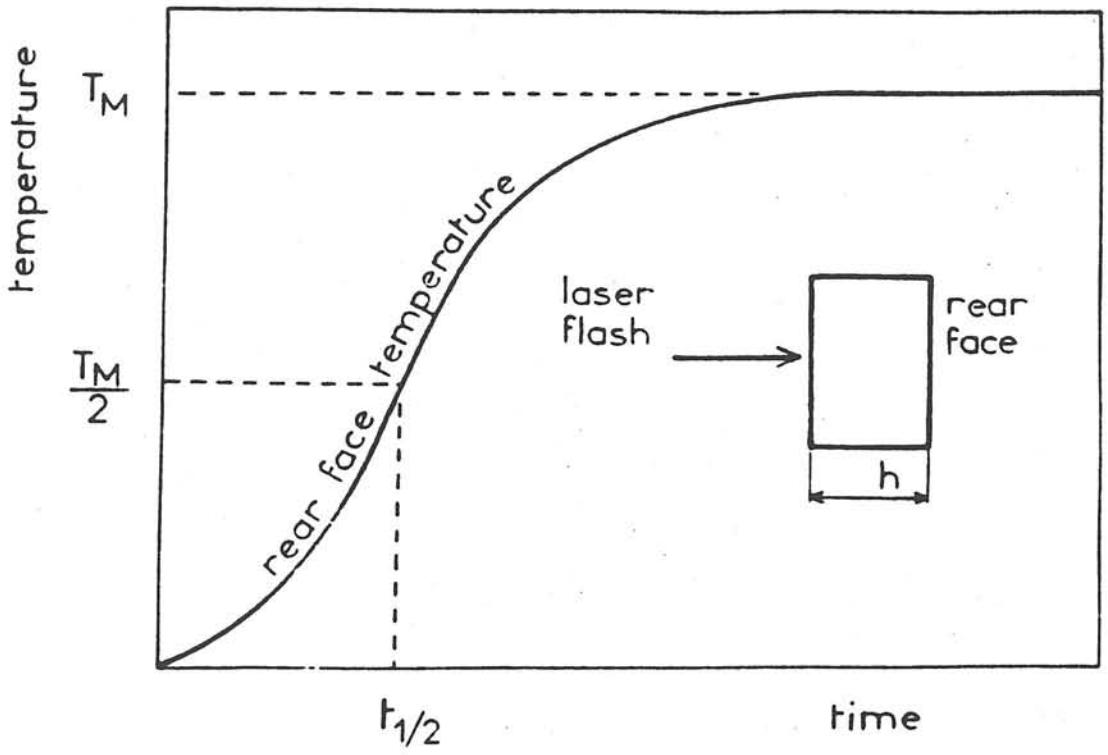

Fig. 1 - Measurement of the thermal diffusivity of zirconia matrix composite materials according to the flash method

Furthermore, in order to derive the **thermal conductivity** λ from the thermal diffusivity data, applying equation (2), the specific heat Cp and the density ρ of the solid have to be known. Therefore, density was measured, at room temperature, according to the conventional Archimede method. Specific heat was measured, on cylindrical samples (d = 5mm; h = 1mm) from 70 to 570 °C under an atmosphere of nitrogen.

In order to access the effect of an oxygen containing gaseous atmosphere on the stability of the composites, tests were run on different samples (i.e. bending test specimens (60 x 12 x 2 mm) or cylindrical specimens (d = 8mm; h = 8mm) cut, as said above, in the preforms prior to ZrO_2-CVI densification), either in air or pure oxygen and at a temperature within the range 1100-1200°C. The weight variations of the samples were usually recorded vs time with a microbalance. After cooling, the samples were analysed by X-ray diffraction (XRD) with Cu-Kα radiation, scanning electron microscopy (SEM) as well as Raman spectroscopy microanalysis (RSM) with a Laser beam ($\approx$ 1 μm in diameter).

3 - RESULTS AND DISCUSSION

3.1. Thermal expansion

The thermal expansion tests were performed, parallelly to the reinforcement layers (direction 1), on three different materials. The first belongs

to the composite 1 series but was incompletely densified, i.e. it had a ZrO_2 volume fraction of only 0.19 (instead of 0.44 as reported in Table 2 part 1 [10]) and therefore a rather large residual porosity (V_p = 0.38). The second is a composite of type 4 and the third a composite of type 5 (with a somewhat lower zirconia volume fraction, i.e. 0.55 instead of 0.62).

The variations of the thermal $\Delta l / l_0 = (l_T - l_0) / l_0$ where l_T and l_0 are respectively the lengths of the specimen at T and ambient), as a function of temperature, are shown in figures 2 - 4. Three heating / cooling cycles are given for each material in order to point out the reversible and irreversible evolutions of the materials induced by temperature. Assuming that the monoclinic-tetragonal transition of zirconia takes place between 1000 and 1200°C [18] even when zirconia is trapped within a fiber skeleton, the first temperature cycle was limited to 800°C, i.e. (i) well below the ZrO_2 (m) ---> ZrO_2 (t) transition, (ii) the temperatures at which ZrO_2 was formed by CVI (≈ 900°C) and (iii) the preforms processed (900 - 1100°C for CVI consolidation by pyrocarbon and 1400°C for slurry impregnation and sintering). On the other hand, the second and third temperature cycles usually exhibit an excursion near or above the ZrO_2 (m) ---> ZrO_2 (t) transition temperature.

Generally speaking, the thermal expansion behavior of the materials is reversible within the 20 - 800°C temperature range. Although the $\Delta l/l_0$ - T curves are almost the same on heating and cooling for the composites of types 1 and 5, they appear to be very different at low temperatures for the

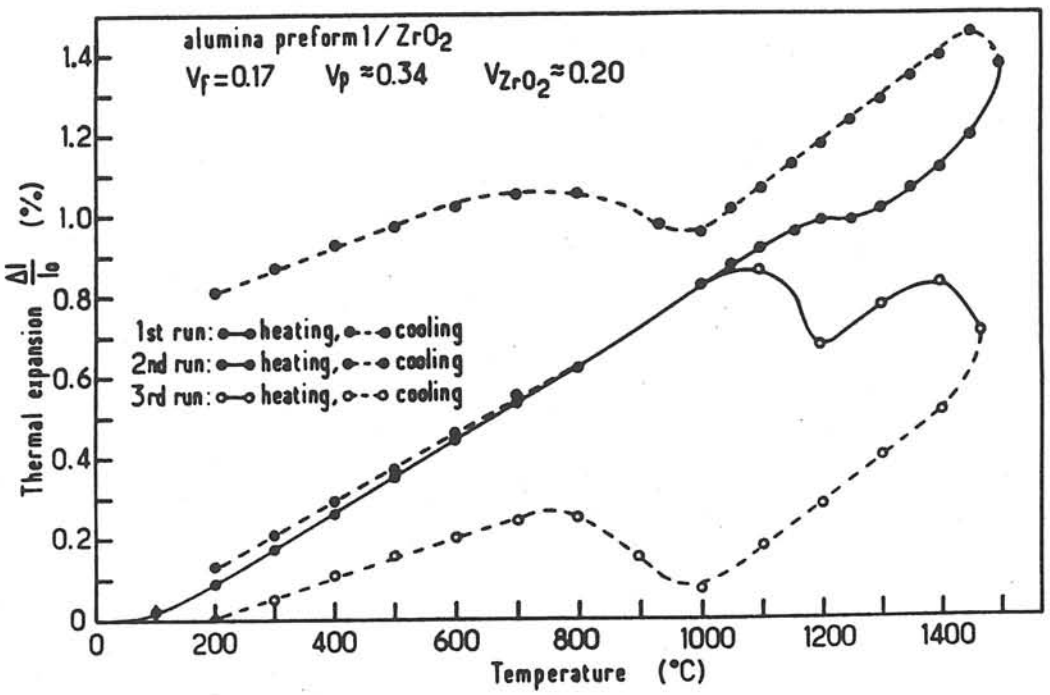

Fig. 2 - Thermal expansion of an alumina-zirconia composite (type 1) as a function of temperature

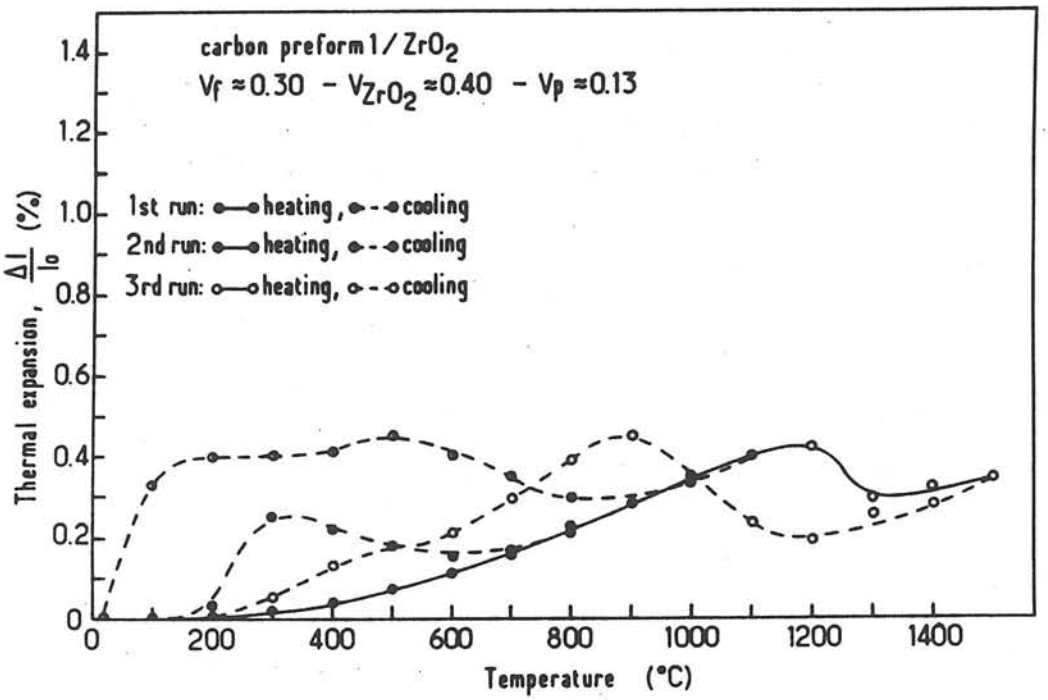

Fig. 3 - Thermal expansion of a carbon-zirconia compoosite (type 4) as a function of temperature

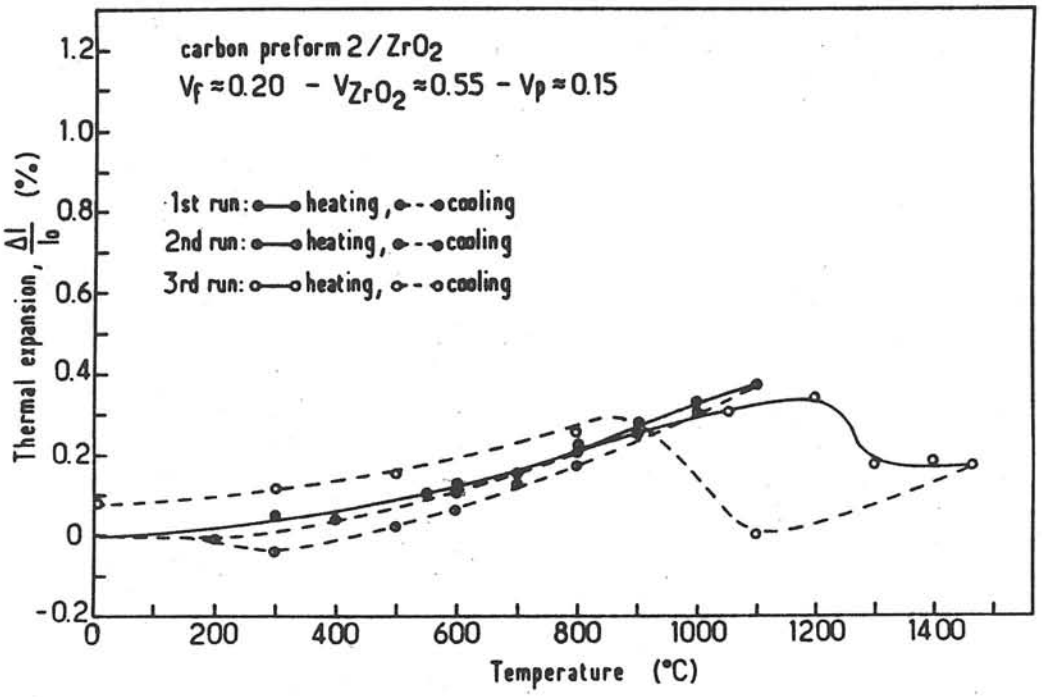

Fig. 4 - Thermal expansion of a carbon-zirconia composite (type 5) as a function of temperature

composite of type 4, which exhibits a significant expansion on cooling between 500 and 200°C (this expansion disappearing below 200°C) (Fig. 3).

Extending the themperature cycle up to 1100°C does not modify significantly the above conclusions. However, the hysteresis effect which was almost negligible for the composite of type 5 between ambient and 800°C is now more pronounced (Fig. 4). In the same manner, the expansion observed on cooling, for the composite of type 4, takes place earlier (i.e. at about 700°C) and disappears only when approaching the ambient (Fig. 3).

The thermal expansion behavior of the composites becomes more or less complex according to the nature of the preform, when the upper limit of the temperature cycle is extended above the ZrO_2 (m) ---> ZrO_2 (t) transition. The simplest case is that corresponding to the composite of type 5 (Fig. 4). It is characterized by: (i) a hysteresis loop due to the reversible ZrO_2 (m) $\rightleftharpoons$ ZrO_2 (t) transition which takes place at 1200 - 1300°C on heating and at 1100 - 900°C on cooling, i.e. in temperature ranges slightly higher than those reported for unreinforced zirconia (Fig. 5) [18, 19], and (ii) a small permanent expansion (about + 0.1%) when the specimen is cooled back to the ambient. A rather similar behavior is apparent from figure 3 for the composite of type 4. However, the expansion effect due to the polymorphic transition of ZrO_2 is smaller (a feature which could be simply related to the lower ZrO_2 volume fraction). Furthermore, the expansion at low temperatures on cooling, which has been reported above for the temperature cycles limited to 800 - 1100°C, is found to have almost disappeared after heating at 1500°C. This feature suggests that further cycling at 1500°C could

result in thermal expansion curves similar to that observed for the composite of type 5 after one single cycle at 1500°C (Fig. 4). Finally, the material never exhibits a permanent expansion when cooled back the ambient.

As shown in figure 2, the thermal expansion curves for the composite deriving from the alumina-based preform (composite of type 1) become much complex when the temperature cycle is extended up to 1500°C, whith the main following features: (i) during the first heating at high temperatures (cycle 2), the ZrO_2 (m) ---> ZrO_2 (t) transition is hardly detectable whereas it is well apparent on cooling as well as on both heating and cooling during the second high temperature cycle (cycle 3), (ii) the ZrO_2 (m) $\rightleftharpoons$ ZrO_2 (t) transitions are shifted about 100°C below those reported above for the carbon fiber reinforced composites, i.e. they take place within temperature ranges which are in better agreement with those of unreinforced zirconia (Fig. 5) [19], (iii) finally, after the first heating at 1500°C, the specimen has kept a large permanent expansion when cooled back to a temperature close to the ambient (i.e. + 0.8% at 200°C).

Although a detailed understanding of the thermal expansion behavior of ZrO_2 - based fiber composites would require obviously complementary experiments, some general comments can be made on the basis of the present exploratory study. Figures 2 - 4 show, as said above, that below the ZrO_2 (m) ---> ZrO_2 (t) transition, the thermal expansion behavior of the composites is neither perfectly reversible nor linear. However, assuming in a first approximation a linear $\Delta l / l_0$ - T relationship in a given temperature range, CTE can be calculated from the thermal expansion data. Their values, given in

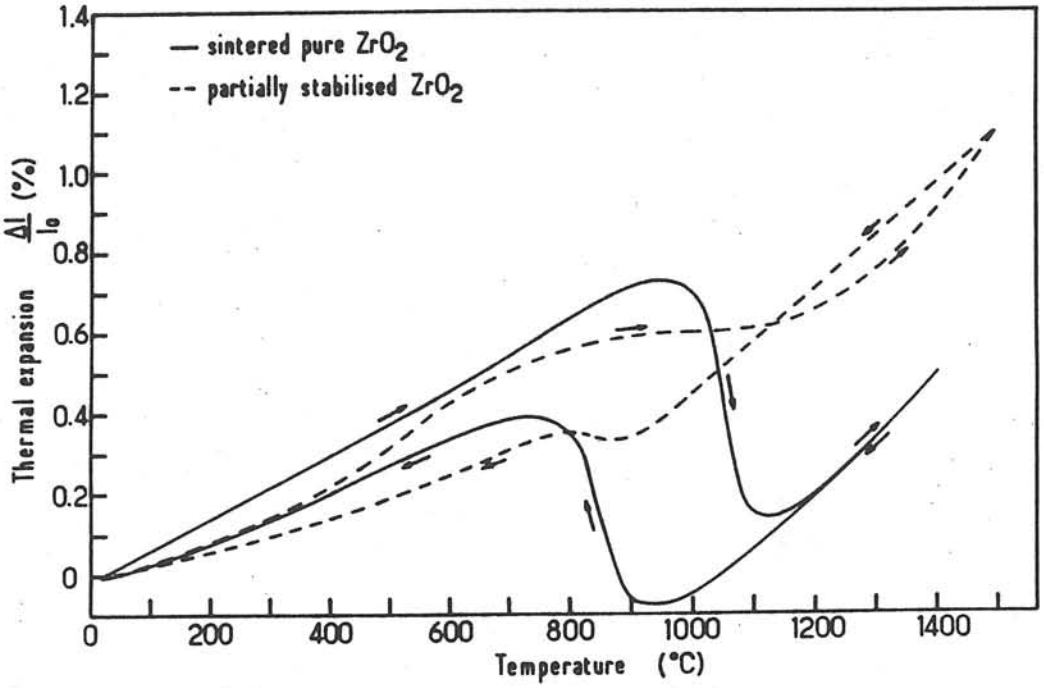

Fig. 5 - Thermal expansion of unreinforced zirconia as a function of temperature

table 1, show that the composites with a carbon fiber skeleton have a better dimension stability than those deriving from the alumina preforms, due to the much lower CTE of the 2D-C-C preform. As already established for other matrices (e.g. glass-ceramics or metals), this effect of the carbon reinforcement on the thermal expansion of ZrO_2-matrix composites should be still more pronounced if HM or UHM carbon fibers are used. Furthermore, the shift, of the ZrO_2 (m) $\rightleftharpoons$ ZrO_2 (t) transitions towards the high temperatures, which has been pointed out in the present study and for the first time as far as we know, when zirconia is trapped within a carbon fiber skeleton, is consistent with the stress-dependent character of the transition. Again, this effect could be still more important for say pure orthogonal 3D woven preforms built from carbon fibers exhibiting higher negative CTE (e.g. the P100 fiber series from Union Carbide). On the other hand, the origins of the other phenomena which have been reported here remain a matter of speculation regarding the limited amount of data and samples. Thus, the permanent expansion observed for the composite of type 1, after heating at 1500°C and cooling, could be related to at least two complementary phenomena: (i) the absence of contraction at the ZrO_2 (m) ---> ZrO_2 (t) on heating which does not balance the expansion on cooling at the reverse transition and (ii) some creep, at high temperatures, of the poorly densified composite (which contains moreover a significant amount of silica). However, these two phenomena are no longer observed during the second cycle at 1500°C. Similarly, the expansion on cooling which appears at low temperatures for the composite of type 4 may have to be connected to the strong 2D anisotropy of the material. As a matter of fact, it is not present for the composite of type 5 whose main difference is the occurence of fibers bonding the carbon 2D layers together in the third direction.

COMPOSITES	Temperature range (°C)	Mean α_1 ($°C^{-1}$)
Type 1 (alumina preform)	200 to 1000	9.2×10^{-6}
Type 4 (2D-C-C preform)	500 to 1100	5.5×10^{-6}
Type 5 (3D-C-C preform)	500 to 1100	3.8×10^{-6}

Table 1 : Thermal expansion characteristics of the composites of types 1, 4 and 5 (assuming a $\Delta l / l_0 = f(t)$ linear relation within the temperature range considered).

3.2. Thermal diffusivity

The thermal diffusivity measurements were performed on four different materials, parallely (direction 1) or perpendicularly (direction 3) to the ceramic fiber layers: composites of type 1 ($V(ZrO_2)$ = 0.40; V_p = 0.22), type 2 ($V(ZrO_2)$ = 0.75; V_p = 0.10), type 4 ($V(ZrO_2)$ = 0.32; V_p : 0.15) and type 5 ($V(ZrO_2)$ = 0.60; V_p = 0.10).

The variations of the thermal diffusivities a_1 et a_3 (measured respectively in a direction parallel or perpendicular to the fiber layers) as a function temperature are shown in figures 6 and 7. Their values at the ambient, 1000 and 1500°C are listed in table 2.

The thermal diffusivities of the ZrO_2 - matrix composites decrease regularly as temperature increases. They are lower for the composites derived from the alumina preforms than for those measured on the composites reinforced with a carbon fiber skeleton (carbon fibers consolidated with pyrocarbon), a feature which is directly the result of the insulating and conducting characters of alumina and carbon respectively. Furthermore and as shown in figure 6, the thermal diffusivity of the Al_2O_3 (SiO_2)-ZrO_2 composites decreases as the volume fraction of zirconia increases due to the fact that zirconia is a better insulating material. Thus, the composites obtained by ZrO_2-densification of Al_2O_3 (SiO_2) preforms have a lower thermal diffusivity than those derived from the same preforms by Al_2O_3-densification. As an example, $a_1 = 4.5.10^{-6}$ and $2.7.10^{-6} m^2 s^{-1}$ at the ambient for composites of type 1 densified according to the same

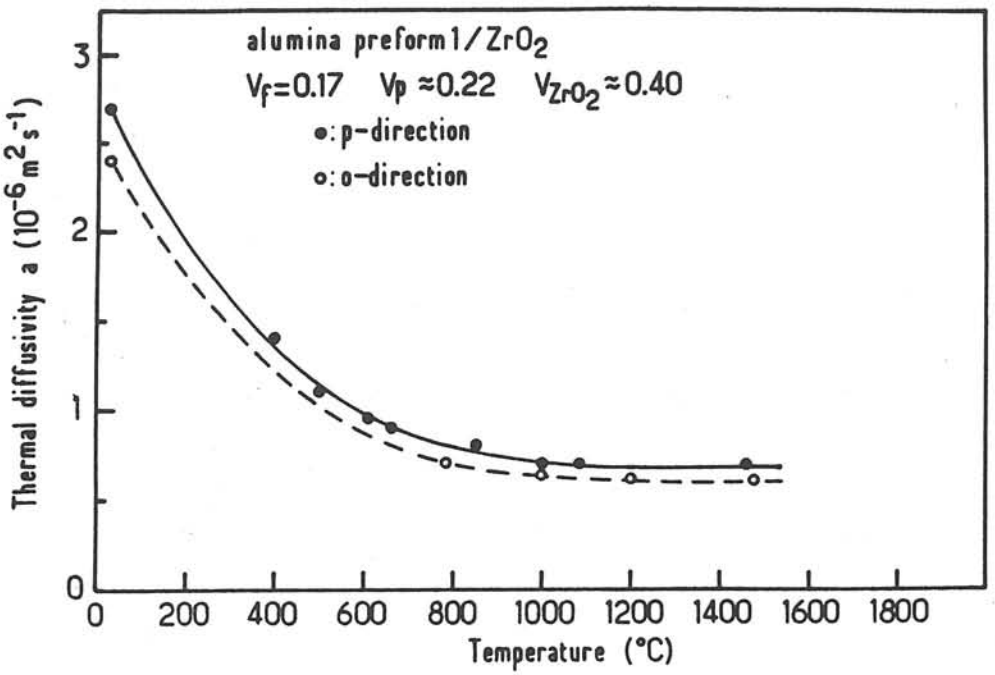

(a)

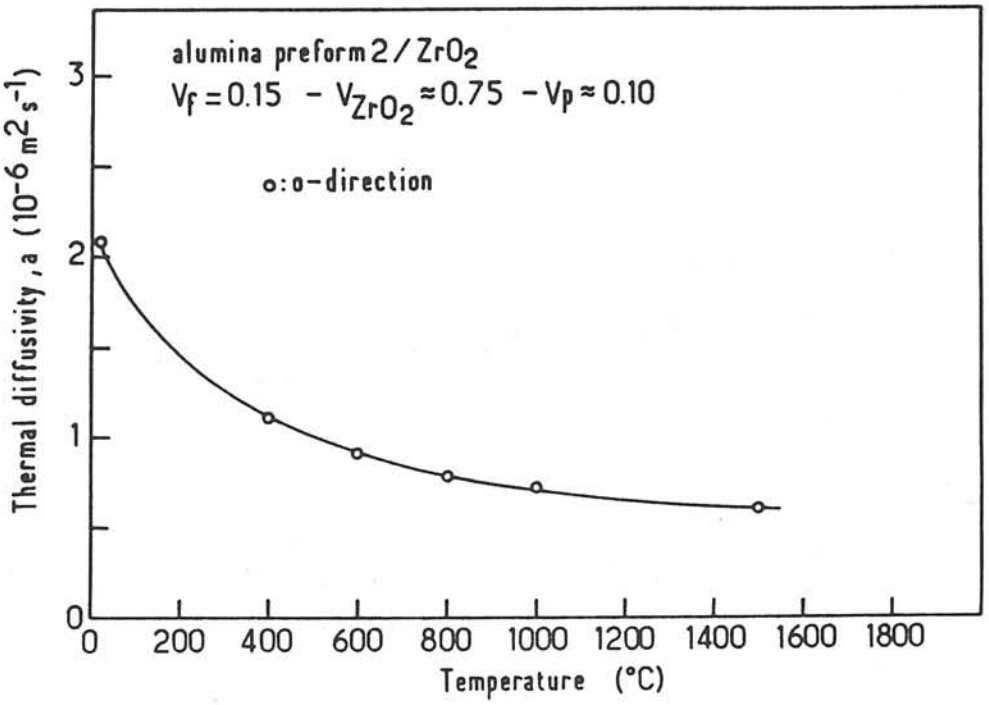

(b)

Fig. 6 - Thermal diffusivity of alumina-zirconia composites (a) type 1, (b) type 2, as a function of temperature

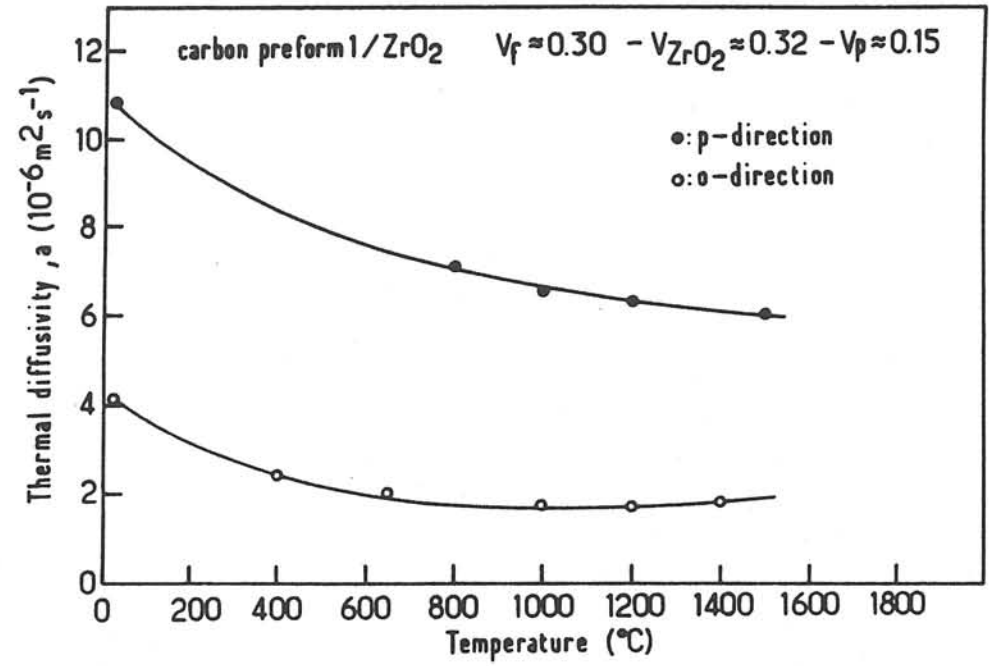

(a)

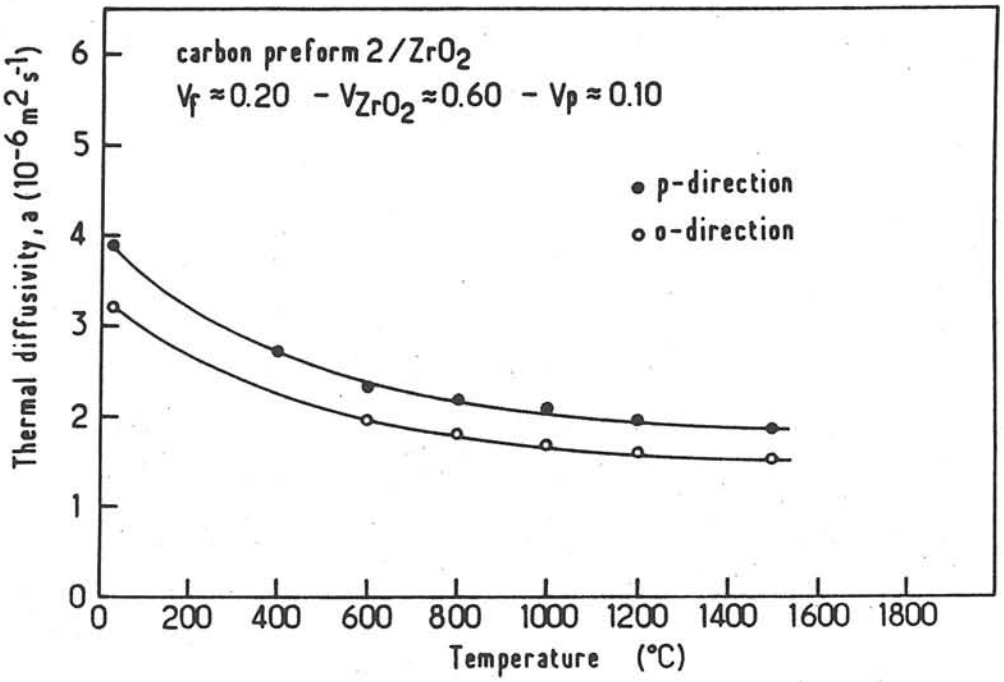

(b)

Fig. 7 - Thermal diffusivity of carbon-zirconia composites (a) type 4, (b) type 5, as a function of temperature

COMPOSITES	20°C		1000°C		1500°C	
	a_1	a_3	a_1	a_3	a_1	a_3
Type 1 (alumina preform)	2.7	2.4	0.7	0.65	0.7	0.6
Type 2 (alumina preform)	-	2.1	-	0.75	-	0.6
Type 4 (carbon preform)	11	4	6.6	1.7	6	1.8
Type 5 (carbon preform)	4	3.2	2.1	1.7	1.9	1.5

Table 2 : Thermal diffusivity (in 10^{-6} m^2 s^{-1}) of ZrO_2 - matrix fibrous composites

CVI-technique by alumina and zirconia respectively [13]. Finally, the anisotropy of thermal diffusivity of the composites derived from the alumina-based preforms is weak as it could have been predicted from the insulating character of both alumina and zirconia.

On the contrary, the thermal diffusivity anisotropy of the composite of type 4, made of a 2D-C-C skeleton densified with zirconia, is much pronounced due to the texture of the composite, the conducting character of carbon and the insulating properties of zirconia. The thermal diffusivity is higher is a direction parallel to the carbon fabrics (due to the continuity of the carbon skeleton) than in an orthogonal direction where there is a stacking of alternating layers of conducting and isolating materials. This feature is general for all the composites derived from a 2D-C-C preform. It has been reported already for the 2D-C-C / SiC and 2D-C-C/TiC composites [20, 21]. It is even true for the 2D-C-C composites themselves [22]. As it could have been predicted, the thermal diffusivity anisotropy of the composite of type 5 is much lower due to the occurence of carbon fibers running in a direction perpendicular to the carbon fabrics, a feature which is specific to the NOVOLTEX fiber architecture (Fig. 7). The low values of the thermal diffusivities measured on this composite are due to the high volume fraction (i.e. 0.60) of the isolating ZrO_2 matrix.

3.3. Specific heat and thermal conductivity

Specific heat measurements have been performed on two different materials, i.e. on composites of types 2 and 4 derived from alumina-based and

carbon-based preforms respectively (table I). The variations of the specific heats C_p as a function of temperature are shown in figure 8. For both materials, a slight modification of the slope of the curve occurs at about 350°C whose origin is presently unknown.

The specific heat appears to be higher for the composite with a carbon skeleton than for the composite prepared from the alumina-based preform, whatever the temperature, the gap being higher at high temperatures. This feature is in agreement with the facts that: (i) carbon has itself a higher C_p than both alumina and zirconia and (ii) its C_p increased more rapidly with rising temperatures than those of alumina and zirconia [24].

Assuming that the specific heat of the composites obeys the rule of mixtures, the C_p values of the composites have been calculated from the compositions of the materials and from the C_p values of the constituents taken from [24]. The calculated C_p values are given in figure 8.

It clearly appears from figure 8, that there is a rather good agreement between the calculated and measured C_p values for the composite of type 4 (prepared from the 2D-C-C preform). On the contrary, for the composite of type 2 (obtained from Al_2O_3 (SiO_2) preform), the measured C_p values are systematically higher than the calculated values and they increase more rapidly with rising temperatures. These features could result from the facts that (i) both the fibers and their binder are not pure alumina but are made of alumina and silica (silica has not been taken into account in the calculation of C_p) and (ii) the

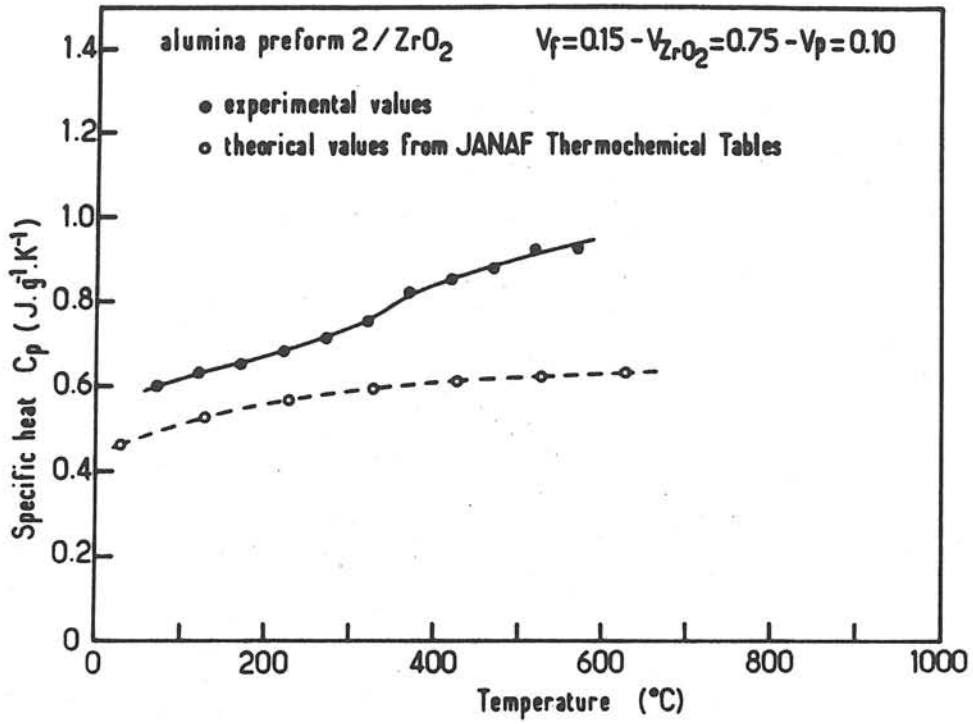

(a)

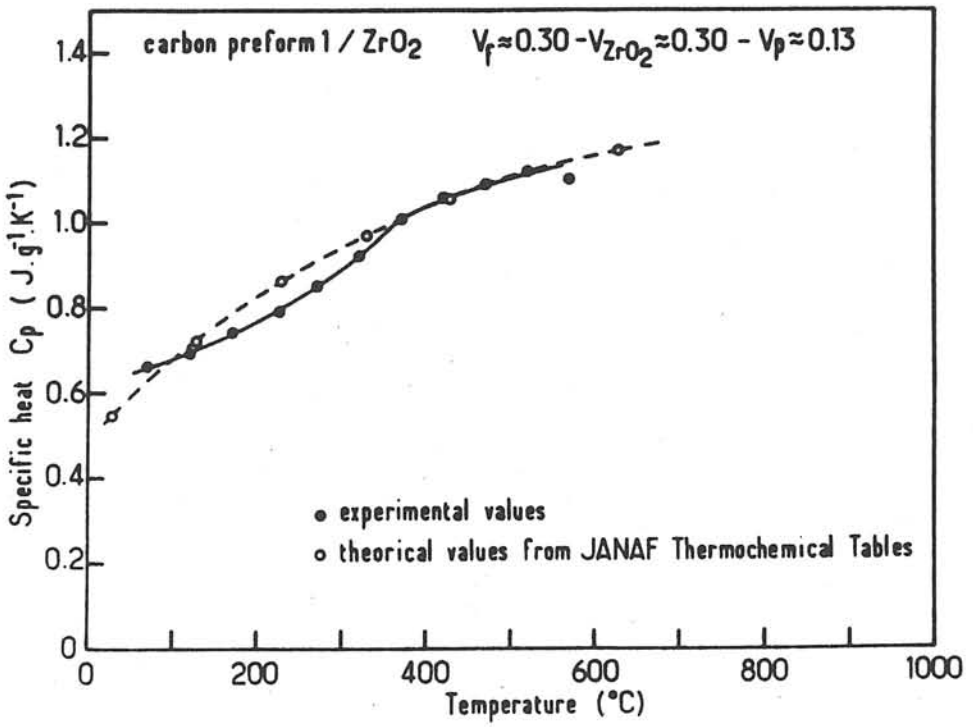

(b)

Fig. 8 - Variations of the specific heat of (a) alumina-zirconia composite (type 2), (b) carbon-zirconia composite (type 4), as a function of temperature

ZrO_2 matrix deposited by CVI often contains a small amount of free carbon, as established by J. Minet et al [7, 8].

From the measured values of density, thermal diffusivity and specific heat, the thermal conductivity λ can be calculated from equation (2). The variations of λ as a function of temperature are shown in figure 9 for different Zro_2-matrix composites as well as those for several related monolithic materials (i.e. pyrolytic graphite, sintered alumina and zirconia).

The Al_2O_3 (SiO_2) - ZrO_2 fibrous composites have, at room temperature, thermal conductivities which are very similar in directions parallel and perpendicular to the fiber layers (directions 1 and 3, respectively), as discussed above for the thermal diffusivities (i.e. $\lambda_1 = 5$ and $\lambda_3 = 4$ W $m^{-1}K^{-1}$). As temperature is raised, the thermal conductivities decrease down to values which are close to that of sintered stabilized zirconia at 1500°C. Therefore, the $Al_2O_3(SiO_2)$-ZrO_2 fiber composites can be regarded, above about 1000°C, as materials having insulating properties equivalent to those of zirconia. On the contrary and as expected, the composites prepared from carbon fiber preforms have higher thermal conductivities. Moreover, the strong anisotropy which characterizes the thermal diffusivity of the 2D-C-C/ZrO_2 composite (type 4) results in a similar anisotropy for the thermal conductivity (since ρ and C_p are volumic properties). As an example, at room temperature, $\lambda_1 = 18$ and $\lambda_3 = 7$ W m^{-1} K^{-1}. This is no longer the case for the composite of type 5 obtained from the NOVOLTEX preform which exhibits only a weak anisotropy with λ values

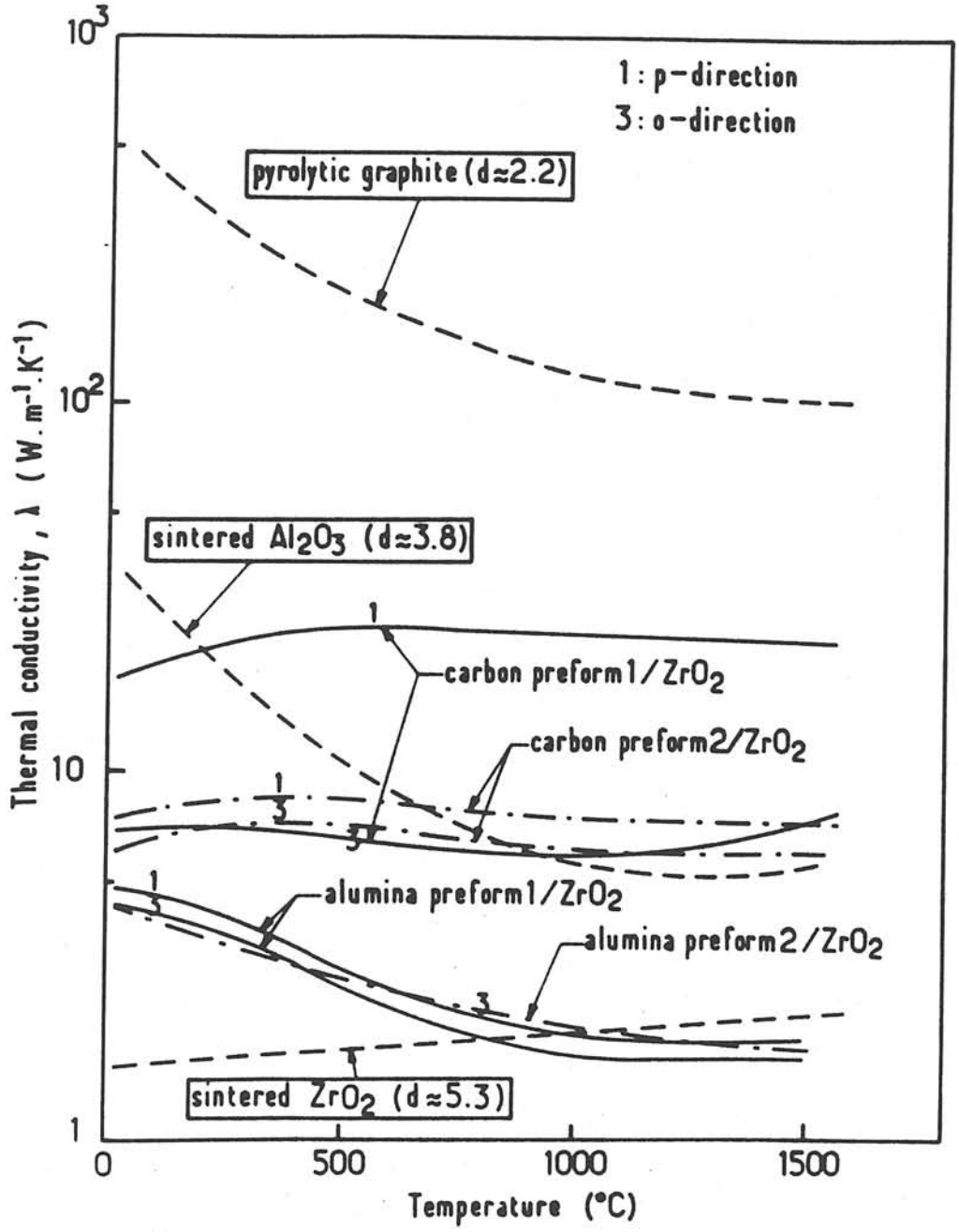

Fig. 9 - Variations of the thermal conductivity of zirconia matrix composite materials vs. temperature

remaining almost constant within the whole 20 - 1500°C temperature range (λ_1 = 7-8 and λ_3 = 6-7 W m^{-1} K^{-1}).

3.4. Resistance to oxidation

The oxidation tests have performed on composites prepared either from alumina-based preforms (composite of type 1) or carbon-based preforms (composite of type 4). Moreover, since hex-BN could be a potential interphase material, the tests were extended to composite of type 3 [2, 14].

- Composites alumina-zirconia

Bending test specimens of composite of type 1 ($V(ZrO_2)$ = 0.40; V_p = 0.20) were heated at 1300°C in air for 6 hours, cooled to the ambient temperature and analyzed. As shown in figures 10 - 12, several important phenomena occur during the oxidation test which modify both the composition and microstructure of the ZrO_2-matrix (which has been formed at a much lower temperature, i.e. about 900°C). The small amount of free carbon codeposited with zirconia from the $ZrCl_4$-CO_2-H_2 precursor, as mentioned above, is burnt off, as illustrated by the evolution of the Raman spectrum (Fig. 10) [8]. Simultaneously, the poorly crystallized monoclinic ZrO_2 - matrix undergoes a recrystallization process, as attested by a sharpening of the Raman and Debye-Scherrer pattern lines (Figs. 10 and 11) and a coarsening of the microstructure (Fig. 12). The evolution of the microstructure of the matrix and simultaneously that of the alumina fibers (not studied here but known to occur

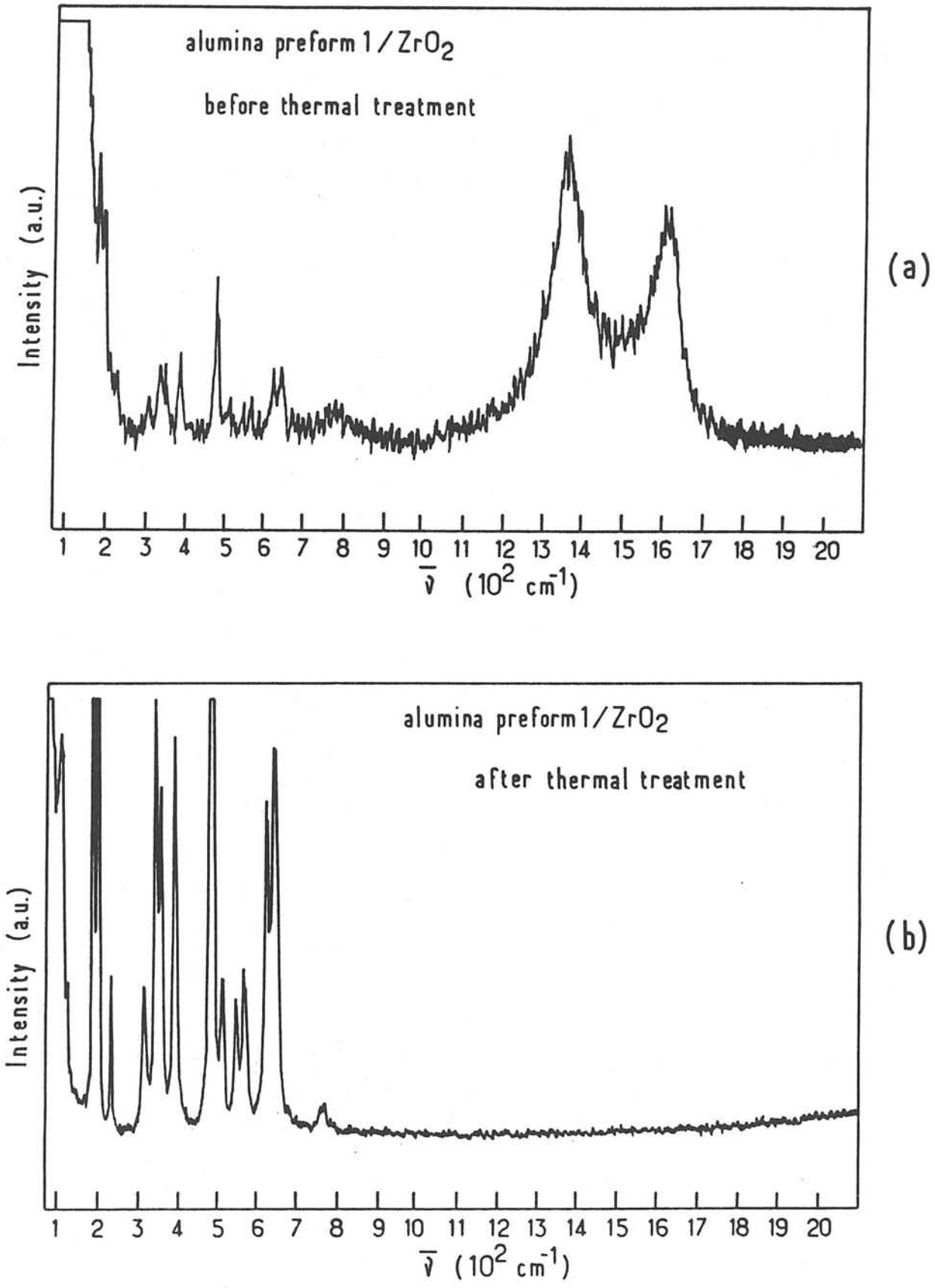

Fig. 10 - Raman spectra of the zirconia based matrix in composite of type 1: (a) as prepared, (b) after an oxidation test in air at 1300° C

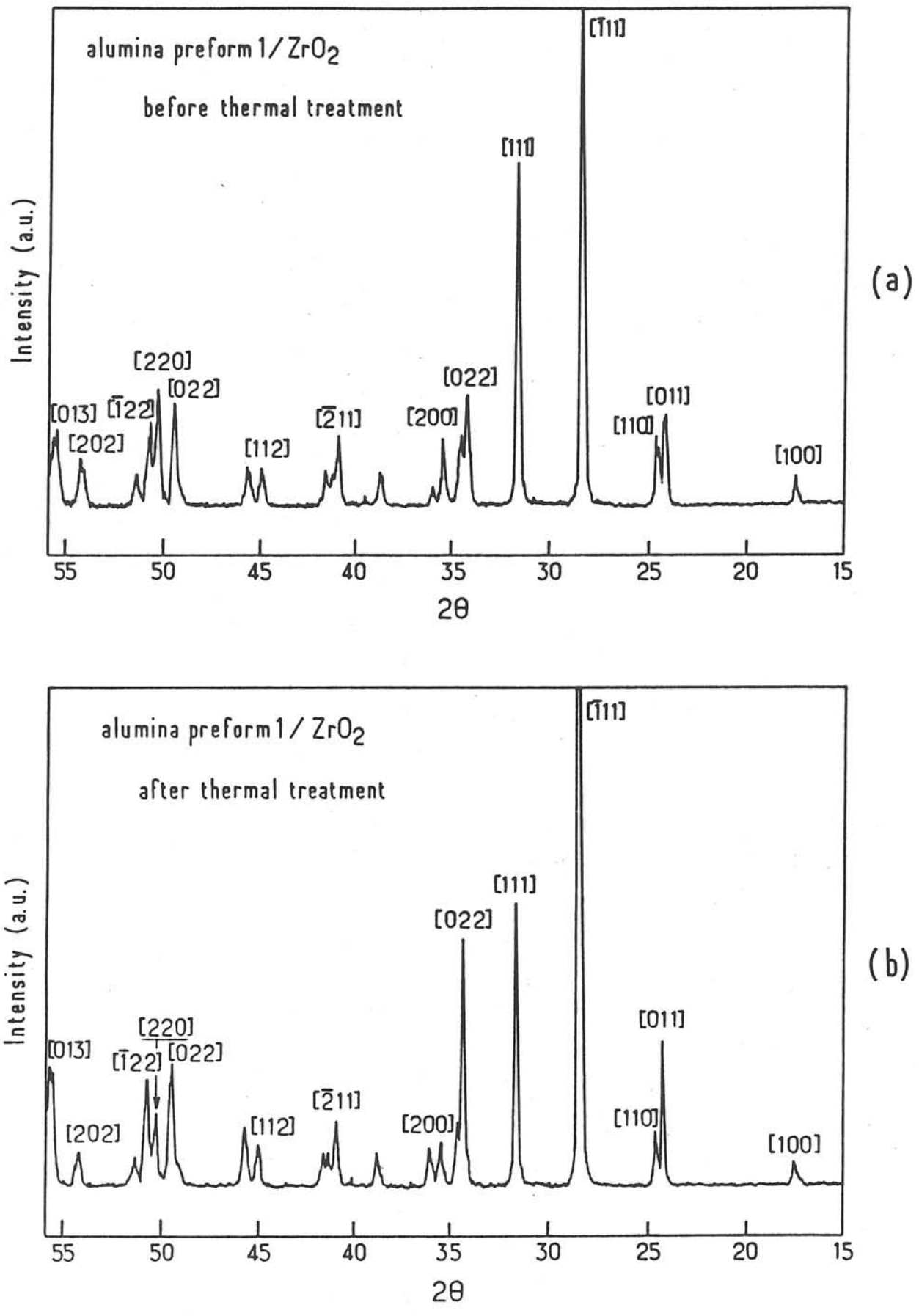

Fig. 11 - Debye-Scherrer pattern of an alumina-zirconia composite (type 1): (a) as prepared, (b) after an oxidation test in air at 1300°C

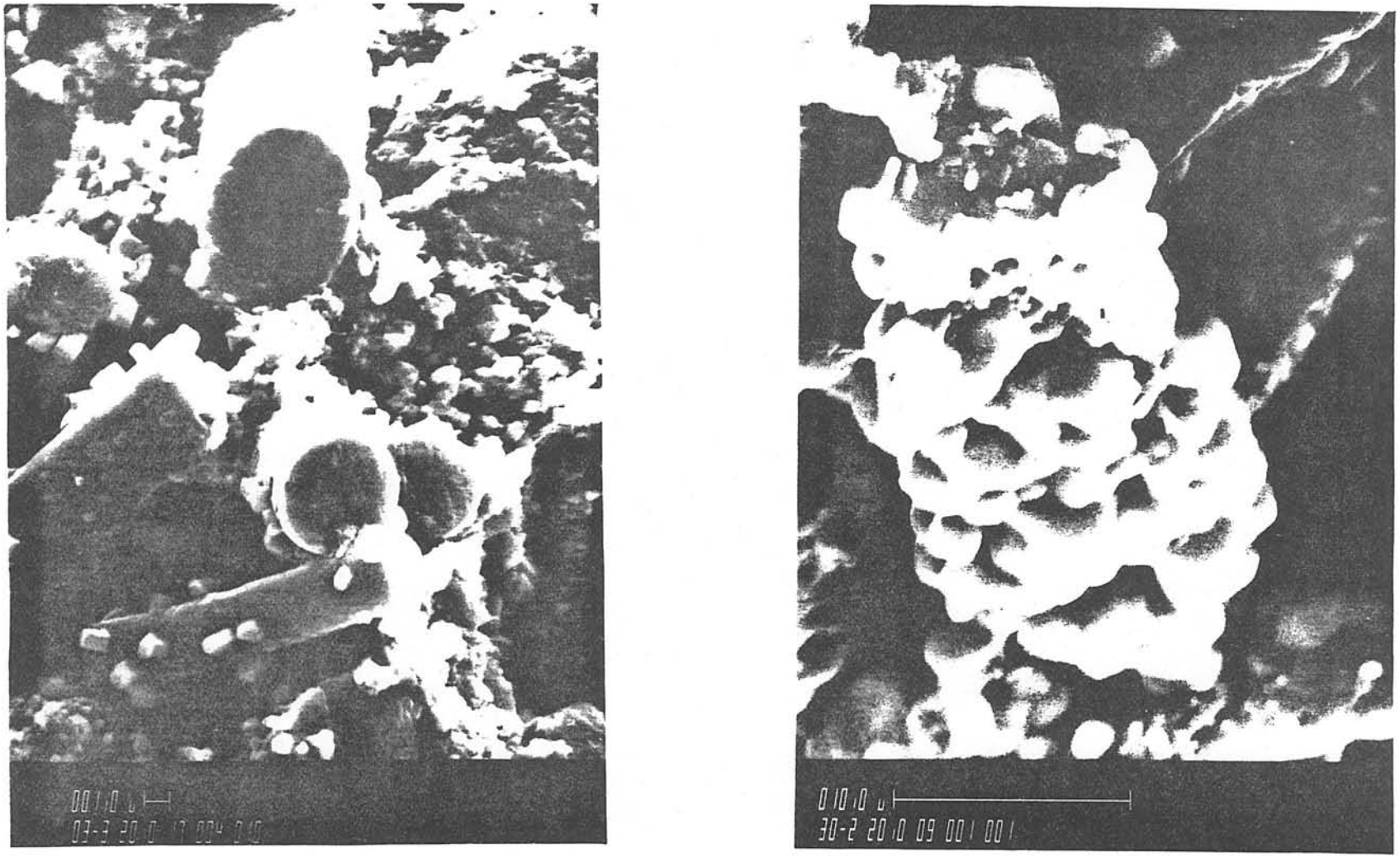

(a) (b)

Fig. 12 - SEM microanalysis of an alumina-zirconia composite (type 1): (a) as prepared, (b) after an oxidation test in air at 1300°C

under such conditions) result in a significant lowering of the bending strength (of the order of 30-50%).

A coarsening of the microstructures of both the alumina fibers and m - ZrO_2 matrix was also observed, after an oxidation test in air at high temperatures (1200°C; 6 hrs), for the alumina-zirconia composite of type 5, as illustrated in figure 13. Moreover and as it could have been predicted, an oxidation of the BN interphase also takes place, as shown in figure 14 which gives the variations of the mass of the sample during the test (temperature was first increased up to 1200°C at a rate of 600°C per hour and then it was maintained at this value for 46 hours). During the first part of the test (when temperature is raised from the ambient to 1200°C), the sample undergoes a small weight loss which could correspond to both and outgasing of the material (whose residual porosity is of the order of 20%) and to the oxidation of the free carbon of the ZrO_2 - matrix. During the second part of the test, there is a weight increase which is thought to be related to the oxidation of BN yielding B_2O_3. Finally, the sample undergoes a new weight loss (part 3) which could correspond to a slow vaporization of the boron oxide.

It appears from the present study that an again treatment in air at 1200-1300°C of an alumina-zirconia composite does result in a microstructural evolution which may be detrimental to some extend to its mechanical behavior (the lack of suitable fibers for high temperature applications is a well established feature of the engineering og CMC).Moreover, although BN has been found to be an efficient interphase material for enhancing fiber pull out and increasing

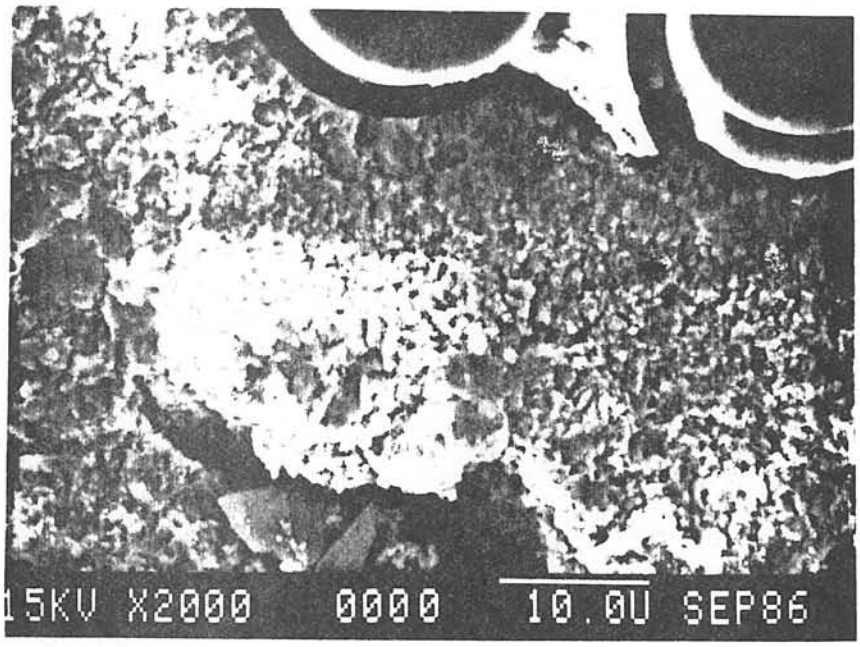

(a)

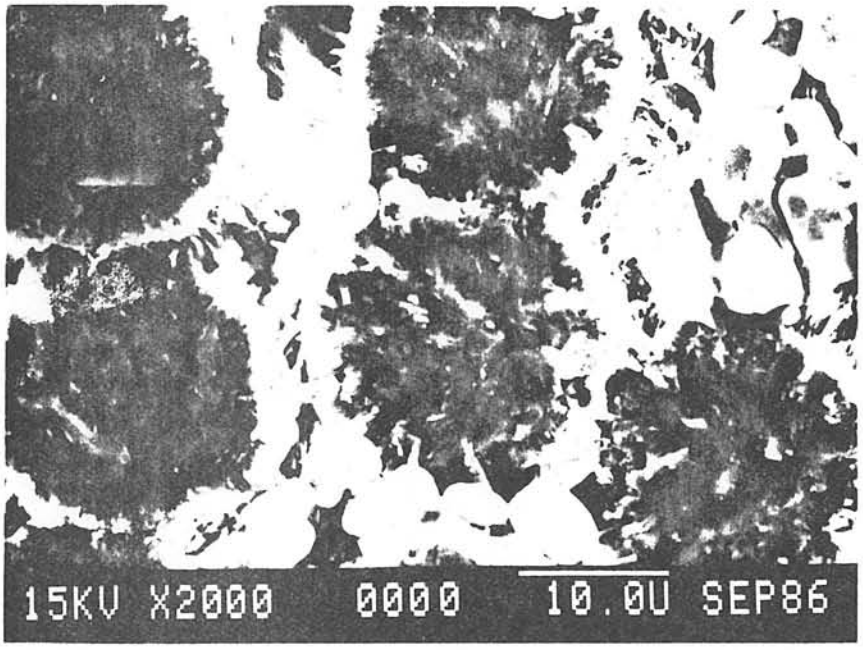

(b)

Fig. 13 - SEM analysis of an alumina-zirconia composite (type 3): (a) as prepared, (b) after an oxidation test in air at 1200°C

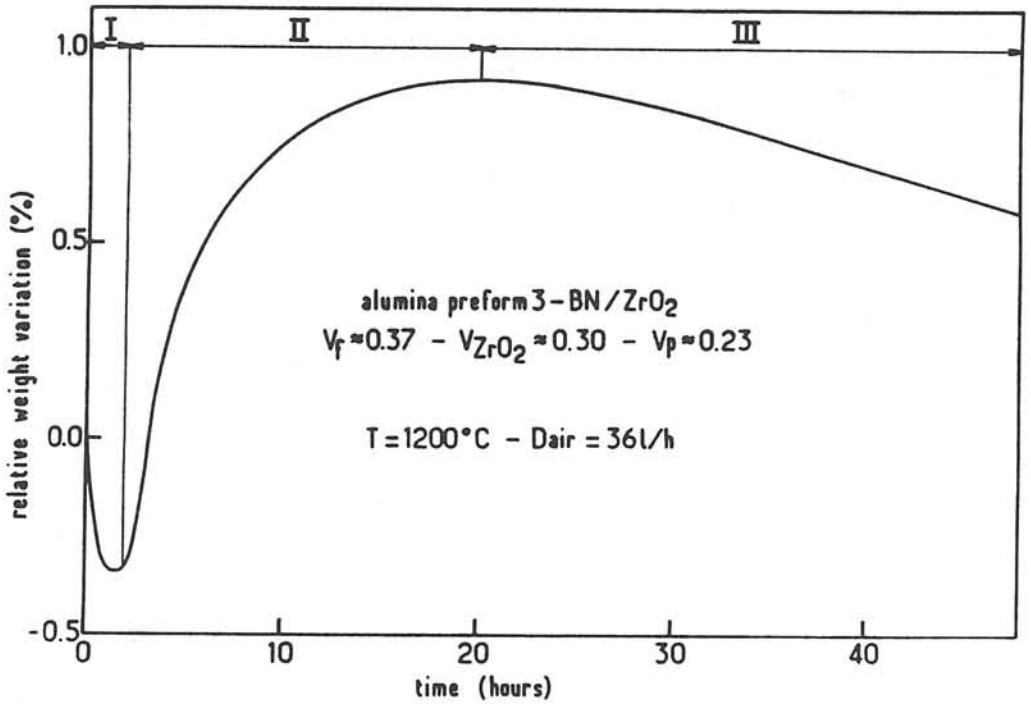

Fig. 14 - Weight variations of a 2D-Al_2O_3 (BN) - ZrO_2 composite (type 3) during an oxidation test in air at 1200°C

toughness at room temperature in oxide-matrix composites [2, 24], its use in materials which have to sustain long exposures in air at high temperatures, may be questionable unless a protective coating is applied to the whole composite.

- Composites carbon-zirconia

Oxidation tests were also performed on carbon-zirconia composites of type 4 (cylindrical samples: d = 8 mm; h = 8 mm) in order to assess the effects of temperature, time and oxygen partial pressure on the materials.

A first series of tests were performed in air at 1100°C on samples prepared from a 2D-C-C preform whose open porosity was $V_p \approx 0.56$ and which was progressively filled with zirconia up to $V(ZrO_2) = 0.30$. As shown in fig. 15, the oxidation kinetics of the initial 2D-C-C porous preform is very rapid, the specimen being totally consumed by oxidation in 90 min. As the volume fraction of zirconia increases, the time necessary to consume the carbon is still very short for $V(ZrO_2) = 0.10$ and 0.15. On the contrary, for $V(ZrO_2) > 0.20$, a protective effect is observed, the rate of the weight loss decreasing as the volume fraction of ZrO_2 increases. For $V(ZrO)_2 = 0.30$, the weight loss is less than 2% after 4 hours of exposure in air at 1100°C which appears to be a rather remarkable result regarding the poor resistance of carbon to oxidation at such a temperature and the high residual porosity of composite (i.e. 0.26).

A second series of experiments were run at 1150°C on the same materials (with $V(ZrO_2) = 0.30$ and $V_p = 0.26$) in order to study the effects of both

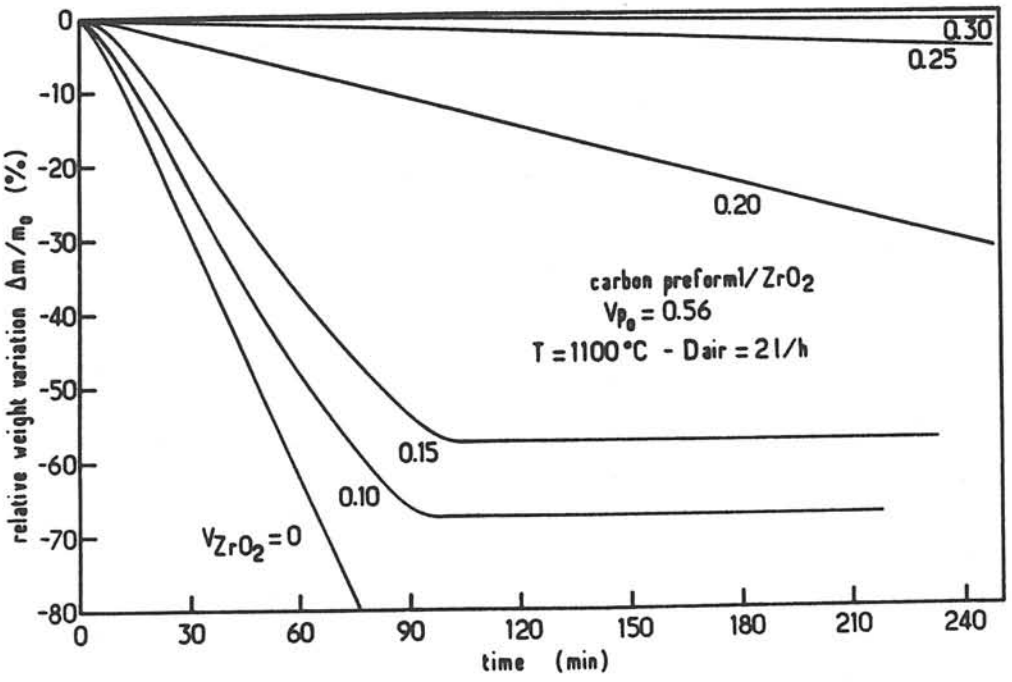

Fig. 15 - Kinetics of oxidation of 2D-C-C / ZrO_2 composites (type 4) in air at variations V_{ZrO_2} values

the gas flow rate and the oxygen partial pressure on the oxidation kinetics (Fig.16). At a fixed oxygen partial pressure, e.g. for tests performed in air, the weight loss due to oxidation increases linearly vs time, the slope of the $\Delta m/m_0 = f(t)$ straight line (where Δm is the weight loss at time t for a sample of initial mass m_0) increasing as the gas flow rate is raised. However, in pure oxygen, an initial non linear regime is observed. Furthermore, at a constant gas flow rate (e.g. 6l / hr.), the weight loss is proportional to the pressure of oxygen (i.e. it is divided by five when pure oxygen is replaced by air).

Thus, the above results show that when carbon fibers are imbedded within a zirconia matrix, protection of the fibers by the matrix, against oxidation, is effective for short exposures at moderate temperatures. On the contrary under more severe oxidation conditions (higher temperatures or and longer exposures) different damaging mechanisms (i.e. oxidation of the carbon preform and of the interphase, preform-matrix chemical reaction as well as grain growth) take place with a detrimental effect on the mechanical behavior Some of them could be inhibited through the use of a coating

ACKNOWLEDGEMENTS

The preforms which have been used in the present study were supplied by SEP and part of the test were performed in its laboratories. The authors acknowledge the contribution of L. RABARDEL and J. VILLOT for the oxydation tests.

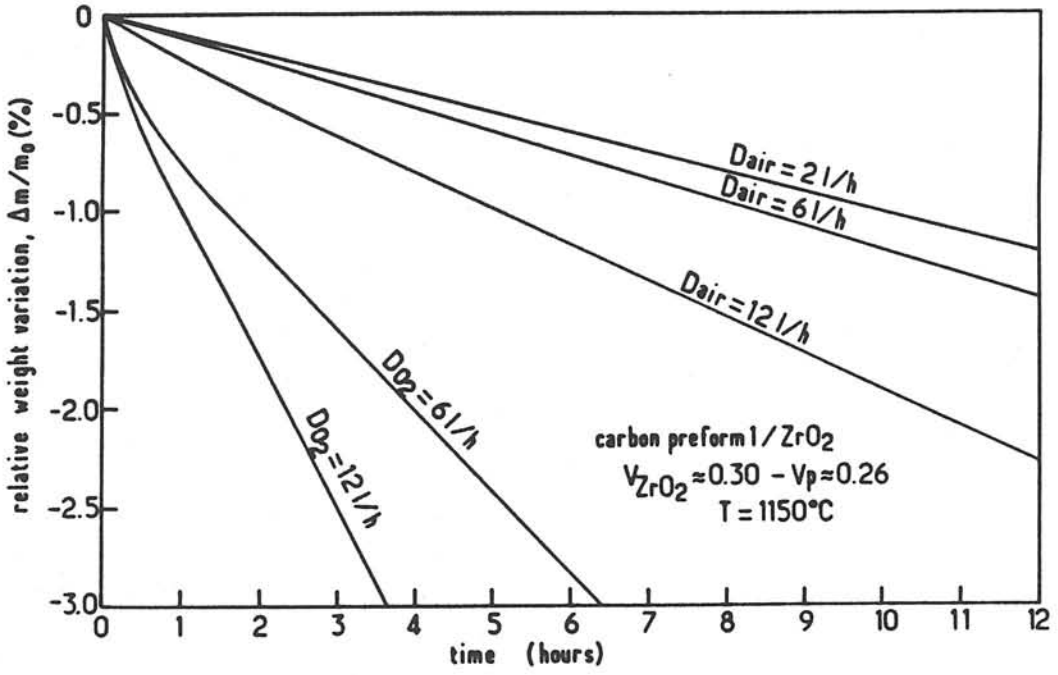

Fig. 16 - Kinetics of oxidation of 2D-C-C / ZrO_2 composites (type 4) as a function of the gaz flow rate and partial pressure of oxygen

REFERENCES

1 - V.K. PUJARI and I. JAWED, "The Alumina Fibre / Tetragonal Zirconia Polycrystal Composite System", Composites, 17/2 (1986) 137 - 140.

2 - B. BENDER, D. SHADWELL, C. BULIK, L. INCORVATI and D. LEWIS, "Effect of Fiber Coatings and Composite Processing on Properties of Zirconia Based Matrix SiC Fiber Composites", Ceram. Bull., 65/2 (1986) 363 - 369.

3 - N. CLAUSSEN and G. PETZOW, "Whisker reinforced Zirconia - Toughened Ceramics", in "Tailoring Multiphase and Composite Ceramics" (Ed. R.E. Tressler et al.), Mater. Sci. Res., Vol. 20 (1986) 649 - 662.

4 - N. CLAUSSEN and G. PETZOW, "Whisker - Reinforced Oxide Ceramics", J. de Physique, Colloque C_1, Suppl. # 2, 47 (1986) C_1 - 693 to C_1 - 702.

5 - H. GREWE, K. DREYER and J. KOLASKA, "Wisker-Reinforced Ceramics Cfi / Ber 8 / 9 (1987) 303 - 317.

6 - L. MAZEROLLES, D. MICHEL and R. PORTIER, "Microstructure and Mechanical Behaviour of Al_2O_3 - ZrO_2 (Y_2O_3) Oriented Eutectics", J. de Physique, Colloque C_1, Suppl. # 2, 47 (1986) C_1 - 335 to C_1 - 339.

7- J. MINET, F. LANGLAIS, R. NASLAIN and C. BERNARD, "On the CVD of Zirconia from $ZrCl_4$-H_2-CO_2-Ar Gas mixture: 1 - Thermodynamic Approach, J. Less-Common Met., 119 (1986) 219 - 235.

8- J. MINET, F. LANGLAIS and R. NASLAIN, "On the CVD of Zirconia from $ZrCl_4$-H_2-CO_2-Ar Gas Mixture: 2 - An experimental Approach, J. Less-Common Met., 132 (1987) 273 - 287.

9- J. MINET, F. LANGLAIS and R. NASLAIN, "Chemical Vapor Infiltration of Zirconia within the Pore Network of Fibrous Ceramic Materials From $ZrCl_4$-H_2-CO_2", submitted to Composite Science and Technology.

10 - J. MINET, F. LANGLAIS, J.M. QUENISSET and R. NASLAIN, "Thermomechanical Properties and Resistance to Oxidation of Zirconia CVI matrix Composites: 1 - Mechanical Behavior", this Journal.

11 - F. CHRISTIN, R. NASLAIN and C. BERNARD, "A Thermodynamic and Experimental Approach of Silicon Carbide CVD. Application to the CVD-Infiltration of Porous Carbon Composites", Proc. Int. Conf. CVD (T.O. Sedwick and H. Lydbin, eds.), The Electrochem. Soc. Princeton, 1979, 499 - 514.

12- R. NASLAIN and F. LANGLAIS, "CVD- Processing of Ceramic Composite Materials in "Tailoring Multiphase and Composite Ceramics" (R.E. Tressler et al., eds.), Mater. Sci. Res., Vol. 20 (1986) 145 - 164.

13 - R. COLMET, I. LHERMITTE-SEBIRE and R. NASLAIN, "Fibrous Alumina-Alumina Composite Materials Obtained According to a CVI-Technique",Adv. Ceram. Mater., 1 [2] (1986) 185 - 191.

14- H. HANNACHE, R. NASLAIN and C. BERNARD, "Boron Nitride Chemical Vapour Infiltration of Fibrous Materials from BCl_3-NH_3-H_2 or BF_3-NH_3-H_2 Mixtures: a Thermodynamic and Experimental Approach", J. Less-Common Met., 95 (1983) 221 - 246.

15- D.B. MARSHALL, F.F. LANGE and P.D. Morgan, "High Strength Zirconia Fibers", J. Am. Ceram. Soc., 70 [9] (1987) C 187 - C 188.

16- D.P.H. HASSELMANN, "Tailoring of the Thermal Transport Properties and Thermal Shock Resistance of Structural Ceramics" in "Tailoring Multiphase and Composite Ceramics" (R.E. Tressler et al. eds.), Mater Sci Res., Vol. 20 (1986) 731 - 754.

17- W.J. PARKER, R.J. JENKINS, C.P.BUTLER and G.L. ABBOT, J. Applied Phys., 32 [9] (1961) 1679 - 1684.

18 - R. STEVENS, "Zirconia and Zirconia Ceramics", a publication of Magnesium Elektron Ltd, Twickenham, July 1986.

19 - A.H. HEUER, "Science and Technology of Zirconia", The American Ceramic Society, 1981.

20 - F. CHRISTIN, Thesis 641, "The C-C/Si Composites: a New Family of Materials for High Temperature Applications", University of Bordeaux, december 13, 1979, pp. 99-102.

21 - J.Y. ROSSIGNOL, Thesis 833, "On the Ceramic - Ceramic Composites Made of a 2D-carbon Fiber Reinforcement Densified by CVI by Hybrid Carbon-Carbide or Carbon-Nitride Matrices", University of Bordeaux, March 18, 1985, pp. 39-41.

22 - B. BROQUERE, B. BUTTAZZONI and J.J. CHOURY "The Carbon-Carbon Composites and their Industrial Applications", in "Introduction to Composite Materials" (R. Naslain, ed.), CNRS - Editions / IMC, Bordeaux 1985, Chap. 17, pp. 405 - 438.

23 - D.R. STULL and H. PROPHET "Janaf Thermochemical Tables" 2nd Edition, NSRDS - NBS 37, 1971.

24 - R.W. RICE, "BN coating of Ceramic Fibers for Ceramic Fiber Composites", US Patent 4, 642, 271, Feb. 10, 1987.

ANNEXE

COMPORTEMENT A L'ABLATION DES MATERIAUX COMPOSITES A MATRICE DE ZIRCONE

L'utilisation des matériaux composites à matrice céramique, à très haute température, dans le secteur aérospatial (e.g. dans les tuyères des moteurs fusées ou pour la protection thermique des corps de rentrée) suppose que soit connue leur **résistance à l'ablation.** Rappelons que la plupart des matériaux, même les plus réfractaires, subissent une dégradation importante lorsqu'ils sont portés à très haute température (e.g. T > 3000°C) au contact d'un fluide s'écoulant à très grande vitesse (gaz de combustion dans un propulseur, gaz constituant la haute atmosphère lors du retour sur terre d'un corps de rentrée). La protection thermique des structures placées dans de telles conditions se fait par ablation d'une partie du matériau sous le double effet de la température et de l'érosion due aux gaz. La résistance à l'ablation est en général d'autant meilleure que le matériau est plus réfractaire et qu'il peut être le siège de **phénomènes fortement endothermiques** (vaporisation, décomposition thermique, réactions chimiques, etc...). Tel est le cas, par exemple, des matériaux à base de carbone ou / et de carbures (1 - 3).

1 - PRINCIPE DE L'ESSAI

La résistance à l'ablation a été étudiée à l'aide d'un chalumeau à plasma d'hydrogène-argon, dont le principe est donné à la figure 1.

L'essai consiste à mesurer le **temps de perforation** d'un échantillon cylindrique (d = 30 mm; h = 10mm) exposé perpendiculairement à l'une de ses bases au dard du chalumeau à plasma (dont la température est estimée à environ 4000 K). Le dispositif est étalonné à l'aide de matériaux de référence dont les temps de perforation ont été antérieurement déterminés.

2 - RESULTATS EXPERIMENTAUX

2.1. Composites à renfort fibreux à base d'alumine

Les essais qui ont été réalisés sur les composites à renfort fibreux à base d'alumine (préforme 1 constituée à partir d'un mat de fibres SAFFIL très riches en alumine (i.e. 97% Al_2O_3, 3% SiO_2) consolidée par imprégnation à l'aide d'une barbotine d'alumine de 1 µm) et à matrice de zircone, montrent que la **fusion locale du matériau est aisément atteinte,** en raison de la faible réfractérité du renfort (l'alumine fond à 2050°C et son point de fusion est abaissé en présence de silice) et du comportement thermique des mélanges Al_2O_3-ZrO_2 (le diagramme binaire comporte un eutectique fondant vers 1900°C).

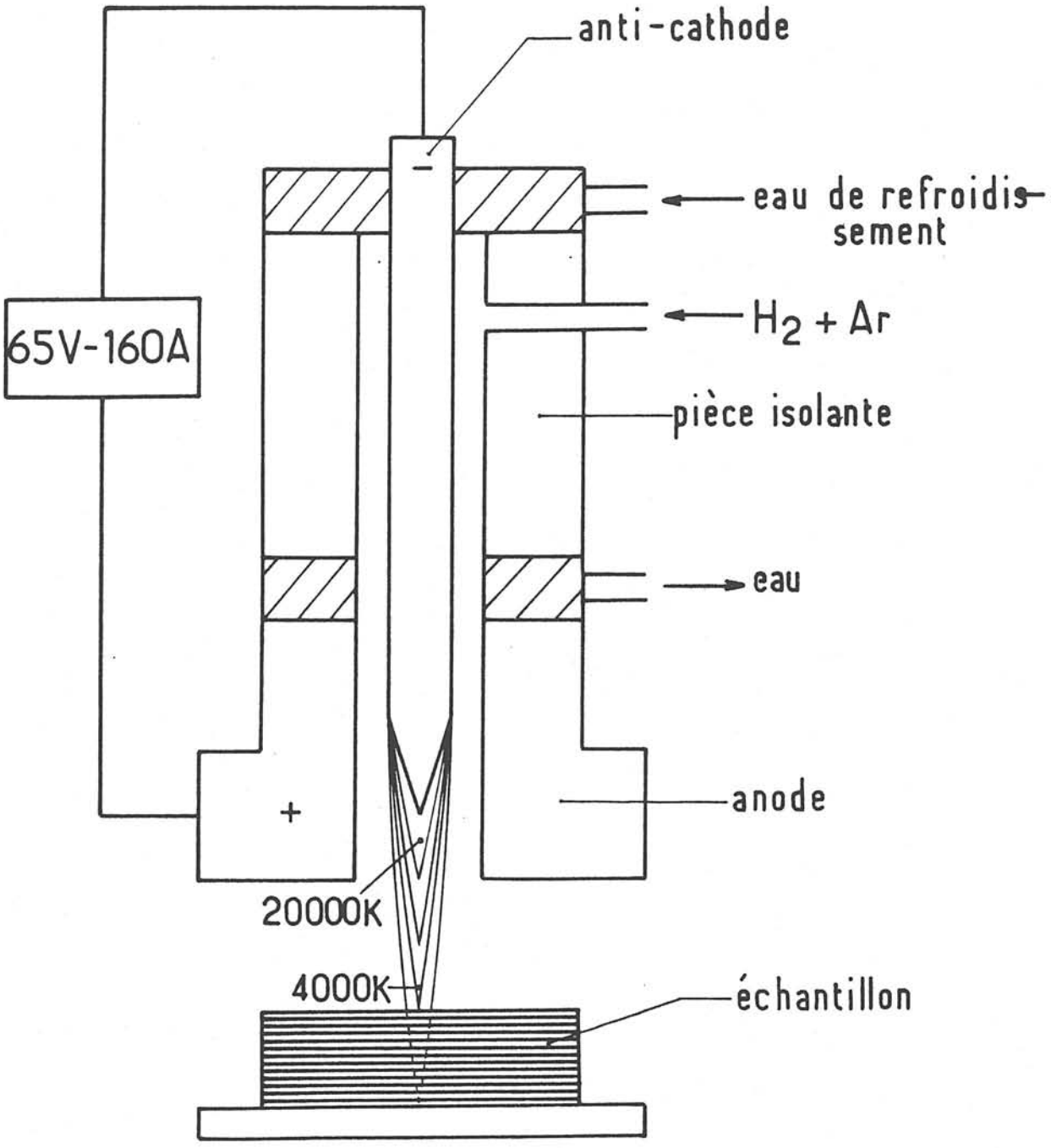

Fig. 1 - Schéma de principe de l'installation de mesure d'ablation au chalumeau à plasma

Il en résulte que le temps de perforation du matériau est très court, i.e. de l'ordre de 6 secondes. De plus, sous l'effet du choc thermique, le matériau subit une importante fissuration (Fig. 2a).

2.2. Composites à renfort fibreux de carbone

Le comportement à l'ablation du composite à renfort de carbone (préforme 1) constituée à partir d'un empilement de tissus de fibres de carbone issues d'un précurseur PAN et consolidée par du pyrocarbone avant densification par la zircone) est notablement différent:

1) le temps de perforation est comparable à celui d'un composite 2D-C-C (40 PAN) totalement densifié par du pyrocarbone (i.e. ne contenant pas de zircone) et de l'ordre de 300 secondes (donc 50 fois supérieur à celui du composite à renfort fibreux d'alumine). La réfractairité du carbone constituant la préforme et sa tenue bien connue à l'ablation expliquent ce résultat.

2) le matériau ne présente pas de macrofissurations apparentes, ainsi que l'illustre la figure 2b (cliché de droite) en dépit de la sévérité du choc thermique et de la différence existant entre les coefficients de dilatation thermique du carbone et de la zircone. On peut penser que cette absence de macrofissuration trouve son origine dans le fait que la matrice de zircone est fragmentée par le renfort fibreux et que le pyrocarbone de consolidation a la propriété bien établie d'arréter ou / et de dévier la propagation des fissures résultant de la microfissuration de la matrice.

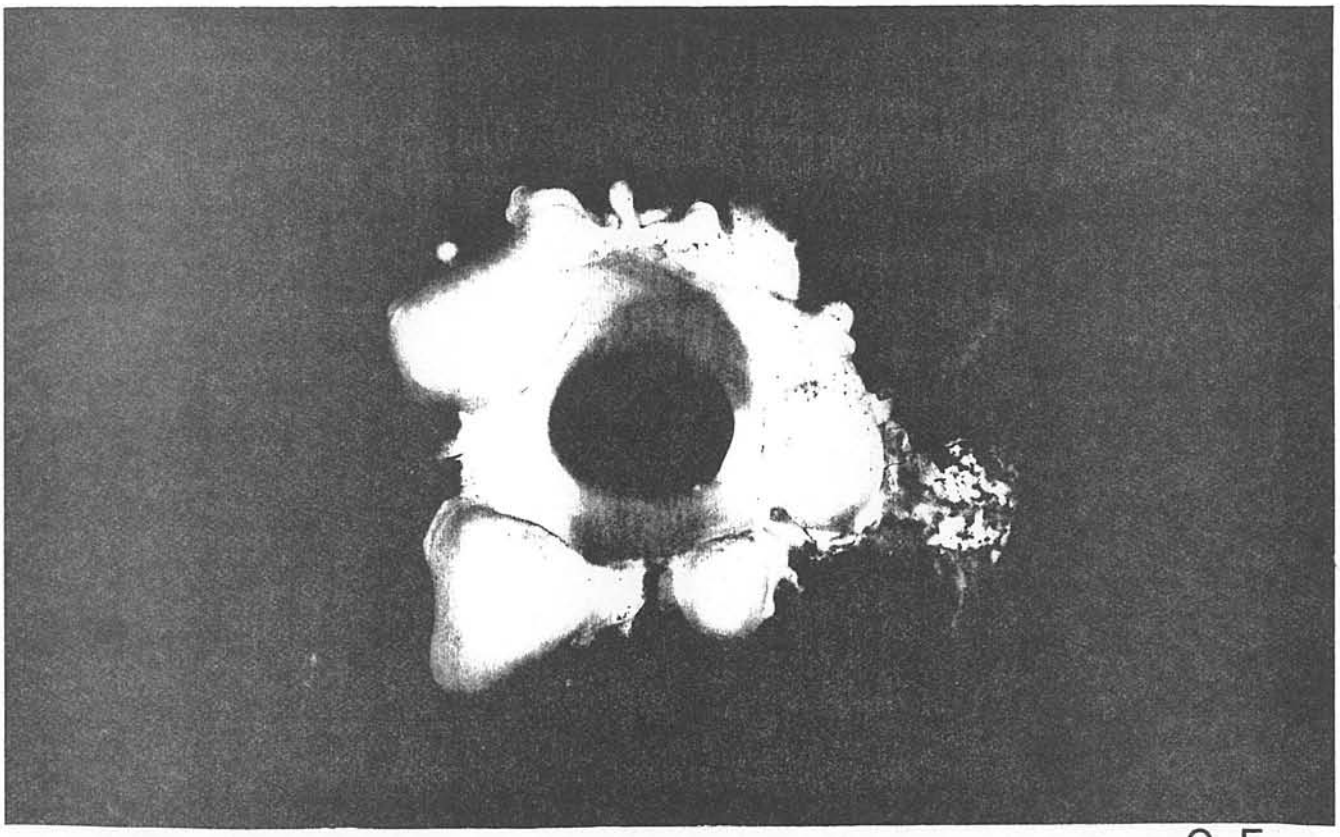

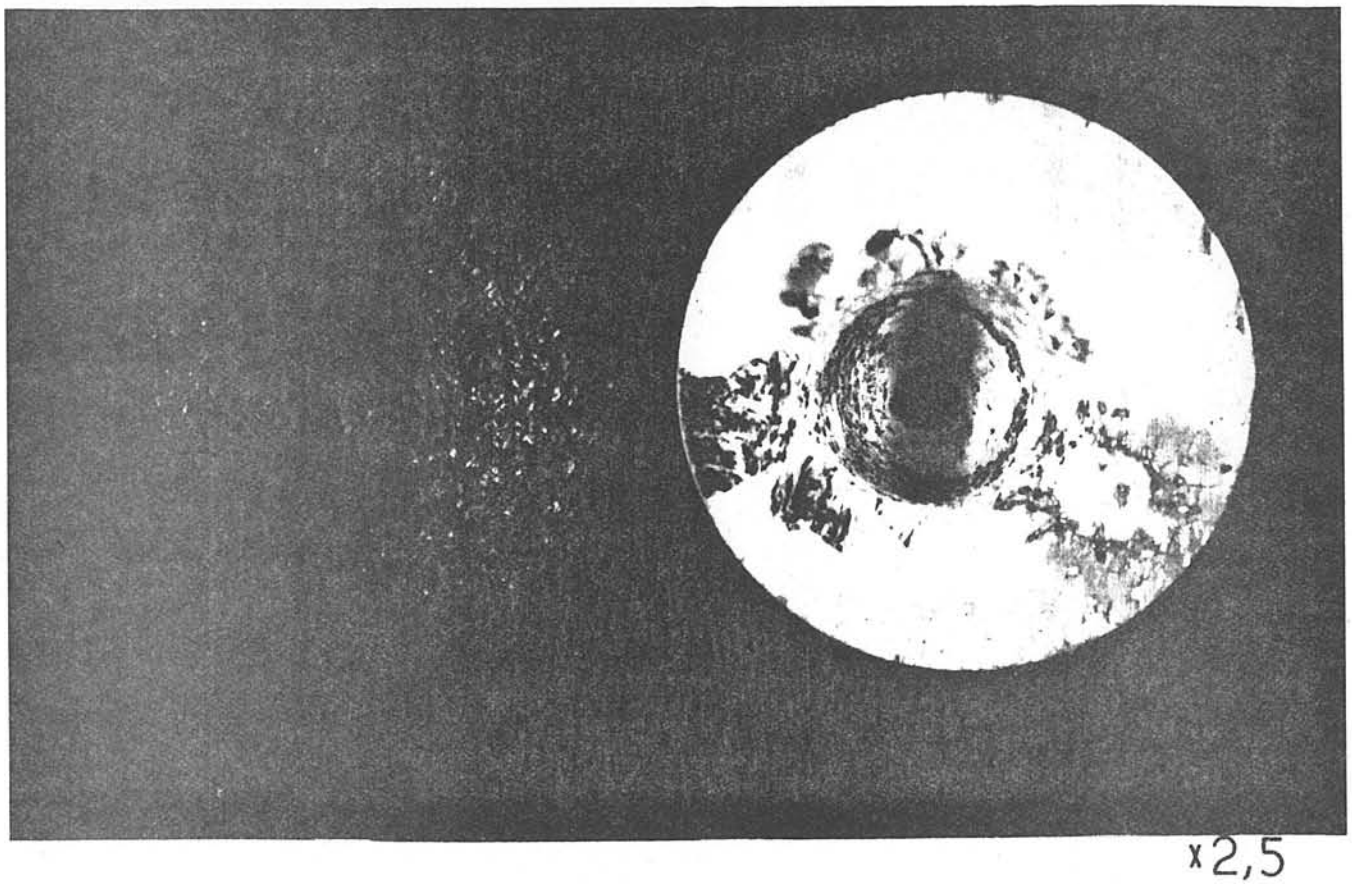

Fig. 2 - Essais de résistance à l'ablation de composites à matrice de zircone: (a) composite à renfort fibreux d'alumine, (b) composites à renfort fibreux 2D de carbone (cliché de gauche : composite densifié au pyrocarbone; cliché de droite: composite à matrice hybride C / ZrO_2

3) enfin, la présence de la matrice de zircone ralentit notablement l'oxydation du renfort fibreux et du pyrocarbone de consolidation par rapport aux phénomènes observés pour le composite homologue 2D-C-C (40 PAN) totalement densifié au pyrocarbone (Fig. 2b). C'est ainsi que le composite à matrice zircone a parfaitement conservé sa forme extérieure et que la quantité de matière ablatée est plus faible.

3 - CONCLUSIONS

L'ensemble des essais d'ablation montre, comme on pouvait s'y attendre, que les composites à renfort fibreux de carbone et à matrice de zircone sont plus résistants à l'ablation et au choc thermique que leurs homologues à renfort fibreux d'alumine.

Il eût été intéressant de comparer la tenue à l'ablation du composite 2D-C-C / ZrO_2 à celle d'un composite 2D-ZrO_2-ZrO_2 à interface fibre-matrice faible. Malheureusement, au moment où se travaille a été réalisé les fibres de zircone pure (ou de zircone stabilisée) n'étaient pas encore disponibles.

4 - BIBLIOGRAPHIE SUCCINCTE

(1) B. BROQUERE, B. BUTTAZZONI et .J. CHOURY, "Les Composites Carbone-Carbone; leurs Applications Industrielles", dans "Introduction aux Matériaux Composites : 2 - Matrices Métalliques et Céramiques" (R. Naslain, éd.), Editions du CNRS / IMC, Bordeaux 1985, chap. XVII, pp. 405 - 438.

(2) F. CHRISTIN, "Les Composites Carbone-Carbone-Carbure de Silicium: Une Nouvelle Famille de Matériaux Destinés à des Applications à Haute Température", Thèse n° 641, 13 décembre 1979, Université de Bordeaux I.

(3) J.Y. ROSSIGNOL, "Sur les Matériaux Composites Céramique-Céramique à Renfort Bidirectionnel de Fibres de Carbone et à Matrice Hybride Carbone-Carbure ou Carbone-Nitrure *Elaborés par CVI", Thèse n° 833, 18 Mars 1985, Université de Bordeaux I.

CONCLUSIONS GENERALES

Ce travail s'inscrivait dans le cadre des études poursuivies au Laboratoire de Chimie du Solide du CNRS sur les composites fibreux de type **céramique-céramique** destinés à des applications à hautes températures, relevant notamment de l'industrie aéronautique et spatiale. Il répondait à des motivations industrielles et se situait dans l'élargissement des travaux de R. COLMET qui avaient montré que des composites fibreux à matrice d'alumine pouvaient être élaborés par infiltration chimique en phase gazeuse (CVI). En dehors de ses aspects finalisés, cette recherche a permis d'aborder trois principaux sujets à caractère fondamental: (1) la compréhension, par des approches thermodynamique et cinétique, du dépôt chimique en phase gazeuse de la **zircone,** (2) l'optimisation expérimentale des conditions (débit, température, pression) de densification par ZrO_2, de milieux poreux et, (3) la compréhension des comportements thermo-mécanique et physico-chimique, de la température ambiante à 1400°C, des matériaux composites céramique-céramique à matrice à base de zircone. Au moment où cette étude a été entreprise, aucun article n'avait été publié sur les composites fibreux à matrice de zircone.

1) Dans un premier temps, afin de préciser la nature des réactions chimiques qui interviennent lors du dépôt de la zircone, à partir de mélanges gazeux $ZrCl_4$-H_2-CO_2-Ar et pour diverses valeurs de température et pression compatibles avec le processus CVI, nous avons étudié ce système, en collaboration avec C. BERNARD du LTPCM - Grenoble, par une **approche thermodynamique**.

Cette étude a été décomposée en deux volets: (1) dépôt sur substrat chimiquement inerte, (2) dépôt sur substrats actifs. Dans le second cas, des substrats en carbone et en mullite ($3Al_2O_3$, $2SiO_2$) ont été choisis, correspondant aux types de fibres qui peuvent être utilisées dans les matériaux composites à matrice à base de zircone.

Dans le cas où le **substrat est chimiquement inerte**, l'étude thermodynamique a montré que la zircone se dépose, à partir de mélanges $ZrCl_4$-H_2-CO_2 dilués à l'argon, dans des conditions modérées de température (1000 K ≤ T ≤ 1400 K) et de pression (0,01 atm ≤ P ≤ 0,5 atm). Tant qu'à l'équilibre, l'eau résultant de la réduction de CO_2 par H_2, est présente en excès, le rendement en ZrO_2 (par rapport à la quantité initiale de $ZrCl_4$) est de 100%. Ainsi, pour une quantité de $ZrCl_4$ donnée, le rendement en zircone demeure-t-il égal à 100% entre deux valeurs limites α_i et α_s (où $\alpha = [H_2]_{in} / [CO_2]_{in}$). A partir de compositions riches en CO_2 ($\alpha < \alpha_i$) ou en H_2 ($\alpha > \alpha_s$), le rendement en zircone tend progressivement vers zéro; la quantité d'eau formée étant limitée soit par la concentration en hydrogène, soit par la concentration en dioxyde de carbone. Par ailleurs, plus la quantité de $ZrCl_4$ initiale diminue, plus la largeur du domaine / $\alpha_s - \alpha_i$ / augmente. De plus, pour les mélanges riches en hydrogène ($\alpha > 1$) et sous excès de chlorure de zirconium ($[ZrCl_4]_{in} > 1/2\ [CO_2]_{in}$, des **codépôts carbone-zircone** se forment à l'équilibre, étant d'autant plus riches en carbone que α est plus élevé. Ce domaine de codépôt se déplace vers les valeurs élevées de α, plus la température augmente et /ou la pression diminue; toutefois, l'influence de la pression totale demeure faible par rapport à celle de la température. L'ensemble de ces résultats est en accord avec ceux déjà obtenus par R. COLMET

et I. LHERMITTE-SEBIRE dans le cas de dépôt chimique en phase gazeuse d'alumine à partir de mélanges Al_2Cl_3-H_2-CO_2.

Dans le cas où le dépôt de zircone est réalisé au contact du **substrat de carbone** - qui est simulé en introduisant un excès de carbone dans la composition initiale - l'étude thermodynamique montre qu'un tel substrat ne peut être considéré comme inerte vis à vis de la phase gazeuse que si cette dernière est suffisamment riche en hydrogène ($\alpha > \alpha_s = \alpha_c$). Le dépôt est alors constitué d'un mélange de zircone et de carbone libre. Dans le cas contraire (i.e. $\alpha < \alpha_s$), il se produit une oxydation du substrat sous l'effet conjugué du dioxyde de carbone et de l'eau en excès conduisant à la formation de monoxyde de carbone. Dans ces conditions, seul un dépôt de zircone est formé, son rendement demeure égal à 100% entre deux valeurs limites α_i et α_s ; toutefois, pour une quantité de $ZrCl_4$ initiale donnée, la largeur du domaine / α_s - α_i / apparaît plus faible que dans le cas d'un dépôt de zircone sur substrat inerte.

Enfin, dans le cas où le dépôt de zircone est effectué au contact d'un **substrat de mullite ($3Al_2O_3$, $2SiO_2$)** , simulant des renforts à base de fibres silico-alumineuses, l'étude thermodynamique montre qu'un tel substrat ne peut être considéré comme inerte vis à vis de la phase gazeuse que pour les compositions comprises entre α_i et α_s ; le dépôt étant alors constitué uniquement de ZrO_2, avec un rendement égal à 100%. Au contraire, pour les compositions riches en CO_2 (i.e. $\alpha < \alpha_i$), le substrat est attaqué, vraisemblablement par $ZrCl_4$ en excès, conduisant à la formation de nouvelles espèces à l'équilibre, telles que $AlCl_3$ et $ZrSiO_4$. Egalement, pour les compositions riches en H_2 (i.e. $\alpha > \alpha_s$), et

plus particulièrement pour les compositions comprises entre α_s et α_{SiC}, le chlorure de zirconium en excès semble réagir avec le substrat, formant les mêmes espèces que précédemment, accompagnées simultanément de la réduction du CO par H_2 qui conduit à un codépôt carbone-zircone. Puis, pour $\alpha > \alpha_{SiC}$, le substrat de mullite réagit, à l'état solide, en présence du carbone libre pour former, à l'équilibre, du SiC et Al_2O_3.

2) Dans un second temps, l'approche thermodynamique a été complétée par une **étude cinétique sur substrats plans**, non poreux, d'alumine. Il est apparu que la vitesse de dépôt de la zircone croît exponentiellement avec la température (pour 800°C ≤ T ≤ 1000°C). L'énergie d'activation est de l'ordre de 100 kcal.mole^{-1}: valeur comparable à celle obtenue par K. BREENFLECK et al. . Ainsi, il a pu être établi, tout comme pour l'alumine, que la réaction de dépôt de la zircone est thermiquement activée. Toutefois, il n'a pas été possible - contrairement à ce qui avait pû être fait pour TiC et B_4C - de mettre en évidence, compte tenu des possibilités limitées du four résistif disponible, la transition entre un dépôt contrôlé par les réactions de surface et un dépôt contrôlé par la diffusion des espèces gazeuses dans la couche limite. Egalement, il est apparu que la vitesse de dépôt de la zircone croît avec le débit total. Néanmoins, pour des débits élevés (i.e. D > 500 cm^3.mn-1), il se forme une importante nucléation en phase gazeuse qui entraîne des dépôts peu adhérents, se traduisant, en apparence, par une diminution de la vitesse de dépôt. Ces résultats sont à rapprocher de ceux obtenus par J.S. CHUN et al. pour les dépôts d'alumine, d'une part, et de carbure et/ou de nitrure de titane, d'autre part. Des variations analogues de la vitesse de dépôt, en fonction du débit total, ont été notées sans, toutefois, observer le phénomène de

nucléation en phase homogène. D'après ces auteurs, pour les faibles débits, le processus cinétique est gouverné par la diffusion des espèces gazeuses dans la couche limite (dont l'épaisseur décroît lorsque le débit augmente), la vitesse de dépôt est alors proportionnelle à la racine carrée du débit total, ce que nous observons également dans le cas de la zircone. Pour les débits élevés, la vitesse de dépôt est indépendante du débit total car, selon ces auteurs, la cinétique serait alors gouvernée par les réactions de surface. Dans le cas de la zircone, la faible dépendance de la vitesse de dépôt avec le débit total peut également être attribué à la présence de nucléation homogène. Enfin, en fonction de la pression totale, la vitesse de dépôt passe par un maximum pour 3 KPa à 300 $cm^3. mn^{-1}$ et, pour 4 KPa à 420 $cm^3. mn^{-1}$, puis décroît pour tendre vers une valeur limite qui semble être indépendante du débit total. Ce résultat peut être étroitement lié à l'importante nucléation en phase gazeuse qui apparaît aux pressions supérieures à 4 KPa, perturbant considérablement le processus de dépôt de zircone.

Par ailleurs, cette étude cinétique a été complétée par des **caractérisations physico-chimiques** des divers **dépôts de zircone** obtenus par CVD. Ainsi, il a pu être établi que les dépôts de zircone sont constitués de deux variétés allotropiques: ZrO_2-monoclinique et ZrO_2-quadratique. La proportion de zircone quadratique dans le dépôt est maximale à la température d'environ 975°C. Egalement, cette proportion de ZrO_2 quadratique est d'autant plus élevée que le débit total est élevé et que la pression totale est faible; néanmoins, ces paramètres n'ont qu'une influence relativement négligeable. De plus, il est apparu que les dépôts de zircone contiennent du carbone libre dont la proportion augmente quand la température augmente et quand la pression totale diminue. Enfin, une étude

morphologique a montré que les dépôts de zircone sont formés de "grains" dont la taille moyenne est d'autant plus grande que la température et la pression totale sont plus élevées. C'est par une approche théorique de la transformation martensitique due à F.F. LANGE et al. qu'il serait permis de justifier les résultats expérimentaux et d'expliquer la présence de la variété quadratique de la zircone, à température ambiante, sur la base d'un effet de taille de grains. Toutefois, à ce stade de l'étude, afin de confirmer ces investigations, il serait nécessaire de définir une méthode fiable pour la mesure du diamètre moyen des grains de zircone constituant les divers dépôts.

3) A partir des résultats acquis lors des études thermodynamique et cinétique sur substrats plans, une troisième étape a permis de définir les **conditions optimales d'infiltration chimique par voie gazeuse (CVI) de ZrO_2**, au sein de milieux microporeux, par une approche expérimentale. Cette optimisation à été établie sur la base de: (i) **une étude cinétique** qui permet de connaître la vitesse globale de dépôt de zircone (i.e. infiltration et dépôt à la surface externe) en fonction du temps; (ii) **une caractérisation par porosimétrie à mercure** qui à un certain stade de la densification limité dans le cas présent à environ 100 heures, conduit à la porosité résiduelle du matériau (V_p) et par conséquent à la proportion de zircone infiltrée; (iii) **une caractérisation par spectrométrie X** qui renseigne sur la qualité du matériau ainsi préparé (i.e. homogénéité de l'infiltration). Cette étude a porté principalement sur deux types de préformes: l'une à base de fibres d'alumine de transition consolidées par une barbotine Al_2O_3, l'autre à base de tissu de carbone consolidé par du pyrocarbone (ou 2D-C-C). Ainsi, il est apparu que la qualité de la densification augmente (en

général au détriment de sa vitesse) lorsque le débit total, la température et la pression totale diminuent. Toutefois, la densification semble être plus facile avec les préformes 2D-C-C que les préformes à base d'alumine, compte tenu de leurs structures poreuses différentes. De ce fait, une faible porosité globale et un réseau de pores constitué de petits pores (diamètres ≤ 0,1 μm) sont défavorables à une bonne densification. En tenant compte de la géométrie de la chambre réactionelle, il a été établi que les conditions d'infiltration par ZrO_2 de préformes fibreuses et microporeuses, sont les suivantes: débit total = 100 $cm^3.mn^{-1}$, température = 910°C, pression totale = 2 kPa, et $\alpha = [H_2] / [CO_2] = 3$. Le choix de ces paramètres, adoptés quel que soit le substrat de départ, représente un compromis entre (1) une vitesse de densification acceptable, mais qui demeure encore trop lente (plusieurs centaines d'heures), (2) l'obtention d'une densification homogène et (3) la limitation des risques d'oxydation des substrats carbonés.

Ainsi, du point de vue cinétique, il a été démontré que la variation de la porosité résiduelle en fonction du temps de densification suit une loi exponentielle, confirmant les résultats déjà obtenus sur l'infiltration de préformes 2D-C-C par des carbures (TiC, B_4C) ainsi que la densification de préformes à base d'alumine par Al_2O_3. A l'issue des différentes densifications, les matériaux composites à matrice à base de zircone ont été caractérisés aux plans physico-chimiques et morphologiques. Il est apparu, à la température ambiante, que la matrice ZrO_2 au sein des diverses préformes, est cristallisée sous la forme monoclinique exclusivement. De plus, il a été établi que la matrice ZrO_2 contient du carbone libre, en très faibles proportions (inférieures à quelques pour cent). D'autre part, l'étude morphologique a révélé que les composites

Al_2O_3 - ZrO_2 présentent un faciès de rupture de type fragile (i.e. sans aucun déchaussement de fibres), avec une forte adhésion entre la fibre et la matrice. Ce comportement apparaît analogue à celui des composites Al_2O_3 - Al_2O_3. Par contre, les composites C-ZrO_2 montrent un important déchaussement entre la fibre et le pyrocarbone, ainsi qu'une mauvaise adhésion de la matrice zircone vis-à-vis du pyrocarbone. Cette adhésion relativement faible entre les matrices ZrO_2 et pyrocarbone résulte de la nature différente de chacun des matériaux. Ainsi, les matériaux composites C-ZrO_2 semblent-ils présenter une meilleure ténacité que les composites Al_2O_3 - ZrO_2.

En vue d'éventuelles applications thermo-mécaniques, une dernière étape a consisté à caractériser succinctement les divers composites céramique-céramique à matrice à base de zircone au plan mécanique, thermique et chimique.

4) Au plan **mécanique**, les matériaux composites à matrice ZrO_2 ont été caractérisés en **compression** dans les directions 1 et 3 (i.e. parallèlement et perpendiculairement aux strates formés par les fibres), ainsi qu'en **flexion trois points**, en fonction du degré de densification par ZrO_2 ($V(ZrO_2)$) et / ou de la température (de l'ambiante jusqu'à 1400°C). Pour un stade de densification donné, la fraction volumique de ZrO_2, $V(ZrO_2)$, est définie par la relation $V(ZrO_2) + V_c = 1 - V_p$ (où $1 - V_p$ est la comparité et V_c la constante pour une série de matériaux issue d'une même préforme).

Dans le cas de **sollicitations en compression** (directions 1 et 3), les **composites Al_2O_3 - ZrO_2** (particulièrement : fibres alumine + barbotine Al_2O_3 / ZrO_2) présentent trois types de comportement mécanique, mis en évidence pour des contraintes croissantes:

1) un comportement non-linéaire, résultant d'une rigidification apparente qui peut être attribuée à la mise en appui des faces, non parfaitement parallèles, de l'éprouvette,

2) un comportement élastique quasi-linéaire et,

3) un comportement non linéaire qui correspond à divers mécanismes d'endommagement, précédant la rupture du matériau. De plus, la rupture de ces matériaux, de caractère fragile, est du type translaminaire quelle que soit la direction des efforts, comme on pourvait l'attendre d'une texture faiblement anisotrope, mais aussi d'une liaison fibre-matrice forte. Dans le cas des **composites 2D-C-C / ZrO_2**, il est apparu des comportements mécaniques similaires. Toutefois, compte tenu de leur texture bidirectionnelle (fortement anisotrope), les modes de rupture diffèrent suivant que le matériau est sollicité en compression dans la direction 1 (la rupture est alors interlaminaire) ou dans la direction 3 (la rupture est translaminaire). De plus, en raison de leur nature, et leurs performances plus élevées les composites carbone-ZrO_2 ont un travail de rupture plus élevé que celui des composites Al_2O_3 - ZrO_2. Par ailleurs, les évolutions des modules d'Young (E_1 et E_3), des résistances à la rupture (σ^R_1 et σ^R_3) et des déformations (ε_1 et ε_3), en fonction de la fraction volumique en zircone

V(ZrO_2) ont confirmé les résultats obtenus antérieurement au laboratoire sur les composites 2D-C-C / céramique (où céramique = SiC, SiC + C, TiC, B_4C ou BN).

Dans le cas de **sollicitations en flexion trois points;** les matériaux **composites Al_2O_3 - ZrO_2** sans interphase présentent, quel que soit le degré de densification, un comportement élastique quasi-linéaire, jusqu'à la rupture, sans révéler de domaine pseudo-plastique. Le mode de rupture, typiquement "fragile" semble être gouverné par la propagation de fissure(s) initiée(s) à la surface de l'éprouvette, par des défauts critiques. Cette propagation brutale est rendue possible par une liaison fibre-matrice forte, empêchant toute relaxation de contraintes en fond de fissures.

Par contre, dans le cas de **matériaux Al_2O_3** - BN / **ZrO_2**, le comportement mécanique fait apparaître, en plus du comportement linéaire quasi-élastique, un comportement pseudo-plastique, non linéaire, traduisant divers mécanismes d'endommagement et, par conséquent une certaine dissipation d'énergie. Le mode de rupture, beaucoup plus "ductile", témoigne d'un mécanisme de microfissurations de la matrice. Ce phénomène est possible en raison de la présence du nitrure de bore, à l'interface fibre-matrice, qui permet, en raison de sa faible rigidité, de diminuer les concentrations de contraintes dues à la microfissuration de la matrice au voisinage de la surface des fibres. La rupture des fibres peut, alors, ne pas se produire au droit des microfissures de la matrice provoquant ainsi les mécanismes de décohésion fibre-matrice, de frottement et de fibres rompues, de déchaussement qui sont à

l'origine du domaine pseudo-plastique. Par ailleurs, il convient de noter qu'un renfort constitué d'une texture tissée, à fibres continues, permet d'atteindre des niveaux de rupture supérieurs à ceux atteints avec une texture élaborée à partir de fibres courtes. Enfin, il est à signaler que l'ensemble des matériaux composites Al_2O_3 - ZrO_2 ne peuvent pas être envisagés pour des applications au dessus de 1200°C, en raison des quantités, non négligeables, de silice contenue dans les fibres commercialisées.

Pour les **composites C-C / ZrO_2**, la sollicitation en flexion fait apparaître un comportement mécanique similaire à celui des composites Al_2O_3-BN/ZrO_2. Dans ce cas, le pyrocarbone qui a servi à la consolidation de la préforme, contribue aux mécanismes de dissipation d'énergie en favorisant les phénomènes de déchaussements entre fibre et pyrocarbone d'une part, puis entre pyrocarbone et matrice zircone, d'autre part. Le mode de rupture et l'important travail de rupture laisse à penser que ces matériaux sont tenaces. Quelle que soit la répartition du renfort, les évolutions des caractéristiques mécaniques (σ^R, E), en fonction de la température, de composites C-C/ZrO_2 présentent des similitudes avec, toutefois, des niveaux de rupture différents, étroitement liés aux performances de la fibre de carbone de départ. Néanmoins, les composites C-C/ZrO_2 présentent de meilleures tenues en températures que les composites Al_2O_3-ZrO_2.

5) Au plan **thermique**, la caractérisation a porté sur la **dilatation,** la **diffusivité** et la **chaleur spécifique.** Ces caractéristiques ont été mesurées sur les

les fibres d'alumine (ou silico-alumineuse), les composites carbone-zircone sont plus conducteurs de la chaleur que les composites alumine-zircone.

Enfin, les mesures de **chaleur spécifique** confirment que les composites alumine-zircone sont plus isolants que les composites carbone-zircone.

L'ensemble de ces mesures thermiques ont permis d'établir que les composites Al_2O_3 - ZrO_2 ont des conductivités thermiques (directions 1 et 3) inférieures à 5 watt. m^{-1} . K^{-1}, tandis que les composites 2 D-C-C / ZrO_2 ont des conductivités thermiques autour de 7 watt. m^{-1} K^{-1} dans la direction 3, et de 20 watt. m^{-1} · K_{-1}, dans la direction 1, étroitement liées à l'anisotropie de la préforme 2D-C-C.

Au plan **chimique** , la caractérisation a été limitée à l'étude de la **résistance à l'oxydation** et à **l'ablation.**

Ainsi, il est apparu qu'en raison de sa microstructure polycristalline, de la présence de carbone libre et d'une porosité résiduelle significative, la matrice zircone, déposée par CVI, ne permet pas une complète protection des fibres (alumine, carbone) vis à vis des gaz oxydants. Sous l'effet de la température, la taille des grains élémentaires augmente, s'accompagnant d'importantes porosités, propices à la diffusion de l'oxygène de l'air. L'utilisation des composites à matrice zircone en athmosphère oxydante et à haute température, est limitée, en durée, par la dégradation des fibres

silico-alumineuses, par l'oxydation des fibres de carbone ou des interphases, et par la recristallisation de la matrice.

Par ailleurs, en présence d'un important flux de chaleur, il a été montré que les composites alumine-zircone sont rapidement perforés tandis que les composites carbone-zircone ont un temps de perforation analogue aux 2D-C-C (~ 300 s).

En résumé, cette étude a permis d'élaborer une nouvelle famille de matériaux composites céramique-céramique. Les caractérisations au plan mécanique, thermique et chimique ont montré que les composites Al_2O_3 - ZrO_2 peuvent être envisagés en vue d'applications à moyenne température, alors que les composites C-ZrO_2 peuvent être utilisés pour de courtes durées à très haute température (plus de 2000°C) en tant qu'isolant thermique. De plus, ce travail a permis de dégager un certain nombre de directions nouvelles de recherche tant fondamentale qu'appliquée. C'est ainsi qu'il reste à: (1) approfondir la corrélation entre la taille des grains, la présence de carbone et la stabilisation de la variété quadratique de la zircone (2) optimiser les infiltrations en les rendant compatibles avec celle de la zircone quadratique soit par le contrôle de la taille de grain, soit par le dopage de la phase gazeuse à l'aide d'un oxyde, enfin (3) étudier l'influence de la microstructure de la matrice zircone (taille de grains, variété allotropique) sur la ténacité et / ou la tenue à l'oxydation.

Vu et approuvé
Talence, le
Le président de
l'Université de Bordeaux I